Università degli Studi di Padova

Department of Chemical Sciences

Ph.D. Course in Molecular Sciences

Curriculum Chemical Sciences – 38th cycle

PEPTIDE-POLYSACCHARIDE CONJUGATES: A CLICK APPROACH TO FUNCTIONAL WOUND DRESSINGS

Coordinator: Prof. Stefano Corni

Supervisor: Prof. Cristina Peggion

Co-Supervisor: Lorenzo Beretta

Ph.D. Student: Francesca Albini

Thesis written with the financial contribution of the European Union - Next Generation EU and I.R.A. – Istituto di Ricerche Applicate S.p.a.

ABSTRACT

This thesis investigates the synthesis of bioactive materials capable of enhancing the wound healing process by preventing bacterial infections or accelerating wound closure. This was achieved by combining natural polysaccharides with peptides using a click chemistry approach. The polysaccharides cotton, chitosan, and hyaluronic acid were selected due to their nontoxicity, biocompatibility, and intrinsic bioactivities. Peptides were used as active molecules due to their versatile biological properties, which include antimicrobial, antiviral, anti-inflammatory, and collagen-stimulating activities. **PMAP-36$_{12\text{-}24}$**, **Pal-HAaH, 3.1** and **(RW)$_3$** were selected for their broad-spectrum antimicrobial activity, while **PP4** and **Ac-SDKP** were chosen for their potential skin regenerative properties. This work reports on (***1***) three chemoselective strategies for conjugating peptides to cotton; (***2***) a dual chemoselective ligation approach for conjugating peptides **3.1** and peptide **PP4** to chitosan; (***3***) the use of thiazolidine conjugation to bind peptides to hyaluronic acid and the electrospinning of the peptide-hyaluronic acid conjugates to form textiles made of nanometric fibers.

Cotton is the most widely used material for wound bandages but lacks intrinsic bioactivity. Therefore, aldehydes were introduced to its backbone through TEMPO/laccase/O_2 catalyzed oxidation, enabling thiazolidine and oxime ligations with active peptides. The reaction conditions for the two types of chemoselective ligation were studied using model peptides. Consecutive thiazolidine bonds of **PMAP-36$_{12\text{-}24}$** and **Pal-HAaH** or **PP4** were successfully carried out, producing double functionalized peptide-cotton conjugates capable of inhibiting the growth of *Acinetobacter baumannii*. **PMAP-36$_{12\text{-}24}$** was also successfully bound to norbornene-functionalized cotton through a photoinitiated thiol-ene reaction. The resulting peptide-cotton conjugates demonstrated comparable peptide loading and antibacterial activity to that of the conjugates obtained via thiazolidine bond.

The intrinsic antibacterial and hemostatic properties of chitosan make it a promising wound-healing material, and the presence of an hydroxyl and amine group in its repeating unit permit a double functionalization of the polysaccharide. Aldehydes and azides were introduced onto chitosan to enable binding of peptide **cys3.1** via thiazolidine chemistry and peptide **PraPP4** via azide–alkyne cycloaddition. The binding of both peptides to modified chitosan was confirmed by FT-IR, XPS and amino acid analyses. Antibacterial tests against *Staphylococcus aureus* and *Pseudomonas aeruginosa* demonstrated the ability of the **3.1**–chitosan conjugate to strongly inhibit the growth of both bacterial strains. However, the tests also revealed the dual conjugate **3.1**–chitosan–**PP4** to be less effective.

Hyaluronic acid is a key component in the wound healing process. Conjugating hyaluronic acid with active peptides and electrospinning the resulting conjugate enables the creation of nanostructured textiles with enhanced healing properties. $NaIO_4$ and TEMPO/laccase/O_2 oxidation were compared as

methods to introduce the aldehyde onto hyaluronic acid. TEMPO/laccase/O_2 was chosen because it has a better environmental impact and preserves the integrity of hyaluronic acid better. Electrospun nanofibers were successfully fabricated from aldehyde-functionalized hyaluronic acid/polyethylene oxide blends, and the same electrospinning setup was used for the successful electrospinning of peptide-hyaluronic acid conjugates with analogues of **Ac-SDKP** and **$(RW)_3$**. The conjugation and electrospinning processes did not impair the ability of **$(RW)_3$** to inhibit the growth of *Staphylococcus aureus*.

Abbreviations

A. alternata	Alternaria alternata
A. baumannii	Acinetobacter baumannii
A. flavus	Aspergillus flavus
A. fumigatus	Aspergillus fumigatus
A. tumefaciens	Agrobacterium tumefaciens
AAA	Amino acid analysis
ACE	Angiotensin-converting enzyme
ACTH	Adrenocorticotrophic hormone
Ahx	Aminohexanoic acid
Aib	2-Aminoisobutyric acid, α-methylalanine
Ala, A	Alanine
AMPs	Antimicrobial Peptides
Aox, Ax	Aminoxyacetic acid
Arg, R	Arginine
Asn, N	Aspargine
Asp, D	Aspartic acid
ATCC	American Type Culture Collection
B. cinerea	Botrytis cinerea
B. subtilis	Bacillus subtilis
Boc	tert-Butyloxycarbonyl
C. albicans	Candida albicans
C. heterostrophus	Cochliobolus heterostrophus
C. neoformans	Cryptococcus neoformans
Carbic Anhydride	5-norbornene-2,3dicarboxylic anhydride
CFU	Colon forming Unit
COPD	Chronic obstructive pulmonary disease pathophysiology
CuAAC	Copper Catalyzed Azide-Alkyne Cycloaddition
Cys, C	Cysteine
DCM	Dichloromethane
DD	Degree of deacetylation
Dde	1-(4,4-dimethyl-2,6-dioxocyclohex-1-ylidene)ethyl
DIC	N,N'-Diisopropylcarbodiimide
DIPEA	N,N-Diisopropylethylamine

DMF	Dimethylformammide
DMSO	Dimethylsulfoxide
DO	Degree of oxidation
DODT	2,2 -(Ethylenedioxy)diethanethiol
E. amylovora	Erwinia amylovora
E. coli	Escherichia coli
E. faecalis	Enterococcus faecalis
E. faecium	Enterococcus faecium
ECM	Extracellular Matrix
EDTA	Ethylenediaminetetraacetic acid
Et2O	Diethylether
FDA	Food and Drug Administration (US)
Fmoc	Fluorenylmethoxycarbonyl
GAGs	Glycoaminoglycans
Gln, Q	Glutamine
Glu, E	Glutamic acid
Gly, G	Glycine
GPC	Gel permeation chromatography
HA	Hyaluronic Acid
HARP	HepA-related protein
HaCaT	Human keratinocytes
HBTU	Hexafluorophosphate Benzotriazole Tetramethyl Uronium
HCF	Human corneal fibroblasts
HCTU	O-(1H-6-Chlorobenzotriazole-1-yl)
HDF	Human dermal fibroblasts
HEPES	N-2-hydroxyethylpiperazine-N-2-ethane sulfonic acid
HFF-1	Human foreskin fibroblasts
HFIP	Hexafluoro-2-propanol
His, H	Histidine
HMW	High Molecular Weight
HOBt	Hydroxybenzotriazole
IL	Interleukin
Ile, I	Isoleucine
ISA·HCl	Imidazole-1-sulfonyl azide hydrochloride
K. pneumoniae	Klebsiella pneumoniae
Leu, L	Leucine

LMW	Low Molecular Weight
Lys, K	Lysine
M. luteus	Micrococcus luteus
MBC	Minimal bactericidal concentration
MDR	Multi drug resistant
Met, M	Methionine
MIC	Minimal inhibitory concentration
MTBE	Methyl-tertbuthylether
MTT	3-(4, 5-dimethylthiazolyl-2)-2, 5-diphenyltetrazolium bromide
NMM	N-Methylmorpholine
OD	Optical Density
Oxima	Ethyl cyano(hydroxyimino)acetate
P. aeruginosa	Pseudomonas aeruginosa
P. syringae	Pseudomonas syringae
P. syringae pv. actinidiae	Pseudomonas syringae pv. actinidiae
Pal	Palmitic Acid
Pbf	2,2,4,6,7-pentamethyldihydrobenzofuran-5-sulfonyl residue
PBS	Phosphate-buffered saline
Pc	Zinc phthalocyanine
PCL	Polycaprolactone
PEG	Polyethylenglycol, Polyethylenoxide
PEO	Polyethylenoxide, Polyethylenglycol
Phe, F	Phenilalanine
PLGA	Poly(lactic-co-glycolic)
POP	Propyl oligopeptidase
Pra	Propargylglicine
Pro, P	Proline
PU	Polyurethane
PVA	Polyvinyl alcohol
RH	Relative humidity
S. aureus	Staphylococcus aureus
S. dysenteriae	Shigella dysenteriae
S. enterica	Salmonella enterica
S. epidermidis	Staphylococcus epidermidis
S. typhimurium	Salmonella enterica serovar Typhimurium

Ser, S	Serine
SPPS	Solid Phase Peptide Synthesis
TCC	Trichloroisocyanuric acid
TCEP	Tris(2-carboxyethyl)phosphine
TEMPO	(2,2,6,6-tetramethylpiperidin-1-yl)oxyil radical
TFA	Trifluoroacetic acid
TGF-β	Transforming growth factor-β
THP-1	Monocyte cell line
THPTA	Tris(3-hydroxypropyltriazolylmethyl)amine
Thr, T	Threonine
TIS	Triisopropylsilane
TNF-α	Tumor necrosis factor alpha
Trp, W	Tryptophane
Trt	Triphenylmethane
Tyr, Y	Tyrosine
Tβ4	Thymosin-beta 4
VA-086	2,2'-Azobis[2-methyl-N-(2-hydroxyethyl)propionamide]
Val, V	Valine

Contents

ABSTRACT ..... *i*

Abbreviations ..... *iii*

Chapter I: Aim and Introduction *1*

1.1 Aims and Structure of the Thesis 1

1.2 Skin: Structure and Wounds 4

1.2.1 Anatomy of the Skin 4

1.2.2 Wound Healing 4

1.2.3 Bacteria on Skin and Wounds 6

1.2.4 The Ideal Wound Dressing 7

1.3 Peptides as Active Agents 9

Antimicrobial Peptides (AMPs) 10

1.4 Click Chemistry 13

1.4.1 Thiazolidine 13

1.4.2 Oxime 14

1.4.3 Thiol-ene 16

1.4.4 Azide-alkyne (CuAAC) 17

References 19

Chapter II: Antibacterial Cotton for Wound Healing via Chemoselective Peptide Conjugation Strategies *22*

2.1 Introduction 23

2.1.1 Cotton 23

2.1.2 The Peptides 26

2.2 Results and Discussion 33

2.2.1 Peptide Choice 33

2.2.2 Project 1: Model Peptides for Oxime and Thiazolidine Chemoselective Ligation Reactions 37

2.2.3 Project 2: Multiple Cotton Functionalization by Thiazolidine bond 39

2.2.4 Project 3: PMAP-Cotton Functionalization by Thiol-Ene click reaction 46

2.3 Conclusions and Future Perspectives 53

2.4 Methods 55

2.4.1 Instruments 55

2.4.2 Peptide Synthesis 55

2.4.3 Cotton Modification 62

2.4.4 Peptide-Cotton Conjugation 65
2.4.5 Amino Acid Analysis 67
References 69
Chapter III: Bi-functional Chitosan: an Orthogonal Approach to Peptide Grafting 72
3.1 Introduction 73
3.1.1 Chitosan 73
3.1.2 The Peptides 76
3.2 Results and Discussion 80
3.2.1 Choice of Peptides 80
3.2.2 Chitosan Modification 81
3.2.3 Peptide-Chitosan conjugations- Preliminary 83
3.2.4 Peptide-Chitosan conjugations 85
3.2.5 XPS Analysis of Chitosan and Derivatives 88
3.2.6 Amino Acid Analysis 89
3.2.7 Antibacterial Activity of the Conjugates 90
3.2.8 Collagen-Boosting Activity of the Conjugates 92
3.3 Conclusions and Future Perspectives 93
3.4 Methods 95
3.4.1 Peptide Synthesis 95
3.4.2 Chitosan modification 97
3.4.3 Peptide-Chitosan conjugations - Preliminary 98
3.4.4 Peptide-Chitosan conjugations 100
3.4.5 Amino acid analysis 101
3.4.6 Antibacterial tests 102
References 103
Chapter IV: Nanofibrous Textiles with Antibacterial and Skin-regenerative Properties Based on Hyaluronic Acid and Peptides 105
4.1 Introduction 106
4.1.1 Hyaluronic acid 106
4.1.2 The Peptides 108
4.1.3 Electrospinning 112
4.2 Results and Discussion 116
4.2.1 Choice of Peptides 116
4.2.2 CHO grafting on Hyaluronic Acid 120
4.2.3 Peptide-HA Conjugates – Preliminary 125
4.2.4 Peptide-HA Conjugates for electrospinning 127

4.2.5 Electrospinning 130
4.2.6 Antibacterial Activity 132
4.3 Conclusions and Future Perspectives 134
4.4 Methods 136
4.4.1 Instruments 136
4.3.2 Peptide Synthesis 136
4.3.3 Peptide Resistance in Human Serum 140
4.3.4 CHO grafting on Hyaluronic Acid 140
4.3.5 Peptide-HA conjugations 142
4.3.6 Electrospinning 143
4.3.7 Antibacterial tests 144
References 146
Chapter V: Supporting Information 149
5.1 Materials 150
Reagents and solvents 150
5.2 Supporting Images – Chapter II 151
5.2.1 Chromatograms (HPLC) of the synthesized peptides 151
5.2.2 Peptide Loading overtime 156
5.2.3 FT-IR Spectra – Project 2 158
5.2.4 FT-IR Spectra – Project 3 159
5.2.5 Amino acid analysis 161
5.2.6 XPS Analysis 163
5.2.7 Antibacterial tests - Optical Density measurements 165
5.2 Supporting Images – Chapter III 166
5.3.1 Chromatograms (HPLC-MS) of the synthesized peptides 166
5.3.2 FT-IR Spectra of modified chitosan 167
5.3.3 Schiff test 167
5.3.4 XPS Analysis 168
5.3.5 Amino acid analysis 171
5.3.6 Raw Data of Antibacterial tests 172
5.4 Supporting Images – Chapter IV 173
5.4.1 Chromatograms (HPLC) of the synthesized peptides 173
5.4.2 HPLC of the degradations in human serum 175
5.4.3 FT-IR Spectra 178
5.4.4 ^{1}H-NMR results 181

5.4.5 Gel Permeation chromatography - Molecular weight 184
5.4.6 SEM images of electrospun hyaluronic acid 186
5.4.7 Immunomodulatory activity 190
5.4.8 Antibacterial Activity 193
Ringraziamenti ***195***

Chapter I:

Aim and Introduction

1.1 Aims and Structure of the Thesis

Skin wounds, especially when they become chronic, are a major public health problem, with several risks of complications and a significant negative impact on the quality of life of patients[1]. Thus, the preparation of active dressings that can enhance the heling process is of utmost relevance. Natural polysaccharides, such as cellulose, chitosan, or hyaluronic acid, are especially attractive as primary material due to their non-toxicity, biocompatibility, and intrinsic biological activities like hemostatic or antibacterial properties[2]. Depending on their amino acid sequence, peptides exert various properties and can be antibacterial, antiviral, anti-inflammatory, but also trigger the production of collagen[3,4]. This versatility makes them particularly appealing as functionalization agent.

Within this context, the present thesis focuses on designing and producing innovative wound dressings that actively support the healing process with the ultimate goal of improving quality of life for patients dealing with issues like chronic wounds. Peptides were selected as the active agents to provide a specific functionality to the final materials, and different types of click chemistry will be employed to selectively and covalently graft the peptides onto natural polysaccharides. Thus, the aims of this thesis are:

1) Integrate functional biomolecules into natural, biocompatible matrices

The potential of cellulose, chitosan, and hyaluronic acid, in combination with bioactive peptides, will be investigated to create multifunctional, biocompatible materials through:

a) Synthesis, purification, and evaluation of the activity of peptides with antibacterial or wound healing properties. The parent sequence will be modified to include the moiety required for the selective ligation to the polysaccharide (e.g thiol, β-aminothiol, α-nucleophile, or alkyne).
b) Chemical functionalization of cotton cellulose, chitosan and hyaluronic acid to allow for the click chemistry with the modified peptides (e.g. aldehyde, norbornene, or azide).

2) Explore selective chemical strategies for biofunctionalization

Click chemistry approaches will be employed to covalently conjugate peptides to polysaccharide substrates. Specifically:

c) Peptide-polysaccharide conjugates will be synthetized by thiazolidine, oxime, thiol-ene, or azide-alkyne reactions
d) The reaction conditions will be optimized in terms of efficiency and environmental impact.
e) The activity of the conjugates will be evaluated to investigate whether the peptides activity and the intrinsic benefit of the polysaccharides were not lost after conjugation.

3) Contribute to innovation in biomaterials through electrospinning technologies.

The electrospinning technique is of particular interest because it enables the production of nanofibrous textiles that resemble the extracellular matrix of cells, but are also characterized by good hemostasis, absorbability and oxygen permeability, and that can act as support and help in healing damaged tissues[5]. Thus, hyaluronic acid will be used as a substrate to develop next-generation biomedical devices by:

f) Setting up the conditions for the production of an electrospun textile based on hyaluronic acid and peptides with a particular emphasis on using water-based solvent systems to improve the sustainability and biocompatibility of the fabrication process.
g) Confirm that the activity of the peptides was not lost due to the presence of the polysaccharide, conjugation, or electrospinning.

The thesis is divided into five chapters, where ***Chapter I*** provides the background required to put into context the original research work reported in ***Chapter II-IV***, and ***Chapter V*** contains the supporting information for the previous chapters. More specifically, ***Chapters I-III*** are divided depending on the polysaccharide used as a substrate for the conjugation with peptides:

Chapter II gives an overview on the studies performed using ***cotton*** for the production of an antibacterial material to be used in wound care. Four sets of peptides were synthesized: (*1*) model peptides to study the reaction conditions, (*2-3*) derivatives of two AMPs (**PMAP$_{12\text{-}24}$** and **Pal-HAaH**) modified to include the moiety required for the selective ligation (e.g thiol, β-aminothiol, α-nucleophile) to the polysaccharide, and (*4*) derivatives of the collagen boosting peptide **PP4**. This chapter is divided into three sections. The *first* and *second section* focus on the use thiazolidine and oxime bonds for the functionalization of cotton with peptides. In the former, model peptides are used to optimize the reaction conditions. In the latter, the double functionalization of cotton by consecutive thiazolidine ligations of different active peptides is explored. The *third section* briefly investigates the feasibility of the thiol-ene click chemistry for the conjugation of an antibacterial peptide to cotton functionalized with norbornene. Finally, the antibacterial properties of the synthetized materials were evaluated against *A. baumannii*.

Chapter III focuses on the synthesis of a bi-functional (antibacterial and collagen boosting) ***chitosan*** by a Click orthogonal approach. Chitosan was chemically modified to introduce the aldehydes and azides required to bind two peptides by two click chemistry. A β-aminothiol was introduced to the antimicrobial peptide **3.1**, and an alkyne was introduced to the collagen boosting peptides **PP4** to allow for thiazolidine and copper catalyzed azide-alkyne reaction, respectively. The activity of the peptide-chitosan conjugates was tested against *S. aureus* and *P. aeruginosa* to evaluate whether the properties of the peptides could be maintained in the final materials.

Chapter IV delineates the research carried out on the conjugation of peptides to ***hyaluronic acid*** by thiazolidine bond formation, and its electrospinning to produce peptide/hyaluronic acid-based textiles. Two sets of peptides were synthesized: derivatives of the antibacterial peptide **$(RW)_3$**, and derivatives of the skin regenerative peptide **Ac-SDKP**, modified to include the moiety required for the selective ligation. The $NaIO_4$ and TEMPO/laccase/O_2 catalyzed oxidation of hyaluronic acid were compared as methods to introduce the aldehyde needed for the thiazolidine bond in hyaluronic acid. The electrospinning setup to produce nanometric fibers from water-based solutions of hyaluronic acid and the peptide-hyaluronic acid conjugates was investigated. Finally, the antibacterial properties of the synthetized materials were evaluated against *S. aureus*.

The third project of ***Chapter II*** and the work of ***Chapter III*** was carried out at the University of Porto, under the supervision of Prof. Paula Gomes (LAQV-REQUIMTE, Departamento de Química e Bioquímica, Faculdade de Ciências) and Prof. M. Cristina L. Martins (i3S, Instituto de Investigaçãoe Inovação em Saúde). Part of the work of ***Chapter IV*** was performed at I.R.A – Istituto di Ricerche Applicate during a six-month internship.

1.2 Skin: Structure and Wounds

1.2.1 Anatomy of the Skin

Skin is the largest organ or the human body and serves a physical barrier against the entrance of microbial, physical and chemical agents, but also the against exit of liquids, preventing excessive water loss and dessication[6].

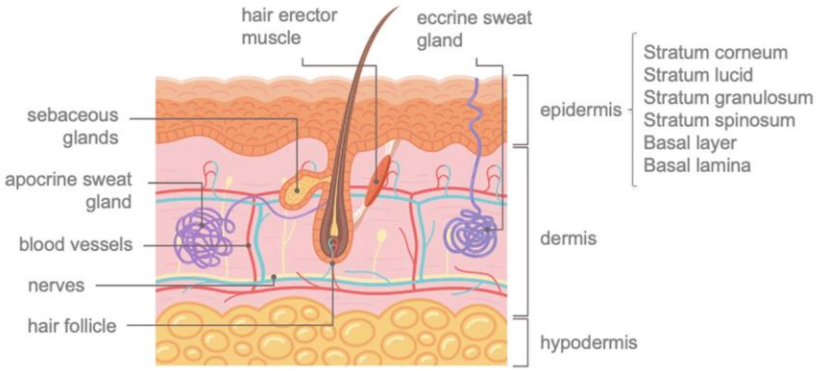

***Figure 1.1**: Schematic representation of the skin anatomy. Reported with permission from De-Luna-Gallardo et al.[7]*

The skin is organized in three main layers (Fig 1.1):

1. *The epidermis* is the layer in direct contact with the environment. It lacks vascular vessels and consists of keratinized, stratified squamous epithelial tissue. Based on cell arrangement, the cell layers of the epidermis have been differentiated in four main types: *stratum corneum*, *stratum granulosum*, *stratum spinosum* and *stratum basale* (from outside to inside)[8]. Some areas that are defined as thick (e.g. palms or plantars) have an additional layer between the first two: the *stratum lucid.* It is important to note that the only cells that exhibit mitotic activity are found in the basal layer[7].

2. *The dermis* is located below the epidermis. This layer consists of sweat glands (regulate body temperature), blood vessels, lymph vessels, hair follicles, nerves and sebum. Of particular interest in this layer is the presence of fibroblasts: cells responsible for the secretion of elastic fibers and procollagen[8]. Other cells present in this layer are macrophages, plasmatic cells and mast cells[7].

3. *The hypodermis* (or subcutaneous tissue) consists of loose connective tissue and adipose tissue that function as a storehouse of energy[7,9].

1.2.2 Wound Healing

Wounds are defined as a damage or disruption of the normal anatomical architecture and function of a tissue. They can be classified in superficial or deep wounds according to the number of skin layers

affected. The former include breaks in the integrity of the epidermis, the latter can extend the damage to lower layers, even up to the bones. Wounds can also be clinically classified as acute if their timeframe of healing is concluded within 30 days. On the other hand, when there is an interference in the normal wound healing process by factors that include infection, tissue hypoxia, necrosis, exudate and excess of inflammatory cytokines, chronic wounds may result and the tissue could remain in a non-healing state for much longer than 30 days[10,11]. Wound healing aims at limiting the loss of tissues and fluids, but also avoiding the invasion of particulate or microorganisms. This complex and dynamic process can be rationalized in the four main phases illustrated in Figure 1.2[10-13]:

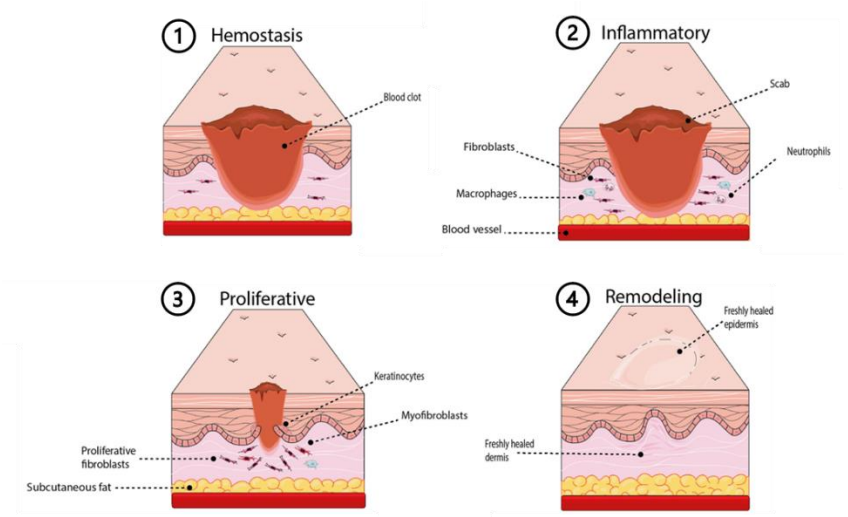

Figure 1.2*: The four stages of wound healing, from Canchy et al.[1]*

The first step of ***coagulation and hemostasis*** begins right after wound formation and includes (**1**) the *formation of a temporary barrier* against exsanguination by contraction of the injured vessels, formation of the platelet plug by aggregation, and activation of the coagulation cascade that brings to the conversion of fibrinogen to insoluble fibrin; and (**2**) the *arrival of a matrix of invading cells* needed for later phases of healing[11,12].

Inflammation is the second step of the wound healing process, it can be divided in early and late inflammatory phase, and has a major role in removing tissue debris from the wound site[11,13]. The early state starts within the first 24-36h after the trauma, and is characterized by *neutrophils* infiltration. This molecules, once at the wound site, prevent bacterial infections and ulterior damage by phagocytosing foreign material and bacteria. The late inflammatory phase takes place 48-72h after wound formation and includes the elimination of the neutrophils *via* phagocytosis by *macrophages,* but also the arrival of *inflammatory cytokines* (such as TNF-α and IL-1), and the *antimicrobial chemokines*. In normal acute wounds the inflammatory stage lasts for 2-5 days[11,12].

As the inflammation recedes, the ***proliferative phase*** starts in order to repair the tissue. This stage is characterized by (**1**) *fibroblast migration* that then synthetize the new extracellular matrix proteins such

as hyaluronan, fibronectin, proteoglycans and procollagen that replace the provisional fibrin network, (**2**) *synthesis of collagen* that is essential for the intracellular matrix, (**3**) *angiogenesis and granulation tissue formation* to partially recover the structure and function of the skin, (**4**) *epithelization* by migration of the newly formed epithelial cells[11,12].

The last step of wound healing is the ***remodeling*** of the wound, and it could take up to two years to complete. In this phase the granulation tissue that is composed mainly of *collagen III* is replaced by the healthy scar tissue, mainly composed of *collagen I*[12]. The fully matured scar presents a decreased number of cells and blood vessels and a high tensile strength[11].

1.2.3 Bacteria on Skin and Wounds

As stated in the previous section, avoiding bacterial infections is a crucial part of the wound healing process because it may delay the healing process by prolonging the inflammatory phase, but also cause serious complications, such as ulcers or even sepsis.

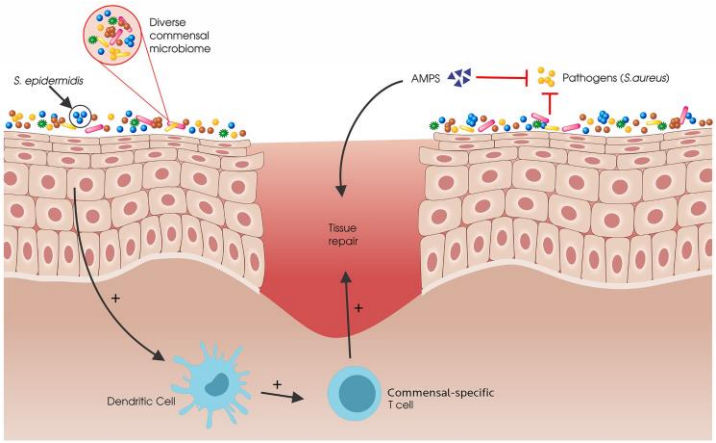

Figure 1.3*: Normal skin with its microbiome, from Canchy et al.*[1]

It is important to note that healthy skin has a symbiotic relationship with the complex community of commensal bacteria, fungi and viruses that compose the skin microbiome. These resident microorganisms (e.g. *S. epidermidis*) have a major role in limiting the colonization of skin pathogens (e.g. *S. aureus*) and can have an active positive effect on wound healing by limiting the inflammation at the skin injury, improving re-epithelization and tissue granulation, and stimulating the production of the host antimicrobial peptide (AMPs)[1]. Thus, in every wound there is certain amount of bacterial contamination regardless of cause, size, location and management of the wound itself[11,14], however the problem lays on whether the bacterial colonization becomes critical, and turns into infection. In fact, a wound is defined as (**1**) *contaminated* when the bacteria are present without active proliferation, (**2**) *colonized* when the bacteria are multiplying but do not determine a reaction in the host, (**3**) *critically colonized* when there host response is activated and (**4**) *infected* when the bacterial population is increasing despite the ongoing host reaction[14]. The formation of bacterial communities living in

aggregates at the liquid interface (biofilms) poses an additional complication to healing because in the biofilm the bacteria are physically protected by a self-produced matrix composed of polymeric extracellular substances[14,15]. The formation of biofilms is particularly relevant in chronic wounds where the accumulated proteins and damaged tissue provide an excellent attachment site for biofilm formation, making the treatment of chronic wounds even more difficult[15].

Since their ideal pH for growth is around 7, the first bacteria that colonize wounds are usually gram-positive (e.g. *Staphylococci*). At later times, *P. aeruginosa* and *E. faecalis* can also be found due to their ability to survive in a wider range of pH. As the pH of the wound turns more alkaline, also anaerobic bacteria (e.g *Peptostreptococci*) colonize the wound[14]. In particular, while *S. aureus* appears to be the most common colonizer in acute wound burns, these wounds also present a variety of gram-negative pathogens like *Pseudomonas* and *Acinetobacters*[16,17]. In addition, it is important to note that, in 2024, 86.6% of the *S. aureus* strains found in burn wounds were methicillin-resistant[17]. Thus, there is a call for new antibiotics with a mechanisms of action that are not so easily circumvented by bacteria prone to develop multidrug resistance, such as the so-called ESKAPE pathogens: *Enterococcus faecium, Staphylococcus aureus*, *Klebsiella pneumoniae*, *Acinetobacter baumannii*, *Pseudomonas aeruginosa*, and *Enterobacter species*[18].

1.2.4 The Ideal Wound Dressing

Considering the utmost importance of protecting wounds from infections and promote their healing in a fast manner, wound dressings have been employed for centuries to avoid these issues. While a variety of materials can achieve this desired effect, they all share some key features. Beside the basic mechanical protection against bacterial infection, to enhance the healing process an ideal wound dressing should[19,1,20,21]:

- *Maintain a balanced moist environment* by avoiding the wound to dry out, but also preventing an excessive moisture that could allow for bacterial infections and tissue maceration.
- *Absorb the excess exudate.* This is particularly relevant in chronic wounds because their exudate negatively affects wound remodeling and repair due to the presence of proteases and proinflammatory cytokines.
- *Prevent excess scarring.*
- Allow for *the exchange of gases*, especially oxygen.
- Be *comfortable*, *non-toxic*, *biocompatible* and *durable.*
- Be *easy to apply, remove* and *dispose of.*

Gauzes and bandages are the oldest and most traditional form of wound dressing. They satisfy the basic requirement of covering the wound and preventing secondary injuries, but they present some disadvantages (e.g. low exudate absorption and absence of the ideal moist environment) making them

effective for clean and dry wounds, but not for more challenging chronic wounds[21,22]. Other common forms of wound dressing are hydrogels and foams. The former are excellent at maintaining the ideal moisture at the wound site, but lacks in mechanical properties, making them less suitable for motion-related wounds. The latter are characterized by great hemostatic properties, but are particularly difficult to remove, causing pain in the patient[22]. Thus, in recent years there has been a surge in the research on smart wound dressings that could tackle some of the flaws of the most common wound dressings. Of particular note is the development of materials that can actively monitor the wound status, or deliver drugs, cell or cell derivatives, and can even manage the scar development or be stimuli-responsive[21,22].

As bulk materials for wound dressings natural polysaccharides are of great interest due to their excellent biocompatibility, biodegradability, non-toxicity, rapid manufacturing, and, especially their high level of biomimicry of the native ECM[2]. The most commonly used are:

- *Cellulose* due to its low costs and high abundance. In addition, depending on the original source it could also have a different moisture retaining capacity and exudate absorption (e.g. bacterial cellulose)[23]. A more detailed description of cotton cellulose is found in *Chapter 2.1.1*.
- *Chitosan* due to its intrinsic antimicrobial, analgesic and hemostatic properties, but also its ability to support neovascularization and dermis regeneration[24,25]. A more detailed description of chitosan is found in *Chapter 3.1.1*.
- *Hyaluronic acid* due to its wide spread ubiquitous role during the wound healing process, but also its intrinsic anti-inflammatory activity, exudate absorption capacity and ability to induce cell adhesion and reduce biofilm formation[26,27]. A more detailed description of hyaluronic acid is found in *Chapter 4.1.1*.
- *Alginate* due to its high adsorption capacity, antimicrobial, antifungal and immunomodulatory activity, but also regenerative and angiogenic properties[28,29].

1.3 Peptides as Active Agents

Peptides are organic molecules consisting of a small number of amino acids linked together by amide bonds. They occupy an intermediate position between small organic molecules and large biological compounds like antibodies or proteins. They are particularly interesting because depending on their amino acid composition and sequence they exert a wide range of activities such as antioxidant, immunomodulatory, cytomodulatory, opioid, mineral-binding, antihypertensive, antithrombotic, collagen regenerative, antimicrobial, or anticancer[3,30-32].

The use of peptides therapeutics started in the 1920s with the isolation of insulin and adrenocorticotrophic hormone (ACTH) from animal sources[32]. Even though the discovery of these two molecules revolutionized the field in the first half of the 19th century, the invention of solid phase peptide synthesis by Merrifield in 1963[33] opened the way for a fast and automatable method for large scale peptide synthesis[34]. The use of peptides as therapeutics has increased over time reaching the 5% of the global pharmaceutical market in 2019[31]. In particular, as of March 2017, 60 therapeutic peptides had been approved in the US, Europe and Japan, and 155 were in clinical development with half of those in Phase 2 studies. Interestingly, 30% of peptides that entered clinical development since the start of 2010 are conjugates with PEG, lipids, proteins, cytotoxins, synthetic polymers or imaging agents[32]. Notable examples of peptide drugs currently on the market are Leuprolide for cancer therapy, Semaglutide/Liraglutide/Tirzepatide for diabetes, the antimicrobial Dalbavancin, and the anti-inflammatory Voclosporin[30].

Two of the main challenges in the broad use of peptides as active agents are (**1**) their *susceptibility to peptidases* which results in a short plasma half-life and rapid elimination from the body, making very difficult to achieve the therapeutic concentration *in vivo*, and (**2**) their *poor oral bioavailability* due to degradation of the amide bond by digestive enzymes that forces a systematic administration, which then results in poor patient compliance[32,35]. Anyhow, their uniqueness does not only rise from their versatility, but also by their specificity and safety, as well as their well-defined mechanisms of action[30,35]. In fact, when compared to small organic drugs, they have fewer off-target effects and reduced cytotoxicity due to a general greater precision in targeting cell receptors, but are also characterized by a lower immunogenicity[30]. Compared to monoclonal antibodies, they have lower costs of production, better tumor penetration, and greater flexibility in structural modification[35]. In addition, the metabolism of peptide drugs does not usually lead to the formation of toxic metabolites[36].

Over the years several strategies have been applied to improve peptide stability against proteases without drastically altering their activity and cytotoxicity. Some of the most successful methods include[37,38]: (**1**) *N/C-terminus modification* such as acetylation, acylation and methylation at the uniquely

reactive site of the terminal nitrogen and amidation at the C-terminus. In some cases acylation could impact the activity and cytotoxicity of the molecules[31,37,39], (**2**) *side chain modifications* such as alkylation, PEGylation or glycosylation of the amino acid side chains[37], (**3**) use of *non-proteinogenic amino acids* makes peptide less recognizable to proteases[40], and (**4**) c*yclization* of the peptide reduces the flexibility and access to the cleavage sites[41,42].

Of particular relevance for the aims of this manuscript are peptides with wound healing properties and antimicrobial peptides to be used as active agents for the functionalization of natural polysaccharides.

As previously stated, wound healing is a complex and dynamic process that involves a series of specific and coordinate phases. Several natural peptides are involved in this process and can be administrated to enhance the wound healing process:

- *Neuropeptides* are the largest and the most diverse signaling group of molecules in multicellular organisms. Their positive contribution to wound healing is currently being studied and is thought to be due to the activation of endothelial cells, fibroblasts, and keratinocytes to express their functions, by direct activation of the intracellular G protein signaling cascade[43,44].
- *Collagen peptides* are derived from the enzymatic degradation of collagen and show potential in improving wound healing. These peptides are derived from different sources such as fishes, shellfish, arthropods, but also bovine Achille tendons[43].
- *Growth factors* natively act as regulators of wound healing and their exogenous application can modify the process. In particular, the healing of various wounds has been enhanced by treatment with epidermal growth factor (EGF) or transforming growth factor alpha (TGF-α)[45,46].

Antimicrobial Peptides (AMPs)

Gramicidin, being active against *Pneumococcus* infections, was the first antimicrobial peptide (AMP) to be discovered, in 1939[47,48]. Most living organisms (bacteria, fungi, plants, invertebrates, arthropods, fishes, amphibians, reptile, birds and mammals) are producers of AMPs as part of their innate immune response to viruses, fungi, bacteria, but also protozoa and even cancer cells[49]. These molecules are of particular interest because their broad-spectrum mechanism of action means they are at low risk of developing resistance, making them promising candidates for pharmacological applications, even in a synergetic administration with classical antibiotics[50]. Cationic antimicrobial peptides are the most abundant and studied class of AMPs. Although they are quite heterogeneous, they are still characterized by some distinctive features[51,52]: (**1**) *small size*: from 10 to 25 amino acid residues and 1-5 KDa. The length of the chain can count up to 60 residues but usually, shorter AMPs are usually preferred for clinical treatments for the lower costs and lower cytotoxicity, (**2**) *cationic* (Arg and Lys) and *hydrophobic* (with aliphatic and aromatic side chains) *residues* as the main constituting types of amino acids, (**3**) tendency to adopt *amphipathic structures* and (**4**) *net positive charge* that ranges from +2 to +9.

Overall, AMPs are particularly interesting functionalization agents due to their broad spectrum of activity, even at low concentrations, target specificity, synergistic effect with conventional antibiotics, and low tendency to induce pathogen resistance[52,53].

Based on their mechanism of action, cationic AMPs are divided into two categories: **membrane-targeting** and **non-membrane targeting** AMPs. The former act by damaging the structural integrity of the cell membrane, while the others exert their antimicrobial properties by inhibiting essential cell components or cellular functions[50].

Membrane Targeting AMPs

The selectivity of membrane-targeting AMPs for bacterial membranes is due to their differences from mammalian membranes. Mammalian membranes do not expose negative charges that can attract cationic AMPs. In fact, the anionic lipids are located in the inner leaflet of their plasma membrane. Additionally, the presence of cholesterol in both leaflets increases the membrane thickness and density making more difficult for the peptides to penetrate. On the other hand, bacterial membranes lack sterols and contain at least 15% anionic lipids. . Thus, bacterial membranes tend to be highly negatively charged, and therefore attractive to AMPs[54].

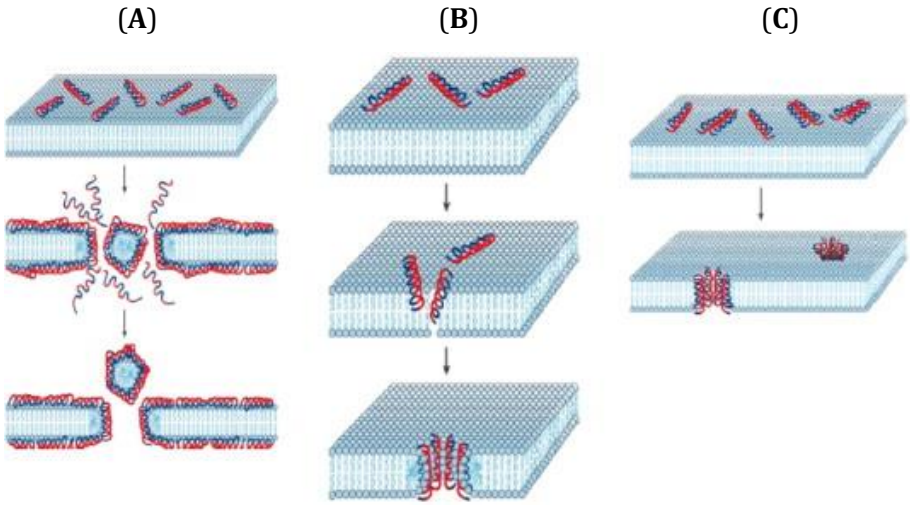

Figure 1.4*: Current models of the mechanism of action of membrane-active antimicrobial peptides (AMPs, from left to right): (**A**) **carpet model**: the peptides accumulate and spread all over the membrane surface in a parallel arrangement. The reaching of a critical concentration causes the reorientation of the peptides towards the inside of the membrane and the degeneration of the membrane into smaller micelles with a hydrophobic core; (**B**) **toroidal pore model**: pore formation is triggered by a peptide-lipid interaction. This causes a local curvature of the bilayer and the formation of a toroidal pore ; (**C**) **barrel-stave model**: first the peptides attach to the membrane surface parallelly. Then the interaction between the hydrophobic regions of the peptides with the inner hydrophobic core of the membrane causes their insertion and the formation a transmembrane pore. In this model the hydrophilic regions of AMPs face the inner part of the channel. Reported with permission from Costa et al.[52]*

Upon accumulation of AMPs, the membrane reaches its critical aggregation concentration, and AMPs begin to affect the membrane integrity[50]. The specifics of exactly how the peptides disrupt membranes are not the same, but the three principal identified models of action are: (**1**) the *barrel-stave* pore model[55], (**2**) *toroidal pore* model[55], (**3**) *carpet* model[56] (Fig. 1.4).

Non-Membrane Targeting AMPs

Many AMPs are proven to act with different mechanisms that do not involve the bacterial membrane as their primary target. The non-membrane targeting AMPs act by first translocate into the cytoplasm, without damaging the membrane, by different mechanisms such as the formation of transient toroidal pores or stereospecific binding of AMPs to inner membrane transporters[57]. Then, they can interfere with various critical cellular processes. Some notable intracellular targets of these AMPs are the DNA, proteins or cell wall biosynthesis inhibition, nucleic acids binding, and ribosomes or intracellular proteins (e.g. DnaK and GroEL) inhibition that leads to protein misfolding[50,57].

1.4 Click Chemistry

The term *Click Chemistry* was first introduced in a paper by *Kolb et al*.[58] to define a set of chemoselective reactions that can be used to synthesize new chemical entities by joining smaller units in an easy and efficient manner. In particular, the reactions must be "modular, wide in scope, give very high yields, generate only inoffensive byproducts that can be removed by nonchromatographic methods, and be stereospecific. The required process characteristics include simple reaction conditions, readily available starting materials and reagents, the use of no solvent or a solvent that is benign (such as water) or easily removed, and simple product isolation"[58]. The most commonly employed click chemistry include the Dies-Alder cycloaddition, ring-opening reactions of strained heterocyclic electrophiles, Staudinger reaction, copper catalyzed azide-alkyne cycloaddition (CuAAC), thiol-ene, thiol-maleimide but also the formation of oximes, hydrazones, disulfides and amides[58-60].

In the context of peptides, the work of Tam, Liu, and Kent[61-64] in the early 1990s, demonstrated the feasibility of using click reactions to assemble unprotected peptide fragments in aqueous solutions. This marked a fundamental change in peptide synthesis. In fact, this innovative method overcame the limitations imposed by the steric hindrance that was inevitable with previous methods, which required the use of protective groups for the side chains of amino acids, and allowed the synthesis of complex molecules by convergent synthesis using unprotected peptides and biorthogonal reactions. On the other hand, the click chemistry approach is particularly suited in the context of functionalized materials with biological applications. In fact, provided the insertion of two chemoselective moieties, one on the material and the other on the active molecule, the use of click chemistry allows for an easy, one-step and tunable functionalization process that uses reagents and reaction conditions that are biocompatible (inoffensive by-products, benign solvents and simple product isolation), without the need of further purification.

1.4.1 Thiazolidine

A chemoselective reaction that has not yet been fully explored in the context of bioconjugations is the condensation reaction between β-aminothiols and aldehydes to form a thiazolidine[65].

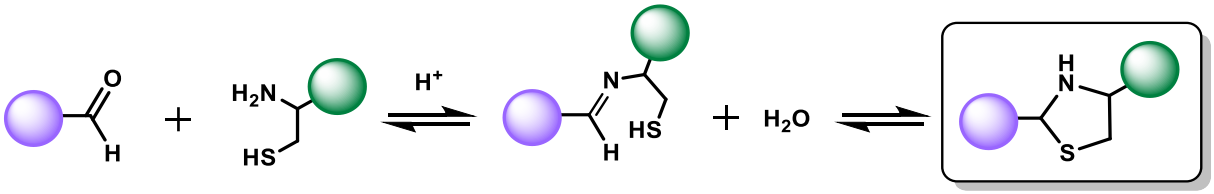

***Figure 1.5**: Reaction mechanism for the formation of a thiazolidine ring.*

The reaction was first described in 1994 by *Liu et al.*[61] for the synthesis of a tetradecapeptide starting from two shorter sequences using water as the solvent. The highly specificity of this reaction lies in the formation of a stable five membered ring, that is not present in the concurrent reaction with an amine Schiff base that would be reversible and unstable[61]. The original paper reported an ideal pH of 4.5 for the reaction to prevent the reaction between aldehydes and nucleophiles by protonation, however recent data showed that the reaction is fast and efficient in a broader range of pH (5-9), even for the conjugation of N-terminal cysteine peptide with a model short interfering aldehyde grafted RNA[65].

The reaction mechanism is reported in Figure 1.5. Specifically, the N_α-terminal amine attacks the C_α-terminal to form an imine bond with the elimination of a water molecule. Then, the thiol side chain attacks the electrophilic carbon forming a five membered ring.

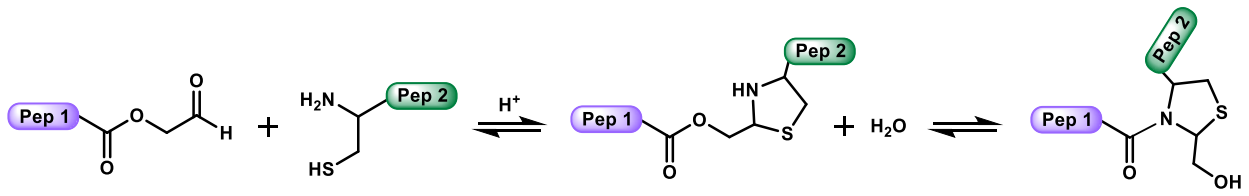

***Figure 1.6**: Reaction mechanism for condensation reaction between an aldehyde introduced at the C-terminus of a peptide and the β-aminothiol of a N-terminus cysteine.*

When the aldehyde is introduced at the C-terminus of a peptide sequence (Fig. 1.6), the presence of an ester carbonyl near the N_α-amine of the ring favors the subsequential intramolecular O- to N-acyl transfer and the formation of an amide bond. In this way, the final product has a proline mimetic structure. The back reaction is triggered by the presence of electrophiles, that is why this type of ligations are also used as temporary protection of Cys in peptide synthesis[61,63]. It is important to note that the β-amino hydroxyl of Thr of Ser can also act as a nucleophile similarly to the thiol of Cys to form heterocyclic rings, but the reaction rates are much lower[63]. The thiazolidine ligation product was demonstrated to be stable at a pH range of 3-9 in a dendrimer synthesis study[62].

The thiazolidine ring formation has been exploited in different fields, from the synthesis of antibody–drug conjugates, to protecting group for N-terminal cysteines, and for developing cyclic peptides[65]. Overall, the rapid reaction rate, the stable product formed also in aqueous solvents and the catalyst free ligation makes thiazolidine a highly attractive type of click reaction.

1.4.2 Oxime

The condensation reaction between an alkoxyamine with a carbonyl moiety to form an oxime has been known since the end of the 19th century[66,67].

As shown in Figure 1.7, the conjugation if fully reversible and starts with a proton-catalyzed attack of the α-nucleophile to the carbonyl atom. The tetrahedral intermediate obtained upon proton transfer undergoes dehydration and determines the formation of a protonate intermediate and water.

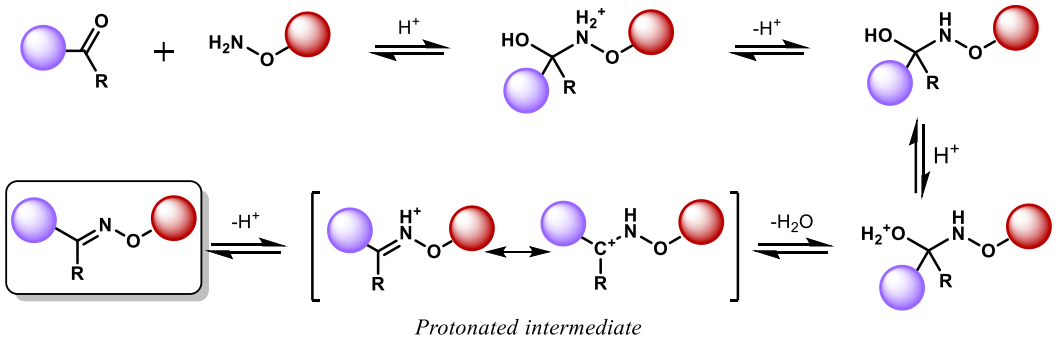

***Figure 1.7**: Mechanism of reaction for the oxime formation. R is an hydrogen in the case of aldehydes and a generic alkyl group in the case of ketones.*

The final deprotonation of double bonded resonance form of the dehydrated product determines the formation of the final product. Due to the catalytic role of the proton, the reaction is typically performed at acidic pH (Fig. 1.8)[68]:

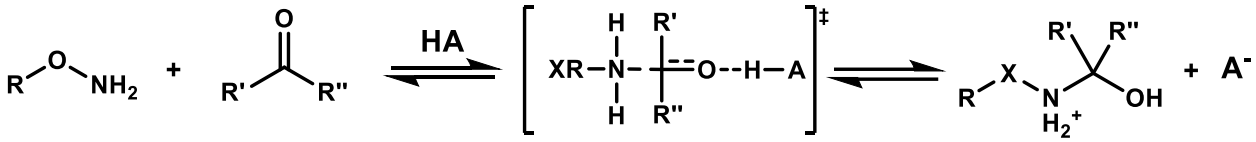

***Figure 1.8**: Proton-catalyzed attack of the α-nucleophile to the carbonyl atom. R is the linking group and R' and R'' are generic alkyl groups. The transition state proposed by Kolmel et al.[68] is also illustrated.*

At pH from 3 to 7 the dehydration of the tetrahedral intermediate is the rate determining step. But at pH lower than 3 the nitrogen atoms of the α-nucleophiles tend to be protonated. Thus, also the nucleophilicity is lower and the first nucleophilic attack becomes the rate determining step. Taken all this into account, a pH of 4.5 is typically ideal for the formation of oximes. The back reaction is initiated by a protonation of the imine nitrogen[68]. The bond was demonstrated to be stable at physiological pH, making the reaction suitable for the use in biological context[69]. In addition, the stability of the final product depends also on the carbonyl counterpart of the reaction. The higher the electrophilicity the more stable the ligation, that is why aromatic aldehydes are frequently used for this type of reaction[68].

This click reaction has been extensively applied in field that span from the decoration of nanoparticles to the synthesis of molecular switchers. The success of these ligations is attributable to the small size of the bond, which does not significantly interfere with the structure of the native biomolecule, and the reversibility of the conjugation, that can be exploited for the controlled release of biomolecules. Other reasons for the success include the low interference with biological processes and metabolites and the fact that the only byproduct is water[68]. In the context of polymer science the use of this type of reaction is fairly recent and involves the synthesis of step-growth polymers or hydrogels, as well as the functionalization of polymers and surface patterning[70].

1.4.3 Thiol-ene

The hydrothiolation of alkenes by thiol-ene reaction has been known since the beginning of the 19th century[71], and was extensively used for the production of polymer materials by photopolymerization of thiol-enes, but was upstaged by the low-cost acrylate based polymers[72]. However, in the last decades the interest in click reactions that take place in mild conditions without the need of a catalyst has grown, and so has the research around thiol-ene chemistry[73-75]. In addition, the versatility of this type of chemistry makes it applicable in a wide selection of applications such as protective polymers, cross-linked hydrogels, biomedical and bioconjugated molecules, or drug delivery systems[76].

Depending on the reaction conditions, the thiol-ene hydrothiolation can proceed by different pathways: radical pathway, base or nucleophilic mediated catalysis, solvent promoted process, but also *via* supramolecular catalysis using β-cyclodextrin[73].

The most used reaction mechanism involves the photochemical induction of the radical conditions, and proceeds by the typical chain process with initiation, propagation and termination steps.

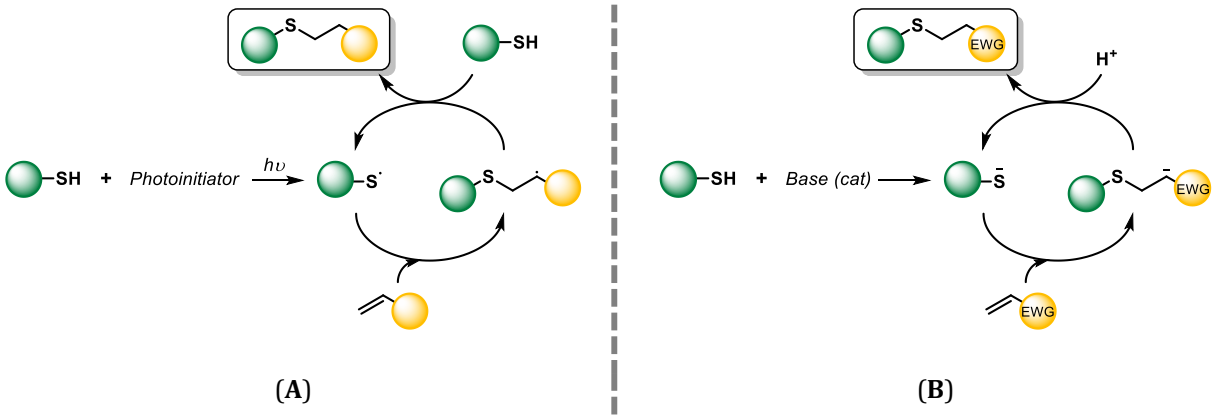

***Figure 1.9**: (**A**) Photoinitiated radical mechanism for the hydrothiolation of alkenes. (**B**) Base-catalyzes mechanism for the hydrothiolation of electron-deficient alkenes.*

The initiation involves the production of a thiyl radical by phototriggering a photoinitiator (Fig.1.9A). Propagation involves two steps: direct addition of the thiyl radical to the alkene, followed by chain transfer to a second molecule of thiol to give the thiol-ene addition product in anti-Markovnikov orientation and a new radical. Norbornenes are particularly reactive with this type of reaction not only for by being electron rich, but also due their bond angle distortion and associated loss of ring strain upon addition of a thiyl radical[73,75].

Electron deficient alkenes can react under mild base or nucleophilic catalysis without the need for the formation of a radical[73] (Fig 1.9B). Differently from traditional Michael reactions, in this case a weak base (i.e., NEt_3) is sufficient to catalyze the deprotonation of the thiol, which initiates the reaction cycle illustrated in Figure 1.10. Similar results are obtained when using primary/secondary amines or phosphines as nucleophilic catalysts[73].

Independently from the mechanism, the appeal of this reaction is due to its high yields and regioselectivity with fast reaction rates, while lacking interference by ambient oxygen or water[75].

1.4.4 Azide-alkyne (CuAAC)

Copper catalyzed azide-alkyne cycloaddition has been the most prevalent type of click chemistry in recent decades, due to its versatility, general ease of execution, quantitative yields, mild reaction conditions and orthogonality with other chemical processes [77,78].

The mechanism of action for the CuAAC has not yet been completely disclosed[79]. In particular, it is not yet known how the azide coordinates with the copper catalyst or whether the C-2 in the Cu_2-alkyne complex has a electrophilic or nucleophilic character. Additionally, the direction of the electron movement in the transition state of the reaction is unclear[78].

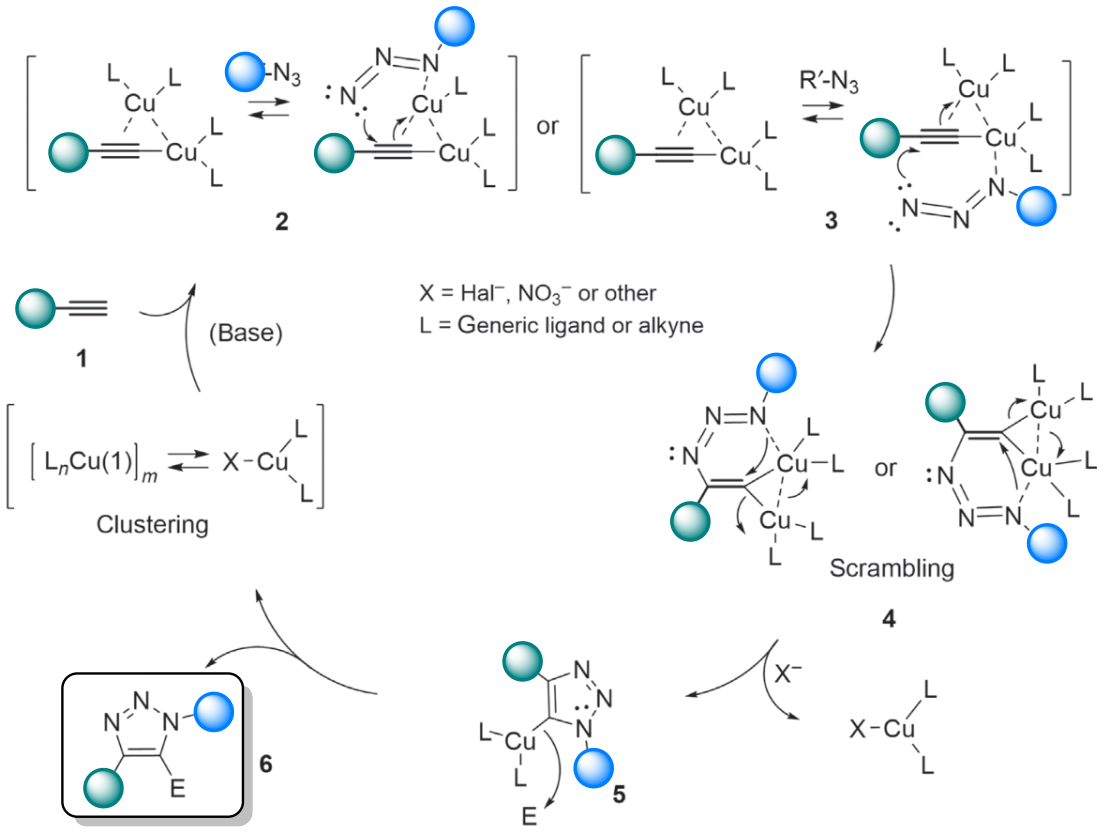

Figure 1.110*: Best representation of the current view on the reaction mechanism as illustrated by Meldal et al.[78]: the exact nature of the azide coordination has not yet been determined. A particularly important feature of the reaction mechanism is the exchange of copper with an electrophile at the end of the catalytic cycle. Figure reported with permission from Meldal et.al[78].*

The most recent rationalization on the reaction dinuclear catalytic mechanism was carefully elucidated by *Meldal et al.*[78] in 2020 (Fig 1.10). Briefly, the C-2 of the alkyne is assumed to be electrophilic and forms a complex with two clustered Cu(I) atoms. During the formation of the heterocycle, one catalytic Cu(I) atom is released, allowing the adduct to act as a soft-metal organic compound and end the cycle by exchanging the remaining copper with a large variety of electrophiles, including the hydrogen of the

unreacted alkynes[78]. Therefore, 1,4-disubstituted 1,2,3-triazoles are produced starting from organic azides and alkynes thanks to the copper catalyst[80].

A downside of this reaction is the production of reactive oxygen species (ROS) that threaten the integrity of any biological material (proteins, peptides, DNA, lipids, sugars) but also polymers present during the reaction. ROS are produced from the Cu(I)-catalyzed disruption of oxygen or oxygen peroxide that could be generated by the reduction of oxygen by ascorbate or the reducing agent used to create Cu(I) *in situ* from Cu(II) [78]. However, the use of a THPTA ligand in a 5eq excess with respect to copper, beside accelerating the reaction[81,82], was demonstrated to mitigate this effect by acting as a sacrificial reductant for the interception of ROS generated during CuAAC[78,83]. Finally, the toxicity of copper to humans is a factor to be taken in consideration when using this type of chemistry, and thus the amount of copper traces left in the final product must be carefully controlled[84].

References

1 Canchy, L., Kerob, D., Demessant, A. L. & Amici, J. M. Wound healing and microbiome, an unexpected relationship. *Journal of the European Academy of Dermatology and Venereology* **37**, 7-15 (2023).

2 Gardikiotis, I., Cojocaru, F.-D., Mihai, C.-T., Balan, V. & Dodi, G. Borrowing the features of biopolymers for emerging wound healing dressings: a review. *International Journal of Molecular Sciences* **23**, 8778 (2022).

3 Sanchez, A. & Vazquez, A. Bioactive Peptides: A Review. *Food Quality and safety* **1**, 29-46 (2017).

4 Zhang, L. & Falla, T. J. Cosmeceuticals and peptides. *Clinics in dermatology* **27**, 485-494 (2009).

5 Castelletto, V., Hamley, I. W., Perez, J., Abezgauz, L. & Danino, D. Fibrillar superstructure from extended nanotapes formed by a collagen-stimulating peptide. *Chemical Communications* **46**, 9185-9187 (2010).

6 Proksch, E., Brandner, J. M. & Jensen, J. M. The skin: an indispensable barrier. *Experimental dermatology* **17**, 1063-1072 (2008).

7 De-Luna-Gallardo, D., Mena-Garza, A. A. & Ettinger, R. E. in *Plastic and Reconstructive Surgery Fundamentals: A Case-Based and Comprehensive Review* 3-12 (Springer, 2024).

8 Yadav, N., Parveen, S., Chakravarty, S. & Banerjee, M. in *Skin Aging & Cancer: Ambient UV-R Exposure* 1-10 (Springer, 2019).

9 Kolarsick, P. A., Kolarsick, M. A. & Goodwin, C. Anatomy and physiology of the skin. *Journal of the Dermatology Nurses' Association* **3**, 203-213 (2011).

10 Lodhi, S. & Vadnere, G. P. Relevance and perspectives of experimental wound models in wound healing research. *Asian Journal of Pharmaceutical and Clinical Research* **10**, 57 (2017).

11 Velnar, T., Bailey, T. & Smrkolj, V. The wound healing process: an overview of the cellular and molecular mechanisms. *Journal of international medical research* **37**, 1528-1542 (2009).

12 Cioce, A., Cavani, A., Cattani, C. & Scopelliti, F. Role of the skin immune system in wound healing. *Cells* **13**, 624 (2024).

13 McCarty, S. *et al.* in *Biofilms in Infection Prevention and Control* 339-358 (Elsevier, 2014).

14 Scalise, A. *et al.* in *Seminars in vascular surgery.* 151-159 (Elsevier).

15 Zulkowski, K. Skin bacteria: implications for wound care. *Advances in skin & wound care* **26**, 231-236 (2013).

16 Park, H.-S. *et al.* Early pathogenic colonisers of acute burn wounds: a retrospective review. *Burns* **43**, 1757-1765 (2017).

17 Roy, S. *et al.* Microbial infections in burn patients. *Acute and Critical Care* **39**, 214 (2024).

18 De Oliveira, D. M. *et al.* Antimicrobial resistance in ESKAPE pathogens. *Clinical microbiology reviews* **33**, 10.1128/cmr. 00181-00119 (2020).

19 Kaya, S. & Derman, S. Properties of ideal wound dressing. *Journal of Faculty of Pharmacy of Ankara University* **47**, 1119-1131 (2023).

20 Barbari, S. & Asayesh, A. Effect of surface layer design on the physical properties of weft-knitted spacer fabrics for wound dressing applications. *The Journal of The Textile Institute*, 1-13 (2025).

21 Farahani, M. & Shafiee, A. Wound healing: from passive to smart dressings. *Advanced Healthcare Materials* **10**, 2100477 (2021).

22 Dong, R. & Guo, B. Smart wound dressings for wound healing. *Nano Today* **41**, 101290 (2021).

23 Portela, R., Leal, C. R., Almeida, P. L. & Sobral, R. G. Bacterial cellulose: a versatile biopolymer for wound dressing applications. *Microbial biotechnology* **12**, 586-610 (2019).

24 Ahmed, S. & Ikram, S. Chitosan based scaffolds and their applications in wound healing. *Achievements in the life sciences* **10**, 27-37 (2016).

25 Patrulea, V., Ostafe, V., Borchard, G. & Jordan, O. Chitosan as a starting material for wound healing applications. *European Journal of Pharmaceutics and Biopharmaceutics* **97**, 417-426 (2015).

26 Graça, M. F., Miguel, S. P., Cabral, C. S. & Correia, I. J. Hyaluronic acid—Based wound dressings: A review. *Carbohydr. Polym* **241**, 10.1016 (2020).

27 Della Sala, F., Longobardo, G., Fabozzi, A., di Gennaro, M. & Borzacchiello, A. Hyaluronic acid-based wound dressing with antimicrobial properties for wound healing application. *Applied Sciences* **12**, 3091 (2022).

28 Barbu, A. *et al.* Current trends in advanced alginate-based wound dressings for chronic wounds. *Journal of personalized medicine* **11**, 890 (2021).

29 Aderibigbe, B. A. & Buyana, B. Alginate in wound dressings. *Pharmaceutics* **10**, 42 (2018).

30 Rosson, E. *et al.* Focus on therapeutic peptides and their delivery. *International Journal of Pharmaceutics*, 125555 (2025).

31 Muttenthaler, M., King, G. F., Adams, D. J. & Alewood, P. F. Trends in peptide drug discovery. *Nature reviews Drug discovery* **20**, 309-325 (2021).

32 Lau, J. L. & Dunn, M. K. Therapeutic peptides: Historical perspectives, current development trends, and future directions. *Bioorganic & medicinal chemistry* **26**, 2700-2707 (2018).

33 Merrifield, R. B. Solid Phase Peptide Synthesis. I. The Synthesis of a Tetrapeptide. *Journal of the American Chemical Society* **85**, 2149-2154 (1963).

34 Amblard, M., Fehrentz, J., Martinez, J. & Subra, G. Methods and Protocols of Modern Solid Phase Peptide Synthesis. *Molecular Biotechnology* **33**, 239-254 (2006).

35 Fetse, J., Kandel, S., Mamani, U.-F. & Cheng, K. Recent advances in the development of therapeutic peptides. *Trends in pharmacological sciences* **44**, 425-441 (2023).

36 Slominsky, P. & Shadrina, M. Peptide pharmaceuticals: Opportunities, prospects, and limitations. *Molecular Genetics, Microbiology and Virology* **33**, 8-14 (2018).

37 Han, Y., Zhang, M., Lai, R. & Zhang, Z. Chemical modifications to increase the therapeutic potential of antimicrobial peptides. *Peptides* **146**, 170666 (2021).
38 Pollaro, L. & Heinis, C. Strategies to prolong the plasma residence time of peptide drugs. *MedChemComm* **1**, 319-324 (2010).
39 Jiang, H., Chen, W., Wang, J. & Zhang, R. Selective N-terminal modification of peptides and proteins: Recent progresses and applications. *Chinese Chemical Letters* **33**, 80-88 (2022).
40 Ding, Y. *et al.* Impact of non-proteinogenic amino acids in the discovery and development of peptide therapeutics. *Amino acids* **52**, 1207-1226 (2020).
41 Ji, X., Nielsen, A. L. & Heinis, C. Cyclic peptides for drug development. *Angewandte Chemie* **136**, e202308251 (2024).
42 Zorzi, A., Deyle, K. & Heinis, C. Cyclic peptide therapeutics: past, present and future. *Current opinion in chemical biology* **38**, 24-29 (2017).
43 Liu, C., Yang, Q. Q. & Zhou, Y. L. Peptides and Wound Healing: From Monomer to Combination. *International Journal of Peptide Research and Therapeutics* **30**, 46 (2024).
44 Pradhan, L., Nabzdyk, C., Andersen, N. D., LoGerfo, F. W. & Veves, A. Inflammation and neuropeptides: the connection in diabetic wound healing. *Expert reviews in molecular medicine* **11**, e2 (2009).
45 Schultz, G., Clark, W. & Rotatori, D. S. EGF and TGF-α in wound healing and repair. *Journal of cellular biochemistry* **45**, 346-352 (1991).
46 Namjoshi, S., Caccetta, R. & Benson, H. A. Skin peptides: biological activity and therapeutic opportunities. *Journal of pharmaceutical sciences* **97**, 2524-2542 (2008).
47 Dubos, R. J. Studies on a Bactericidal Agent Extracted from a Soil Bacillus: II. Protective Effect of the Bactericidal Agent Against Experimental Pneumococcus Infections in Mice. *The Journal of experimental medicine* **70**, 11-17 (1939).
48 Dubos, R. J. Studies on a Bactericidal Agent Extracted from a Soil Bacillus: I. Preparation of the Agent. Its Activity in Vitro. *The Journal of experimental medicine* **70**, 1-10 (1939).
49 Ageitos, J. M., Sanchez-Perez, A., Calo-Mata, P. & Villa, T. G. Antimicrobial Peptides (AMPs): Ancient Compounds that Represent Novel Weapons in the Fight Against Bacteria. *Biochemical Pharmacology* **133**, 117-138 (2017).
50 Büyükkiraz, M. E. & Kesmen, Z. Antimicrobial Peptides (AMPs): A Promising Class of Antimicrobial Compounds. *Journal of Applied Microbiology* **132**, 1573–1596 (2021).
51 Wang, J. *et al.* Antimicrobial Peptides: Promising Alternatives in the Post Feeding Antibiotic Era. *Medicinal research reviews* **39**, 831-859 (2019).
52 Costa, F., Carvalho, I. F., Montelaro, R. C., Gomes, P. & Martins, M. C. Covalent Immobilization of Antimicrobial Peptides (AMPs) onto Biomaterial Surfaces. *Acta Biomaterialia* **7**, 1431-1440 (2011).
53 Barbosa, M., Vale, N., Costa, F. M., Martins, M. C. L. & Gomes, P. Tethering antimicrobial peptides onto chitosan: Optimization of azide-alkyne "click" reaction conditions. *Carbohydrate polymers* **165**, 384-393 (2017).
54 Ciumac, D., Gong, H., Hu, H. & Lu, J. R. Membrane Targeting Cationic Antimicrobial Peptides. *Journal of Colloid and Interface Science* **537**, 163-185 (2019).
55 Yang, L., Harroun, T. A., Weiss, T. M., Ding, L. & Houang, H. W. Barrel-Stave Model or Toroidal Model? A Case Study on Melittin Pores. *Biophysical Juournal* **81**, 1475–1485 (2001).
56 Gazit, E., Miller, I. R., Biggin, P. C., Sansom, M. S. P. & Shai, Y. Structure and Orientation of the Mammalian Antibacterial Peptide Cecropin P1 within Phospholipid Membranes. *Journal of Molecular Biology* **258**, 860–870 (1996).
57 Cardoso, M. H. *et al.* Non-lytic antibacterial peptides that translocate through bacterial membranes to act on intracellular targets. *International journal of molecular sciences* **20**, 4877 (2019).
58 Kolb, H. C., Finn, M. & Sharpless, K. B. Click chemistry: diverse chemical function from a few good reactions. *Angewandte Chemie International Edition* **40**, 2004-2021 (2001).
59 Degirmenci, A., Yeter Bas, G., Sanyal, R. & Sanyal, A. "Clickable" Polymer Brush Interfaces: Tailoring Monovalent to Multivalent Ligand Display for Protein Immobilization and Sensing. *Bioconjugate Chemistry* **33**, 1672-1684 (2022).
60 Luu, T., Gristwood, K., Knight, J. C. & Jorg, M. Click chemistry: reaction rates and their suitability for biomedical applications. *Bioconjugate Chemistry* **35**, 715-731 (2024).
61 Liu, C.-F. & Tam, J. P. Chemical ligation approach to form a peptide bond between unprotected peptide segments. Concept and model study. *Journal of the American Chemical Society* **116**, 4149-4153 (1994).
62 Shao, J. & J.P., T. Unprotected Peptides as Building Blocks for the Synthesis of Peptide Dendrimers with Oxime, Hydrazone, and Thiazolidine Linkages. *Journal of American Chemical Society* **117**, 3893-3899 (1995).
63 Tam, J. P., Rao, C., Liu, C. F. & Sha, J. Specificity and formation of unusual amino acids of an amide ligation strategy for unprotected peptides. *International Journal of Peptide and Protein Research* **45**, 209-216 (1995).
64 Kent, S. B. H. Total Chemical Synthesis of Proteins. *Chemical Society Reviews* **38**, 338-351, doi:10.1039/B700141J (2009).
65 Bermejo-Velasco, D., Nawale, G. N., Oommen, O. P., Hilborn, J. & Varghese, O. P. Thiazolidine chemistry revisited: a fast, efficient and stable click-type reaction at physiological pH. *Chemical Communications* **54**, 12507-12510 (2018).
66 Fischer, E. Ueber die Hydrazone. *Ber. Dtsch. Chem. Ges.* **21**, 984–988 (1888).
67 Meyer, V. & Janny, A. Ueber Stickstoffhaltige Acetonderivate. *Ber. Dtsch. Chem. Ges.* **15**, 1164–1167 (1882).
68 Kolmel, D. K. & Kool, E. T. Oximes and Hydrazones in Bioconjugation: Mechanism and Catalysis. *Chemical Reviews* **117**, 10358-10376 (2017).
69 Kalia, J. & Raines, R. T. Hydrolytic stability of hydrazones and oximes. *Angewandte Chemie International Edition* **47**, 7523-7526 (2008).
70 Collins, J., Xiao, Z., Müllner, M. & Connal, L. A. The emergence of oxime click chemistry and its utility in polymer science. *Polymer Chemistry* **7**, 3812-3826 (2016).

71 Posner, T. Beiträge zur Kenntniss der ungesättigten Verbindungen. II. Ueber die Addition von Mercaptanen an ungesättigte Kohlenwasserstoffe. *Berichte der deutschen chemischen Gesellschaft* **38**, 646-657 (1905).
72 Hoyle, C. E., Lee, T. Y. & Roper, T. Thiol–enes: Chemistry of the past with promise for the future. *Journal of Polymer Science Part A: Polymer Chemistry* **42**, 5301-5338 (2004).
73 Lowe, A. B. Thiol-ene "click" reactions and recent applications in polymer and materials synthesis. *Polymer Chemistry* **1**, 17-36 (2010).
74 Lowe, A. B. Thiol–ene "click" reactions and recent applications in polymer and materials synthesis: a first update. *Polymer Chemistry* **5**, 4820-4870 (2014).
75 Hoyle, C. E. & Bowman, C. N. Thiol–ene click chemistry. *Angewandte Chemie International Edition* **49**, 1540-1573 (2010).
76 Machado, T. O., Sayer, C. & Araujo, P. H. Thiol-ene polymerisation: A promising technique to obtain novel biomaterials. *European Polymer Journal* **86**, 200-215 (2017).
77 Meldal, M. Polymer "clicking" by CuAAC reactions. *Macromolecular Rapid Communications* **29**, 1016-1051 (2008).
78 Meldal, M. & Diness, F. Recent fascinating aspects of the CuAAC click reaction. *Trends in Chemistry* **2**, 569-584 (2020).
79 Buckley, B. R. & Heaney, H. in *Click Triazoles* 1-29 (Springer, 2012).
80 Chassaing, S., Bénéteau, V. & Pale, P. When CuAAC'click chemistry'goes heterogeneous. *Catalysis Science & Technology* **6**, 923-957 (2016).
81 Chouhan, G. & James, K. CuAAC macrocyclization: high intramolecular selectivity through the use of copper–tris (triazole) ligand complexes. *Organic Letters* **13**, 2754-2757 (2011).
82 Chan, T. R., Hilgraf, R., Sharpless, K. B. & Fokin, V. V. Polytriazoles as copper (I)-stabilizing ligands in catalysis. *Organic letters* **6**, 2853-2855 (2004).
83 Hong, V., Presolski, S. I., Ma, C. & Finn, M. a. G. Analysis and optimization of copper-catalyzed azide–alkyne cycloaddition for bioconjugation. *Angewandte Chemie (International ed. in English)* **48**, 9879 (2009).
84 Ahmad Fuaad, A. A., Azmi, F., Skwarczynski, M. & Toth, I. Peptide conjugation via CuAAC 'click'chemistry. *Molecules* **18**, 13148-13174 (2013).

Chapter II:

Antibacterial Cotton for Wound Healing *via* Chemoselective Peptide Conjugation Strategies

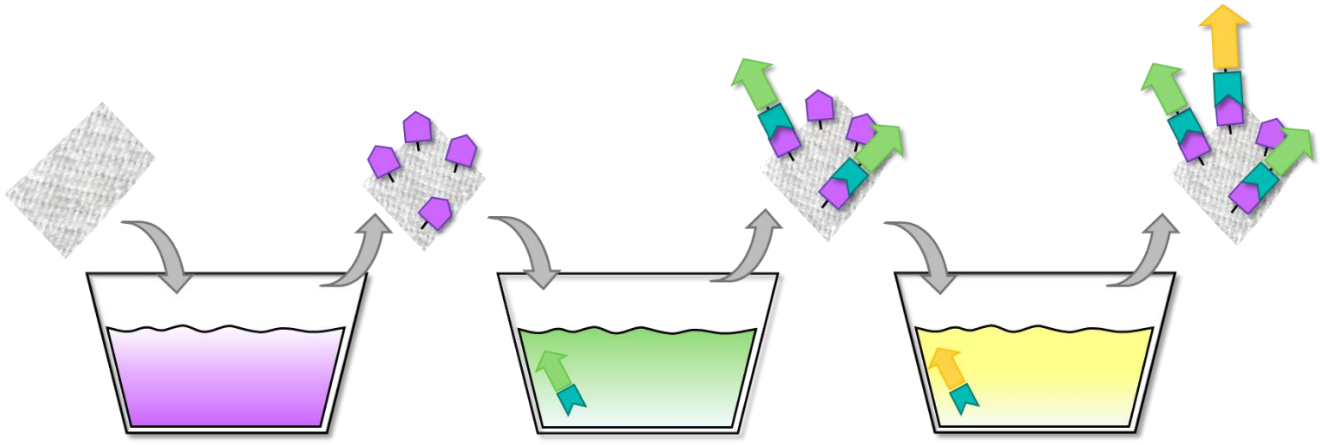

Acknowledgements:

- Dr. Adriana Di Stasi for the tests on the antibacterial activity of the peptides, and the biofilm growth assays on the cotton samples.
- Prof. Antonella Glisenti for the XPS measurements and data analysis.
- Dr. Renato Schiesari for some of the FT-IR measurements

2.1 Introduction

Cotton has several distinctive properties that make it widely used not only in the apparel industry but also for gauze, gowns, and other medical devices. However, a major drawback to the use of cotton is the microorganism growth promotion caused by its hydrophilicity[1]. This phenomenon not only promotes the transmission of bacteria[2], but can also be the cause of unpleasant odors, degradation of fabric color, allergic reactions when the fabric comes in contact with the skin, and deterioration of the fabric itself. Therefore, it would be important to find methods that can improve its properties for a safe use.

In this chapter, the covalent conjugation of peptides to a cotton fabric was explored as a method to improve the functionality of cotton in the context of wound patches. In particular, model peptides were used to finalize the reaction conditions to form thiazolidine and oxime bonds (*Chapter 1.4.1 and 1.4.2*). between peptides and cotton grafted with aldehydes. The antibacterial peptides PMAP(12-24) and Pal-HAaH, and the collagen-boosting peptide PP4 were used to give cotton multiple functionalities through the formation of consequent thiazolidine bonds. In addition, the thiol-norbornene (*Chapter 1.4.3*) conjugation was explored as an alternative chemoselective method for the functionalization of cotton with PMAP(12-24) to produce an antibacterial material.

2.1.1 Cotton

Cotton plants belong to the family *Malvaceae*, the tribe *Gossypieae*, and the genus *Gossypium*.[3] Of the thirty-three species currently recognized, only four have a real commercial value: *hirsutum, barbadense, arboreum,* and *herbaceum*. The first two originate from the USA and South America, respectively, and constitute over 90% of the world cotton production. The last two species are known as "Desi", come from Asia and Sub-Saharan Africa, and produce shorter and coarser fibers than the American ones[4].

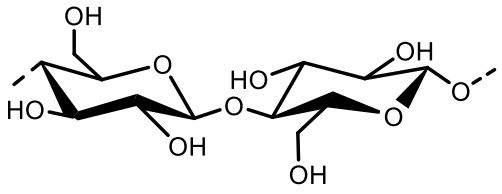

Cotton main component, cellulose, is a linear carbohydrate polymer made of β-D-glucopyranose (or glucose) molecules that are linked to one another by glycosidic bonds between C_4-OH of one molecule and the C_1-OH of an adjacent unit. Each glucose molecule is rotated 180° with respect to the previous, making the union of two glucose molecules (cellobiose) the repeating unit of the polymer[3]. Furthermore, cotton cellulose is the purest form of natural cellulose and has the highest molecular weight and structural order[5]. The presence of hydroxyl groups in the chain in abundance permits the creation of both intra- and inter-molecular hydrogen bonds. The former give rigidity and strength to the chain, whereas the latter are needed to form higher ordered aggregates[3,6]. Specifically, thirty-six cellulosic chains compose an elementary fibril, which in turn is arranged to form

microfibrils, which in turn aggregate into microfibril bundles, whose union forms the cellulose fiber[3,7]. A cotton fiber is the dried cell walls of an elongated (to >2.5 cm in *hirsutum*), thickened and formerly living cell. It derives from the epidermis of the cottonseed and constitutes the seed hairs (trichomes) [3,8]. Overall, a mature cotton fiber is composed of 88.0–96.5% cellulose, 1.0–1.9% proteins, 0.4–1.2% waxes, 0.4–1.2% pectins, 0.7–1.6% inorganics and 0.5-8.0% other substances[3]. The variations in the percentage of the components arises from differences in the fiber maturity, variety of cotton and environmental growth conditions.[4] After harvesting, ginning, mechanical cleaning and spinning, cotton is approximately composed of 95% of cellulose. Then after scouring, bleaching and mercerization, the final obtained textile has a cellulose content of over 99%[3,4].

The reactions that are most commonly performed on the internal hydroxyls of cellulose are substitution (esterification or etherification), deoxyhalogentation (to C-Cl, C-Br or acetylation) and oxidation. These chemical modifications do not affect drastically the physical-chemical properties of cellulose and make cellulose more reactive towards possible functionalization agents.[5]

Aldehyde grafting on cotton

Among the reported methods[9-13] periodate oxidation is one of the most widely used for the oxidation of polysaccharides hydroxyls[14]. This oxidation takes place at the C_2-OH and C_3-OH positions and leads to ring scission, altering the structure of the polysaccharide chain. Furthermore, *Scapin et al.*[15] demonstrated that periodate oxidation on yarn cotton fabrics alters the mechanical proper ties of the fiber itself, resulting in a damaged material.

On the other hand, the (2,2,6,6-tetramethylpiperidin-1-yl)oxyil radical (TEMPO) was proven to be highly effective in the conversion of primary alcohols to aldehydes of high molecular weight polysaccharides and ensured high reaction rates, yields, selectivity and modest degradation of the polysaccharide[16]. The most common molecules used for the catalyst regeneration are NaBr/NaClO or NaClO/$NaOCl_2$. Both imply the use of halogenated-based reagents that rise concerns about environmental and safety issues[17,18]. Therefore, the use of laccase for the regeneration of TEMPO is of particular interest[19-22]. The ability of laccase to regenerate TEMPO was first investigated by Vikari *et al.*[19], the mechanism of action is not yet fully disclosed but the major part was illustrated by Tromp *et al.*[20] (Fig. 2.1), and Aracri *et al.*[9] were the first to use the TEMPO/laccase/O_2 system on cellulose fibers.

TEMPO (Fig. 2.1C and D) binds chemoselectively to the C_6 primary alcohol of cellulose and oxidize it to aldehyde or carboxyl moiety[20]. Aracri *et al.* demonstrated that the higher the TEMPO percentile and the reaction time, the higher is the aldehyde content[21,23]. The radical form of TEMPO is regenerated by a comproportionation reaction with TEMPO+ (Fig. 2.1E). At the end, laccase regenerates TEMPO+ by reduction (Fig. 2.1B)[18,20]. In particular, the catalytic site of the laccase is composed of four copper atoms in three redox sites (T1, T2 and T3). The oxidation of the substrate takes places at T1, whereas the T2

copper and T3 copper couple are 12 Å away from T1 and responsible for the simultaneous reduction of molecular oxygen to water. In the native laccase when all copper centers are in the +1-oxidation state, the enzyme is in the fully reduced state. The interaction with O_2 determines the oxidation of one T3 and T2 copper. Then, the O_2 bond is reduced, all the copper atoms are oxidized, resulting in the production of two molecules of water[24]. Therefore, the oxygen present in the air causes the laccase to be in its oxidized state (Fig. 2.1A). It was speculated that step-E could be catalyzed by laccase, but there is yet no evidence of this. In the case of cellulose, the rate limiting step was demonstrated to be cellulose oxidation (Fig. 2.1D) with an ideal pH of 4-5[18].

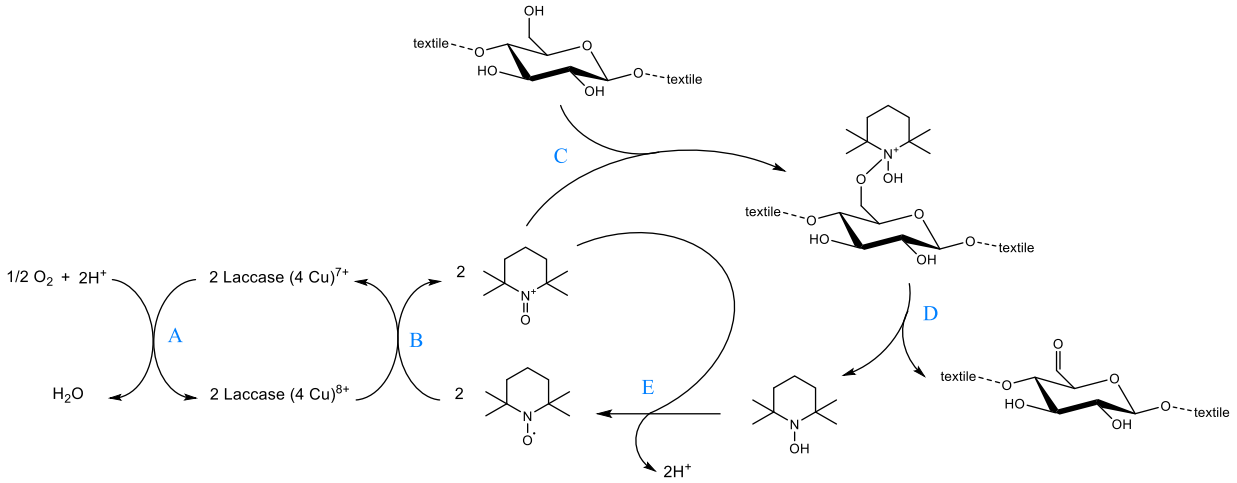

***Figure 2.1**: Mechanism* of the *TEMPO/laccase/O_2 redox system. Copper charges conform to the reaction stoichiometry but do not represent the real laccase oxidation state. (**A**) O_2 reduction (**B**) Regeneration of reduced Laccase (**C**) TEMPO chemoselective linkage to the C_6 primary alcohol of cellulose (**D**) Cellulose oxidation (**E**) Compropornation of TEMPO[20]*

It is important to notice that the oxoammonium salts could deactivate the enzyme by oxidation of the amino acid alcohols[25]. The enzyme stability could be improved by immobilization, for example by cross-linking.[26] Overall, the TEMPO/laccase/O_2 system is a more ecological and efficient process than $NaIO_4$: (**1**) it does take place at a pH near neutrality and not in an alkali media, thus the β-elimination is disfavored[21], (**2**) it happens at room temperature and in ca. 20 hours [21], (**3**) the only byproduct is water, and (**4**) it does not involve halogenated reagents. In conclusion, using this system the primary alcohols of cellulose are selectively oxidized to aldehydes under mild reaction conditions without altering structural integrity of the polysaccharide[9,19,20,27].

Norbornene grafting on cotton

Thiol–norbornene reactions have been extensively studied for biomaterial functionalization in recent years, and specifically norbornene grafting on cellulose has been studied by several authors[28-32]. However, to this author knowledge norbornene grafting has not yet been tested directly on cotton textiles, even though *Bao et al.*[33] used the thiol-ene reaction to link photochromic compounds to cotton fabric by introducing the thiol groups on cotton with a 3-mercaptopropyltriethoxysilane treatment.

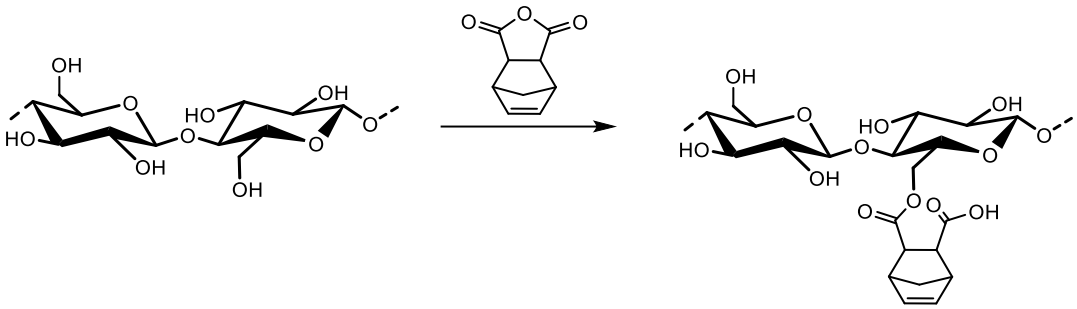

***Figure 2.2**: Norbornene grafting on cellulose by reaction with 5-norbornene-2,3dicarboxylic anhydride (carbic anhydride).*

The most common method to introduce norbornene is via an esterification reaction between the available hydroxyl groups of cellulose and of 5-norbornene-2,3-dicarboxylic anhydride (carbic anhydride, Fig. 2.2)[29,32]. *Dadoo et al.*[29,32] performed the reaction on cellulose nanofibrils, using alkaline water as the solvent. In fact, in order to minimize the unwanted hydrolysis of anhydride, the ideal pH range for the reaction was of 9.5-10.5. A 20-fold molar excess (with respect to the repeating unit) of carbic anhydride was used due to its low solubility in water and its tendency to hydrolyze in the acidic environment created by the free carboxylic acid formed in the esterification. Interestingly, in a recent report of *Long et al*.[28] the authors managed to reduce the amount of carbic anhydride needed to functionalize cellulose nanofibrils to an 8-fold excess by using a mixed solvent of DMSO:H_2O (40:6) and KOH in a concentration of 0.015M. In addition, *Long et al*.[28] obtained a degree of substitution around 1.6 mmol/g of norbornene, which is only slightly lower what could be obtained using the best conditions in *Dadoo et al.*[29,32] (10% substitution of the hydroxyls, 1.9 mmol/g).

2.1.2 The Peptides

For our studies the ideal peptide to be used as the active agent on cotton should (**1**) have an intrinsic activity useful in the treatment of wounds, (**2**) be soluble in the solvent used for the conjugation, (**3**) have a short sequence, and (**4**) have high resistance towards proteases. Therefore, three peptides were selected in this chapter: the shortened analogue of the porcine myeloid antimicrobial peptide PMAP(12-24), the ultrashort antibacterial lipopeptide Pal-HAaH, and the collagen-boosting peptide PP4.

PMAP(12-24)

Up to date, three porcine myeloid antimicrobial peptides have been discovered: PMAP-23, -36 and -37 [34-37]. Out of these three host-defense antimicrobial peptides, PMAP-36 is of particular interest due to its moderate cytotoxicity and broad spectrum of activity that includes Gram-positive and Gram-negative bacteria, but also some Candida strains [38-40], and its additional immunomodulatory effects[41,42].

PMAP-36 is a 36 amino acid, highly cationic cathelicidin. The 23 cationic residues are collocated in the N-terminal region, the peptide is organized in an amphipathic α-helix structure interrupted by two Pro in positions 25 and 26. The additional longitudinal amphipathicity of this peptide is determined by the

presence of a more loosely structured hydrophobic C-terminal tail. Finally, its Cys_{35} residue allows the formation of dimers, through an intermolecular disulfide bridge (Fig. 2.3)[40,42].

The mechanism of action of PMAP-36 is membranolytic and both PMAP-36 and its dimer PMAP-36(1-35)$_2$ are able to permeabilize the inner and outer membrane of *E. coli* in a dose dependent manner [40].

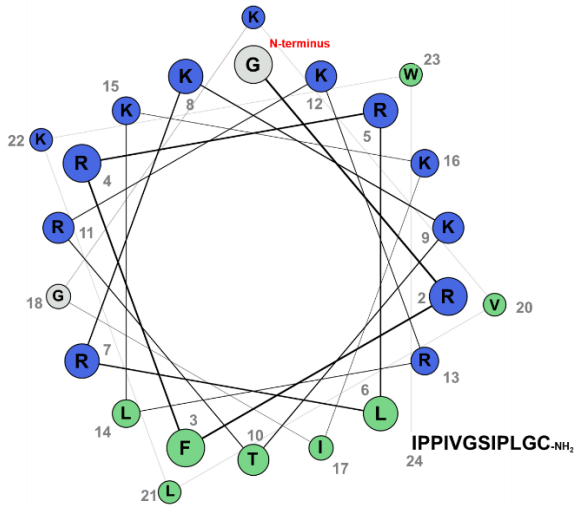

***Figure 2.3**: Helical wheel projection of PMAP-36. Cationic residues are in blue, hydrophobic residues in green. The projection concerns residues until Ile$_{24}$, all further residues are schematically shown as a linear tail.*

The main disadvantage of this peptide is its selectivity with respect to human cells. In fact, PMAP-36 and its dimer PMAP-36(1-35)$_2$ showed moderate cytotoxicity to human erythrocytes, with a 10–30% hemoglobin release at concentrations comparable to their MIC values[40].

Series of shortened analogues allowed to investigate the parts of the peptide sequence that are essential for the activity, and at the same time search for residues with a decreased cytotoxicity[38,39,42-44] (Table 2.1). These studies revealed that :

1) Dimerization favors helix formation, and does not greatly affect the antibacterial potency or the cytotoxicity *in vitro*, however the monomer shows a less efficient immunomodulatory effect, especially when some of the N-terminus amino acids are truncated [40,42].
2) Deletion of the first 11 amino acids to form peptide PMAP-36(12-36) does not strongly affect helicity, activity against *E. coli* or cytotoxicity, whereas a further deletion of 4 more amino acids of the fragment PMAP-36(16-36) results in a decreased cytotoxicity but also a complete loss of activity[42].
3) The hydrophobicity of the fragment $L_{21}K_{22}W_{23}I_{24}$ is essential for the activity. In fact, even though the fragment that comprises only the cationic and amphipathic α-helix, PMAP-36(1-20), did not result cytotoxic against human erythrocytes, it loses in antimicrobial potency; whereas the fragment containing also the $L_{21}K_{22}W_{23}I_{24}$ amino acids, PMAP-36(1-24), retains an antibacterial activity comparable to PMAP-36 and its lower hemolytic activity demonstrates an increased selectivity towards prokaryotic cells.

4) Interestingly, when W_{23} of PMAP-36(1-24) was substituted with the hydrophobic Leu, the antimicrobial properties were maintained, but in the case of Lys or Ala substitution, the resulting peptide had a complete or partial loss in activity, respectively [40,44].

Peptide	Sequence	Ref
PMAP-36	GRFRRLRKKTRKRLKKIGKVLKWIPPIVGSIPLGCG-NH_2	-
PMAP(1-35)$_2$	(GRFRRLRKKTRKRLKKIGKVLKWIPPIVGSIPLGC-NH_2)$_2$	40
N-terminus truncations		
PMAP-36(12-36)	KRLKKIGKVLKWIPPIVGSIPLGCG-NH_2	42
PMAP-36(16-36)	KIGKVLKWIPPIVGSIPLGCG-NH_2	
C-terminus truncations		
PMAP-36(1-20)	GRFRRLRKKTRKRLKKIGKV-NH_2	40
PMAP-36(1-24)	GRFRRLRKKTRKRLKKIGKVLKWI-NH_2	44
PMAP-36[L_{23}](1-24)	GRFRRLRKKTRKRLKKIGKVLK**L**I-NH_2	
PMAP-36[K_{23}](1-24)	GRFRRLRKKTRKRLKKIGKVLK**K**I-NH_2	
PMAP-36[A_{23}](1-24)	GRFRRLRKKTRKRLKKIGKVLK**A**I-NH_2	
N- and C-terminus truncations		
PMAP-36(7-24)	RKKTRKRLKKIGKVLKWI-NH_2	39
PMAP-36(10-24)	TRKRLKKIGKVLKWI-NH_2	
PMAP-36(13-24)	RLKKIGKVLKWI-NH_2	39,44
PMAP-36(12-31)	KRLKKIGKVLKWIPPIVGSI-NH_2	43
PMAP-36[$A_{25}K_{26}$](12-31)	KRLKKIGKVLKWI**AK**IVGSI-NH_2	
PMAP-36(12-24)	KRLKKIGKVLKWI-NH_2	
PMAP-36(12-24) ***allD***	krlkkigkvlkwi-NH_2	45,46
PMAP-36[U_{21}](12-24)	KRLKKIGKV**U**KWI-NH_2	43

Table 2.1: *Sequences of the reported PMAP-36 shortened analogues. D-amino acids in lower case.*

These results, suggesting that the central part of PMAP-36 is the pharmacophore, were confirmed by the works of *Biondi et al.*[43] and *Lyu et. al.*[39], where shorter PMAP-36 analogues truncated both at the N- and C-terminal end were studied. In particular, *Lyu et al.* demonstrated that PMAP-36(7-24) had an activity comparable to the parent peptide against the tested bacteria (different strains of *E. coli* and *S. aureus*, *S. epidermidis*, *B. subtilis*), but also had an improved activity against *C. albicans* and showed a lower cytotoxicity to human erythrocytes, with only 5% hemolysis at 128 μM, where PMAP-36 had the same level of hemoglobin release at 4 μM. Furthermore, even though the shorter PMAP-36(10-24) and PMAP-36(13-24) did not resulted hemolytic at all the tested concentrations (up to 128 μM), they lost in potency against *S. aureus* having a MBC of 128 μM, that is much lower than the 4 μM of the parent peptide, and did not gain in activity against *C. albicans*. The authors argued that a charge of +6 is the threshold for driving peptides to the bacteria membrane via electrostatic interactions, and the higher the charge the higher the antibacterial activity, thus this is probably the reason of the loss in activity of the shorted

peptides that have lower charge [39]. On the other hand, *Biondi et al*. demonstrated, by a viability assay on HaCaT cell line and a hemolysis test on human erythrocytes, that the shortened analogue PMAP-36(12-31) is not cytotoxic and is active at concentrations lower than 4 μM against all the tested bacteria (*E. coli*, *A. baumannii*, *K. pneumoniae*, *P. aeruginosa*, *S. epidermidis*) except for *S. aureus*. The prolongation of the α-helix of PMAP-36(12-31) by substitution of Pro_{25} and Pro_{26} with Ala and Lys, respectively, resulted in a broadened spectrum of action that includes also *S.aureus*. However, the modified peptide lost a little in potency against *P. aeruginosa* and *K. pneumoniae* (MIC 8 and 16 μM, respectively) and lost also in selectivity, resulting cytotoxic both in the viability and hemolysis assays[43].

In addition, PMAP-36(12-24) and its analogue where Lys_{21} was substituted with the non-proteogenic amino acid Aib were studied by *Biondi et al*.[43] (Table 2.2*).* Interestingly, both peptides did not present the pure α-helix secondary structure typical of the parent peptide, but were arranged in a 3_{10}-helix in membrane mimetic environments and displayed a disordered structure in water. Also, they both maintained the broad activity of PMAP-36(12-31) with MIC lower than 8 μM for all the tested bacteria strains (except for *S. aureus*). Even though the Aib modified analogue was more resistant to degradation by chymotrypsin and did not show any hemolysis, it resulted cytotoxic to HaCaT cells. Instead, PMAP-36(12-24) did not result cytotoxic in any of the performed assays[43]. Furthermore, the low resistance to proteases of PMAP-36(12-24) was overcome by the use of D-amino acids. In fact, the D-enantiomer was not cytotoxic, showed a slightly improved antimicrobial activity, and was not degraded by trypsin or in the presence of human serum (Table 2.2)[45,46].

		PMAP-36(12-24)	**PMAP-36[U_{21}](12-24)**	**PMAP-36(12-24) *allD***
MIC (μM)	*E. coli ATCC 25922*	4	4	2
	A.baumannii ATCC 19606	2	2	2
	K. pneumoniae ATCC 700603	4	8	4
	P. aeruginosa ATCC 27853	8	8	4
	S. aureus ATCC 25923	>64	>64	16
	S. epidermidis ATCC 12228	4	8	4

***Table 2.2**: Reported minimal inhibitory concentrations of PMAP-36(12-24) analogues[43,45].*

C_{16}-HAaH

The ultrashort lipopeptides with the general sequence of C_n-XYyX-NH_2 were first described by *Makovitzki et al*.[47]. They are of particular interest due to their short peptide chain and broad activity against Gram-positive and Gram-negative bacteria as well as a variety of fungi.

More specifically, they are composed of four amino acids, two cationic and two lipophilic, and an aliphatic chain linked at the N-terminus of the peptide chain; in each peptide, one of the residue is

replaced with its D-enantiomer (lower case) to confer a better resistance against enzymatic degradation. Interestingly, the activity and selectivity of these peptides were found to depend not only on the amino acid chain but also on the length of the aliphatic moiety (Table 2.3). For example, C_{16}-KA*a*K is active against all the tested strains of bacteria and fungi at low MICs, whereas C_{14}-KA*a*K is active, with MICs below 25μM, only against *S. aureus, A. flavus and C. neoformans*, and C_{12}-KA*a*K is not active against any of the tested strains. Furthermore, C_{16}-KL*l*K is active, with MIC below 12μM, against the tested fungi strains but shows much higher MICs for bacteria, and loses its activity when linked to shorter aliphatic chains. Also, where C_{16}-KA*a*K showed low hemolysis (3% at 50 μM), C_{16}-KL*l*K was much more cytotoxic (50% at 50 μM). Despite the short length of these peptides, their mechanism of action was found to involve the permeation and disintegration of the membrane, similarly to that of many classical AMPs[47]. From this set of analogues C_{16}-KA*a*K resulted the most promising in terms of broad activity, high potency and low cytotoxicity.

		C_{12}-KL*l*K	**C_{14}-KL*l*K**	**C_{16}-KL*L*K**	**C_{12}-KA*a*K**	**C_{14}-KAaK**	**C_{16}-KAaK**
MIC (μM)	*E. coli D21*	50	25	100	>100	50	6.25
	E. coli ATCC 25922	50	25	100	100	50	6.25
	P. aeruginosa ATCC 27853	25	12.5	100	>100	50	12.5
	A. baumannii ATCC 19606	>100	>100	50	>100	100	12.5
	S. aureus ATCC 6538P	12.5	3.12	3.12	100	12.5	6.25
	A. fumigatus ATCC 26430	25	6.25	6.25	>100	25	6.25
	A. flavus ATCC 9643	100	12.5	12.5	>100	100	100
	C. albicans ATCC 10231	12.5	6.25	6.25	>100	50	12.5
	C. neoformans ATCC MYA-422	3	2.3	1.5	50	6.25	3
	Hemolysis, % at 50μM	0	50	45	0	0	3

Table 2.3*: Reported minimal inhibitory concentrations and hemolysis of ultrashort lipopeptides reported in Makovitzki et al.*[47] *D-amino acids are in lower case.*

Further investigations demonstrated that C_{16}-KA*a*K is also active against some plant fungi and pathogens: *P. syringae, A. tumefaciens* and *A. alternata, B. cinerea, C. heterostrophus* [48], but also that it is more efficient than the current commercial drug (amphotericin B deoxycholate) in the treatment of *A. fumigatus* in mice[49].

Cotton grafted with C_{16}-KAaK and some analogues where Lys was substituted with the other positively charged amino acids Arg and His was studied by *Orlandin et al*.[50] In this work cotton was used as the solid support for the growth of the peptide chain by attaching a NH_2-CH_2-CH_2-NH- linker to cotton. Surprisingly, the C_{16}-KAaK grafted on cotton was found inactive against the tested bacterial species (*E.*

coli and *S. aureus*), whereas its analogue C_{16}-HAaH-$NH_2(CH_2)_2NH$-cotton was active against both these species[50,51].

Pentapeptide-4

The discovery of the collagen-boosting properties of the peptide sequence Lys-Thr-Thr-Lys-Ser (also known as Pentapeptide-4 or PP4) started with a paper from *Aycock et al.*[52] where the inhibitory activity against type I procollagen and fibronectin of the C-terminal 22 amino acids of the COOH-propeptide of human α2(I) procollagen were found.

This result was followed by a more extensive study on the complete COOH-propeptide of the α2(I) procollagen sequence by the synthesis of a series of overlapping 16-45 residue peptides and testing their biological activity. Surprisingly, three of the tested peptides stimulated, rather than inhibited the production of extracellular matrix (ECM) proteins such as type I and III procollagen and fibronectin in subconfluent human lung fibroblasts in a dose- and time-dependent manner[53].

Later, in a study from *Katayama et al.*[54] done in 1993, the longest of those three fragments (residues 197-241) was selected to individuate the minimum sequence able to increase ECM production by synthesizing a series of subfragments of its sequence. By retaining 80% of the original activity, the sequence Lys-Thr-Thr-Lys-Ser (fragment 212-216) was the shortest to stimulate ECM biosynthesis, even though it needed higher concentrations to exert the same effect of its longer counterparts. Further shortening of KTTKS dramatically reduced its stimulatory activity, both when truncated at the N-terminus or at the C-terminus. Interestingly, the addition of an inactive sequence (fragment 205-211, GKTVEY) to the sequence of KTTKS resulted in a peptide that was slightly more active than KTTKS**,** suggesting that the inactive sequence either stabilizes the pentapeptide or facilitates its uptake[54].

The mechanism of action of KTTKS is yet to be fully clarified, but it was reported to promote the expression of type I collagen and maintain its mRNA stability by being involved in the upregulation of the transforming growth factor-β (TGF-β)[55,56].

The palmitoylated analogue of KTTKS (Pal-KTTKS) is commercially known as Matrixyl®[57] and is widely used as a cosmetic[55]. The addition of a C_{16} moiety at the N-terminus is an optimization for its use in topical care, in particular the addition of a palmitoyl moiety should enhance the chance of the hydrophilic peptide to pass across the epidermal barrier[55,58]. The first report of this improved activity was reported in 2002 with a short communication by *Lintner et al.*[58], where the authors claimed that Pal-KTTKS not only permeates in the skin without passing the dermis, but is also able to stimulate the production of ECM proteins including collagen I and elastin in *vitro*, *ex vivo* and *in vivo*. However, no data were shown to support their claims. Subsequential studies by *Jones et al.*[59] on human corneal and dermal fibroblasts (HCF and HDF) showed that Pal-KTTKS had some inhibitory effects on cell proliferation but, similarly to its parent peptide, was effective in stimulating collagen production.

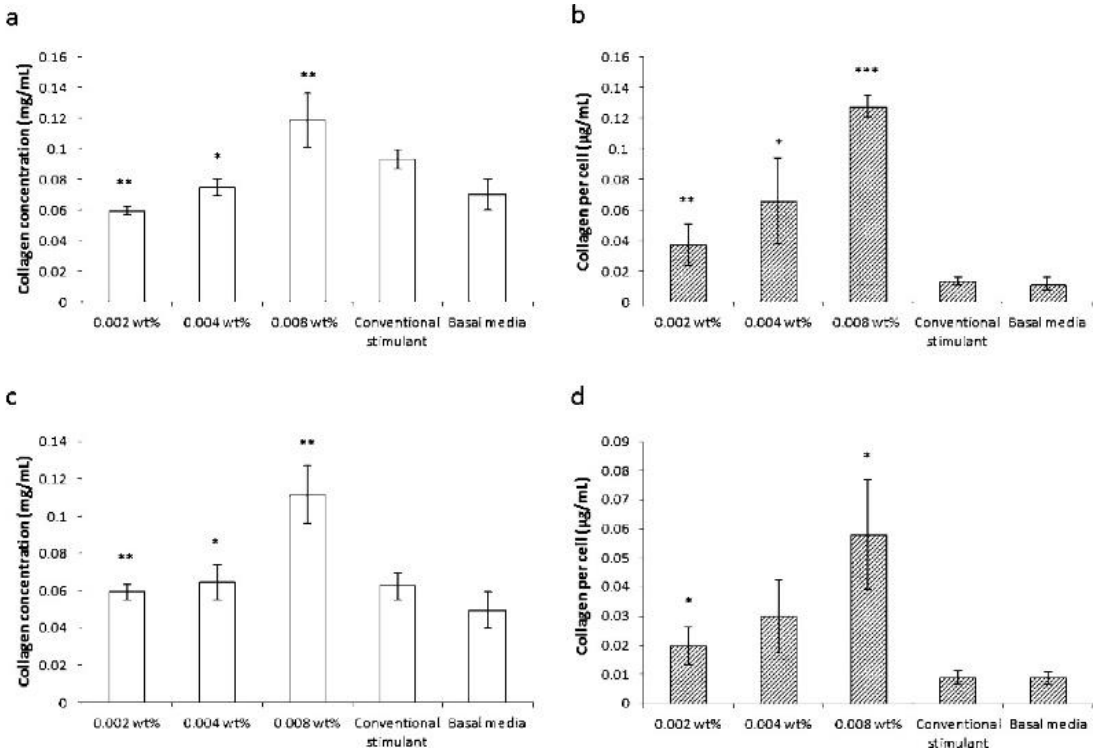

Figure 2.4: *Stimulation of collagen by Pal–KTTKS from Jones et al.[59] in (**a,b**) human corneal and (**c,d**) human dermal fibroblasts. Figures **a** and **c** report the total amount of collagen deposited. Figure **b** and **d** report the amount of collagen mediated by the number of cells (n =3; *P ≤ 0.005, **P ≤ 0.01, and ***P ≤ 0.001). Reported with permission from Jones et al.[59]*

In particular (Fig. 2.4), Pal-KTTKS was tested in concentrations from 0.002% to 0.008% and demonstrated a concentration-dependent effect with amounts of produced collagen per cell significantly higher than the positive control. Furthermore, *Castelletto et al.[60]* speculated that the tendency of Pal-KTTKS to form macroscopic fibrillar structures could be related to its collagen boosting action, in fact the palmitoyl-driven aggregates could act as a suitable scaffold for collagen deposition[59,60]. On the other hand, in a paper from *Choi et al*.[61] from 2014, Pal-KTTKS was also demonstrated to be more stable than KTTKS in skin extracts and homogenate, and able to penetrate stratum corneum, the epidermis, and the dermis of mice models.

Even though the efficacy of Pal-KTTKS as an anti-wrinkle agent has been clearly established by several clinical studies[55,62,63], lately there has been a growing interest in the use of KTTKS as an active agent in the treatment of wounds[64,65]. In particular, Pal-KTTKS was demonstrated to have a role in accelerating wound closure, but also to have pro-fibrotic abilities, and thus create scar tissue, in a dose-dependent manner. Therefore, it is also important to notice that the therapeutic dose for wound healing, especially when Pal-KTTKS is administered directly to the dermis, should be taken in careful consideration[65].

2.2 Results and Discussion

Cotton has several properties that makes it an optimal material for bandages and wound patches. The implementation of a sustainable reaction to merge the properties of a cotton fabric with the biological activity of peptides into a single material would be quite significant. To ensure that the functionalized fabric maintains the acquired properties over time, an efficient method of conjugation is the use of a covalent bond. In this context, we explored the use of three different chemoselective ligation reactions to bind peptides to a cotton fabric: thiazolidine[15] and oxime bonds, and thiol-ene click chemistry (*Chapter 1.4*).

Thus, the work on cotton functionalization was divided into three subprojects:

(1) Model peptides to study thiazolidine and oxime reaction conditions[66].
(2) Multiple functionalization of cotton by thiazolidine bond.
(3) Development of a PMAP(12-24)-cotton conjugate by thiol-norbornene click chemistry.

2.2.1 Peptide Choice

Three types of peptides were used in this work: model peptides to study the thiazolidine and oxime bond reaction conditions, antibacterial peptides, and collagen regenerative peptides to confer additional properties to cotton (Table 2.5).

The amino acid chains of the model peptides **1a** and **1b** were designed to contain the minimal number of amino acids needed to (1) bind the peptide to CHO-cotton, (2) monitor the cotton-conjugation reactions, and (3) confirm the presence of the peptide on the material. Therefore, for the thiazolidine and oxime reactions, an aldehyde-selective reactive group (Cys or Aox, respectively) was inserted at the peptides' N-terminus. Trp is the aromatic amino acid with the highest extinction coefficient ($\varepsilon_{Trp\text{-}280nm}$ in H_2O = 5630 $M^{-1}cm^{-1}$)[67]. Therefore, Trp was used to provide the peptides with a chromophore to follow the reaction and quantify the peptide on cotton by UV–Vis. Additionally, a free amine (Lys side chain) was added to further confirm the presence of the peptide on cotton by a *Kaiser test*[68].

Peptide	Short name	Sequence	Purity	MW (g/mol)
Model Peptides				
1a	CGWK	H-CGWK-NH_2	95.3%	491.61
1b	AxGWK	H-A_xGWK-NH_2	74.5%	461.24
Antibacterial Peptides				
2a	CysPMAP(12-24)	H-CKRLKKIGKVLKWI-NH_2	92.1%	1712.27
2b	PMAP(12-24)cys	H-KRLKKIGKVLKWIC-NH_2	93.4%	1712.27
2c	AoxPMAP(12-24)	H-A_xKRLKKIGKVLKWI-NH_2	96.0%	1682.19

3a	Pal-HAaH	C_{16}-HAaH-NH_2	92.3%	671.89
3b	-	C_{16}-K(WC)-HAaH-NH_2	98.5%	1089.42
3c	-	C_{16}-HAaH-K(WC)-NH_2	98.7%	1089.42
Collagen Regenerative Peptides				
4a	PP4	H-KTTKS-OH	94.9%	563.65
4b	PP4-NH_2	H-KTTKS-NH_2	96.4%	562.67
4c	Pal-PP4	Pal-KTTKS-NH_2	97.1%	801.08
4d	CW-PP4	H-CWKTTKS-NH_2	89.6%	852.02
4e	-	H-CWK(Pal)KTTKS-NH_2	85.8%	1218.60
4f	-	H-CWKTTKSK(Pal)-NH_2	86.7%	1218.60

***Table 2.5**: List of the synthesized peptides. The D-amino acids are in lower-case. A_x is aminooxyacetic acid. Details about the synthesis and HPLC-MS characterization are in Section 2.4.2 in Chapter 5.2.1, respectively.*

The antibacterial peptides used in this study are divided in two sets: the analogues of PMAP(12-24) (**2a** to **2c**) and the analogues of Pal-HAaH (**3a** to **3c**). The studies performed in our group[43,46] highlighted PMAP(12-24) as an interesting candidate to confer antibacterial properties to cotton. In fact, the peptide (1) has a broad spectrum antibacterial properties and low cytotoxicity, (2) has a membranolytic mechanism of action that helps in avoiding resistance development of bacteria, and (3) its D-enantiomer was demonstrated to be also resistant to human proteases[46], allowing for the production of a material with durable antibacterial properties. In addition, its high solubility in water is useful for the thiazolidine or oxime reactions whose ideal solvent is slightly acidic water. Therefore, to provide the peptide with the β-amino thiol or thiol needed for the thiazolidine or thiol-ene reactions, an additional Cys was introduced at the N-terminus or C-terminus of PMAP(12-24) sequence to form peptide **2a** and **2b**, respectively. Similarly, to allow the oxime bond, an aminooxyacetic acid (Aox) is present at the N-terminus of peptide **2c**. A downside of PMAP(12-24) is the length of its amino acidic sequence (13 aa) that makes the synthesis of higher amounts of peptide more difficult, and its inactivity against *S.aureus*. Therefore, as an alternative the short sequence of peptide Pal-HAaH (**3a**) was tested for the thiazolidine bond. Since the N-terminus of peptide **3a** is occupied by the palmitoyl chain, the additional Trp and Cys were introduced at the side chain of an additional lysine.

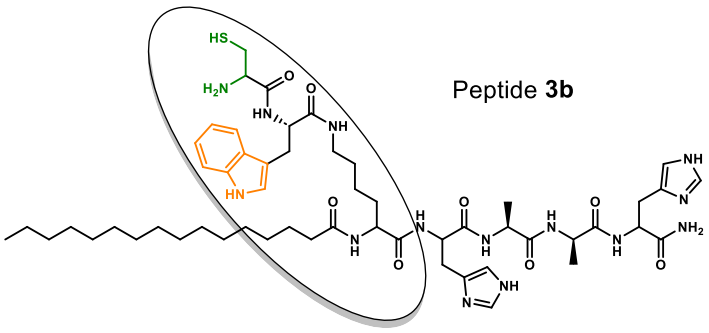

***Figure 2.5**: Chemical structure of peptide **3b**. Highlighted is the "conjugation arm" made of Lys(Trp-Cys). In orange is the chromophore and in green the β-amino thiol.*

This was possible by the use of Dde-Lys(Fmoc)-OH and Fmoc-Cys(Boc)-OH for the synthesis: the Fmoc protecting group of Lys was removed by standard protocol (20% piperidine in DMF), then Trp and Cys were attached to Lys side chain, and the deprotection of the Dde protecting group was performed with a strategy that is orthogonal to both Fmoc and Boc removal (2% hydrazine in DMF). Peptides **3b** and **3c** differ only in the position of the "conjugation arm" made of Lys(Trp-Cys).

The sequence of the pentapeptide PP4 was selected to equip cotton with an additional functionality useful in the treatment of wounds. In fact, PP4 has shown promising collagen-boosting properties. Peptide **4d** was synthesized with an additional Cys and Trp at the N-terminal end to allow the thiazolidine bond and follow the reaction by UV-Vis, respectively. Since its palmitated analogue (**4c**, Pal-KTTKS-NH_2) is being studied as the active agent in the treatment of wounds[64,65], we tested different positions for the palmitoyl chain by introducing it at the side chain of an additional Lys in peptides **4e** and **4f**.

All peptides were synthesized in high purity by solid phase peptide synthesis using the Fmoc/Boc strategy. Peptide **1b** presented an impurity attributable to the formation of conjugates with residual traces of acetone (Fig. S2.1, *Chapter 5.2.1*). Thus, to avoid this issue in the cleavage solution of peptide **2c** Aox was added as a scavenger for acetone[69]. The cleavage from the resin was performed by acidic treatment with trifluoroacetic acid (TFA). In this way also the side chain protecting groups of the amino acids could be removed simultaneously. The peptides were recovered by precipitation and washed in cold diethyl ether. When necessary, medium pressure flash chromatography was performed to further purify the peptides (*Section 2.4.2*). All synthesized peptides were characterized by HPLC-MS (*Chapter 5.2.1*).

Biological Activity

The **cytotoxicity** of peptides **3a, 3b** and **4a** to **4f** was studied at the University of Trieste on mouse fibroblast 3T3 cells.

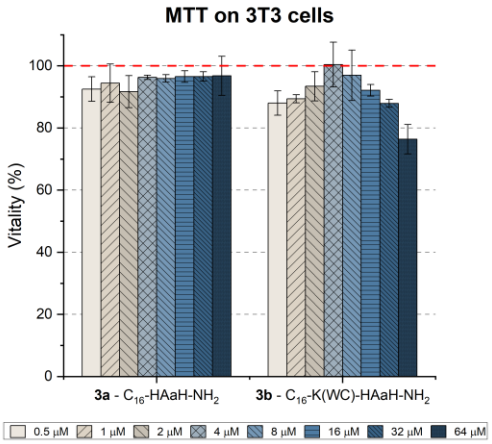

Figure 2.6: *Cytotoxicity to 3T3 cells of the Pal- HAaH analogues **3a** and* **3b**.

Peptides **3a**, **4a**, **4b**, **4c**, and **4d** did not result cytotoxic against 3T3 cells at none of the tested concentrations. On the other hand, the "conjugation arm" of peptide **4b** made it slightly cytotoxic at the highest concentration (64 μM), and the PP4 analogues with additional palmitated Lys (**4e** and **4f**) demonstrated cytotoxicity at the highest concentrations. In particular, it seems that the palmitoyl chain at the C-terminus of peptide **4f** determined highest cytotoxicity against 3T3 cells. In fact, at 64 μM all the cells in contact with **4f** were not viable any more, whereas the ones in contact with **4e** expressed a vitality of around 40%.

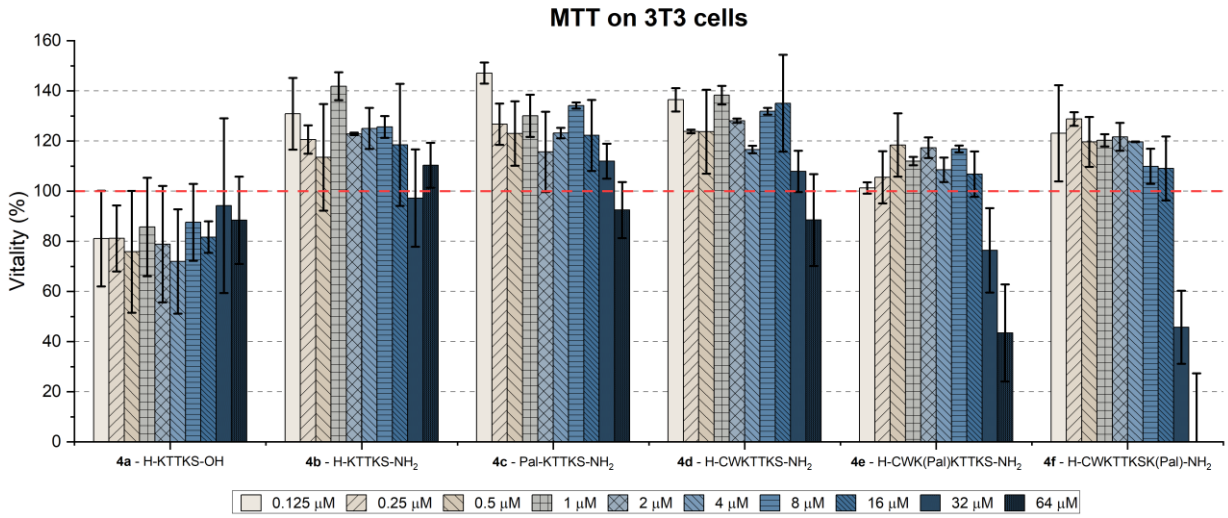

Figure 2.7: *Cytotoxicity to 3TT cells of PP4 analogues, peptides **4a** to **4f**.*

To evaluate whether peptide **3b** maintained the same **antibacterial activity** of peptide **3a** against *S. aureus*, their minimal inhibitory concentration (MIC) was evaluated at the University of Trieste. Unexpectedly, neither of them resulted active up to 64 μM. This results are in contradiction with the activity against *S.aureus* of cotton bound to Pal-HAaH reported by *Orlandin et al.*[50]. However, they are coherent with a recent report of our group about Pal-HAaH analogues with non-coded amino acids where the peptide was found active only against *S. enterica*[70].

2.2.2 Project 1: Model Peptides for Oxime and Thiazolidine Chemoselective Ligation Reactions

During the author's master thesis[71], peptides **1a** and **1b** were used to test the conditions for the thiazolidine and oxime conjugations of peptides with cotton, quantify the amount of peptide linked to cotton, and evaluate the stability of the ligation in different media. To complete the study, the peptides were used to test unmodified cotton as negative control for the reactions to ensure that the peptides were covalently bound to the cellulose matrix by thiazolidine or oxime ligations and not just absorbed into the fiber.

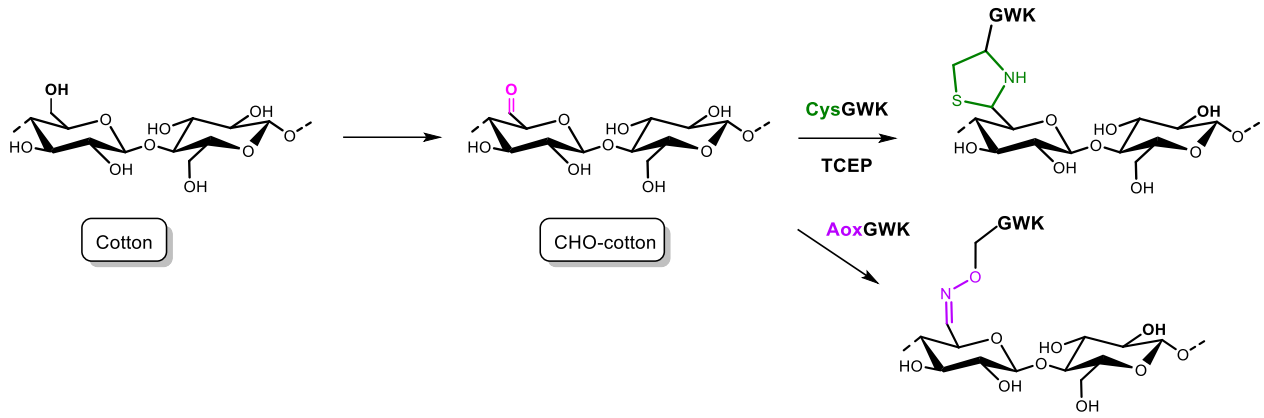

***Figure 2.8**: Schematic representation of the thiazolidine and oxime reactions between model peptides and CHO-cotton.*

For the reaction to take place a weighted piece of cotton or aldehyde functionalized cotton (CHO-cotton, *Section 2.2.3*) was dipped into the same solution of the chosen peptide (in 50 mM acetate buffer at pH 4.5) that was split into two reaction vessels (**r1**-**r2** and **r3**-**r4**). In the case of peptide **1a**, 1 eq (with respect to the peptide) of tris(2-carboxyethyl)phosphine (TCEP) was also added to avoid the formation of dimers. Unfortunately, the amount of CHO-cotton of this batch was not enough for a quantification of the aldehydes by titration (see *Section 2.2.3*), therefore amount and concentration of peptide that were used were the ones that gave the better results in previous studies[66]. The reaction was monitored by UV-Vis following the absorbance of Trp (at 280 nm) in solution.

	Sample	Cotton mass (mg)	Peptide exc* ($mmol/g_{cot}$)	Peptide conc (mM)	Reaction time	Peptide loading ($mmol/g_{cot}$)
r1	Cotton + **1a**	9.0	0.80	0.72	1day	0.01
r2	CHO-Cotton + **1a**	10.5	0.69	0.72	1day	0.08
r3	Cotton + **1b**	10.0	0.76	0.77	1day	0.004
r4	CHO-Cotton + **1b**	10.1	0.77	0.77	1day	0.09

***Table 2.6**: Reaction conditions for the conjugation of peptides **1a** and **1b**. *exc = excess.*

As the reaction proceeds, cotton "captures" some of the peptide and the concentration of peptide in solution and the absorbance of Trp decrease (Fig. 2.9A and B). The reactions were considered complete when there was no further decrease in Trp absorbance, indicating that the cotton had reached saturation

(Fig. 2.9A and B). The amount of bound peptide was calculated by assuming that all the peptide that left the solution was on cotton. In fact, the difference between the final and initial absorbance at 280 nm allows the determination of the moles of peptide bound to cotton. The peptide loading was calculated as the ratio between the mmol of bound peptide and grams of cotton used for the reaction (Table 2.6). The absorbance of both peptide solutions did not decrease significantly over time when unoxidized cotton was present. In contrast, the behavior in the presence of CHO-cotton was similar to previous experiments[66,71]. The Kaiser test confirmed the presence of the free amine of the peptides only on the materials produced by CHO-cotton (Fig. 2.9C and D).

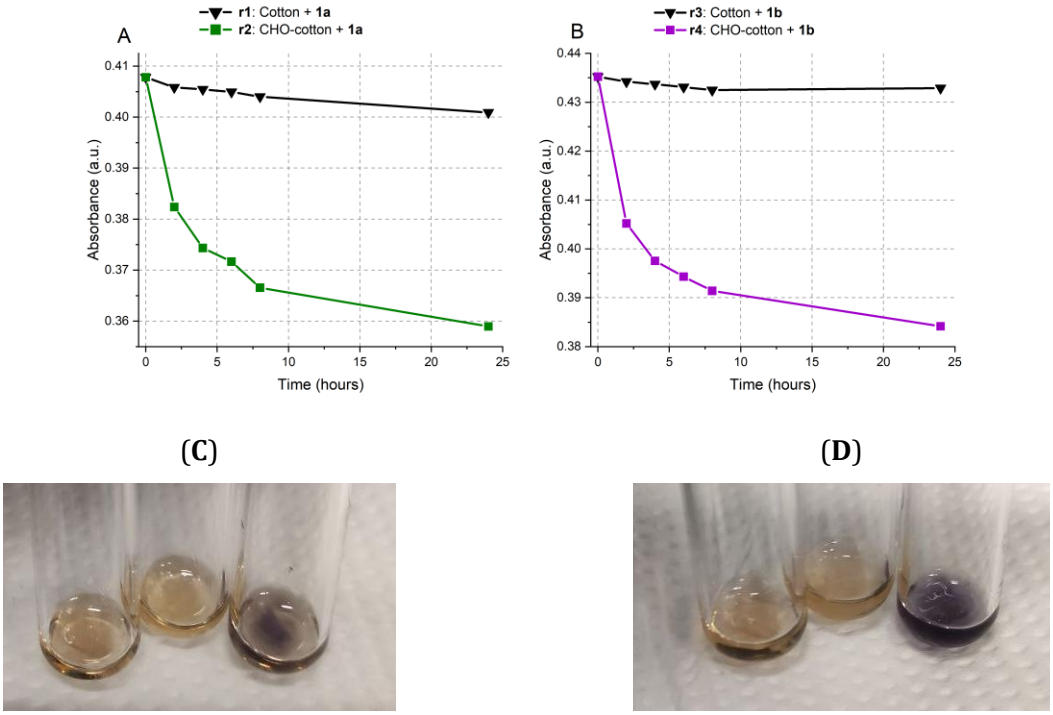

Figure 2.9: Absorbance at 280nm over time of (**A**) peptide **1a**/TCEP solution in reaction **r1-2** (**B**) peptide **1b** solution in reaction **r3-4.** In black is shown the absorbance of the peptide solution in the presence of unmodified cotton, in green or purple in the presence of CHO-cotton. (**C**) From left to right Kaiser test on CHO-cotton, **r1** and **r2**. (**D**) From left to right Kaiser test on CHO-cotton **r3** and **r4**.

To conclude, the peptide loading obtained with **1a** and **1b** was similar: around 0.1 mmol/g with CHO-cotton and at least 10 times lower with unmodified cotton, confirming that the peptides were successfully covalently conjugated on CHO-cotton when performing a thiazolidine ring (peptide **1a**) or an oxime bond (peptide **1b**), and the low amount of unmodified cotton is assumed to be only adsorbed in the cotton matrix.

2.2.3 Project 2: Multiple Cotton Functionalization by Thiazolidine bond

One disadvantage of cotton is its low solubility in most common solvents that forces most reactions to be heterogeneous. However in this project we took advantage of this property to develop an easy and step-by-step method for the multiple functionalization of cotton.

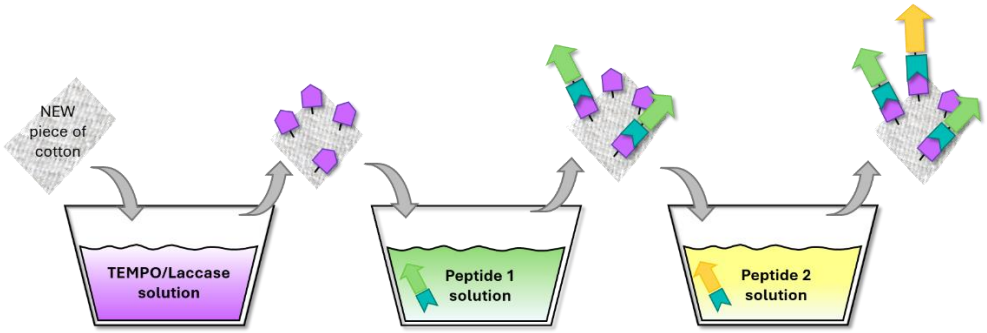

In fact, an aldehyde was introduced on cotton using the TEMPO/laccase/O_2 system described in *Section 2.1.1*. Then, the piece of CHO-cotton could be easily removed from the oxidizing solution, washed and put in the peptide solution to form the thiazolidine or the oxime bond. The peptide loading was monitored by the absorbance of the peptide in solution, and can be tuned by changing the reaction time. After that, the piece of cotton functionalized with the first peptide could be easily removed from the solution, washed and put in another peptide solution to equip cotton with a second functionality. Specifically, PMAP(12-24) sequence was used to give cotton the primary antibacterial functionality, and PP4 or Pal-HAaH sequences were used with the idea of equipping cotton with either an additional collagen boosting activity or with an amplified antibacterial activity against *S. aureus*, respectively.

Aldehyde grafting on cotton

The TEMPO/laccase/O_2 catalyzed system was employed to introduce the aldehyde directly on cotton as a milder oxidation method, largely selective for C_6-OH position [9,66]. Indeed, in this reaction, the primary alcohols of cellulose are selectively oxidized to aldehydes under mild reaction conditions without altering structural integrity of the polysaccharide. In addition, the possible re-use of the oxidizing reaction makes the reaction particularly attractive[66].

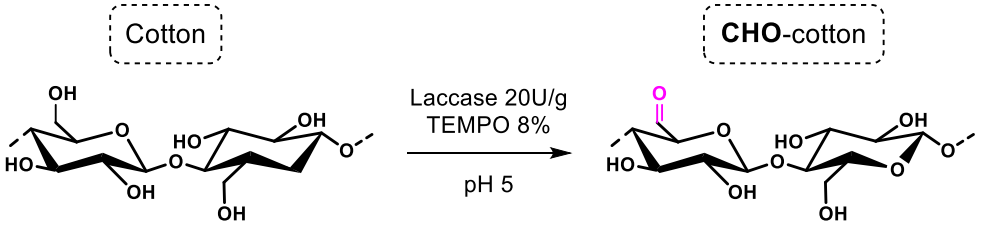

***Figure 2.10**: Schematic representation of the oxidation reaction of cotton to introduce aldehydes.*

The reaction took place in an aqueous NaOAc/AcOH buffer at a pH 5. In order to maximize the aldehyde content, the reaction conditions were those suggested by *Aracri et al.*[9] of 20U of laccase per gram of

material, 8%$_{wt}$ TEMPO and 24h as reaction time. Differently from *Aracri et al.*[9], we did not apply any oxygen pressure to the solution. The success of the reaction was indicated by the change in color upon the Schiff reagent addition: CHO-cotton became pink already after 4h of reaction, whereas the unreacted cotton remains white (Fig. 2.11).

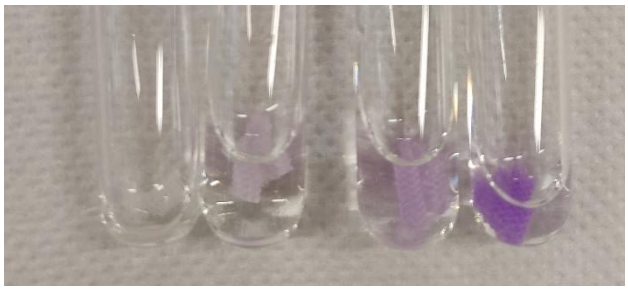

Figure 2.11*: Schiff test on cotton (left) and CHO-cotton after 4h, 8h and 24h (from the second on the left to the right) of reaction with TEMPO/laccase.*

The amount of aldehydes on cotton was quantified by adapting a titration procedure described by *Saito et al.*[72].In particular, the aldehydes were converted into carboxyl groups by a treatment in $NaClO_2$ for 48h, and quantified by an alkaline titration. The difference between the amount of carboxyl groups in the samples that were treated with $NaClO_2$ and those that were not treated was assumed to be the amount of aldehydes (Table 2.7).

Sample	Amount of COOH (mmol/g)	Amount of CHO* (mmol/g)
Cotton	0.025 ± 0.001	0 ± 0.0015
Cotton treated with $NaClO_2$	0.025 ± 0.0005	-
CHO-cotton	0.048 ± 0.003	0.075 ± 0.013
CHO-cotton treated with $NaClO_2$	0.123 ± 0.010	-

Table 2.7*: results of the titration of the carboxyl groups on the materials using with 0.01 M NaOH as the titrant. *calculated as the difference between the carboxyl groups in the samples treated with $NaClO_2$ and the untreated samples. These results are the average of three different titrations on three pieces of cotton from the same batch (Section 2.4.3).*

As expected, no aldehydes were found on unmodified cotton. The amount of aldehydes introduced in CHO-cotton of 0.075 ± 0.013 mmol/g is coherent with the 0.083 mmol/g reported by *Aracri et al.*[9] for cellulose using the same conditions. On the contrary, the amount of added carboxyls in CHO-cotton (0.023 ± 0.004 mmol/g) is much lower than the 0.137 mmol/g found by *Aracri et al.*[9], indicating that the primary product in the absence of external oxygen pressure is the aldehyde.

Peptide-Cotton conjugation reactions – Preliminary

To evaluate the best reaction conditions, the thiazolidine bond with the active peptides **2a**, **2c**, **3b** and **4d** was preliminary tested with small samples of cotton (50-100 mg). The first peptide tested for the conjugation with CHO-cotton was the sequence of the antibacterial PMAP(12-24). Therefore, reaction conditions similar to those used for peptides **1a** and **1b** were employed with peptides **2a** and **2c** (Table 2.8), and unmodified cotton was used as negative control (**r5** and **r7**). The absorbance of the peptide

solution was monitored at 280 nm and the reaction was stopped when the absorbance value reached a plateau (Fig. S2.11A and B, *Chapter 5.2.2*).

	Sample	Cotton mass (mg)	Peptide exc (μmol/g_{cot})	Peptide conc (mM)	Reaction time	Peptide loading (μmol/g_{cot})
r5	Cotton + **2a**	101.8	50.0	0.68	3 days	3.0
r6	CHO-Cotton + **2a**	112.7	45.1	0.68	3 days	7.1
r7	Cotton + **2c**	99.6	50.8	0.67	3 days	4.2
r8	CHO-Cotton + **2c**	102.6	49.3	0.67	3 days	11.4

Table 2.8*: Reaction conditions for the preliminary conjugation of peptides **2a** and **2c**. Moles of peptide bound to the material calculated by the difference in the peptide solution concentration after the reaction and before cotton was added to the solution. *exc = excess.*

Interestingly, the reaction time required for conjugating peptides **2a** and **2c** was longer than that observed in **r1**-**r4** for the model peptides. However, since the CHO-cotton batch was different, a direct comparison cannot be made. The much lower peptide loading values (compared to those of the model peptides) could be attributed to the much greater steric hindrance of PMAP(12-24). The amount of peptide adsorbed to unmodified cotton was comparable to the absolute value of model peptides results, but it results more impactful when compared to the amount of peptide that was actually covalently bound. As expected, the peptide loading of the thiazolidine (**r6**) and oxime bond (**r8**) was similar (Table 2.8).

For simplicity, the other peptide sequences (Pal-HAaH and PP4) were tested only for the thiazolidine bond, using the same rection conditions of peptide **2a**. Since peptide **3c** was not soluble in the NaOAc/AcOH buffer (pH 4.5) needed for the thiazolidine bond, its reaction was not tested.

	Sample	Cotton mass (mg)	Peptide exc (μmol/g_{cot})	Peptide conc (mM)	Reaction time	Peptide loading (μmol/g_{cot})
r9	Cotton + **3b**	60.5	61.7	0.83	3 days	14.8
r10	CHO-Cotton + **3b**	60.1	62.1	0.83	3 days	18.6
r11	Cotton + **4d**	105.6	132.2	0.69	3 days	10.4
r12	CHO-Cotton + **4d**	106.3	131.3	0.69	3 days	38.0

Table 2.9*: Reaction conditions for the preliminary thiazolidine conjugation of peptides **3b** and **4d**. Moles of peptide bound to the material calculated by the difference in the peptide solution concentration after the reaction and before cotton was added to the solution. *exc = excess.*

As shown in Table 2.9, the peptide loading is higher when the peptides are less sterically hindered. The loading of peptide **3b** on unmodified cotton (**r11**) was only slightly lower than the peptide found on CHO-cotton (**r10**), and higher than the amount of **1a** or **2a** adsorbed on cotton (r1 and r5). However, the difference between the two amounts is similar to that of peptide **2a** on CHO-cotton (**r6**), suggesting that the thiazolidine reaction between **3b** and CHO-cotton was successful, and that the "conjugation arm" of peptide **3b** and **3c** can be used to bind peptides *via* a thiazolidine bond.

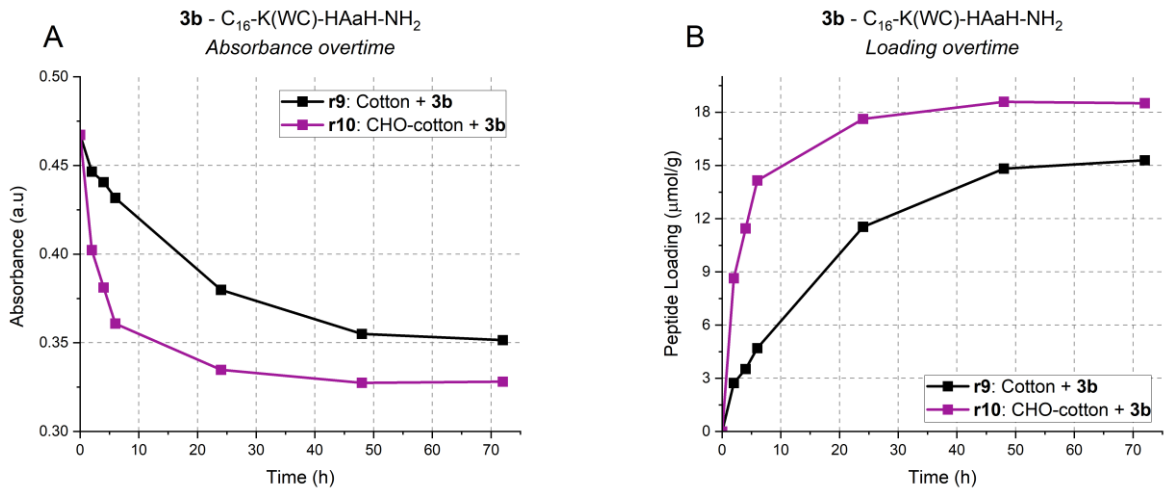

***Figure 2.12**: Reported as an example (**A**) Absorbance of the peptide **3b**/TCEP solution upon the addition of cotton (**r9**), or CHO-cotton (**r10**) (**B**) Peptide loading over time of reactions **r9**, and **r10**. The data of the other reactions is reported in Chapter 5.2.2.*

On the other hand, **4d** loading on CHO-cotton was drastically higher than on unmodified cotton, confirming the success of the reaction and that more than half of the aldehyde sites were occupied by the peptide.

It is important to notice that for the larger peptides **2a**, **2c** and **3b**, the amount of solution needed to reach a concentration around 1mM (used in the tests and with the model peptides) was just sufficient to cover the piece of cotton. Therefore in the following section, a lower peptide concentration was used to allow for a better stirring. In addition, considering the low peptide loading obtained especially with peptide **2a** and **3b**, in the next part of the study a lower excess of peptide was used to minimize the costs of the synthesis by lowering the amount of peptide lost.

Double peptide functionalization on cotton

The materials produced in this section were synthesized to be evaluated for the antibacterial tests. The control reactions with unmodified control took place in a smaller scale (10-20mg) than the reactions with CHO-cotton. Considering the results of the preliminary tests, the peptide with the lowest loading (**2a**) was bound to CHO-cotton first. This was done to maximize the amount of free aldehydes available for the binding of the second peptide. To ensure that the results obtained with the same peptide were comparable, the same peptide/TCEP solution was used for **r13-14** (peptide **2a**), **r15-16-17** (peptide **3b**) and **r18-19-20** (peptide **4d**).

	Sample	2a loading ($\mu mol/g_{cot}$)	3b loading ($\mu mol/g_{cot}$)	4d loading ($\mu mol/g_{cot}$)	Time of Reaction
r13	Cotton + **2a**	1.5	-	-	3days
r14	CHO-Cotton + **2a**	3.5	-	-	3days
r15	Cotton + **3b**	-	6.2	-	2days
r16	CHO-cotton + **3b**	-	9.4	-	2days

r17	**r14** + **3b**	3.5	8.2	-	2days
r18	Cotton + **4d**	-	-	8.6	2days
r19	CHO-cotton + **4d**	-	-	30.7	2days
r20	**r14** + **4d**	3.5	-	21.3	2days

***Table 2.10**: Reaction conditions for the conjugation of peptides **2a, 3b** and **4d** for the production of the double functionalized cottons **2a/3b**-cotton and **2a/4d**-cotton. Peptide **2a**, **3b** and **4d** initial concentrations in solution were of 0.069, 0.073 and 0.64mM, respectively. The moles of peptide bound to the material were calculated by the difference in the peptide solution concentration before cotton was added to the solution and after the end of the reaction.*

Using a lower concentration and excess of **2a** and **3b** determined lower loading of peptide with respect to the preliminary tests. However, the amount of **2a** present on unmodified cotton was also lower, suggesting the success of the thiazolidine bond. Similar results were obtained with **3b:** the peptide loading in **r15**-**16** is less than half the value obtained in the preliminary tests (**r9**-**10**). In addition, **3b** loading obtained in **r17** is slightly lower than **r16**, but higher than **r15**, suggesting that the thiazolidine binding of peptide **3b** was effective both on CHO-cotton and on cotton already grafted with **2a** (Table 2.10).

Since the reaction conditions used for **4d** were the same of the preliminary tests, as expected the peptide loading of **r18** and **r19** were similar to **r11** and **r12**, respectively. Similarly to **r17,** the amount of peptide **4d** bound to CHO-cotton (**r19**) was slightly higher than the amount bound on cotton already grafted with peptide **2a** (**r20**), using the same reaction conditions (Table 2.10).

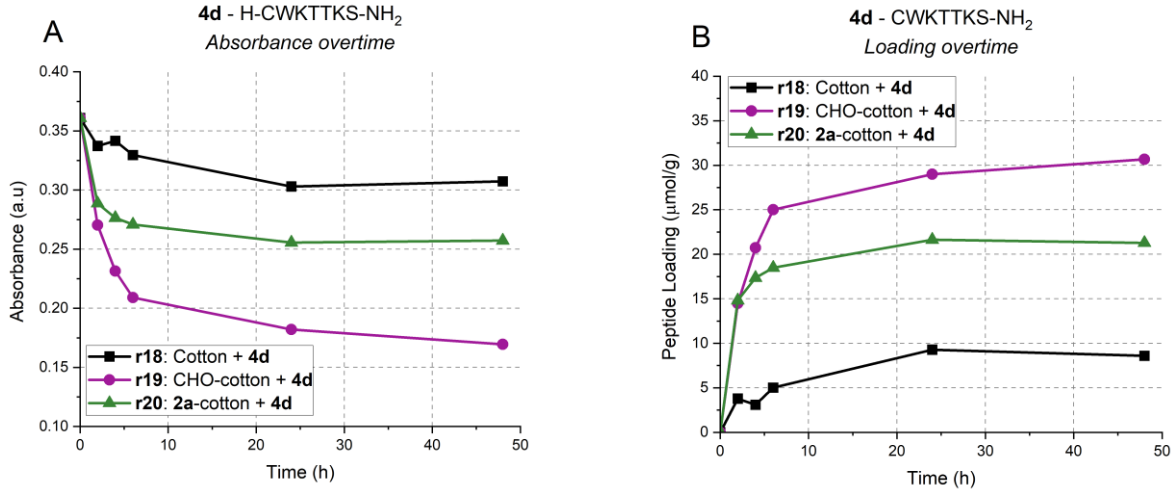

***Figure 2.13**: Reported as an example (**A**) Absorbance of the peptide **4d**/TCEP solution upon the addition of cotton (**r18**), CHO-cotton (**r19**), or **2a**-cotton from **r14** (**r20**), (**B**) Peptide loading over time of reactions **r18**, **r19**, and **r20**. The data or the other reactions is reported in Chapter 5.2.2.*

To summarize, the thiazolidine bond was successfully employed to bind two peptides, **2a** and **3b** or **2a** and **4d**, to the same piece of cotton, demonstrating the feasibility of a step-by-step system to produce cotton matrices with multiple functionalities provided by peptides.

The presence of the peptide after the reaction was concluded was confirmed by FT-IR for the peptide-cotton conjugates obtained in reaction **r16**, **r17**, **r19** and **r20.** In fact, the FT-IR spectra presented a weak

(**r17**, **r19** and **r20**) or very weak (**r14** and **r16**) band at 1532 cm^{-1}, that can be attributed to the *amide II* stretching signal of the amides present in the peptide backbone. The presence of the peptides in the cotton controls (**r13**, **r15** and **r18**) could not be confirmed by FT-IR, probably due to the low amount of adsorbed peptide present after washing the materials (Fig. 2.14 and S2.13, *Chapter 5.2.3*).

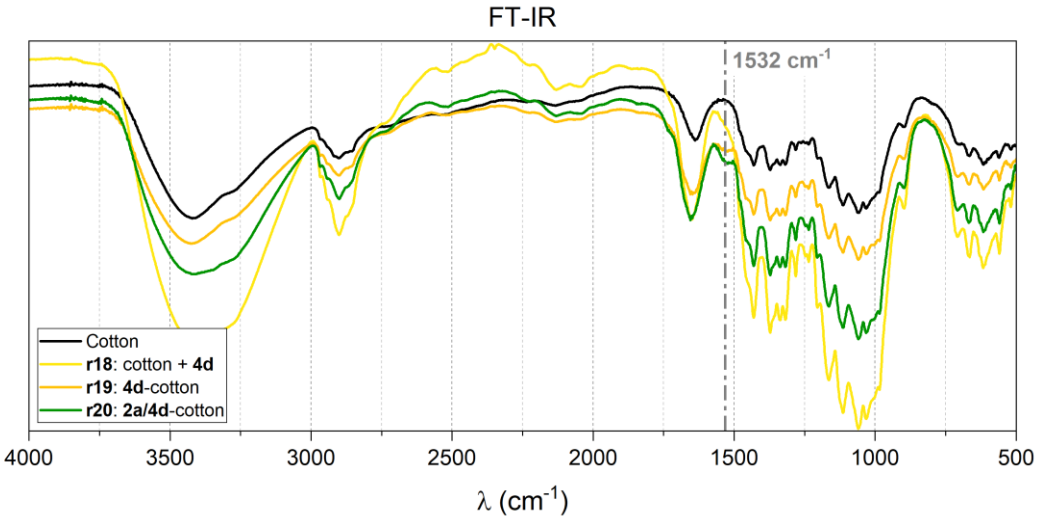

***Figure 2.14**: FT-IR of cotton, **r18** (cotton+ **4d**), **r19** (**4d**-cotton) and **r20** (**2a/4d**-cotton). Reported as an example, FT-IR data for **r13** to **17** in chapter 5.2.3.*

Antibacterial Tests

Considering the negative results of the antibacterial activity of peptides **3a** and **3b** (*Section 2.1.2*), the antibacterial activity of the cotton grafted with **3b** was not evaluated. Samples from reaction **r5**, **r14**, **r19** and **r20** were sent to the University of Trieste to test their antibacterial activity by a biofilm growth test against the bacteria species that was most susceptible to PMAP(12-24): *A. baumannii*.

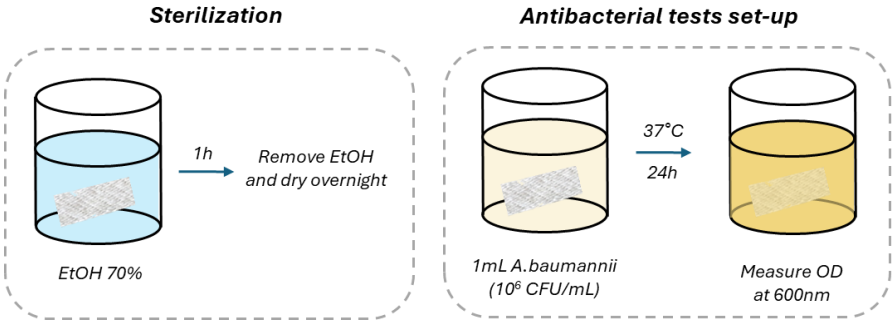

***Figure 2.15**: schematic representation of the antibacterial tests set-up.*

Briefly, CHO-cotton and peptide-cotton conjugate samples (ca. 15 mg) were first sterilized by submerging the materials in EtOH 70%. The next day, the sterilized cotton samples were added to 10^6 CFU/mL solution of *A. baumannii,* and incubated for 24h (37°C). The procedure was performed in three independent triplicates using three pieces of material from the same batch. Optical density (OD_{600}) measurements of the solutions were used to evaluate the bacterial growth. In particular, the percentage of bacterial growth was calculated as the ratio between the OD_{600} of the sample and the control without

cotton multiplied by 100 (Fig. 2.16 and Table S2.1, details about the experimental procedure in *Chapter 5.2.7*).

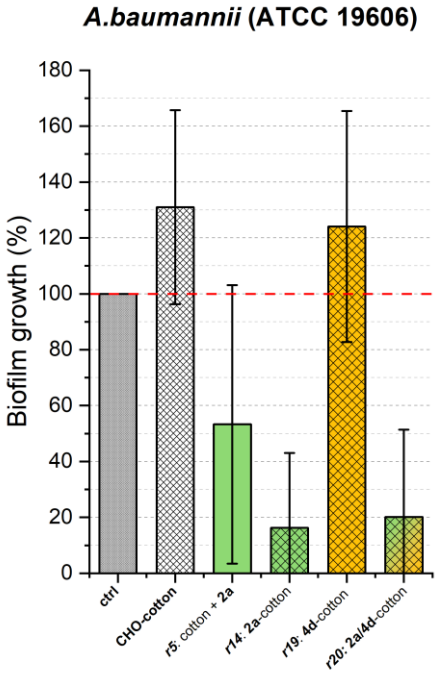

***Figure 2.16**: Test of the biofilm growth of A. baumannii in the presence of CHO-cotton and cotton conjugates from **r14**, **r19** and **r20**. Cotton from **r5** used as a control for the antibacterial activity of adsorbed **2a**. The results are obtained from the average out of three independent measurements. The percentage of biofilm growth is expressed as of ratio between the OD_{600} of the sample and the control without cotton multiplied by 100. In gray is the control without cotton, in green the samples with peptide **2a** and in yellow the samples with peptide **4d**. When CHO-cotton was used the bars are squared.*

The presence of CHO-cotton in the bacterial solution determined a slightly higher growth of *A. baumannii*, and similar results were obtained with the conjugate of the collagen boosting peptide and CHO-cotton (**4d**-cotton from **r19**), proving that cotton matrices can be potential centers for bacterial growth.

On the other hand, the conjugate formed between the antibacterial peptide **2a** and CHO-cotton (**r14**) impaired the bacterial biofilm growth. The double conjugate **2a/4d**-cotton from **r20** demonstrated the same antibacterial properties, confirming that the additional presence of 21.3 µmol/g of the collagen boosting peptide **4d** did not interfere with the antibacterial properties of peptide **2a**.

Unmodified cotton that was in the presence of peptide **2a** in reaction **r5** had a similar peptide loading (3.0 µmol/g) of the **2a**-cotton conjugate from **r14** (3.5 µmol/g). Thus, it was selected as a control to evaluate the antibacterial properties of a cotton material where the peptide was just adsorbed on the matrix. Unfortunately, the assay did not provide reliable results. In fact, while the biofilm growth obtained from two of the three measurements is of 98% and 60%, in the third measurement the bacterium did not grow at all (Table S2.1, *Chapter 5.2.7*). Therefore, without a repetition of the measurements, this behavior cannot be rationalized because it could be attributed to an error during the procedure, but also to an uneven distribution of the adsorbed peptide on cotton.

2.2.4 Project 3: PMAP-Cotton Functionalization by Thiol-Ene click reaction

Considering the successful binding of the antibacterial peptide PMAP(12-24) to CHO cotton and the reported efficiency of the thiol-ene reaction (*Chapter 1.4.3*), the feasibility of the production of a PMAP(12-24)-cotton conjugate by thiol-ene reaction was investigated. In addition, in this project the impact of the orientation of the peptide at the ligation site on peptide loading or activity was also evaluated. This was done by using peptides **2a** and **2b**, that only differ in the position of the Cys needed for the conjugation.

Norbornene grafting on cotton

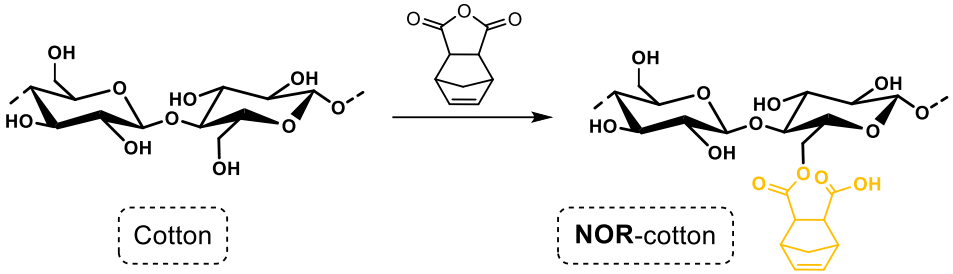

***Figure 2.17**: Schematic representation of the introduction of norbornene on cotton.*

Norbornene grafting of cotton was preliminary tested using the same reaction conditions of *Long et al.*[28]: 8 eq of carbic anhydride (with respect to the moles of hydroxyls) were dissolved in dimethyl sulfoxide (DMSO), and aqueous KOH was added up to a concentration of 0.015M. Then, cotton was added to the solution and stirred for 30min.

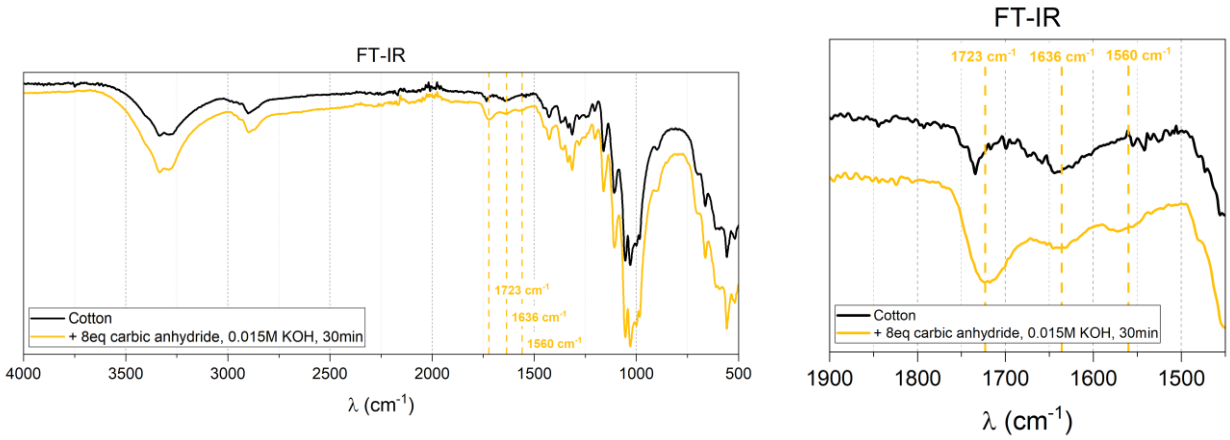

***Figure 2.18**: FT-IR spectra of cotton (black) and NOR-cotton synthesized using 8 eq of carbic anhydride (with respect to the moles of hydroxyls) in DMSO, with addition of KOH up to a concentration of 0.015M. On the right is a zoom of the fingerprint zone for the norbornene functionalization.*

The success of norbornene grafting was confirmed by the appearance of three new peaks in the FT-IR spectra of the material after the reaction, that overlap with the data found by *Dadoo et al.*[30] In particular, the peak at 1723 cm^{-1} is assigned to the stretching band of the ester bond formed with cotton, the peak at 1636 cm^{-1} is assigned to the C=C stretching from the alkene in the same moiety, and the peak at

1560cm^{-1} to the C=O stretching band of the carboxylic acid of the norbornene moiety [30] (Fig. 2.18). To assess the repeatability of the reaction in DMSO, the experiment was repeated in the same conditions twice, however the new signals at the FT-IR spectra were not as clear as in the first experiment (Fig. S2.14A, *Chapter 5.2.4*). Similar spectra were obtained when using lower amounts of carbic anhydride (4eq and 2eq, Fig. S2.14A, *Chapter 5.2.4*). The reaction was also tested using dimethylformamide (DMF) as the solvent and 5eq of carbic anhydride, following a report on norbornene functionalization of chitosan[73]. However, also in this case no difference from the FT-IR spectra of cotton could be detected (Fig. S2.14B, *Chapter 5.2.4*).

Therefore, to confirm the presence of norbornene on cotton, a bigger batch of NOR-cotton was synthesized using 2eq of carbic anhydride and the same conditions described above (*NOR-cotton 1*, Table 2.11). The carboxyls present on the material, thus the moles of norbornene, were quantified by alkaline titration using the same procedure described in *Section 2.2.3* for CHO-cotton.

In addition, since cotton could be easily removed from the solution, the re-use of the carbic anhydride was tested by adding a fresh piece of unmodified cotton to the solution right after the first reaction (*NOR-cotton 2*).

Sample	**Reaction Conditions**	**COOH loading (mmol//g_{cot})**	**Norbornene loading (mmol//g_{cot})**
Cotton	-	0.030 ± 0.003	-
NOR-cotton 1	2 eq carbic anhydride, 0.015M KOH, solvent DMSO, RT 30min	0.058 ± 0.002	0.028 ± 0.005
NOR-cotton 2	Re-use of NOR-cotton 1 solution	0.032 ± 0.003	0.002 ± 0.006
NOR-cotton 3	2 eq carbic anhydride (0.025 eq every 30min), 0.015M KOH, solvent DMSO, RT 24h	0.081 ± 0.005	0.051 ± 0.008

Table 2.11*: results of the titration of the carboxyl groups on the materials using with 0.01M NaOH as the titrant. The results are the average of two/three different titrations on two/three pieces of cotton from the same batch or reaction. Detailed procedure in Section 2.4.3.*

The amount of norbornene grafted on cotton was calculated as the difference of the carboxyls present in the material and those found on unmodified cotton, and resulted much lower than the results obtained by *Long et al*.[28] or *Dadoo et al*.[29] In addition, as shown by the titration results, the re-use of the carbic anhydride solution was not successful, probably due to hydrolysis of the anhydride.

Inspired by the work of *Alves et al*.[73] for the norbornene functionalization of chitosan, the fractional addition of carbic anhydride was tested (*NOR-cotton 3*). In particular, a freshly prepared solution of carbic anhydride in DMSO was added to the reaction solution every 30min for 4h, then the solution containing a total of 2eq of the reagent was left stirring for 24h. This procedure was successfully carried out to minimize the hydrolysis of carbic anhydride and increase the norbornene loading. In fact, the titration of *NOR-cotton 3* revealed almost double the amount of norbornene with respect to *NOR-cotton*

1. The norbornene loading of *NOR-cotton 3* was still not comparable to the amount found in the literature, but since it was compatible to the amount of aldehydes grafted on cotton in the previous section, for our purposes it was enough and we proceeded with the thiol-ene conjugations of the peptides without further optimizing the reaction.

Since only *NOR-cotton 3* was used for the thiol-ene conjugations, in the following Sections *NOR-cotton 3* will simply be referred as NOR-cotton.

PMAP-cotton thiol-ene click chemistry

Peptides **2a** and **2b** were conjugated to NOR-cotton by using the same reaction conditions used by *Alves et al.*[73] for the grafting of an antibacterial peptide to NOR-chitosan. In particular, the peptides were present in a concentration of 0.8mM in water, the photoinitiator (VA-086) was in a concentration of 0.4 mg/mL and was activated by irradiation with light at 365nm and 10mW microwaves, after which the solution was stirred for 5 minutes.

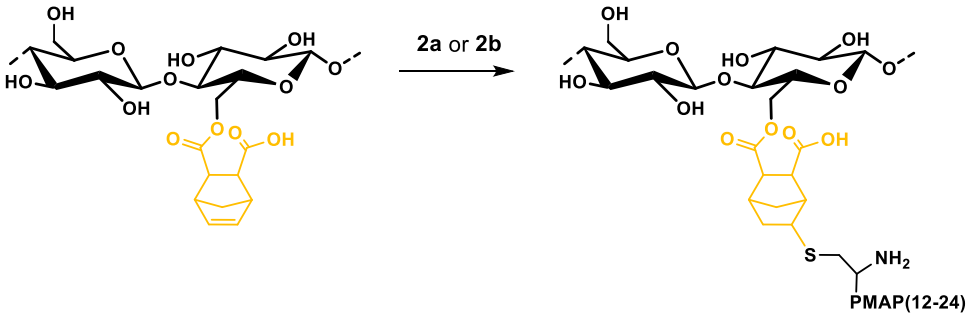

Figure 2.19*: Schematic representation of the thiol-ene reaction between the peptides and NOR-cotton.*

Considering the low amount of norbornene grafted on NOR-cotton and to maximize the yield, peptides **2a** and **2b** were added in a 1:1 ratio with respect to the moles of norbornene, instead of 0.1:1 as in the reference. After the reaction, the pieces of cotton were thoroughly washed with water and sonicated to remove all the excess peptide. As a control, unmodified cotton was subjected to the same reaction conditions. As an ulterior control, the reaction was also performed without promoting photo-triggered peptide conjugation (absence of photoinitiator, UV and microwave exposure).

	Material	Peptide	Reaction Conditions
r21	Cotton	**2a**	**2a** 0.8mM, VA-086 4%, 5min, 365nm/10mW
r22	NOR-cotton	**2a**	**2a** 0.8mM, VA-086 4%, 5min, 365nm/10mW
r23	NOR-cotton	**2a**	**2a** 0.8mM, 5min
r24	Cotton	**2b**	**2b** 0.8mM, VA-086 4%, 5min, 365nm/10mW
r25	NOR-cotton	**2b**	**2b** 0.8mM, VA-086 4%, 5min, 365nm/10mW
r26	NOR-cotton	**2b**	**2b** 0.8mM, 5min

Table 2.12*: Reaction conditions for the thiol-ene reactions of cotton and peptides **2a** and **2b**. All reactions were performed on 9 independent pieces of cotton (of around 15mg) using the same peptide solution.*

The presence of the peptide after the thiol-ene reaction was confirmed by FT-IR for the peptide-cotton conjugates obtained in reaction **r22**, **r23**, **r25** and **r26.** In fact, the FT-IR spectra presented a weak band at around 1530 cm^{-1} that can be attributed to the *amide II* stretching signal of the amides in the peptide backbone. Similarly to what was obtained in the previous *section 2.2.3*, the presence of the peptides in the unmodified cotton controls (**r21** and **r24**) could not be confirmed by FT-IR, probably due to the low amount of adsorbed peptide present after washing the materials (Fig. 2.20 and S2.15, *Chapter 5.2.4*).

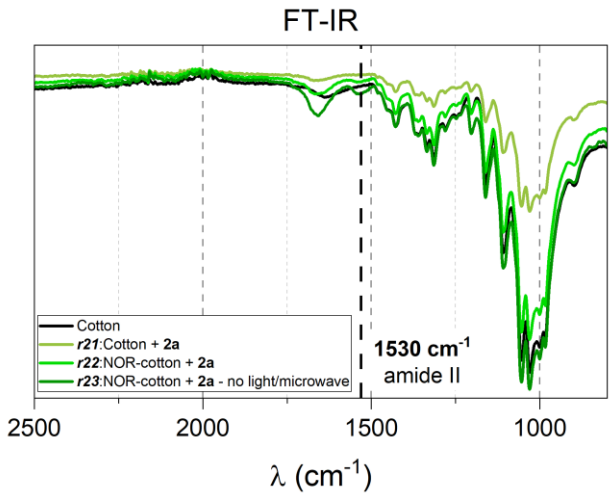

***Figure 2.20**: FT-IR of cotton, **r21** (cotton+ **2a**), **r22** (NOR-cotton **+ 2a**) and **r23** (NOR-cotton + **2a** – NO UV/mW). Reported as an example, the complete FT-IR spectra of **r21** to **126** are reported in chapter 5.2.4.*

Amino Acid Analysis

Amino acid analysis was performed to quantify the amount of PMAP(12-24) conjugated on NOR-cotton by determining the relative amino acid composition. Briefly, weighted cotton pieces were first degraded in harshly acidic conditions to form free amino acids and the products of hydrolysis of the polysaccharide backbone. The former were detected and quantified by ion exchange chromatographic analysis, and the latter did not interfere with the measurements. The results are summarized in Table 2.13.

		Mass (mg)	**n peptide (nmol)**	**Loading** (µmol/g)**
-	Cotton	4.33	-	-
-	NOR-cotton	4.93	-	-
r21	Cotton + **2a**	4.74	7.382	1.56
r22	NOR-cotton + **2a**	4.35	23.824	5.52
r23	NOR-cotton + **2a** – NO UV/mW	5.43	22.291	4.13
r24	Cotton + **2b**	4.51	8.259	1.84*
r25	NOR-cotton + **2b**	4.47	19.725	4.45
r26	NOR-cotton + **2b** – NO UV/mW	4.35	17.190	3.98*

***Table 2.13**: Peptide loading calculated by amino acid analysis. *the value was calculated taking into account only Ile and Lys (<30% of the total number of amino acids). **Calculated as the mmol of peptide divided by the difference between the total mass of the sample and the mass of peptide. Detailed data in Chapter 5.2.5.*

Experimental and theoretical ratios of the amino acids in the PMAP(12-24) sequence were similar for all the tested materials, suggesting that the amino acid sequence of the peptide remained unchanged during thiol-ene reaction (*Chapter 5.2.5*).

Approximately 10% of the norbornene groups available in NOR-cotton (4.5-5.5 μmol of the 50 μmol norbornene groups per gram of NOR-cotton) reacted with peptide **2a** or **2b** (**r22**-**r25**). In addition, the amount of PMAP(12-24) grafted on NOR-cotton was similar independently from the peptide, and was the same range of what was found when using the thiazolidine reaction (*Section 2.2.3*). The amount of peptide present on unmodified cotton that was in contact with both peptides (**r21**-**r24**) was lower than the peptide grafted on NOR-chitosan, and is coherent with the amount of peptide **2a** found on cotton when testing for the thiazolidine bond formation (*Section 2.2.3*). Unexpectedly, the amount of **2a** and **2b** in **r23** and **r26** is only slightly lower than the materials where the photoinitiator was present (**r22**-**r25**). This could be due to a different adsorbent capability of NOR-cotton with respect to unmodified cotton, but also that the reaction could proceed without the photoinitiation. Therefore, the thiol-norbornene reaction could be considered successful, but unfortunately the amount of peptide that is actually covalently bound and not just absorbed cannot be precisely determined.

XPS Analysis

Cotton, NOR-cotton, and the materials obtained from reaction **r21** to **r26** were further analyzed by XPS. Table 2.15 shows the relative atomic percentages of carbon, nitrogen, oxygen and sulfur.

Description	C %	O %	N %	S %	N/C	O/C	N/O	S/C
Cotton	65.24	34.76	-	-	0.000	0.533	0.000	0.000
NOR-Cotton	62.27	37.73	-	-	0.000	0.606	0.000	0.000
***r21*:** Cotton + **2a**	63.54	32.82	3.29	0.35	0.052	0.517	0.100	0.006
r22: NOR-cotton + **2a**	63.4	32.86	3.27	0.71	0.052	0.518	0.100	0.011
r23: NOR-cotton + **2a** – NO UV/mW	62.31	33.51	3.66	0.52	0.059	0.538	0.109	0.008
r24: Cotton + **2b**	60.62	37.42	1.74	0.22	0.029	0.617	0.046	0.004
r25: NOR-cotton + **2b**	60.12	35.05	4.2	0.32	0.070	0.583	0.120	0.005
r26: NOR-cotton + **2b** – NO UV/mW	62.2	32.05	5.31	0.44	0.085	0.515	0.166	0.007

Table 2.14*: elemental analysis data (% C, N, O) as determined by XPS analysis of NOR-cotton, and the materials obtained from reaction **r21** to **r26**.*

The results obtained with cotton are coherent with the data in the literature[74] and previous findings of our group[50], even though atomic percentage of oxygen is slightly lower than the theoretical value. The higher percentage of oxygen present in NOR-cotton is coherent with the insertion of the norbornene moiety. The presence of sulfur and nitrogen in the elemental analysis of **r21**, **r22**, **r23**, **r24**, **r25** and **r26** confirms the presence of peptide in all the samples, coherently with the amino acid analysis. Overall,

these data are in agreement with the results of the amino acid analysis: both peptides (**2a** and **2b**) are present in the controls with unmodified cotton but in lower amounts, further confirming previous findings about the possible adsorption of the peptide onto unmodified cotton (*Section 2.2.3*). The only outlier is amount of peptide **2b** in samples **r25**. In fact, when considering the amount of nitrogen and sulfur present in the samples (expressed as N/O and S/C), the amount of peptide **2b** present in **r25** is slightly lower than in **r26** (where the reaction was not photoinitiated), in contrast to the values found by amino acid analysis. The XPS spectra are reported in *Chapter 5.2.6*.

Antibacterial Tests

Samples from reaction **r21**, **r22**, **r24** and **r25** were sent to the University of Trieste to test their antibacterial activity by a biofilm growth test against the bacterial species that was most susceptible to PMAP(12-24): *A. baumannii*. The same procedure described in *Section 2.2.3* for the antibacterial tests on **r5**, **r14**, **r19** and **r20** was used.

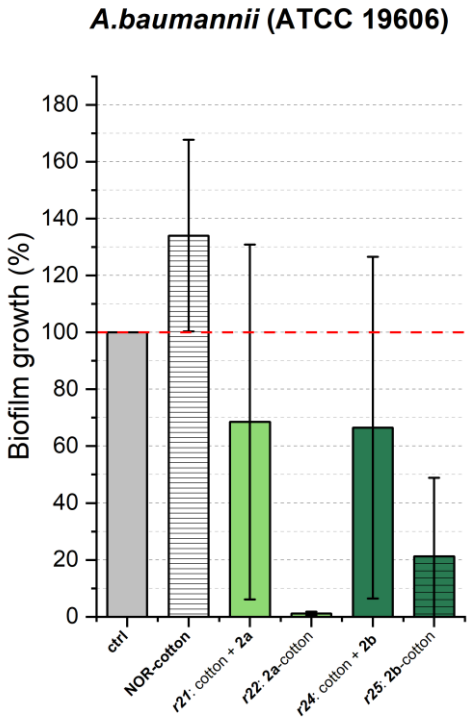

***Figure 2.21**: Test of the biofilm growth of A. baumannii in the presence of NOR-cotton and cotton conjugates from **r22** and **r25**. Cotton from **r21** and **r24** used as controls for the antibacterial activity of adsorbed **2a** and **2b**, respectively. The percentage of biofilm growth is expressed as the ratio between the OD_{600} of the sample and the control without cotton multiplied by 100. In gray is the control without cotton, in light green the samples with peptide **2a** and in dark green the samples with peptide **2b**. When NOR-cotton was used the bars are striped.*

Similarly to CHO-cotton, the presence of NOR-cotton in the bacterial solution determined a slightly higher growth of *A.baumannii*, proving that cotton matrices can be potential centers for bacterial growth.

On the other hand, the thiol-ene conjugates between the antibacterial peptide PMAP(12-24) and NOR-cotton impaired the biofilm growth of *A.baumanni* (Fig 2.21, **2a**-cotton and **2b**-cotton). Interestingly, the

results obtained suggest the orientation of the peptide determined by the different positions of Cys in peptides **2a** and **2b** could have an impact on the antibacterial properties of the final material. In fact, where the **2a**-cotton conjugate (**r22**) almost completely prevented the growth of the bacteria, the presence of the **2b**-cotton conjugate (**r25**) in the bacterial solution determined, in average, a lowered bacterial growth than the control, but not in the same range of **2a**-cotton. However, the high variability in the results of the three measurements of the **2b**-cotton samples did not allow for a definitive rationalization (Table S2.1, *Chapter 5.2.7*).

Similarly, the results obtained with unmodified cotton that was in the presence of peptide **2a** (**r21**) and **2b** (**r24**) are not completely reliable. In fact, in both cases, the biofilm growth obtained from two of the three measurements is higher than 70%, suggesting that the absorbed peptide (if there is after the washes) is not enough to determine a significant inhibition of the bacterial growth. However, in both cases, the third measurement provided very low bacterial growths of 0.2% and 3.5% for **r21** and **r24**, respectively (Table S2.1, *Chapter 5.2.7*). Therefore, without a repetition of the measurements, the antibacterial activity of the samples from **r21** and **r24** cannot be rationalized. Similarly to the results of **r5**, this behavior could be attributed to an error during the procedure, but also to an uneven distribution of the adsorbed peptide on cotton.

2.3 Conclusions and Future Perspectives

Cotton is the most widely used material as an inert coverage in the context of wound healing. In the last years intensive research has been done to improve the properties of cotton, especially to enhance its antibacterial properties. This chapter explores various chemoselective methods to covalently bind active peptides to cotton to enhance its wound-healing potential. In addition, a particular focus was given to the use of environmentally friendly reagents and methods.

The active molecules selected for the functionalization of cotton were the antibacterial peptides PMAP(12-24) (H-KRLKKIGKVLKWI-NH_2) and Pal-HAaH (C_{16}-HAaH-NH_2), and the collagen-boosting peptide PP4 (H-KTTKS-NH_2). Three sets of analogues were synthesized in order to equip the peptides with the β-amino thiol, thiol or aminooxyacetic acid needed for the conjugations, as well as a UV-Vis active probe for quantifying the peptides in the material. In the case of Pal-HAaH, the position of the Lys(Trp-Cys) "conjugation arm" revealed to be relevant for the peptide solubility. On the other hand, in the case of the PP4 analogues the position of the palmitoyl chain determined a difference in the cytotoxicity of the peptides to 3T3 cells.

The aldehyde required for the thiazolidine or oxime conjugations was introduced into cotton by the TEMPO/laccase/O_2 catalyzed system to avoid the environmental hazards and the polysaccharide degradation caused by the common $NaIO_4$ oxidation. The amount of aldehydes grafted on cotton was determined by titration to be 0.075 mmol/g_{cot}. The comparison of the peptide loading on CHO-cotton and on unmodified cotton confirmed the success of the thiazolidine conjugation with all the tested active peptides: **2a** (H-CKRLKKIGKVLKWI-NH_2), **3b** (C_{16}- K(WC)-HAaH-NH_2)and **4d** (H-CWKTTKS-NH_2). In addition, peptides **3b** and **4c** were successfully conjugated to cotton that was already functionalized with peptide **2a**, proving the feasibility of a multiple cotton functionalization *via* consecutive thiazolidine bonds. The antibacterial properties of the **2a**-cotton conjugate obtained with a thiazolidine ligation (**r14**) was confirmed by the low growth of *A. baumannii* in the biofilm assay. Furthermore, the same assay demonstrated that the binding of the additional collagen boosting peptide on **2a**/**4d**-cotton (**r20**) did not impair the antibacterial properties of the final material.

Introducing the norbornene moiety to cotton proved to be more challenging than what reported with other materials. The best results (0.051 ± 0.008 mmol/g_{cot}) were obtained using a fractional addition of carbic anhydride in solution. Preliminary tests of a photoinitiated thiol-norbornene reaction between NOR-cotton and peptide PMAP(12-24) were encouraging. In fact, the peptide loading on unmodified cotton (1-2 μmol/g_{cot}) was lower than what was obtained using NOR-cotton (4-5 μmol/g_{cot}) independently on the position of the cysteine in the peptide (**2a**, H-CKRLKKIGKVLKWI-NH_2 or **2b**, H-KRLKKIGKVLKWIC-NH_2). In addition, the peptide loading on NOR-cotton were in the same range of the

one obtained with the thiazolidine or oxime reaction, while the reaction time was much lower (5min) when compared to the 24h needed for the other two ligations. However, more studies are needed to understand the results obtained in the absence of the photoinitiator. The **2a**-cotton and **2b**-cotton conjugates were proven to have an antibacterial activity against *A. baumannii* that was not present in NOR-cotton, demonstrating that binding the peptides to cotton by thiol-norbornene bond did not impact their antibacterial activity.

Overall, in this chapter the use of the thiazolidine ligation was thoroughly investigated for the production of antibacterial peptide-cotton conjugates using a shortened analogue of PMAP-36. The feasibility of an easy step-by-step multiple functionalization of CHO-cotton by consecutive thiazolidine ligations was also demonstrated using two different peptides. The conjugates obtained from the reaction between the antibacterial peptide and CHO-cotton presented an inhibition of *A. baumannii* growth, independently on the presence of an additional peptide. In addition, the use of the thiol-ene click chemistry was explored to produce antibacterial peptide-cotton conjugates. This last project gave encouraging results both in terms of efficacy of the ligation and antibacterial activity of the final material. However, the optimization of the reaction conditions of the norbornene grafting and the peptide conjugation could be explored in more detail.

2.4 Methods

2.4.1 Instruments

HPLC for peptide analysis: Phenomenex C_{18} reverse phase column (4.6 × 250 mm, 5 μ, 100 Å) using a VWR HITACHI Chromaster instrument with spectrophotometric detection at λ = 214 nm and λ = 280 nm.

ESI–MS: Agilent technologies 1260 Infinity II instrument equipped with an Agilent technologies quadrupole LC–MS 6130.

HPLC for peptide purification:

- *Akta Pure*: preparative RP-HPLC on a Phenomenex C_{18} column (22.1 mm × 250 mm, 10 μm, 300 Å) using an Akta Pure GE Healthcare (Little Chalfont, U.K.) LC system equipped with an ultraviolet detector (flow rate of 15 mL/min) and a binary elution system (A: H_2O, B: CH_3CN/H_2O [9:1 (v/v)].
- *Sigma*: preparative HPLC system (LaPrep Sigma VWR with UV detector LP 3104 and LP 1200 pump) with a reverse-phase Merck C_{18} column (250 × 25 mm ID and 5 m pore size) at a flow rate of 10 mL/min and binary elution system (A: 0.05% aqueous TFA eluent A, B: CH_3CN)

UV-Vis: A Shimadzu UV-Vis 250 1PC with a 350–230 nm interval, 2 nm slit, and a 0.1 nm sampling interval was used. Depending on the experiment, quartz Hellma Analytics cuvettes with an optical path of 1 cm or 1 mm were used.

FT-IR: A Nicolet nexus 670 spectrophotometer was used to collect the FT-IR spectra. The cotton samples were mechanically frayed and incorporated in a KBr pellet. The chamber where the samples sit was maintained under a constant N_2 flow to minimize the contributions of H_2O and CO_2. The spectra were collected through 20 scans in the range 4000–400 cm^{-1}, with a resolution of 2 cm^{-1}.

2.4.2 Peptide Synthesis

All peptides were synthesized by solid phase synthesis using standard by Fmoc strategy[75]. Manual solid phase peptide synthesis can be rationalized with the following steps:

- SWELLING: degassed DMF is added to the resin and the dispersion stirred for 30min. Then, DMF is removed.
- AA COUPLING: To activate the amino acid, 3eq (with respect to the mmol of binding sites on the resin) of protected amino acid and 3eq of Oxima Pure are dissolved in DMF. Then, 3eq of DIC are added and the solution is left stirring for 3-5min. The activated amino acid solution is added to

the resin and the dispersion is left stirring. After 50min, the solution is filtered and the resin is washed 5 times with DMF.

- ⇨ When using 2-chlorotrityl chloride resin, a different protocol is used for the first amino acid coupling. In particular, 2.5eq of protected amino acid and 5eq of DIPEA are dissolved in DMF and added to the swelled resin. The dispersion is stirred for 1h. Then, the resin is capped by adding a DCM/MeOH/DIPEA (80:15:5) solution and stirring for 10min. The capping is repeated two times. Finally, the resin is washed 5 times
- ⇨ The last amino acid of the sequence is also washed 5 times with DCM.

- ❖ Palmitic acid COUPLING: To activate palmitic acid, 3eq (with respect to the mmol of binding sites on the resin) of palmitic acid and 3eq of Oxima Pure are dissolved in DMF. Then, 3eq of DIC are added and the solution is left stirring for 3-5min. The activated palmitic acid solution is added to the resin and the dispersion is left stirring. After 2h, the solution is filtered and the resin is washed 5 times with DMF.
- ❖ FMOC DEPROTECTION: the resin is submerged in a solution of 20% piperidine in DMF for 5min. This procedure is repeated a second time for 15min. Then, the resin is washed 5 times with DMF.
- ❖ DDE DEPROTECTION: the resin is submerged in a solution of 2% hydrazine in DMF for 5min. This procedure is repeated 5 times. Then, the resin is washed 5 times with DMF.
- ❖ CLEAVAGE: a solution of TFA/TIS/H_2O (95:2.5:2.5) is added to the resin and the dispersion is stirred for 2.5h. When the peptide sequence has a cys, a solution of TFA/TIS/H_2O/DODT (94:1:2.5:2.5) is used. Then, a 10-fold excess of cold Et_2O is added to the filtered solution to precipitate the peptide. The solid is recovered by centrifugation (5500 rpm x 5min) and washed 3 times with Et_2O.

In the case of automatic peptide synthesis (Syro Wave, Biotage) the steps are the same but the protocols slightly differ. In particular, the couplings are performed using 3eq of protected amino acid, HBTU, HOBt and 6eq of DIPEA.

After the synthesis all peptides were kept in a desiccator under reduced pressure for two days and then stored in the fridge.

Peptide	Short name	Sequence	MW (g/mol)
1a	CGWK	H-CGWK-NH_2	491.61
1b	AxGWK	H-A_xGWK-NH_2	461.24
2a	CysPMAP(12-24)	H-CKRLKKIGKVLKWI-NH_2	1712.27
2b	PMAP(12-24)cys	H-KRLKKIGKVLKWIC-NH_2	1712.27
2c	AoxPMAP(12-24)	H-A_xKRLKKIGKVLKWI-NH_2	1682.19
3a	Pal-HAaH	Pal-HAaH-NH_2	671.89
3b	-	Pal-K(WC)-HAaH-NH_2	1089.42

3c		Pal-HAaH-K(WC)-NH_2	1089.42
4a	KTTKS-OH	H-KTTKS-OH	563.65
4b	KTTKS-NH_2	H-KTTKS-NH_2	562.67
4c	Pal-KTTKS	Pal-KTTKS-NH_2	801.08
4d	CysWKTTKS	H-CWKTTKS-NH_2	852.02
4e	-	H-CWK(Pal)KTTKS-NH_2	1218.60
4f	-	H-CWKTTKSK(Pal)-NH_2	1218.60

***Table 2.15**: List of the synthesized peptides*

Peptide 1a

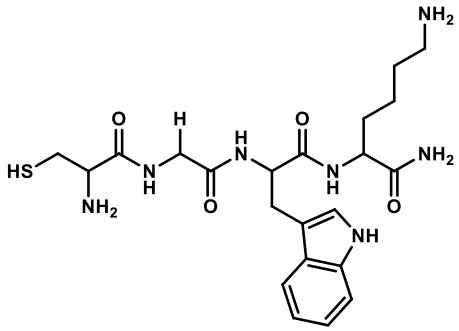

Resin: Fmoc Rink Amide AM (500mg, loading 0.62 mmol/g)

Manual synthesis: SWELL, FMOC DEP, Fmoc-Lys(Boc)-OH COUPLING, FMOC DEP, Fmoc-Trp(Boc)-OH COUPLING, FMOC DEP, Fmoc-Gly-OH COUPLING, FMOC DEP, Fmoc-Cys(Trt)-OH COUPLING, FMOC DEP, CLEAVAGE

Purity **1a**: 95.3%

Peptide 1b

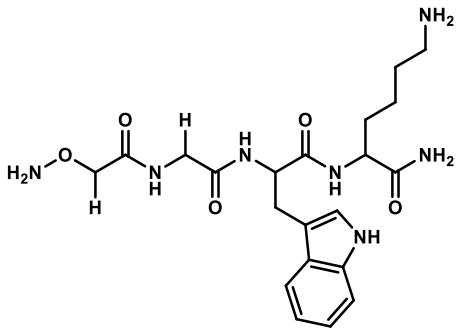

Resin: Fmoc Rink Amide AM (500mg, loading 0.62 mmol/g)

Manual synthesis: SWELL, FMOC DEP, Fmoc-Lys(Boc)-OH COUPLING, FMOC DEP, Fmoc-Trp(Boc)-OH COUPLING, FMOC DEP, Fmoc-Gly-OH COUPLING, FMOC DEP, Fmoc-Aox-OH COUPLING, FMOC DEP, CLEAVAGE

Purity **1b**: 74.5%

Peptide 2a and 2c

2a)

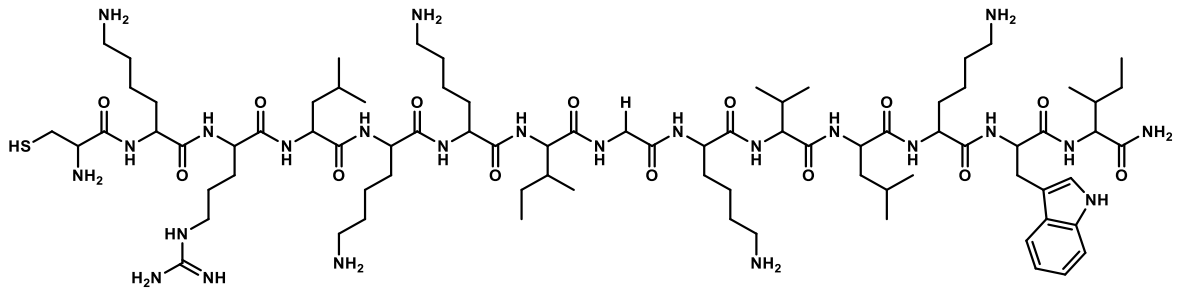

2c)

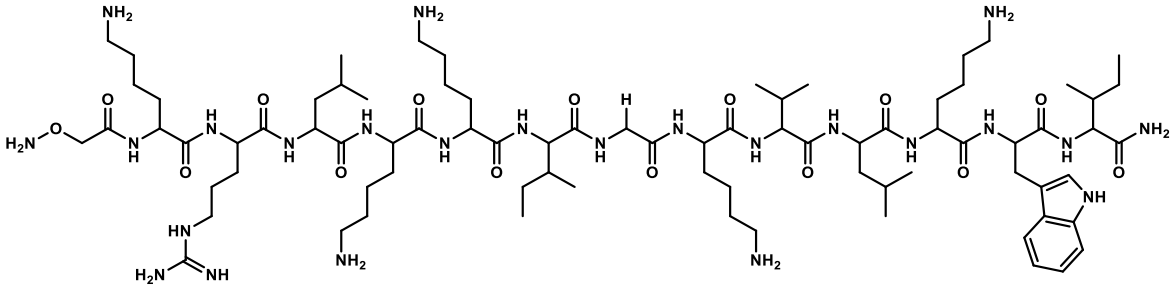

Resin: Fmoc Rink Amide AM (750mg, loading 0.62 mmol/g)

Automatic synthesis: SWELL, FMOC DEP, Fmoc-Ile-OH COUPLING **x2**, FMOC DEP, Fmoc-Trp(Boc)-OH COUPLING **x2**, FMOC DEP, Fmoc-Lys(Boc)-OH COUPLING, FMOC DEP, Fmoc-Leu-OH COUPLING **x2**, FMOC DEP, Fmoc-Val-OH COUPLING **x2**, FMOC DEP, Fmoc-Lys(Boc)-OH COUPLING, FMOC DEP, Fmoc-Gly-OH COUPLING, FMOC DEP, , Fmoc-Ile-OH COUPLING, FMOC DEP, Fmoc-Lys(Boc)-OH COUPLING, FMOC DEP, Fmoc-Lys(Boc)-OH COUPLING, FMOC DEP, Fmoc-Leu-OH COUPLING **x2**, FMOC DEP, Fmoc-Arg(Pbf)-OH COUPLING **x2**, FMOC DEP, Fmoc-Lys(Boc)-OH COUPLING, FMOC DEP.

Manual synthesis:

- Half of the resin for peptide **2a**: SWELL, Fmoc-Cys(Trt)-OH COUPLING, FMOC DEP, CLEAVAGE.
- Half of the resin for peptide **2c**: SWELL, Fmoc-Aox-OH COUPLING, FMOC DEP, CLEAVAGE. Note: to the cleavage solutions 5eq of Aox were added as scavenger for residual

Both peptides were purified with the *Akta Pure* preparative HPLC, gradient 10-45%B in 40min.

Purity **2a**: 92.1%

Purity **2c**: 96.0%

Peptide 2b

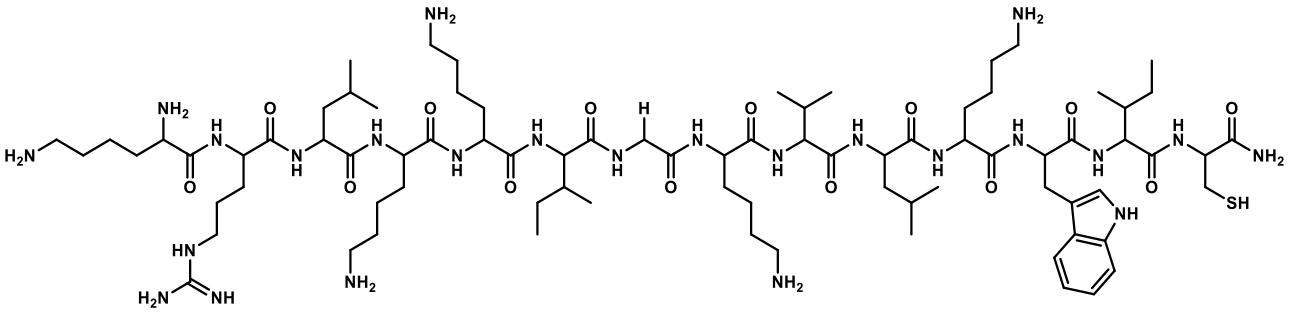

Resin: Fmoc Rink Amide AM (750mg, loading 0.62 mmol/g)

Automatic synthesis: SWELL, FMOC DEP, Fmoc-Cys(Trt)-OH COUPLING, FMOC DEP, Fmoc-Ile-OH COUPLING **x2**, FMOC DEP, Fmoc-Trp(Boc)-OH COUPLING **x2**, FMOC DEP, Fmoc-Lys(Boc)-OH COUPLING, FMOC DEP, Fmoc-Leu-OH COUPLING **x2**, FMOC DEP, Fmoc-Val-OH COUPLING **x2**, FMOC DEP, Fmoc-Lys(Boc)-OH COUPLING, FMOC DEP, Fmoc-Gly-OH COUPLING, FMOC DEP, , Fmoc-Ile-OH COUPLING,

FMOC DEP, Fmoc-Lys(Boc)-OH COUPLING, FMOC DEP, Fmoc-Lys(Boc)-OH COUPLING, FMOC DEP, Fmoc-Leu-OH COUPLING **x2**, FMOC DEP, Fmoc-Arg(Pbf)-OH COUPLING **x2**, FMOC DEP, Fmoc-Lys(Boc)-OH COUPLING, FMOC DEP, CLEAVAGE.

Both peptides were purified with *Sigma* preparative HPLC, gradient 10-45%B in 40min.

Purity **2b**: 93.4%

Peptide 3a and 3b

3a)

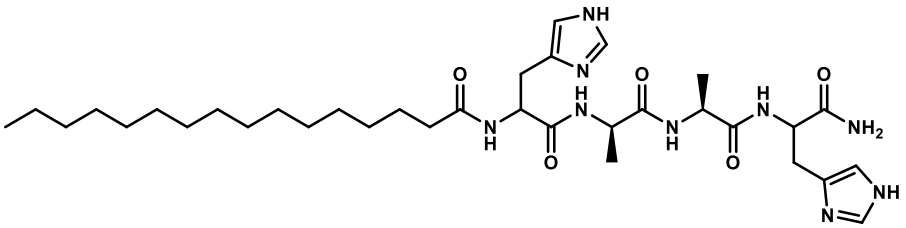

3b)

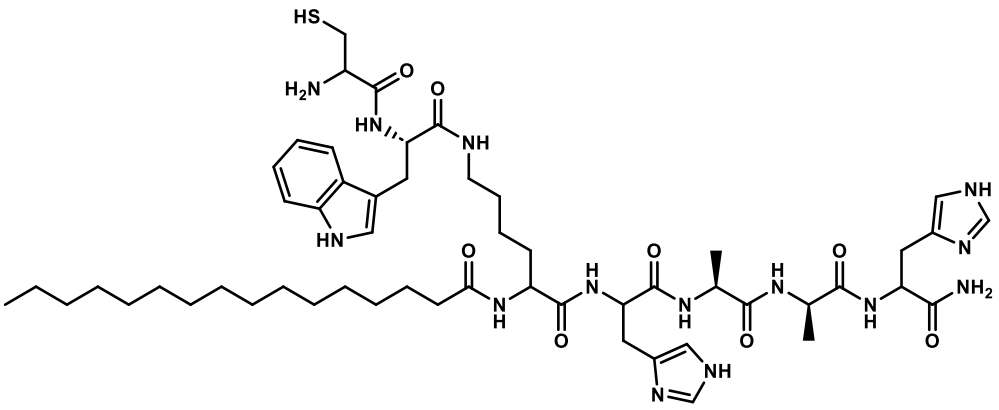

Resin: Fmoc Rink Amide AM (300mg, loading 0.62 mmol/g)

Manual synthesis: SWELL, Fmoc-His(Boc)-OH COUPLING, FMOC DEP, Fmoc-*D-Ala*-OH COUPLING, FMOC DEP, Fmoc-Ala-OH COUPLING, FMOC DEP, Fmoc-His(Boc)-OH COUPLING, FMOC DEP

- 1/3 of the resin for peptide **3a**: Palmitic acid COUPLING **x2**, CLEAVAGE.
- 2/3 of the resin for peptide **3b**: Dde-Lys(Fmoc)-OH COUPLING, FMOC DEP, Fmoc-Trp(Boc)-OH COUPLING **x2**, FMOC DEP, Boc-Cys(Trt)-OH COUPLING, DDE DEP **x2**, Palmitic acid COUPLING **x2**, CLEAVAGE.

Purity **3a**: 92.3%

Peptide **3b** was purified with the *Akta Pure* preparative HPLC, gradient 45-65%B in 20min.

Purity **3b**: 98.5%

Peptide 3c

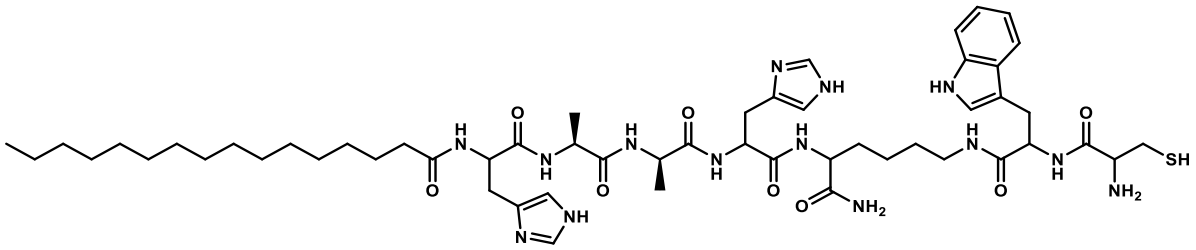

Resin: Fmoc Rink Amide AM (200mg, loading 0.62 mmol/g)

Manual synthesis: SWELL, Dde-Lys(Fmoc)-OH COUPLING, FMOC DEP, Fmoc-Trp(Boc)-OH COUPLING **x2**, FMOC DEP, Boc-Cys(Trt)-OH COUPLING, DDE DEP **x2,** Fmoc-His(Boc)-OH COUPLING, FMOC DEP, Fmoc-*D-Ala*-OH COUPLING, FMOC DEP, Fmoc-Ala-OH COUPLING, FMOC DEP, Fmoc-His(Boc)-OH COUPLING, FMOC DEP, Palmitic acid COUPLING **x2**, CLEAVAGE.

Peptide **3c** was purified with the *Akta Pure* preparative HPLC, gradient 45-65%B in 20min.

Purity **3c**: 98.7%

Peptide 4a

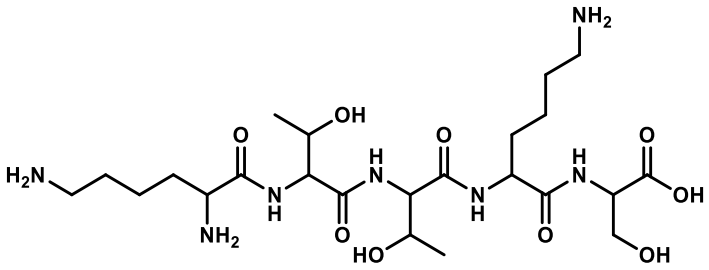

Resin: 2-chlorotrityl chloride resin (100mg, loading 0.98 mmol/g)

Manual synthesis: SWELL, Fmoc-Ser(tBu)-OH COUPLING, FMOC DEP, Fmoc-Lys(Boc)-OH COUPLING, FMOC DEP, Fmoc-Thr(tBu)-OH COUPLING, FMOC DEP, Fmoc-Thr(tBu)-OH COUPLING, FMOC DEP, Fmoc-Lys(Boc)-OH COUPLING, FMOC DEP, CLEAVAGE.

Purity **4a**: 94.9%

Peptide 4b and 4c

4b)

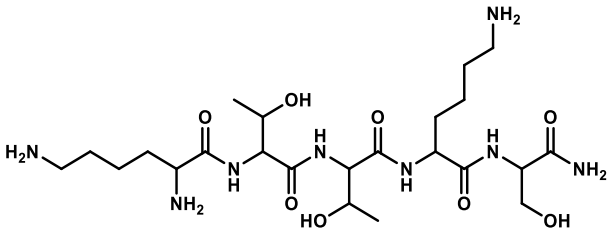

4c)

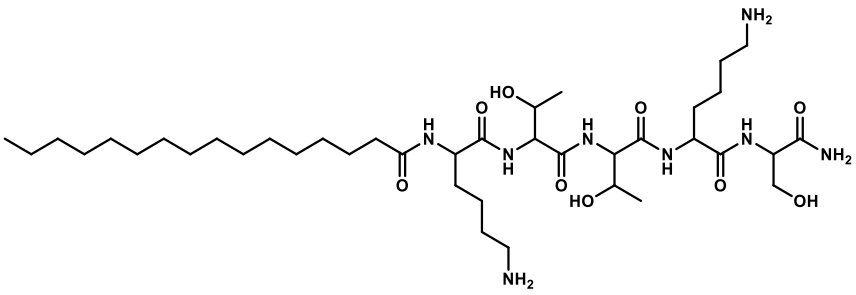

Resin: Fmoc Rink Amide AM (500mg, loading 0.62 mmol/g)

Manual synthesis: SWELL, Fmoc-Ser(tBu)-OH COUPLING, FMOC DEP, Fmoc-Lys(Boc)-OH COUPLING, FMOC DEP, Fmoc-Thr(tBu)-OH COUPLING, FMOC DEP, Fmoc-Thr(tBu)-OH COUPLING, FMOC DEP, Fmoc-Lys(Boc)-OH COUPLING, FMOC DEP

- Half of the resin for peptide **4b**: CLEAVAGE
- Half of the resin for peptide **4c**: Palmitic acid COUPLING **x2**, CLEAVAGE.

Purity **4b**: 96.4%

Purity **4c**: 97.1%

Peptide 4d and 4e

4d)

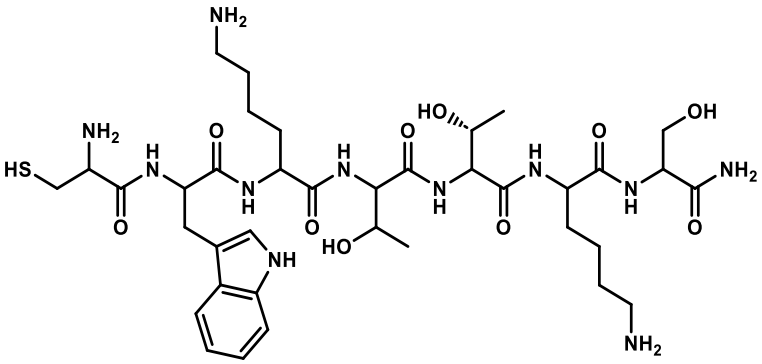

4e)

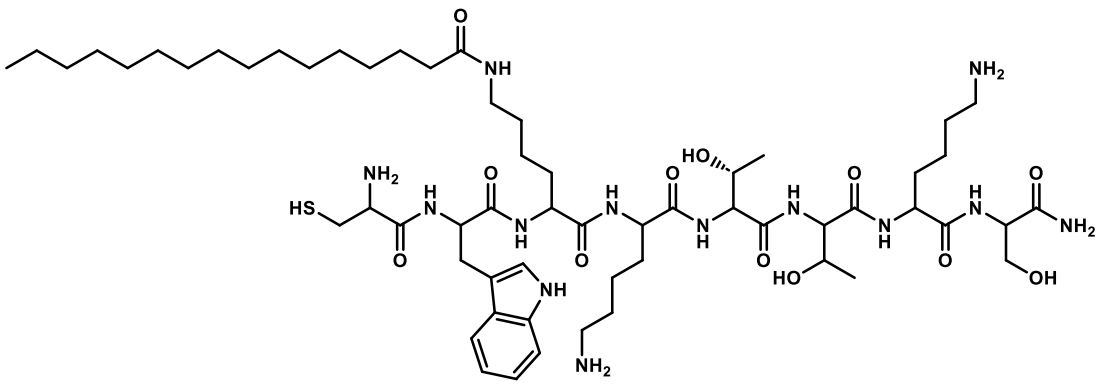

Resin: Fmoc Rink Amide AM (500mg, loading 0.62 mmol/g)

Manual synthesis: SWELL, Fmoc-Ser(tBu)-OH COUPLING, FMOC DEP, Fmoc-Lys(Boc)-OH COUPLING, FMOC DEP, Fmoc-Thr(tBu)-OH COUPLING, FMOC DEP, Fmoc-Thr(tBu)-OH COUPLING, FMOC DEP, Fmoc-Lys(Boc)-OH COUPLING, FMOC DEP,

- Half of the resin for peptide **4d**: Fmoc-Trp(Boc)-OH COUPLING, FMOC DEP, Fmoc-Cys(Trt)-OH COUPLING, FMOC DEP, CLEAVAGE
- Half of the resin for peptide **4d**: Fmoc-Lys(Pal)-OH COUPLING **x2**, FMOC DEP, Fmoc-Trp(Boc)-OH COUPLING, FMOC DEP, Fmoc-Cys(Trt)-OH COUPLING, FMOC DEP, CLEAVAGE

Purity **4d**: 89.6%

Purity **4e**: 85.8%

Peptide 4f

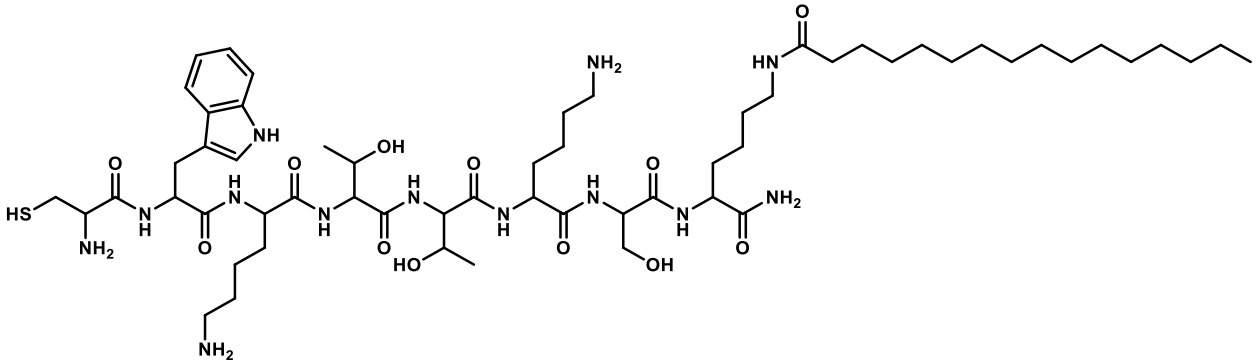

Resin: Fmoc Rink Amide AM (200mg, loading 0.62 mmol/g)

Manual synthesis: SWELL, Fmoc-Lys(Pal)-OH COUPLING **x2**, FMOC DEP, Fmoc-Ser(tBu)-OH COUPLING, FMOC DEP, Fmoc-Lys(Boc)-OH COUPLING, FMOC DEP, Fmoc-Thr(tBu)-OH COUPLING, FMOC DEP, Fmoc-Thr(tBu)-OH COUPLING, FMOC DEP, Fmoc-Lys(Boc)-OH COUPLING, FMOC DEP, Fmoc-Trp(Boc)-OH COUPLING, FMOC DEP, Fmoc-Cys(Trt)-OH COUPLING, FMOC DEP, CLEAVAGE

Purity **4f**: 86.7%

2.4.3 Cotton Modification

CHO grafting on cotton

Cotton (5g) was added to a solution of 20U of laccase per gram of material (0.84 U/mg, 123.2 mg) and 8% m/m_{cot} of TEMPO (414.2mg) in a sodium acetate/acetic acid buffer (pH 5, 50mM) and stirred for 1 day. The course of the reaction was followed by checking the color of cotton upon Schiff's reagent addition. Then, cotton was removed from the reaction, washed 5 times with water and methanol (with added sonication), and stored in the desiccator up to further use.

Norbornene grafting on cotton

The reaction of cotton and carbic anhydride was tested using around 20mg of cotton in the following conditions:

Solvent	Carbic anhydride	Time	KOH	FT-IR
DMF	5eq	3h	-	No difference with cotton
	5eq (1.6eq every 30 min)	3h	-	No difference with cotton
DMSO	8eq	30min	0.015M	New peaks at 1722, 1630 and 1560 cm^{-1}
	4eq	30min	0.015M	New peaks at 1722, 1630 and 1560 cm^{-1}. Less defined than with 8eq
	2eq	30min	0.015M	New peaks at 1722, 1630 and 1560 cm^{-1}. Less defined than with 8eq

Table 2.16*: Tested conditions for the norbornene grafting on cotton. FT-IR spectra reported in Chapter 5.2.4.*

After the reaction, cotton was washed 5 times with the solvent, water (when was not the solvent) and acetone. The textile was kept stored under vacuum at 37°C.

The bigger batches of cotton were prepared using the following conditions:

NOR-cotton 1: cotton (750mg) was added to a solution of 2eq of carbic anhydride and 1.4mL of 0.1M KOH to DMSO (18mL). After 30min cotton was removed from the solution and washed 3 times with DMSO, 3 times with acetone and 9 times with water (with added sonication). The textile was stored under vacuum at 37°C.

NOR-cotton 2: cotton (500mg) was added to the carbic anhydride solution of *reaction 1*. After 1 day of stirring, cotton was removed from the solution and washed 3 times with DMSO, 3 times with acetone and 9 times with water (with added sonication). The textile was stored under vacuum at 37°C.

NOR-cotton 3: cotton (750mg) was added to 10mL of DMSO and 0.5mL of 0.3M KOH. Every 30min 0.025eq of fresh carbic anhydride in DMSO were added to the solution, up to 2eq total. After 1 day of stirring, cotton was removed from the solution and washed 3 times with DMSO, 3 times with acetone and 9 times with water (with added sonication). The textile was stored under vacuum at 37°C.

Cotton titration

Blank measure: 3ml of 0.1M HCl were added to 100mL of 0.5M NaCl and titrated with 0.01M NaOH. The measure was repeated three times.

Quantification COOH: a piece of cotton or modified cotton (around 300 mg) was stirred for 15min in a solution of 0.1M HCl. Then, the material was washed until neutrality, added to 100mL of 0.5M NaCl, and titrated with 0.01M NaOH. The procedure was performed three times.

Quantification of CHO: a piece of cotton or CHO-cotton (around 300 mg) was stirred in a 0.2M $NaClO_2$ solution in 5M acetic acid. After 2 days CHO-cotton was washed 5 times with water and acetone, and kept in the desiccator up to further use. Then, the titration procedure was the same as described above.

Sample	Cotton mass (mg)	V of NaOH (mL)	COOH loading (mmol//g_{cot})	Mean ± error (mmol//g_{cot})
Blank	-	6.20	-	-
Blank	-	6.20	-	-
Blank	-	6.20	-	-
Cotton	313.2	6.95	0.024	0.025 ± 0.001
Cotton	300.2	7.00	0.027	
Cotton	336.0	7.05	0.025	
$NaClO_2$ treated cotton	341.2	7.05	0.025	0.025 ± 0.0005
$NaClO_2$ treated cotton	340.8	7.05	0.025	
$NaClO_2$ treated cotton	328.6	7.05	0.026	
CHO-cotton	308.1	7.65	0.047	0.048 ± 0.003
CHO-cotton	322.0	7.65	0.045	
CHO-cotton	339.6	7.95	0.052	
$NaClO_2$ treated CHO-cotton	356.1	10.40	0.118	0.123 ± 0.010
$NaClO_2$ treated CHO-cotton	308.9	10.40	0.136	
$NaClO_2$ treated CHO-cotton	348.9	10.25	0.116	

***Table 2.17**: **results from the titration of CHO-cotton**. Unmodified cotton used as the control. NaOH used in a concentration of 0.01M (Normex). The volume of NaOH needed to reach the turning point was calculated from the second derivative of the titration curve. The error was calculated as the maximum semi-dispersion.*

Sample	Cotton mass (mg)	V of NaOH (mL)	COOH loading (mmol//g_{cot})	Mean ± error (mmol//g_{cot})
Blank	-	6.45	-	-
Blank	-	6.45	-	
Blank	-	6.46	-	
Cotton	336.4	7.45	0.028	0.030 ± 0.003
Cotton	329.1	7.48	0.029	
Cotton	362.1	7.75	0.033	
NOR-cotton 1	268.1	8.15	0.059	0.058 ± 0.002
NOR-cotton 1	238.4	7.96	0.059	
NOR-cotton 1	238.3	7.87	0.055	
NOR-cotton 2	197.2	7.10	0.030	0.032 ± 0.003

NOR-cotton 2	265.8	7.50	0.035	
NOR-cotton 3	252.0	8.40	0.071	0.081 ± 0.005
NOR-cotton 3	261.1	9.00	0.090	
NOR-cotton 3	233.6	8.52	0.081	

***Table 2.18**: **results from the titration of NOR-cotton.** Unmodified cotton used as the control. NaOH used in a concentration of 0.01M (Normex). The volume of NaOH needed to reach the turning point was calculated from the second derivative of the titration curve. The error was calculated as the maximum semi-dispersion.*

2.4.4 Peptide-Cotton Conjugation

Thiazolidine & Oxime

Peptide loading calculation:

- Initial and final concentration of Trp (and thus of the peptide) in solution calculated as $C = A\ \varepsilon \cdot l$, where l is the optical path, C is the concentration, A the absorbance, ε the extinction coefficient of Trp (assumed 5630 $M^{-1}cm^{-1}$)[67]
- Considering $\Delta C = Ci - Cf$; where C_i is the concentration of peptide in solution before the addition of cotton and C_f is the concentration of the last measure.
- n $bound{-}peptide = \Delta C \cdot V$; where V is the volume of the solution used for the reaction.
- Peptide loading is calculated as $\frac{\text{nbound}-\text{peptide (mmol)}}{\text{mCotton (g)}}$

*Conjugation to **1a** and **1b***: the peptide and 1eq of TCEP (with respect to the peptide) were dissolved in 20 mL of sodium acetate/ acetic acid buffer (50mM, pH 4.5). Unmodified cotton was added to 10mL of the solution, and CHO-cotton was added to the rest. The concentration of peptide in solution was checked overtime by UV-Vis at 280nm. After 1 day, the textiles were removed from solution, washed five times with water and five times with acetone. The materials were stored in the desiccator.

	Sample	Cotton mass (mg)	Peptide exc (mmol/gcot)	Peptide conc (mM)	Reaction time	Peptide loading (mmol/gcot)
r1	Cotton + **1a**	9.0	0.80	0.72	1day	0.01
r2	CHO-Cotton + **1a**	10.5	0.69	0.72	1day	0.08
r3	Cotton + **1b**	10.0	0.76	0.77	1day	0.004
r4	CHO-Cotton + **1b**	10.1	0.77	0.77	1day	0.09

***Table 2.19**: Reaction conditions for the conjugation of peptides **1a** and **1b**.*

*Conjugation to **2a, 2c, 3b** and **4d***: the peptide and 1eq of TCEP (with respect to the peptide) were dissolved in a sodium acetate/ acetic acid buffer (50mM, pH 4.5) in a concentration of around 0.7mM. Unmodified cotton was added to half of the solution, and CHO-cotton was added to the rest. The concentration of peptide in solution was checked overtime by UV-Vis at 280nm. After 3 days, the textiles were removed from solution, washed five times with water and five times with acetone. The materials were stored in the desiccator.

	Sample	Cotton mass (mg)	Peptide exc (μmol/gcot)	Peptide conc (mM)	Reaction time	Peptide loading (μmol/gcot)
r5	Cotton + **2a**	101.8	50.0	0.68	3 days	3.0
r6	CHO-Cotton + **2a**	112.7	45.1	0.68	3 days	7.1
r7	Cotton + **2c**	99.6	50.8	0.67	3 days	4.2
r8	CHO-Cotton + **2c**	102.6	49.3	0.67	3 days	11.4
r9	Cotton + **3b**	60.5	61.7	0.83	3 days	14.8
r10	CHO-Cotton + **3b**	60.1	62.1	0.83	3 days	18.6
r11	Cotton + **4d**	105.6	132.2	0.69	3 days	10.4
r12	CHO-Cotton + **4d**	106.3	131.3	0.69	3 days	38.0

Table 2.20*: Reaction conditions for the conjugation of peptides **2a, 3b** and **4d**.*

Multiple conjugations: The reactions were performed similarly to what is described in the previous paragraph:

- Peptide **2a** and 1eq of TCEP (with respect to the peptide) were dissolved in 100mL of sodium acetate/ acetic acid buffer (50mM, pH 4.5) in a concentration of around 0.07mM. Unmodified cotton was added to 3mL of **2a** solution, and CHO-cotton was added to the rest.
- Peptide **3b** and 1eq of TCEP (with respect to the peptide) were dissolved in 63mL of sodium acetate/ acetic acid buffer (50mM, pH 4.5) in a concentration of around 0.07mM. Unmodified cotton was added to 3mL, CHO-cotton was added to 20mL and **r14** cotton was added to 40mL of **3b** solution.
- Peptide **4d** and 1eq of TCEP (with respect to the peptide) were dissolved in 33mL of sodium acetate/ acetic acid buffer (50mM, pH 4.5) in a concentration of around 0.6mM. Unmodified cotton was added to 3mL, CHO-cotton was added to 10mL and **r14** cotton was added to 20mL of **4d** solution.

After the all reactions, textiles were removed from solution, washed five times with water and five times with acetone. The materials were stored in the desiccator.

	Sample	Cotton mass (mg)	Peptide exc (μmol/gcot)	Peptide conc (mM)	Reaction time	Peptide loading (μmol/gcot)
r13	Cotton + **2a**	14.9	13.8	0.069	3days	1.5
r14	CHO-Cotton + **2a**	501.2	13.3	0.069	3days	3.5
r15	Cotton + **3b**	17.1	17.1	0.073	2days	8.0
r16	CHO-cotton + **3b**	111.6	13.1	0.073	2days	9.4
r17	**r14** + **3b**	166.7	17.6	0.073	2days	8.2
r18	Cotton + **4d**	27.7	57.8	0.64	2days	8.6
r19	CHO-cotton + **4d**	110.9	57.8	0.64	2days	30.7
r20	**r14** + **4d**	173.0	37.0	0.64	2days	21.3

Table 2.21: *Reaction conditions for the double functionalized cottons*

Thiol-norbornene

NOR-cotton 3 or unmodified cotton were added to a 0.8 mM solution of peptide **2a** or **2b** (1eq with respect to the moles of norbornene) and 0.4% VA-086 in water. The solution was stirred and irradiated with light of 365nm and 10mW microwaves for 5min. Then, cotton was retrieved from the solution, washed 5 times with water and kept under vacuum at 37°C. The peptide/photoinitiator solution was used for nine independent reactions with nine *NOR-cotton 3* weighted pieces of around 15 mg, and nine independent control reactions with nine unmodified cotton pieces of around 15mg.

As an ulterior control, *NOR-cotton 3* was added to a 0.8 mM solution of peptide without the photoinitiator. The solution was stirred for 5 min. Then, cotton was retrieved from the solution, washed 5 times with water and kept under vacuum at 37°C.

2.4.5 Amino Acid Analysis

Sample preparation

6M HCl was added to weighted samples of the materials as per Table 2.22. The samples were stirred at 120°C for 24h. Then, the solved was removed by rotavap, and the solvents were sent to the University of Barcelona for the AAA.

	Description	**Mass (mg)**	**Volume of 6M HCl + 10%phenol (µL)**
-	Cotton	4.33	200
-	NOR-cotton	4.93	200
r21	Cotton + **2a**	4.74	200
r22	NOR-cotton + **2a**	4.35	200
r23	NOR-cotton + **2a** – NO UV/mW	5.43	400
r24	Cotton + **2b**	4.51	400
r25	NOR-cotton + **2b**	4.47	400
r26	NOR-cotton + **2b** – NO UV/mW	4.35	400

Table 2.22*: Preparation of the samples of AAA.*

Amino acid analysis

1000 µL of 20 mM HCl was added to the tubes containing the hydrolyzed residue except for those corresponding to samples **r23** and **r28**, which were added to 1500 and 600 µL, respectively. The samples were subsequently shaken for 24 h on an orbital shaker and sonicated in an ultrasonic bath. The solutions were filtered through a PVDF syringe filter (0.45 µm). Finally, dilutions of these samples were prepared in HPLC-grade water, adding norleucine and 2.5 mM α-aminobutyric acid (AABA) as internal standards. An aliquot of the final solution was derivatized with 6-aminoquinolyl-N-hydroxysuccinimidyl

carbamate according to the Waters AccQ-Tag method. The derivatized amino acids were analyzed by HPLC with UV detection (λ = 254 nm).

Instrument: HPLC (WATERS 600 with detector WATERS 2487).

References

1 Granados, A., Pleixats, R. & Vallribera, A. Recent Advances on Antimicrobial and Anti-Inflammatory Cotton Fabrics Containing Nanostructures. *Molecules (Basel, Switzerland)* **26**, 3008, doi:10.3390/molecules26103008 (2021).

2 Gpyal, S., Khot, S. C., Ramachandran, V., Shah, K. P. & Musher, D. M. Bacterial Contamination of Medical Providers' White Coats and Surgical Scrubs: A Systematic Review. *American Journal of Infection Control* **47**, 994-1001 (2019).

3 Fang, D. D. Cotton Fiber: Physics, Chemistry and Biology. *Book* (2018).

4 P.J., W. *et al.* Cotton Fiber: Chemistry and Technology. *Book* (2006).

5 Pinho, E. & Soares, G. Functionalization of Cotton Cellulose for Improved Wound Healing. *J Mater Chem B* **6**, 1887-1898 (2018).

6 Klemm, D., Heublein, B., Fink, H. & Bohn, A. Cellulose: Fascinating Biopolymer and Sustainable Raw Material. *Polymer science* **44**, 3358-3393 (2005).

7 Li, T. *et al.* Developing Fibrillated Cellulose as a Sustainable Technological Material. *Nature* **590**, 47-56 (2020).

8 Haigler, C. H., Betancur, L., Stiff, M. R. & J.R., T. Cotton Fiber: a Powerfull Single-cell Model for Cell Wall and Cellulose Research *Frontiers in plant science* **3** (2012).

9 Aracri, E., Valls, C. & Vidal, T. Paper strength improvement by oxidative modification of sisal cellulose fibers with laccase–TEMPO system: influence of the process variables. *Carbohydrate polymers* **88**, 830-837 (2012).

10 Cumpstey, I. Chemical modification of polysaccharides. *International scholarly research notices* **2013**, 417672 (2013).

11 Pierre, G. *et al.* TEMPO-mediated oxidation of polysaccharides: An ongoing story. *Carbohydrate polymers* **165**, 71-85 (2017).

12 Potthast, A., Kostic, M., Schiehser, S., Kosma, P. & Rosenau, T. Studies on oxidative modifications of cellulose in the periodate system: Molecular weight distribution and carbonyl group profiles. (2007).

13 Potthast, A., Schiehser, S., Rosenau, T. & Kostic, M. Oxidative modifications of cellulose in the periodate system–Reduction and beta-elimination reactions 2nd ICC 2007, Tokyo, Japan, October 25–29, 2007. (2009).

14 Nypelö, T., Berke, B., Spirk, S. & Sirviö, J. A. Periodate oxidation of wood polysaccharides—Modulation of hierarchies. *Carbohydrate Polymers* **252**, 117105 (2021).

15 Scapin, S. *et al.* Sustainable, Site-Specific Linkage of Antimicrobial Peptides to Cotton Textiles. *Macromolecular bioscience* **20**, 2000199 (2020).

16 Semmelhack, M. F., Chou, C. S. & Cortes, D. A. Nitroxyl-mediated Electrooxidation of Alcohols to Aldehydes and Ketones. *Journal of the American Chemical Society* **105**, 4492-1194 (1983).

17 Coseri, S. *et al.* Oxidized Cellulose—Survey of the Most Recent Achievements. *Carbohyd Polym* **93**, 207-215 (2013).

18 Jiang, J. *et al.* Rate-Limited Reaction in TEMPO/Laccase/O2 Oxidation of Cellulose. *Macromolecular rapid communications* **42** (2021).

19 Viikari, L., Kruus, K. & Buchert, J. Method for Modification of Cellulose. *European Pat WO9923117* (2000).

20 Tromp, S. A. *et al.* Mechanism of Laccase–TEMPO-Catalyzed Oxidation of Benzyl Alcohol. *chemical catalysis* **2**, 827-833 (2010).

21 Aracri, E., Valls, C. & Teresa, V. Paper Strength Improvement by Oxidative Modification of Sisal Cellulose Fibers with Laccase–TEMPO System: Influence of the Process Variables. *Carbohyd Polym* **88**, 830-837 (2012).

22 Kunamneni, A. *et al.* Engineering and Applications of Fungal Laccases for Organic Synthesis. *Microbial Cell Factory* **7** (2008).

23 Aracri, E. & Vidal, T. Enhancing the Effectiveness of a Laccase–TEMPO Treatment has a Biorefining Effect on Sisal Cellulose Fibres. *Cellulose* **19**, 867-877 (2012).

24 Jones, S. M. & Solomon, E. I. Electron Transfer and Reaction Mechanism of Laccases. *Cellular and Molecular Life Science* **75**, 869-883 (2015).

25 Arends, I. W. C. E., Li, Y. & Sheldon, R. A. Stabilities and Rates in the Laccase/TEMPO Catalyzed Oxidation of Alcohols. *Biocatalysis and Biotransformation* **24**, 443-448 (2006).

26 Sheldon, R. A. & van Pelt, S. Enzyme Immobilisation in Biocatalysis: Why, What and How. *Chemical Society Reviews* **42**, 6223-6235 (2013).

27 Coseri, S. *et al.* Oxidized cellulose—Survey of the most recent achievements. *Carbohydrate polymers* **93**, 207-215 (2013).

28 Long, J., Li, Z. & Zhong, T. Fabrication of clickable bamboo-sourced cellulose nanofibrils for diverse surface modifications: Hydrophobicity and fluorescence functionalities. *Carbohydrate Polymers* **348**, 122786 (2025).

29 Dadoo, N., Zeitler, S., McGovern, A. D. & Gramlich, W. M. Waterborne functionalization of cellulose nanofibrils with norbornenes and subsequent thiol-norbornene gelation to create robust hydrogels. *Cellulose* **28**, 1339-1353 (2021).

30 Fein, K., Bousfield, D. W. & Gramlich, W. M. The influence of versatile thiol-norbornene modifications to cellulose nanofibers on rheology and film properties. *Carbohydrate polymers* **230**, 115672 (2020).

31 McOscar, T. V. & Gramlich, W. M. Hydrogels from norbornene-functionalized carboxymethyl cellulose using a UV-initiated thiol-ene click reaction. *Cellulose* **25**, 6531-6545 (2018).

32 Dadoo, N. *Chemically Cross-Linked Polysaccharide-Based Hydrogels via Thiol-Norbornene Reaction as Sustainable Biomaterials*. (The University of Maine, 2018).

33 Bao, B. *et al.* A novel and durable photochromic cotton-based fabric prepared via thiol-ene click chemistry. *Dyes and Pigments* **171**, 107778 (2019).

34 Zhang, G., Ross, C. & Blecha, F. Porcine antimicrobial peptides: new prospects for ancient molecules of host defense. *Veterinary Research* **31**, 277-296 (2000).

35 Storici, P., Scocchi, M., Tossi, A., Gennaro, R. & Zanetti, M. Chemical synthesis and biological activity of a novel antibacterial peptide deduced from a pig myeloid cDNA. *FEBS letters* **337**, 303-307 (1994).

36 Tossi, A., Scocchi, M., Zanetti, M., Storici, P. & Gennaro, R. PMAP-37, a novel antibacterial peptide from pig myeloid cells: cDNA cloning, chemical synthesis and activity. *European Journal of Biochemistry* **228**, 941-946 (1995).

37 Zanetti, M., Storici, P., Tossi, A., Scocchi, M. & Gennaro, R. Molecular cloning and chemical synthesis of a novel antibacterial peptide derived from pig myeloid cells. *Journal of Biological Chemistry* **269**, 7855-7858 (1994).

38 Zhou, J. *et al.* Antimicrobial activity of the antibacterial peptide PMAP-36 and its analogues. *Microbial pathogenesis* **136**, 103712 (2019).

39 Lyu, Y., Yang, Y., Lyu, X., Dong, N. & Shan, A. Antimicrobial activity, improved cell selectivity and mode of action of short PMAP-36-derived peptides against bacteria and Candida. *Scientific reports* **6**, 27258 (2016).

40 Scocchi, M. *et al.* Structural aspects and biological properties of the cathelicidin PMAP-36. *The FEBS journal* **272**, 4398-4406 (2005).

41 Balhuizen, M. D. *et al.* PMAP-36 reduces the innate immune response induced by Bordetella bronchiseptica-derived outer membrane vesicles. *Current Research in Microbial Sciences* **2**, 100010 (2021).

42 Scheenstra, M. R. *et al.* Cathelicidins PMAP-36, LL-37 and CATH-2 are similar peptides with different modes of action. *Scientific Reports* **9**, 4780 (2019).

43 Biondi, B. *et al.* Structural and biological characterization of shortened derivatives of the cathelicidin PMAP-36. (2023).

44 Lv, Y. *et al.* Antimicrobial properties and membrane-active mechanism of a potential α-helical antimicrobial derived from cathelicidin PMAP-36. *PloS one* **9**, e86364 (2014).

45 Schivo, A. Analoghi peptidici delle catelicidine PMAP-36 e BMAP-27: relazione struttura-attività e studi di stabilità. *Master Thesis, University of Padova* (2023).

46 Albini, F. *et al.* Fragments of cathelicidins PMAP-36 and BMAP-27 and their D-enantiomers: Effects of all D substitutions on structure, protease resistance and antimicrobial properties. *Bioorganic Chemistry*, 108715 (2025).

47 Makovitzki, A., Avrahami, D. & Shai, Y. Ultrashort antibacterial and antifungal lipopeptides. *Proceedings of the National Academy of Sciences* **103**, 15997-16002 (2006).

48 Makovitzki, A., Viterbo, A., Brotman, Y., Chet, I. & Shai, Y. Inhibition of fungal and bacterial plant pathogens in vitro and in planta with ultrashort cationic lipopeptides. *Applied and environmental microbiology* **73**, 6629-6636 (2007).

49 Vallon-Eberhard, A. *et al.* Efficient clearance of Aspergillus fumigatus in murine lungs by an ultrashort antimicrobial lipopeptide, palmitoyl-lys-ala-DAla-lys. *Antimicrobial agents and chemotherapy* **52**, 3118-3126 (2008).

50 Orlandin, A. *et al.* Covalent graft of lipopeptides and peptide dendrimers to cellulose fibers. *Coatings* **9**, 606 (2019).

51 Orlandin, A. Innovative antimicrobial textiles based on natural fibers functionalized with peptaibiotics. *PhD Thesis, University of Padova* (2015).

52 Aycock, R., Raghow, R., Stricklin, G. P., Seyer, J. M. & Kang, A. H. Post-transcriptional inhibition of collagen and fibronectin synthesis by a synthetic homolog of a portion of the carboxyl-terminal propeptide of human type I collagen. *Journal of Biological Chemistry* **261**, 14355-14360 (1986).

53 Katayama, K., Seyer, J. M., Raghow, R. & Kang, A. H. Regulation of extracellular matrix production by chemically synthesized subfragments of type I collagen carboxy propeptide. *Biochemistry* **30**, 7097-7104 (1991).

54 Katayama, K., Armendariz-Borunda, J., Raghow, R., Kang, A. & Seyer, J. A pentapeptide from type I procollagen promotes extracellular matrix production. *Journal of Biological Chemistry* **268**, 9941-9944 (1993).

55 Abu Samah, N. H. & Heard, C. M. Topically applied KTTKS: a review. *International journal of cosmetic science* **33**, 483-490 (2011).

56 Tsai, W. C. *et al.* The pentapeptide KTTKS promoting the expressions of type I collagen and transforming growth factor-β of tendon cells. *Journal of Orthopaedic Research* **25**, 1629-1634 (2007).

57 Lintner, K. (Google Patents, 2003).

58 Lintner, K. Promoting production in the extracellular matrix without compromising barrier. *Cutis* **70**, 13-23 (2002).

59 Jones, R. R., Castelletto, V., Connon, C. J. & Hamley, I. W. Collagen stimulating effect of peptide amphiphile C16–KTTKS on human fibroblasts. *Molecular pharmaceutics* **10**, 1063-1069 (2013).

60 Castelletto, V., Hamley, I. W., Perez, J., Abezgauz, L. & Danino, D. Fibrillar superstructure from extended nanotapes formed by a collagen-stimulating peptide. *Chemical Communications* **46**, 9185-9187 (2010).

61 Choi, Y. L., Park, E. J., Kim, E., Na, D. H. & Shin, Y.-H. Dermal stability and in vitro skin permeation of collagen pentapeptides (KTTKS and palmitoyl-KTTKS). *Biomolecules & therapeutics* **22**, 321 (2014).

62 Fu, J. *et al.* A randomized, controlled comparative study of the wrinkle reduction benefits of a cosmetic niacinamide/peptide/retinyl propionate product regimen vs. a prescription 0· 02% tretinoin product regimen. *British Journal of Dermatology* **162**, 647-654 (2010).

63 Robinson, L. *et al.* Topical palmitoyl pentapeptide provides improvement in photoaged human facial skin 1. *International journal of cosmetic science* **27**, 155-160 (2005).

64 Kachooeian, M. *et al.* Matrixyl patch vs matrixyl cream: a comparative in vivo investigation of matrixyl (MTI) effect on wound healing. *ACS omega* **7**, 24695-24704 (2022).

65 Park, H., An, E. & Lee, A.-R. C. Effect of Palmitoyl-Pentapeptide (Pal-KTTKS) on Wound Contractile Process in Relation with Connective Tissue Growth Factor and a-Smooth Muscle Actin Expression. *Tissue Engineering and Regenerative Medicine* **14**, 73-80 (2017).

66 Albini, F., Biondi, B., Lastella, L. & Peggion, C. Oxime and thiazolidine chemoselective ligation reactions: a green method for cotton functionalization. *Cellulose* **30**, 5573-5587 (2023).

67 Pace, C. N., Vajdos, F., Fee, L., Grimsley, G. & Gray, T. How to measure and predict the molar absorption coefficient of a protein. *Protein science* **4**, 2411-2423 (1995).
68 Kaiser, E., Colescott, R. L., Bossinger, C. D. & Cook, P. Color test for detection of free terminal amino groups in the solid-phase synthesis of peptides. *Analytical biochemistry* **34**, 595-598 (1970).
69 Mezö, G. *et al.* Efficient synthesis of an (aminooxy) acetylated-somatostatin derivative using (aminooxy) acetic acid as a 'carbonyl capture'reagent. *Journal of Peptide Science* **17**, 39-46 (2011).
70 Peggion, C. *et al.* Synthesis and Biological Activity of Ultrashort Antimicrobial Peptides Bearing a Non-Coded Amino Acid. *Journal of Peptide Science* **31**, e70021 (2025).
71 Albini, F. Study of the cellulose-peptide conjugation for the development of antimicrobial cotton textiles. *Master Thesis, University of Padova* (2022).
72 Saito, T. & Isogai, A. Introduction of aldehyde groups on surfaces of native cellulose fibers by TEMPO-mediated oxidation. *Colloids and Surfaces A: Physicochemical and Engineering Aspects* **289**, 219-225 (2006).
73 Alves, P. M. *et al.* Thiol–norbornene photoclick chemistry for grafting antimicrobial peptides onto chitosan to create antibacterial biomaterials. *ACS Applied Polymer Materials* **4**, 5012-5026 (2022).
74 Topalovic, T. *et al.* XPS and contact angle study of cotton surface oxidation by catalytic bleaching. *Colloids and Surfaces A: Physicochemical and Engineering Aspects* **296**, 76-85 (2007).
75 Atherton, E. *et al.* A mild procedure for solid phase peptide synthesis: use of fluorenylmethoxycarbonylamino-acids. *Journal of the Chemical Society, Chemical Communications*, 537-539 (1978).

Chapter III:

Bi-functional Chitosan: an Orthogonal Approach to Peptide Grafting

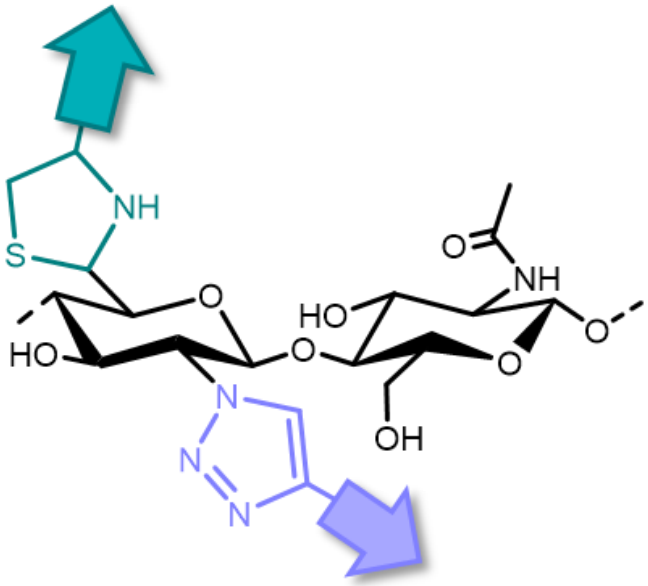

Acknowledgements:

- Dr. Paula Parreira for the antimicrobial tests on the peptide-chitosan conjugates
- Prof. Antonella Glisenti for the XPS measurements and data analysis
- Prof. Paula Gomes and Prof. Cristina Martins for hosting me in their laboratories during my research period at the University of Porto
- Dr. Ana Gomes for tutoring me during my research period at the University of Porto
- European Peptide Society (EPS) for funding my research period at the University of Porto

3.1 Introduction

The use of chitosan in the context of wound healing is widely studied[1-3]. In fact, the biopolymer presents most of the characteristics of the ideal wound dressing material: beside being biodegradable and non-toxic, it is intrinsically antibacterial and hemostatic, but it is also suitable for large scale production and easy to handle. In addition, the presence of different reactive moieties on the N-glucosamine monomer of chitosan, enables multiple functionalization of the biopolymer. Thus, it represents an interesting solution for the delivery of peptides to the wound site by covalent conjugation.

This chapter is a continuation of the work started by *Barbosa et al*.[4,5] on the functionalization of chitosan with an antibacterial peptide by azide-alkyne copper (I) catalyzed chemoselective ligation (*Chapter 1.4.4*). In particular, the azide-alkyne reaction is investigated with a different peptide, the collagen regenerative **PP4** (H-KTTKS-NH_2), and the thiazolidine bond is employed for the conjugation of the broad-spectrum antibacterial peptide **3.1** to chitosan. In addition, the two peptides will be conjugated to the same chitosan to form a double functionalized material for the treatment of wounds.

3.1.1 Chitosan

Chitosan is a natural polysaccharide found in some fungi, and is a linear polymer composed mainly of N-D-glucosamine, and partially of N-acetylglucosamine, liked by glycosidic $\beta(1,4)$ bonds (Fig. 3.1). Chitosan is commercially produced by the chemical deacetylation of chitin, which is recovered from the exoskeleton of crustaceans[6]. Chitosan is distinguished from chitin by its higher solubility in diluted acids, and is always characterized by its degree of deacetylation (DD)[7].

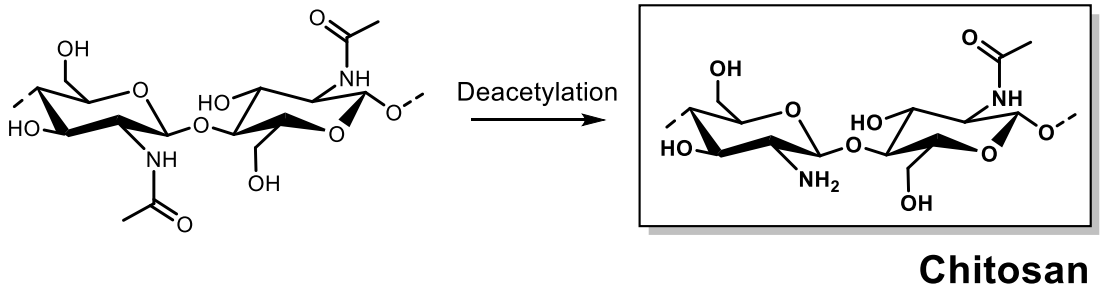

***Figure 3.1**: Schematic representation of the deacetylation of chitin to produce chitosan. Depending on the degree of deacetylation (DD) of chitosan the amount of N-acetylglucosamine units vary.*

The cationic nature of chitosan makes it a great material for treating skin lesions. In fact, its positive charges can either interact with the negative charges present on the bacterial cell walls or the erythrocytes present at the wound site. This gives the polymer both antibacterial and hemostatic properties[8-10]. The interaction with the bacterial cell wall induces a leakage of components from bacterial cells and thus cell death[9]. Conversely, the interaction with erythrocytes induces coagulation,

without activating the intrinsic pathway, by creating a mucoadhesive barrier at the wound site[8]. Interestingly, the antibacterial activity of the polysaccharide depends on several factors, such as the molecular weight, the DD, the concentration, the pH, but even the source[9]. In particular, chitosans with higher DD demonstrates higher antibacterial activity. In addition, the pH plays a fundamental role because at pH higher than 6.3 the amine cannot be protonated and form a positive charge. On the other hand, at present, there is not a definitive correlation between the antibacterial activity and the molecular weight[10].

In vitro analysis of chitosan did not reveal any acute cytotoxicity for the polymer. Animal studies on chitosan allowed to classify the polymer as safe for food application, and as a safe pharmaceutical excipient for parenteral route. Furthermore, the few studies on humans show no toxic effects[11]. In addition, some reports suggest that chitosan has a slight anti-inflammatory activity given by its *N*-acetylglucosamine units[10], and seems to induce wound healing by enhancing vascularization at the wound site[2]. Overall, chitosan is a very promising material to use for skin healing applications, due to its antibacterial and hemostatic effects, as well as its biodegradability, non-toxicity, and biocompatibility[10]. Moreover, since chitin is the second most abundant biopolymer after cellulose[10] and is obtained from sea food waste[6], chitosan is also characterized by relatively low costs of production. The main limitations to its widespread use are the poor solubility and its rigidity and brittleness as a material[8].

Chitosan-peptide conjugates

The *N*-glucosamine repeating unit of chitosan presents an amine at the C_2, a secondary hydroxyl at the C_3 and a primary hydroxyl at the C_6, enabling the modification of the material at three different sites and the consequent conjugation of a wide variety of functionalization agents using different types of chemistry.

In this chapter the focus is on thiazolidine and azide-alkyne chemistry in the context of chitosan-peptide conjugates for wound healing. Thus, the work previously carried out by the group of Prof. Gomes[4,5,12] is of particular interest. In fact, in their first work[12], they managed to chemoselectively bind a PEG-like amino-azide onto a chitosan modified with an alkyne to allow the copper (I) catalyzed azide-alkyne click reaction (CuAAC, *Chapter 1.4.4*). In their following studies[4], they exploited the CuAAC to bind the antibacterial peptide Dhvar5 to chitosan and obtained peptide loading on chitosan of 50μmol/g_{chit}. In this case, the positions of the chemoselective moieties were swapped: the azide was grafted onto chitosan and an alkyne was introduced on the peptide by the use of the unnatural amino acid propargylglycine (Pra) at either the N-terminus or the C-terminus. The amine of chitosan was converted into azide by following the procedure shown by *Castro et al.*[13], where they used the safe-to-handle and commercially available imidazole-1-sulfonyl azide hydrochloride (ISA·HCl) as the diazo-transfer in water mildly alkalinized with potassium carbonate. Given the chitosan's insolubility in basic aqueous medium, the reaction is was performed in heterogeneous conditions.

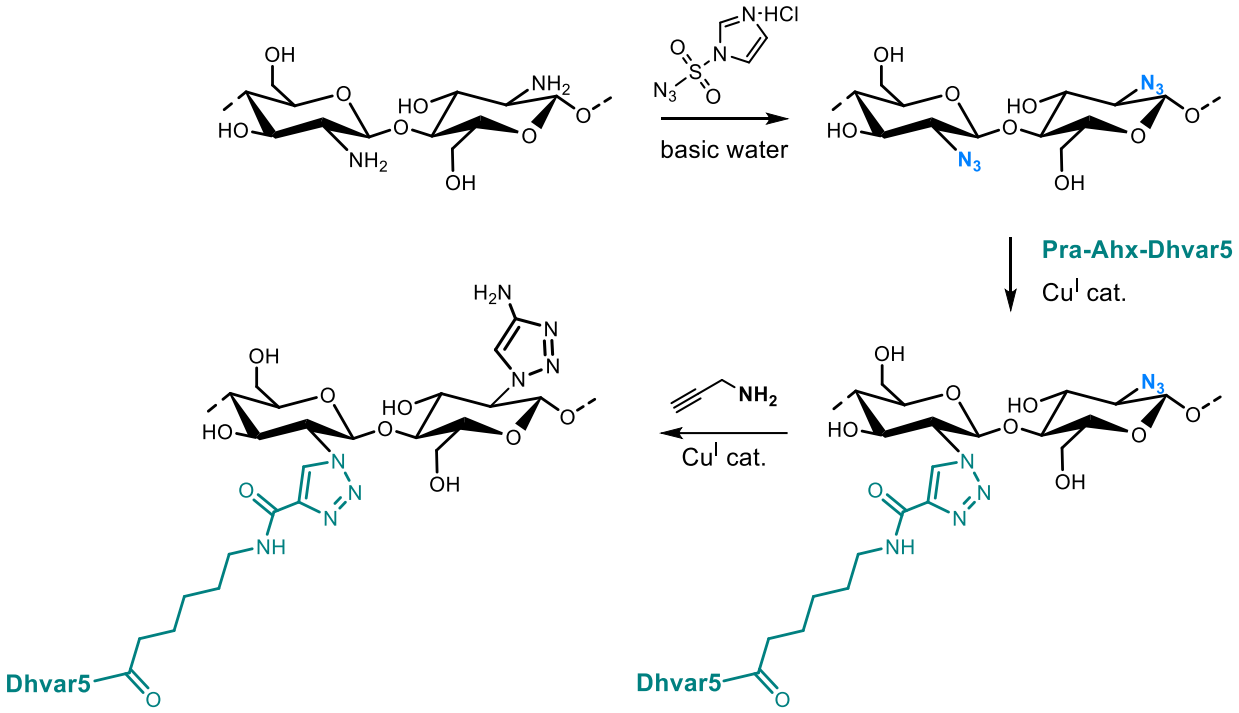

Figure 3.2: *Schematic representation of the peptide-chitosan chemoselective conjugation carried out in the work of Barbosa et al.[4,5]. First the azide was introduced on chitosan by reacting with ISA·HCl following a protocol inspired by the work of Castro et al.[13] Then, the peptides Pra-Ahx-Dhvar5 were conjugated to N_3-chitosan by CuAAC. Finally, the unreacted azides in chitosan were reacted with propargylamine via CuAAC, restoring free primary amines typically present on chitosan matrices.*

Since neither of the Dhvar5-chitosan conjugates exhibit any antibacterial activity in solution, the antibacterial activity was tested on surfaces where the Dhvar5-chitosan conjugates were spin coated. The conjugate with the peptide bound at the C-terminus resulted active against all the tested specis (*S. aureus*, *S. epidermidis*, *E. coli* and *P. aeruginosa*), although the activity against Gram-negative bacteria was primarily due to an inhibition of the bacterial adhesion rather than killing of the adhered cells. Surprisingly, when the peptide was bound at the N-terminus no relevant antibacterial activity was found[5].

Aldehyde grafting on Chitosan

The TEMPO/laccase/O_2 catalyzed system used to introduce the aldehyde required for the thiazolidine reactions in *Chapters 2* and *3*, was explored on chitosan by *da Silva et al.*[14]

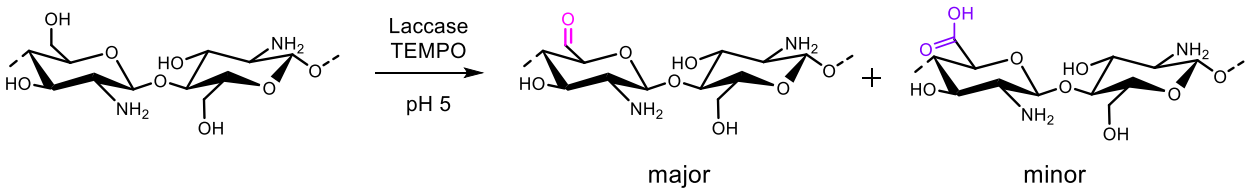

Figure 3.3*: Schematic representation of the products obtained from the TEMPO/laccase/O_2 catalyzed reaction on chitosan.*

Under the reaction conditions employed by these authors (1-70 U/gchit laccase and 1-10%wt TEMPO), they found that in presence of lower amounts of TEMPO and high laccase, low degree of oxidation, short oligomers, and low carbonyl/carboxyl ratio were obtained. Whereas, higher amounts of TEMPO coupled

with a high laccase determined a higher degree of oxidation, larger oligomers, and high carbonyl/carboxyl ratio. Oxidized chitosan produced with this system showed improved solubility in water when acetic acid was used to hydrate the material. On the other hand, when aqueous HCl was used, the aldehydes and the unprotected amines reacted to form an imine, cross-linking the product and allowing the formation a pH dependent hydrogel.

3.1.2 The Peptides

In this chapter, an antibacterial and a collagen-boosting peptide that could work synergically were selected as the active agents to be bound to chitosan. In particular, peptide **3.1** demonstrates promising broad-spectrum antibacterial properties, also in combination with the collagen-boosting peptide **PP4** used in *Chapter 2*.

Peptide 3.1

Kang et al.[15] studied a series of *de novo* synthesized peptides. The idea behind their work was to engineer AMPs structured in perfectly amphiphilic α-helices using the minimum number of amino acids to form the shortest possible chain.

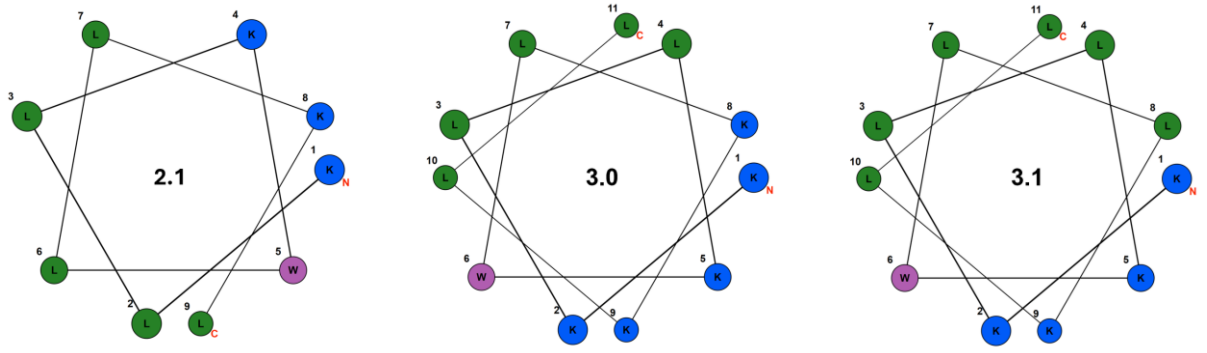

***Figure 3.4**: Helical wheel projection of peptides **2.1**, **3.0** and **3.1** (Table 3.1). Cationic residues are in blue, hydrophobic residues in green, Trp is shown in purple.*

Thus, they synthesized a set of peptides based on Lys for the hydrophilic side, Leu for the hydrophobic side and a Trp at the interface between the hydrophilic and hydrophobic faces. The role of Trp would not only be to stabilize the helix, but also to boost the antimicrobial properties without significant hemolysis of human erythrocytes. Indeed, out of twelve peptides with a length range from 6 to 13 residues, those with more than seven amino acids formed helical structures in membrane mimetic environments and exhibited some antimicrobial activity against the tested bacterial species (*S. subtilis. S. aureus, S. epidermis, M. luteus, E. coli, S. dysentariae, S. typhimorium, K. pneumoniae and P. aeruginosa*). Out of these, peptides **2.1**, **3.0** and **3.1** were the only ones active at μM concentrations against both Gram-positive and Gram-negative bacteria[15,16]. Peptide **3.0** emerged for its low hemolytic activity, with a percentage of hemolysis of only 7% at the higher concentration tested (200 μM). On the other hand, peptide **3.1**

showed higher hemolysis at the higher concentrations, but was also more potent, with MICs of 1.6 μM for Gram-positive bacteria, and in a range of 3-25 μM for Gram negative bacteria (Table 3.1)[15].

		Peptide 2.1	Peptide 3.0	Peptide 3.1
MIC (μM)	*E. coli*	12.5	12.5	6.3
	P. aeruginosa	50	25	25
	S. dysentariae	12.5	6.3	3.1
	S. typhimorium	25	25	25
	K. pneumoniae	6.3	6.3	3.1
	S. aureus	3.1	6.3	1.6
	S. epidermis	12.5	6.3	1.6
	B. subtilis	12.5	6.3	1.6
	M. luteus	25	6.3	1.6

Table 3.1*: Reported minimal inhibitory concentrations of **2.1**, **3.0** and **3.1**[15]. Thick line divides between the Gram-negative (top section) and Gram-positive (bottom section) bacterial species used in the study.*

Interestingly, peptide **3.1** was found to be active against all the tested methicillin-resistant *S. aureus* (MRSA) strains with a MIC of 3.13 μM, making it four times more potent than the current clinical candidate (Omiganan). The same study found the mechanism of action of 3.1 to be bactericidal rather than bacteriostatic, the latter being the case of the only FDA-approved drug for MRSA (retapamulin)[17]. Furthermore, it was also found slightly active against the plant pathogens *E. amylovora* and *P.syringae pv. actinidiae*[18,19].

The amphiphilic helix of **3.1** is an indication of a membranolytic mechanism of action, however the specifics of how the membrane disruption is reached has not yet been thoroughly investigated. Considering that the peptide length is not sufficient to span the bacterial membrane, it was suggested that the peptide could act via a carpet-like mode of action or a via both pore forming and carpet-like[15].

Pentapeptide-4

*For details about the pentapeptide-4 (**PP4**, H- KTTKS-NH_2) refer to Chapter 2.1.2*

Hybrid peptide 3.1-PP4

Taking into account the worldwide emerging problem of multidrug antibacterial resistance and the presence of "ESKAPE" bacteria in skin wounds, *Gomes et. al*[20] decided to combine the properties of two peptides into a single hybrid peptide as a possible candidate to treat diabetic foot ulcers. In particular, the two selected peptides were the antibacterial **3.1** and the collagen boosting **PP4**. Out of the five hybrid peptides that they synthesized (Table 3.2), **3.1-PP4** emerged as the most promising one.

More specifically, all peptides were subjected to a cytotoxicity evaluation on immortalized human foreskin fibroblasts (HFF-1) and antibacterial tests against two Gram-negative and two Gram-positive bacteria: *E. coli* (ATCC 25922), *P. aeruginosa* (ATCC 27853), *S. aureus* (ATCC 25923) and *E. faecalis* (ATCC

29212). As expected, **PP4** did not show any antibacterial properties, while **3.1** was found to be active against all tested strains in MICs ranging from the 3 μM against P. aeruginosa and S. aureus to the 6 μM against E. coli and E. faecalis, confirming the data present in the literature. The addition of the palmitoyl moiety did not prove to give any advantages. In fact, all the palmitoylated peptides showed much higher MICs and cytotoxicity than their N-terminus free counterparts, with the exception of C16-PP4, which could not be tested due to its insolubility.

Peptide	Sequence	Molecular Weight
3.1	H-KKLLKWLLKLL-NH_2	1394.9
C_{16}-3.1	Pal-KKLLKWLLKLL-NH_2	1633.3
PP4	H-KTTKS-NH_2	562.7
C_{16}-PP4	Pal-KTTKS-NH_2	800.6
PP4-3.1	H-KTTKSKKLLKWLLKLL-NH_2	1940.5
C_{16}-PP4-3.1	Pal-KTTKSKKLLKWLLKLL-NH_2	2179.0
3.1-PP4	H-KKLLKWLLKLLKTTKS-NH_2	1940.5
C_{16} -3.1-PP4	Pal-KKLLKWLLKLLKTTKS-NH_2	2179.0
PP4-βala-3.1	H-KTTKS-βAla-KKLLKWLLKLL-NH_2	2011.6

***Table 3.2**: Peptides synthetized by Gomes et al.[20]*

Although both **3.1-PP4** and its reversed counterpart **PP4-3.1** were found to be active against all tested strains and both displayed MICs of 1-2 μM against Gram-negative bacteria, they differed in the activity against Gram-positive bacteria, with **3.1-PP4** showing higher MICs (16-33 μM) than **PP4-3.1** (4-8 μM). However, **3.1-PP4** exhibited much lower cytotoxicity (IC_{50} of 69μM) than both **PP4-3.1** and the original antibacterial peptide **3.1.** The introduction of a spacer amino acid in **PP4-βala-3.1** did not improve either the antibacterial activity or the cytotoxicity.

Therefore, **3.1-PP4** was subjected to antibacterial tests against multidrug-resistant (MDR) bacteria, to antibiofilm assays and collagen stimulation tests:

- **3.1-PP4** resulted bactericidal at 1-4μM against MDR *P. aeruginosa*, *E. coli*, and *K. pneumoniae*.
- At the MIC concentration, **3.1-PP4** was able to inhibit biofilm formation on MDR strains of both *P. aeruginosa* and *K. pneumoniae*. At subinhibitory concentrations, **3.1-PP4** did not significantly inhibit the biofilm formation of any of the three *P. aeruginosa* isolates, but did in the case of the *K. pneumoniae* isolates. In addition, the growth of the preformed biofilms was reduced by the presence of **3.1-PP4** in percentages ranging from 3 to 21% in the cases of *P. aeruginosa* isolates, and from 34 to 56% for *K. pneumoniae* isolates. The obtained results were corroborated by MTT assays that demonstrated that the presence of **3.1-PP4** drastically reduced the metabolic activity of the tested *K. pneumoniae* MDR isolates.

- At concentrations representative of its MIC values against MDR isolates of Gram-negative bacteria, **3.1-PP4** resulted having a collagen-boosting activity *in vitro* comparable to **C_{16}-PP4**.

Overall, the hybrid peptide **3.1-PP4** maintained the collagen boosting activity of **C_{16}-PP4** while enhancing the antibacterial potency of **3.1,** but was also found active against MDR isolates and able to inhibit biofilm formation and reduce preformed biofilms, especially in the case of MDR *K. pneumoniae*.

3.2 Results and Discussion

Considering that:

- the presence of both an amine and a primary hydroxyl at the N-glucosamine monomer of chitosan, enables for a double functionalization of the biopolymer,
- the C_6-OH can be oxidized to aldehyde by a TEMPO/laccase catalyzed reaction[14],
- the use of the thiazolidine conjugation to covalently bind the antibacterial peptide PMAP(12-24) to CHO-cotton gave encouraging results (*Chapter 2*),
- the work of *Barbosa et al.*[4,5] demonstrated the feasibility of the conversion of the C_2-NH_2 to azide and the conjugation of the antimicrobial peptide Dhvar5 to chitosan *via* the CuAAC reaction,

in this chapter the thiazolidine and azide-alkyne chemoselective ligations were used for the functionalization of chitosan with the antibacterial peptide **3.1** and the collagen-boosting peptide **PP4**, respectively.

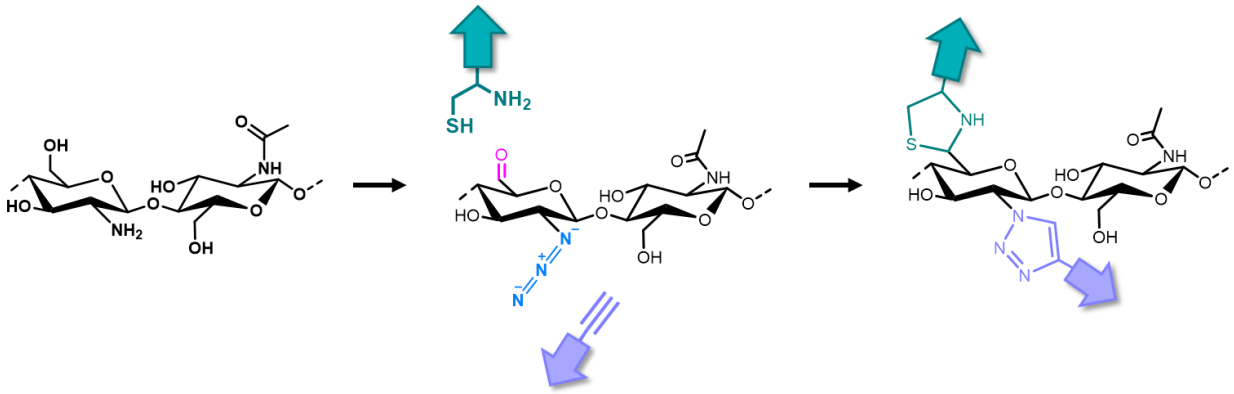

***Figure 3.5**: Schematic representation of the modification of chitosan to introduce the aldehyde and the azide required for the thiazolidine and CuAAC reaction with peptides, respectively. Then, schematic representation of the thiazolidine bond between an Cys-ending peptide (yellow arrow) and CHO-chitosan-N_3, and the CuAAC between a peptide equipped with an alkyne (green arrow) and CHO-chitosan-N_3.*

3.2.1 Choice of Peptides

Peptide **3.1** (H-KKLLKWLLKLL- NH_2) shows great potential for further use as an antibacterial agent due to its broad spectrum activity, low cytotoxicity and non-specific mechanism of action[15]. The palmitated analogue of peptide **PP4** (Pal-KTTKS-NH_2) is being studied as the active agent in the treatment of wounds[21,22]. In addition, the work by *Gomes et. al*[20] on an hybrid peptide of the two (**3.1-PP4**) demonstrated that the sequences of the antibacterial peptide **3.1** and peptide **PP4** can work synergically

and produce a peptide with both antibacterial and collagen boosting activity, and that the addition of a spacer between the two peptides does not negatively affect the activity or the cytotoxicity of the hybrid.

Therefore, the two peptides were selected to functionalize chitosan and form a **3.1**-chitosan-**PP4** double conjugate to be evaluated for its antibacterial and collagen regenerative properties.

Peptide	Short name	Sequence	MW (g/mol)	Purity
4g	PraPP4	H-**Pra**KTTKS-NH_2	657.77	95%
5a	Cys3.1	H-**C**KKLLKWLLKLL- NH_2	1498.04	97%

***Table 3.3**: List of the synthesized peptides and their purity. Pra is the unnatural amino acid propargylglycine. Details about the synthesis and HPLC-MS characterization are in Section 3.4.1 in Chapter 5.3.1, respectively.*

To allow the conjugations with chitosan, the chemoselective moieties needed to form the thiazolidine ring or the azide-alkyne cycloaddition were introduced on the peptides during solid phase peptide synthesis. The alkyne necessary for the CuAAC was introduced by adding the unnatural amino acid propargylglycine (Pra) at the N-terminus of the **PP4** sequence (peptide **4g**), whereas, the β-amino thiol needed for the thiazolidine bond with chitosan was introduced as a Cys at the N-terminus of peptide **3.1** (peptide **5a**). Both peptides were synthesized in high purity by solid phase peptide synthesis using the Fmoc/Boc strategy. The cleavage from the resin was performed by an acidic treatment with TFA. In this way also the side chain protecting groups of the amino acids were removed simultaneously. The peptides were recovered by precipitation and washed in cold methyl tert-butyl ether (MTBE). Preparative HPLC was was performed to further purify the peptides. All synthetized peptides were characterized by HPLC-MS (*Chapter 5.3.1*).

3.2.2 Chitosan Modification

When the TEMPO/laccase/O_2 oxidation was performed on unmodified chitosan, the aldehyde could not be detected either by FT-IR or the Schiff test, probably because they were masked by the imine bond formed with the free amines of chitosan (Fig. S3.3 and S3.5A, *Chapter 5.3*). Therefore, to ensure the synthesis of chitosan grafted with both the aldehyde and the azide (CHO-chitosan-N_3), the oxidation of the hydroxyl to aldehyde needed for the thiazolidine bond with peptide **5a** (**Cys3.1**) was carried out after the introduction of the azide necessary for the reaction with the alkyne on peptide **4g** (**PraPP4**):

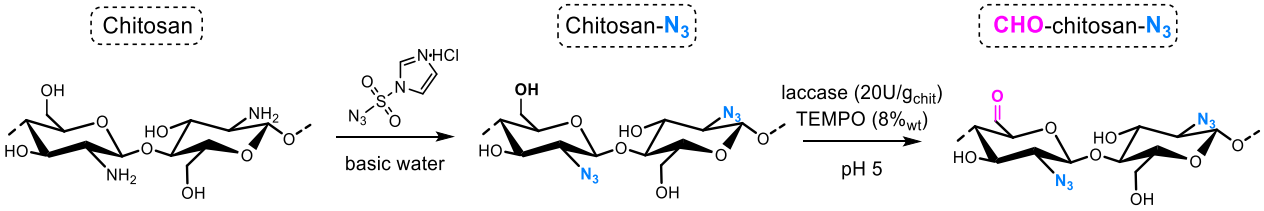

***Figure 3.6**: Schematic representation of the synthetic route to produce CHO-chitosan-N_3.*

The azide was introduced on chitosan following the same procedure of *Barbosa et al.*[4]. Briefly, the amine on chitosan was converted to azide by reacting for 24h with 3eq of ISA·HCl using alkaline water as the solvent. The solid was recovered by centrifugation after full precipitation at pH 12.

The success of the azide grafting on chitosan-N_3 was testified by the appearance of a new FT-IR band at 2110 cm^{-1}, that corresponds to the stretching of the $N^-=N^+=N^-$ bond[4,13] (Fig. 3.7A, in blue). Then, to convert the C_6-OH of N_3-chitosan to aldehyde, the TEMPO/laccase/O_2 catalyzed system was employed, and the same reaction conditions used maximize the aldehyde conversion on cellulose[23,24] were used on chitosan (20U/g_{chit} of laccase and 8%$_{wt}$ of TEMPO).

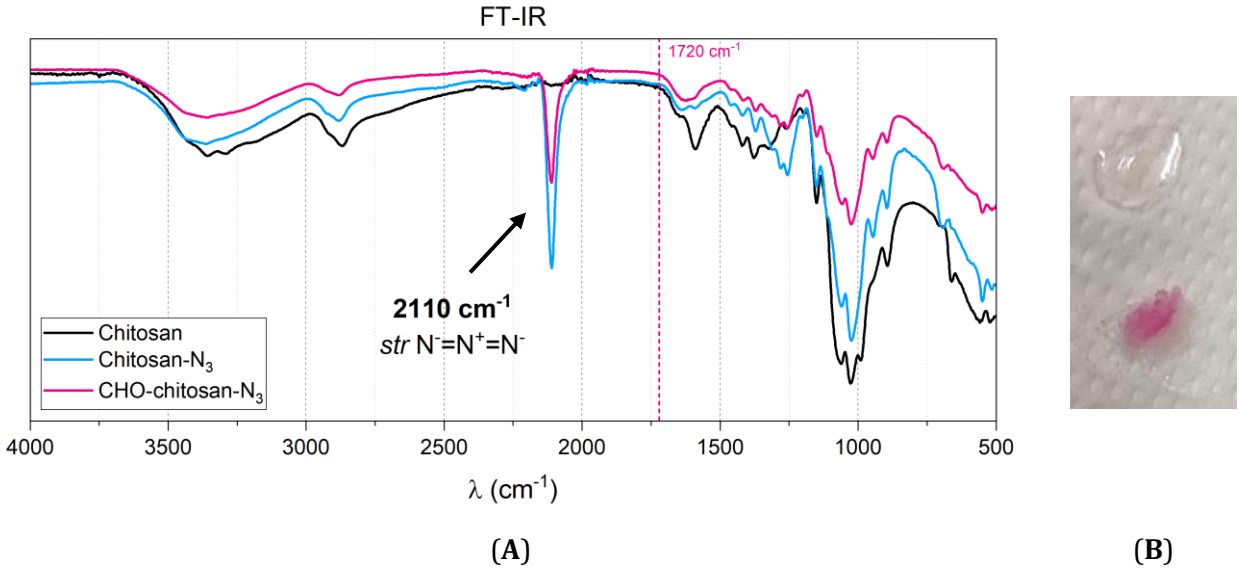

***Figure 3.7**: (**A**) FT-IR spectra of chitosan (black), chitosan-N_3 (blue) and CHO-chitosan-N_3 (pink). Highlighted is the stretching band of the $N^-=N^+=N^-$ bond. (**B**) Schiff test on chitosan (upper sample) and CHO-chitosan-N_3 (lower sample).*

The $N^-=N^+=N^-$ stretching band at the FT-IR is present also for the CHO-chitosan-N_3 sample, confirming that the oxidation of hydroxyl did not interfere with the azide (Fig. 3.7A, in pink). The presence of the aldehyde on CHO-chitosan-N_3 could not be confirmed by FT-IR, but only with the colorimetric Shiff test (Fig. 3.7B). In fact, upon addition of the Schiff's reagent, the sample of CHO-chitosan-N_3 turned pink, whereas chitosan and chitosan-N_3 did not (Fig. 3.7B and S3.5B, *Chapter 5.3.3*). The aldehyde C=O stretching band should be at around 1720 cm^{-1}, but no signal is visible in that range for any sample, probably due to the formation of hemiacetals that shields the aldehydes[25,26], even though the signal at 791 cm^{-1} reported by *da Silva et al.*[14] and attributable to the hemiacetals is not visible.

To quantify the amount of aldehydes present on CHO-chitosan-N_3 we wanted to follow a procedure described by *Alves et al.*[27] where chitosan was dissolved in 0.5% DCl in H_2O (10mg/mL) and characterized by ^{1}H-NMR, however CHO-chitosan-N_3 could not be solubilized in the same conditions. The titration of the aldehyde could be performed as described in *Chapter 2.2.3*. However, this procedure requires big amounts of material, therefore for our scopes we assumed the amount of aldehydes to be

similar to what was found in our studies with hyaluronic acid (*Chapter 4*). Thus, a conversion of around 10% of the hydroxyls that corresponds to 0.54 mmol/g was assumed.

3.2.3 Peptide-Chitosan conjugations- Preliminary

The thiazolidine and azide-alkyne copper(I) catalyzed chemoselective reactions were preliminary tested using small batches (20mg) of CHO-chitosan-N_3, mainly to evaluate the impact of the order of the reactions.

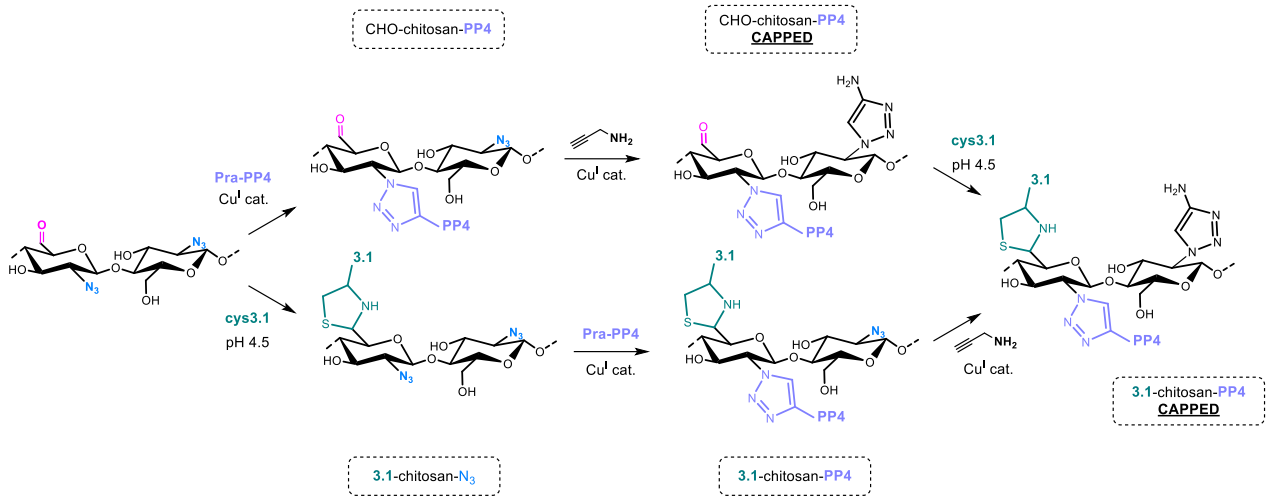

***Figure 3.8**: Outline of the reactions plan for the preliminary tests. The reaction from **3.1**-chitosan-**PP4** to **3.1**-chitosan-**PP4** capped was not performed because no azides were detected by FT-IR after the reaction with **PraPP4**.*

The thiazolidine conjugation between CHO-chitosan-N_3 and peptide **Cys3.1** was performed at a slightly acidic pH (4.5) using a small excess of peptide (1.5 eq with respect to the assumed mmoles of aldehyde), and a reducing agent (TCEP) to avoid the formation of peptide dimers via intermolecular disulfide bonds between cysteine residues. Considering the results described in the previous chapter on the kinetics of the peptide-cotton conjugations, the reaction was allowed to proceed for 24 h under stirring. The solid was recovered by centrifugation after full precipitation upon addition of NaOH. The presence of the peptide on the material was confirmed by the *amide I* and *amide II* bands observed at 1650 cm^{-1} and 1530 cm^{-1}, respectively, by FT-IR spectroscopy (Fig. 3.9, in teal). The amount of peptide present on the material was quantified as 0.47 mmol/g by measuring absorbance of the Trp (in the sequence of peptide **Cys3.1**) in a solution of **3.1**-chitosan-N_3.

The CuAAC between CHO-chitosan-N_3 and peptide **PraPP4** was performed in water under the same reaction conditions used by *Barbosa et al.*[4]. In particular, to calculate the amount of reagents, the conversion of amine to azide was assumed to be complete, and thus the moles of azides corresponded to the moles of repeating units. In addition, the peptide was present in defect (0.25eq with respect to the repeating units), the ligand THPTA was used to form a stabilizing complex with the Cu(I) needed to catalyze the reaction[28,29], and aminoguanidine hydrochloride was present to avoid the modification of Arg side chains by the ascorbate used for in situ reduction of Cu(II) to the Cu(I) catalyst needed to

promote the reaction[4,30]. The solution was stirred for 48h, and the solid was recovered by centrifugation after full precipitation upon addition of NaOH. The excess of copper was removed by washes with EDTA.

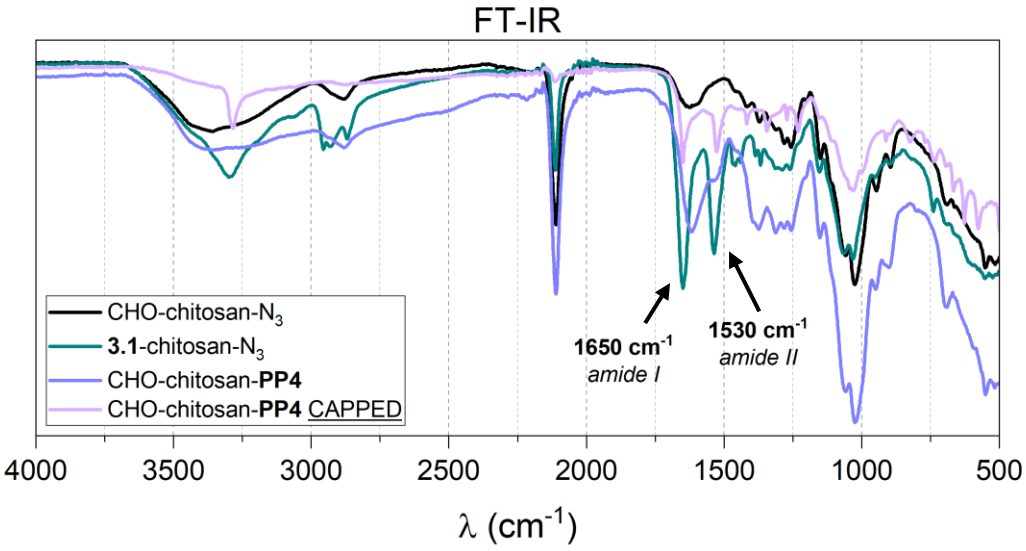

***Figure 3.9**: FT-IR spectra of the materials obtained after the reaction of CHO-chitosan-N_3 with Cys3.1 (teal), PraPP4 (violet), and propargylamine (capping reaction of CHO-chitosan-PP4, light purple).*

The presence of **PraPP4** on the material was confirmed by the *amide I* and *amide II* bands at 1650cm^{-1} and 1530 cm^{-1} in FT-IR spectra, respectively (Fig. 3.9, in purple). To avoid the potential toxic effects of the free azide and restore the primary amines typical of unmodified chitosan, the N_3 group was capped by a CuAAC with an excess of propargylamine. The almost complete disappearance of the $N^-=N^+=N^-$ stretching band at 2110 cm^{-1} confirmed the success of the capping reaction. However, the remaining weak band at 2120 cm^{-1} and the appearance of a sharp peak in the 3333-3267 cm^{-1} region could be attributable to the CΞC and CΞC-H stretching bands of the propargylamine, respectively (Fig.3.9, in pink). This suggests that some of the reagent could still be present and interacting with the aldehyde by imine formation.

The same reaction conditions used to conjugate **Cys3.1** to CHO-chitosan-N_3 were employed to bind the peptide to the capped CHO-chitosan-**PP4** (Fig. 3.7). The FT-IR spectrum of the product (capped **3.1**-chitosan-**PP4**) did not drastically change from the spectrum of capped CHO-chitosan-**PP4**, and presence of a peptide is testified by the *amide I* and *amide II* bands of the amides in the peptide backbone at 1650cm^{-1} and 1530 cm^{-1}, respectively (Fig. 3.10, dark purple). However, this does not confirm the success of the covalent grafting reaction. On the other hand, the UV-Vis analysis of the material revealed 0.09 mmol/g of Trp that corresponds to the amount of grafted **Cys3.1**. The lower peptide loading (with respect to **3.1**-chitosan-N_3) could be attributable to the steric hindrance of **PP4** bound to the material, but could also be due to a partial capping of the aldehydes by imine formation with propargylamine.

Similarly, the same reaction conditions used to conjugate **PraPP4** to CHO-chitosan-N_3 were employed to bind the peptide to **3.1**-chitosan-N_3. The success of the reaction is testified by the disappearance of the

$N^-=N^+=N^-$ stretching band at 2110 cm^{-1} at the FT-IR spectrum. Since the $N^-=N^+=N^-$ stretching band was no longer visible in the FT-IR of the product, the capping reaction with propargylamine was not performed (Fig. 3.10, in aquamarine).

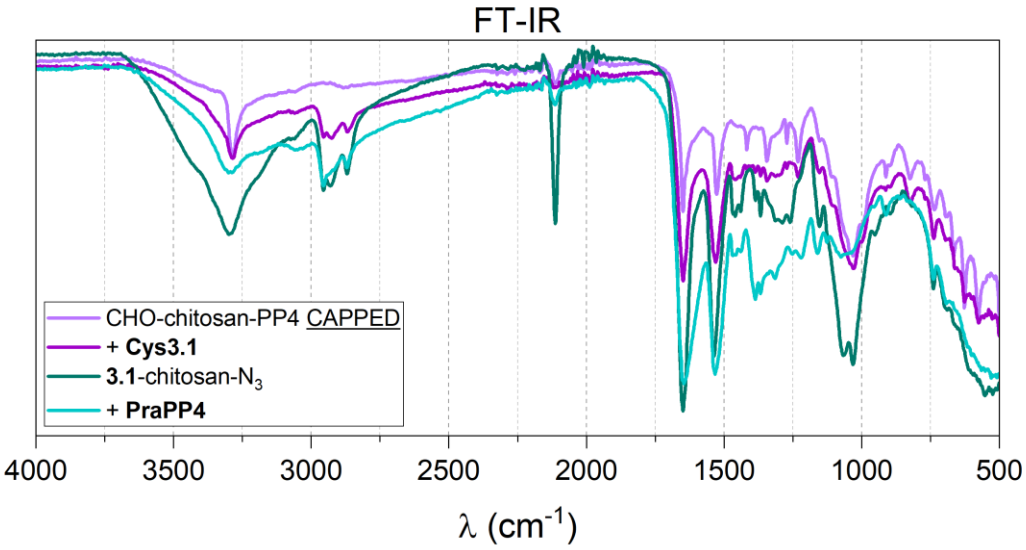

***Figure 3.10**: FT-IR spectra of CHO-chitosan-**PP4** (light purple) and **3.1**-chitosan-**PP4** capped (purple), **3.1**-chitosan-N_3 (teal) and **3.1**-chitosan-**PP4** (aquamarine).*

3.2.4 Peptide-Chitosan conjugations

Considering the preliminary results presented in the previous section, for the synthesis of bigger batches (100 mg) of peptide-chitosan conjugates to be used for the biological assessment: (**1**) propargylamine was substituted with pent-1-yne as the capping reagent to avoid problems of imine formation, (**2**) the double conjugate **3.1**-chitosan-**PP4** was synthesized by conjugating **Cys3.1** first and then **PraPP4**, so the last capping step could be skipped, and (**3**) the azides present on **3.1**-chitosan-N_3 were capped for the biological tests to avoid the potential toxic effects of the azide. In addition, unmodified chitosan was subjected to the same reaction conditions as CHO-chitosan-N_3 to be used as a control for the success of both the thiazolidine and the CuAAC reaction (Fig. 3.11).

The same reaction conditions used in the previous section were employed to bind **Cys3.1** and **PraPP4** to CHO-chitosan-N_3 and chitosan, and **PraPP4** to **3.1**-chitosan-N_3. It is important to notice that for the azide-alkyne reaction it was assumed that the conversion of amine to azide was complete, and thus the moles of azides corresponded to the moles of repeating units. However, the XPS analysis (that was performed afterwards) revealed that only a 30% conversion was reached (*Section 3.2.5*).

The amount of **Cys3.1** bound to **3.1**-chitosan-N_3 and present on unmodified chitosan that was subjected to the same reaction conditions (chitosan+**Cys3.1**) was calculated by measuring the absorbance of Trp, and resulted of 0.89 mmol/g and 0.51 mmol/g, respectively. The higher amount present on **3.1**-chitosan-N_3 confirms the success of the reaction, however it seems that a big amount of peptide could be non-

covalently bound (adsorbed) to the material. The presence of **Cys3.1** in both samples is also testified by the appearance in the FT-IR spectra of the *amide I* and *amide II* peaks at 1650 cm^{-1} and 1530 cm^{-1}, respectively (Fig. 3.12 in teal, and S3.4 *Chapter 5.3. 2* in aquamarine).

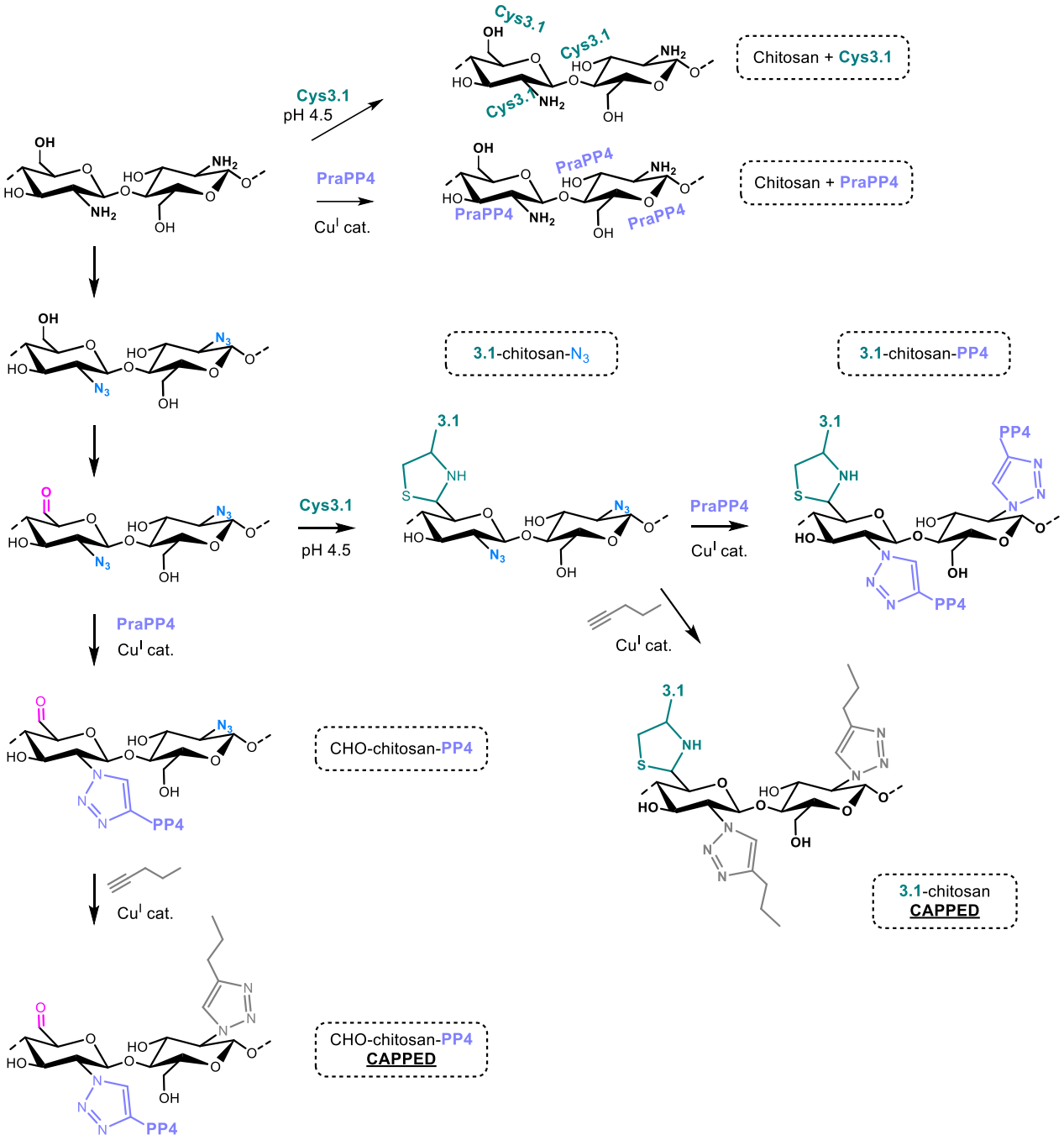

Figure 3.11: *Summary of the reactions to produce the target materials for the biological tests.*

Similarly, the success of the **PraPP4** conjugation to CHO-chitosan-N_3 was confirmed by the appearance of the same bands in the FT-IR spectrum of CHO-chitosan-**PP4** (Fig. 3.12, in purple). Interestingly, the control sample of unmodified chitosan (chitosan+**PraPP4**) did not display the *amide I* and *amide II* bands, suggesting that **PraPP4** was not significantly adsorbed on chitosan (Fig. S3.4 *Chapter 5.3.2*, in pink). In the case of **3.1**-chitosan-**PP4** the disappearance of the $N^{-}=N^{+}=N^{-}$ stretching band at 2110 cm^{-1}

suggests that the reaction between **3.1**-chitosan-N_3 and peptide **PraPP4** was successful (Fig. 3.12, in yellow).

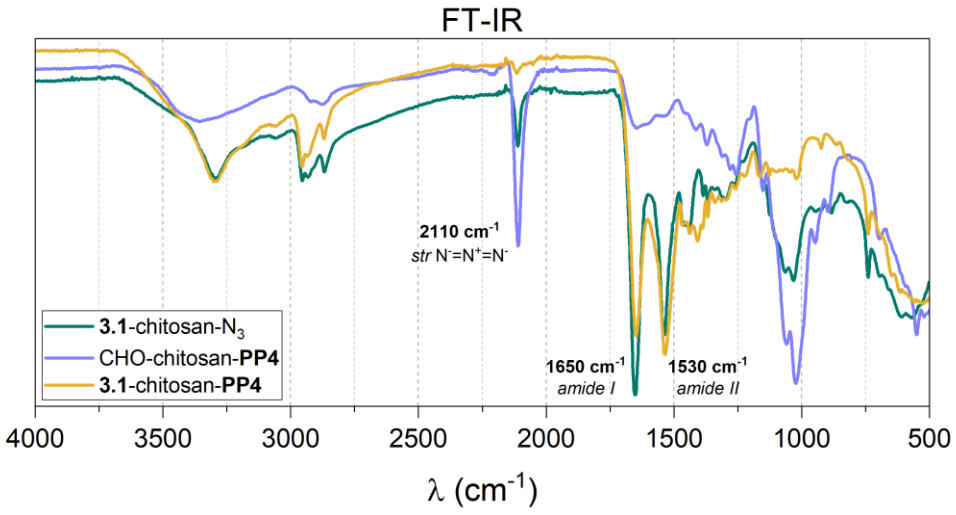

***Figure 3.12**: FT-IR spectra of **3.1**-chitosan-N_3 (teal), CHO-chitosan-**PP4** (violet) and **3.1**-chitosan-**PP4** (yellow).*

The capping of the azides in **3.1**-chitosan-N_3 was confirmed by the disappearance of the $N^-=N^+=N^-$ stretching band at 2110 cm^{-1}, however the same signal is present in the FT-IR spectra of CHO-chitosan-**PP4** suggesting that the capping procedure was not successful (Fig. 3.13). This could be due to the different solubility of the two conjugates in water and/or to the insolubility of pent-1-yne. In fact, **3.1**-chitosan-N_3 partially dissolved in water, whereas CHO-chitosan-**PP4** remained as an insoluble solid. Thus, in the reaction of CHO-chitosan-**PP4** the azides were probably inaccessible to pent-1-yne due to the formation of a three-phase reaction.

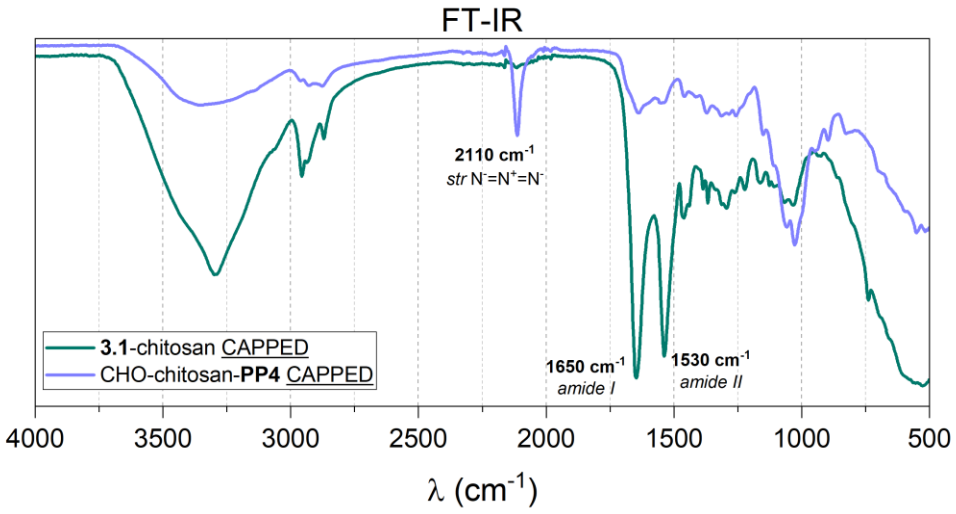

***Figure 3.13**: FT-IR spectra of **3.1**-chitosan-N_3 treated with pen-1-tyne (teal), and CHO-chitosan-**PP4** treated with pent-1-yne (violet).*

In the following sections only the capped materials will be used, unless otherwise noted. Therefore, for simplicity the material formed from the capping of **3.1**-chitosan-N_3 will be referred as **3.1**-chitosan and

the material obtained after the failed capping of CHO-chitosan-**PP4** will be referred simply as CHO-chitosan-**PP4.**

3.2.5 XPS Analysis of Chitosan and Derivatives

Chitosan, modified chitosan, the peptide-chitosan conjugates and their controls were further analyzed by XPS. Table 3.4 shows the relative atomic percentages of carbon, nitrogen, oxygen and sulfur.

Description	C %	N %	O %	S %		N/C	O/C	N/O
Chitosan	53.15	9.41	37.44	-		0.177	0.704	0.251
Chitosan-N_3	53.86	14.6	31.55	-		0.271	0.586	0.463
CHO-chitosan-N_3	52.59	14.58	32.84	-		0.277	0.624	0.444
Chitosan + **Cys3.1**	59.96	5.88	33.32	0.84		0.098	0.556	0.176
3.1-chitosan	68.21	14.19	16.97	0.63		0.208	0.249	0.836
Chitosan + **PraPP4**	45.81	6.73	47.46	-		0.147	1.036	0.142
CHO-chitosan-**PP4**	62.49	14.83	22.69	-		0.237	0.363	0.654
3.1-chitosan-**PP4**	51.99	11.37	35.97	0.68		0.219	0.692	0.316

***Table 3.4**: elemental analysis data (% C, N, O) as determined by XPS analysis of chitosan and derivatives. Chitosan + peptide are the controls done by putting chitosan in the same reaction conditions of CHO-chitosan-N_3.*

The results obtained for chitosan and chitosan-N_3 are coherent with data in the literature[4,31]. As expected, the atomic percentage of nitrogen in chitosan-N_3 and CHO-chitosan-N_3 is higher than chitosan due to the presence of the azide group, and accounts for a conversion of NH_2 to N_3 of around 30% of the repeating units, which corresponds to 1.86 mmol/g. The increase in the percentages of carbon and nitrogen in CHO-chitosan-**PP4** and **3.1**-chitosan testifies the presence of the peptides in the samples. The presence of sulfur in the elemental analysis of **3.1**-chitosan, chitosan + **Cys3.1** and the **3.1**-chitosan-**PP4** confirms the presence of peptide **Cys3.1** in the samples. The XPS spectra and their complete assignment are reported in *Chapter 5.3.4*. The spectra of chitosan and chitosan-N_3 are consistent with the data in the literature[4,31].

The N1s spectrum of chitosan was resolved in one peak assigned to C-N nitrogens corresponding to the amines present in the backbone. The N1s spectra of the controls (chitosan+**Cys3.1** and chitosan+**PraPP4**) was resolved in two peaks: the C-N peak of the amine present on chitosan and the amide peak at 400.0 eV that highlights the presence of the peptides in both samples. The peak at 404-405 eV observed in the spectra of chitosan-N_3 and CHO-chitosan-N_3 confirmed the presence of the azide group and atomic percentage is coherent with the previous assumption of a 30% yield. Surprisingly, CHO-chitosan-**PP4** did not present the peak at 404.4 eV that corresponds to the azide bond, in contrast to the FT-IR measurements, making this dataset not reliable.

The C1s spectrum of unmodified chitosan was resolved into three peaks: the peak at 285.0 eV was assigned to C-C and C-H type carbons, the peak at 286.4 eV was assigned to C-NH_2, C-OH and C-O-C

carbons, whereas the peak at 287.8 eV was assigned to carbons from the O-C-O and N-C=O groups. The presence of the peptides in the control samples was corroborated by the increase in area of the C-C/C-H type carbon peak at 285 eV that are present in the peptide chain. The spectrum of modified chitosan did not drastically change from the spectrum of chitosan, and similarly the presence of the peptides in the conjugated samples was highlighted by an increase in the C-C / C-H peak at 285 eV.

3.2.6 Amino Acid Analysis

Amino acid analysis was performed as a method to quantify the peptides in the conjugates by determining their relative amino acid composition. Briefly, the materials were first degraded in harshly acidic conditions to form free amino acids and the products of hydrolysis of the polysaccharide backbone. The former were detected ant quantified by ion exchange chromatographic analysis, and the latter did not interfere with the measurements. The results are summarized in Table 3.5:

Sample	Loading of Cys3.1 (mmol/g)	Loading of PraPP4 (mmol/g)
Chitosan + **Cys3.1**	0.548	-
3.1-Chitosan	0.919	-
Chitosan + **PraPP4**	-	0.003
CHO-Chitosan-**PP4**	-	0.051
3.1-Chitosan-**PP4**	0.824*	0.043

Table 3.5*: Peptide loading calculated by amino acid analysis. *the value was calculated taking into account only Leu (<30% of the total number of amino acids). Detailed data in Chapter 5.3.5.*

As expected in chitosan and CHO-chitosan-N_3 no amino acids were found. The amount of **Cys3.1** found by amino acid analysis in **3.1**-chitosan and its control, chitosan+**cys3.1**, corresponds to the amount found by UV-Vis and is of 0.919 mmol/g and 0.548 mmol/g. This corroborates the use of the Trp absorbance as a method for peptide quantification.

In addition, the amount of **Cys3.1** on the double conjugate was slightly lower than the monoconjugate **3.1**-chitosan. This could be due to a loss of peptide during the reaction with **PraPP4**, but also due to the use of only one amino acid for the measurement, making the value less accurate. On the other hand, the amount of **PraPP4** found in chitosan+**PraPP4** is minimal when compared to CHO-chitosan-**PP4**, confirming the success of the CuAAC reaction with CHO-chitosan-N_3, as indicated by FT-IR analysis. **PraPP4** loading on CHO-chitosan-**PP4** and **3.1**-chitosan-**PP4** of 51 and 43 μmol/g, respectively, is coherent with the results obtained by *Barbosa et al.*[4] with Dhvar5. Considering the different length of the two peptides and the absence of a linker for **PraPP4**, the low yield may be due to a small number of accessible azides for conjugation rather than steric hindrance.

3.2.7 Antibacterial Activity of the Conjugates

To assess whether the presence of peptide **3.1** improved the antibacterial activity of chitosan, the antibacterial activity of double-layered chitosan ultrathin films was evaluated against Gram-positive and Gram-negative bacteria. This was then compared to the activity of double layered ultrathin films of the peptide-chitosan conjugates **3.1**-chitosan and **3.1**-chitosan-**PP4**, and chitosan+**Cys3.1**.

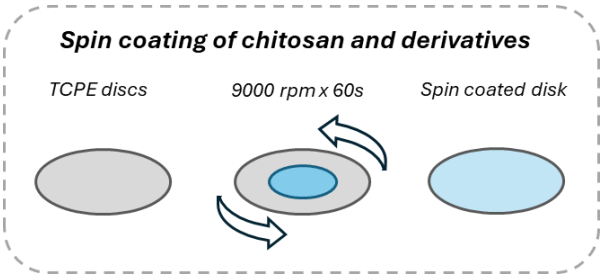

***Figure 3.14**: schematic representation of the spin coating. The procedure was performed twice on each side of the discs.*

In brief, acidic aqueous solutions of the materials were deposited by spin coating on TCPE discs twice, forming double-layered chitosan ultrathin films on both sides of the discs. Unfortunately, CHO-chitosan-N_3 could not be spin coated since it was not soluble in the solvent (Fig. 3.14).

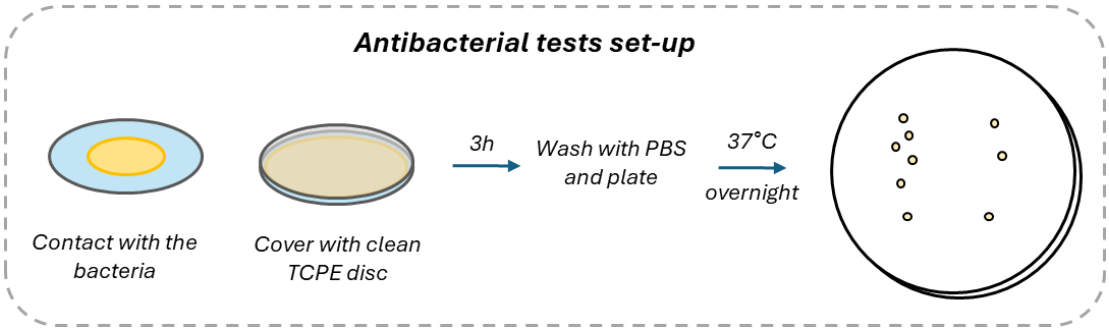

***Figure 3.15**: schematic representation of the antibacterial tests set-up.*

Then, the dried surfaces were placed in contact with the bacteria by depositing a drop of bacterial culture solution on the spin-coated discs, which were then covered with a clean TCPE disc. After 3h, the discs were washed with PBS, and the solution was plated overnight. The number of colonies that grew were used to evaluate the antibacterial properties of the materials (Fig. 3.15). Unmodified TCPE discs were subjected to the same procedure as a control. The results are expressed in Figure 3.15 as colony-forming units per milliliter.

As shown in Figure 3.16A, the antibacterial activity of chitosan is confirmed by the significantly reduced growth of *S. aureus* on a chitosan surface when compared to the controls. The validity of this assessment is confirmed by the presence of a comparable amount of bacteria in the TCPE control and in the *S.aureus* in PBS, confirming that no bacteria was left on the discs. Surprisingly, chitosan control that was in contact with **Cys3.1** (chitosan+**Cys3.1**) had worst performance than chitosan by itself. No colonies grew from the PBS solution used to wash the **3.1**-chitosan surface, suggesting the conjugate bactericidal action

against *S. aureus*. On the other hand, the antibacterial action of **3.1**-chitosan-**PP4** against *S.aureus* is comparable to that of chitosan, suggesting the inefficacy of the double conjugate. Since the amount of peptide **Cys3.1** present on **3.1**-chitosan and **3.1**-chitosan-**PP4** is comparable, and **PP4** present on the double conjugate is not enough to drastically change the weight of the material, the behavior cannot be asserted to a difference in the amount of antibacterial peptide present in the test. However, **3.1**-chitosan-**PP4** solutions were not as viscous as the solutions of the other tested materials, and this could have negatively affected the spin coating, depositing less material than the controls.

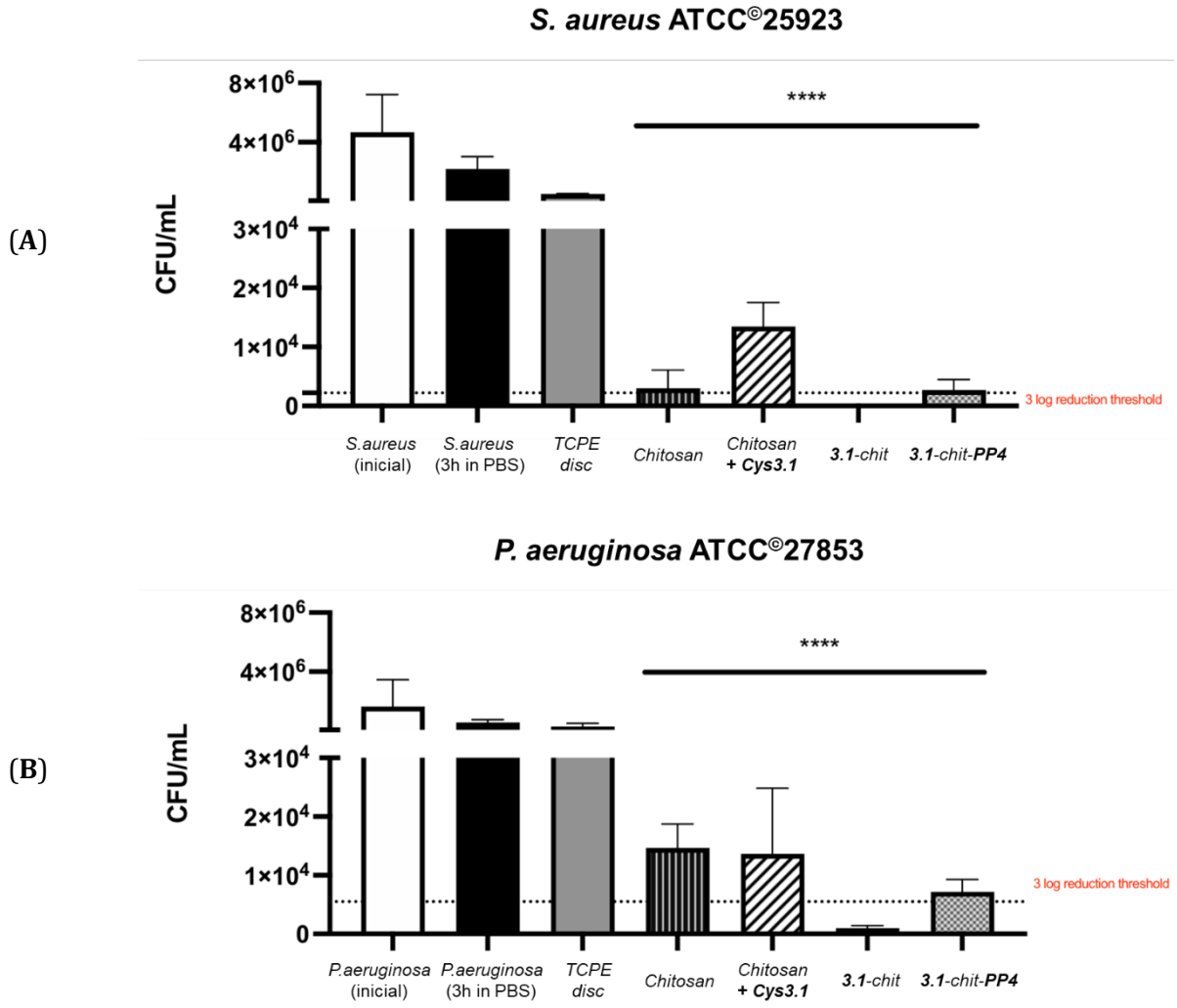

Figure 3.16: *Effect of chitosan and its peptide-grafted derivatives on (**A**) S. aureus, and (**B**) P. aeruginosa; Expressed as colony-forming units per milliliter (CFU/mL). ****- statistically significant different from S. aureus (3 h in PBS) p<0.001 One-Way ANOVA Kruskal Wallis test. Raw data reported in Chapter 5.3.6.*

The difference in the absolute values of the treatment with *P. aeruginosa* can be ascribed to the lower MIC of peptide **3.1** for *S. aureus* (Fig. 3.16B, and *Section 3.1.2*). In this case, chitosan and chitosan+**cys3.1** displayed a comparable antibacterial activity, suggesting that the grafting of the peptide on the surface is necessary to have a higher inhibition of the bacterial growth. In fact, the amount of bacteria that grew on the surface of **3.1**-chitosan was minimal. Unlike the results obtained with *S. aureus*, **3.1**-chitosan-**PP4**

exhibited an enhanced antibacterial effect against *P. aeruginosa* compared to chitosan and chitosan+**cys3.1**. However, it was still not as effective as **3.1**-chitosan.

3.2.8 Collagen-Boosting Activity of the Conjugates

The collagen boosting activity of spin-coated surfaces of chitosan, CHO-chitosan-**PP4** and **3.1**-chitosan-**PP4** is currently undergoing at the University of Porto by scratch test.

3.3 Conclusions and Future Perspectives

Chitosan is a widely used material in the context of wound healing due to its intrinsic antibacterial and hemostatic properties. Its covalent conjugation to peptides offers an interesting approach to the delivery of active agents at the wound site. The work[4,5,12] of the Gomes group proved the feasibility of using antibacterial peptides and azide-alkyne copper(I)-catalyzed chemoselective ligation to create peptide-chitosan conjugates. Thus, in this chapter the use of this chemistry was further explored with a collagen-boosting peptide, alongside with the use of the thiazolidine bond of an antibacterial peptide.

An active wound patch would benefit from avoiding pathogen infections and facilitating wound closure. Since the collagen-boosting peptide **PP4** (H-KTTKS-NH_2) and the *de novo* antibacterial peptide **3.1** (H-KKLLKWLLKLL- NH_2) proved to be able to act in conjunction with each other in the hybrid peptide **3.1-PP4**, the two peptides were selected in this study. A propargylglycine was added at the N-terminal end of the **PP4** sequence to enable reaction with an alkyne-modified moiety via CuAAC. In parallel, the β-amino thiol required for the thiazolidine conjugation was added to the N-terminus of peptide **3.1**.

The chemoselective moieties needed for the two conjugations were grafted onto chitosan to form CHO-chitosan-N_3. The amine was converted to an azide using ISA·HCl as the diazo-transfer agent, whereas the aldehyde was introduced on the C_6-OH via a TEMPO/laccase/O_2 catalyzed system. The success of the reactions was confirmed by FT-IR and Schiff test.

Binding peptide **Cys3.1** through the thiazolidine bond was successful, as evidenced by the higher peptide loading of CHO-chitosan-N_3 (0.9 mmol/g) compared to chitosan (0.5 mmol/g), according to both UV-Vis and AA analysis. The azide-alkyne reaction with peptide **PraPP4** proved to be successful both on CHO-chitosan-N_3 and on **3.1**-chitosan, with peptide loading around 0.05 mmol/g. To avoid the toxic effects of the azide group, pent-1-yne was used instead of propargylamine as the capping reagent, due to the possible side imine reaction of the newly introduced amines and the aldehyde present on CHO-chitosan-N_3 However, in the case of CHO-chitosan-**PP4** the reaction was not successful and the nreacted azides could not be capped.

Surfaces of **3.1**-chitosan proved to have an improved antibacterial activity against both *S.aureus* and *P.aeruginosa*, proving that the binding of the peptide did not negatively affect its antibacterial activity. In addition, the use of pent-1-yne as the capping reagent proved that the high antibacterial activity of this material is mainly due to the peptide and not to the charged amines of chitosan. Unexpectantly, the activity of the double conjugate **3.1**-chitosan-**PP4** was similar to chitosan against *S. aureus* and slightly higher than chitosan against *P. aeruginosa*. Scratch tests on CHO-chitosan-**PP4** and **3.1**-chitosan-**PP4** are currently ongoing to evaluate the collagen boosting activity of the materials.

In conclusion, in this chapter we demonstrated the possibility of binding two different peptides using two different types of chemoselective ligation on the same modified chitosan. Unfortunately, the double-conjugate material is not as antibacterial as its **3.1**.chitosan control, but it still could be promising if the collagen-boosting of PP4 effects are maintained or even improved after grafting.

3.4 Methods

3.4.1 Peptide Synthesis

All peptides were synthesized by automatic solid phase synthesis using standard by Fmoc strategy[32] with a Symphony X automatic synthesizer (Gyros Protein Technologies). The synthesis can be rationalized with the following steps:

- SWELLING: degassed DMF is added to the resin and the dispersion stirred for 30min. Then, DMF is removed.
- AA COUPLING: To activate the Fmoc-protected amino acid, 5eq (with respect to the mmol of binding sites on the resin) of the latter, 5eq of HCTU and 10eq of NMM are dissolved in DMF. The activated amino acid solution is added to the resin and the dispersion is left stirring. After 10min, the solution is filtered off and the resin is washed 5 times with DMF and 5 times with DCM.
- FMOC DEPROTECTION: the resin is submerged in a solution of 20% piperidine in DMF for 2min twice. Then, the resin is washed 5 times with DMF and 5 times with DCM.
- CLEAVAGE AND FULL DEPROTECTION a solution of TFA/TIS/H_2O (95:2.5:2.5) is added to the resin (3mL per 100mg of resin) and the dispersion is stirred for 2.5h. When the peptide sequence has a Cys, a solution of TFA/TIS/H_2O/DODT (94:1:2.5:2.5) is added to the resin and the dispersion is stirred for 2.5h. Then, a 10-fold excess of cold MTBE is added to the filtered solution to precipitate the peptide. The solid is recovered by centrifugation (5500 rpm x 5min) and washed 3 times with MTBE.

Peptide	Short name	Sequence	MW (g/mol)
4g	PraPP4	H-PraKTTKS-NH_2	657.77
5a	Cys3.1	H-CKKLLKWLLKLL-NH_2	1498.04

***Table 3.6**: List of the synthesized peptides*

The peptides were purified in a preparative HPLC system (LaPrep Sigma VWR with UV detector LP 3104 and LP 1200 pump) with a reverse-phase Merck C_{18} column (250 × 25 mm ID and 5 μm pore size) at a flow rate of 10 mL/min using as solvents 0.05% aqueous TFA (eluent A) and acetonitrile (eluent B). Subsequently, collected fractions containing the pure peptide were pooled and the final solution freeze-dried, after which the solid residue was stored at −20°C until use.

Peptide purity degree was determined by analytical HPLC, using a Hitachi-Merck LaChrom Elite system equipped with a quaternary pump, a thermostatically controlled automated sampler, and a diode-array detector (DAD). MS analyses were performed on an LTQ Orbitrap TM XL hybrid mass spectrometer

(Thermo Fischer Scientific, Bremen, Germany) controlled by LTQ Tune Plus 2.5.5 and Xcalibur 2.1.0. The electrospray ionization source settings (ESI) were as follows: source voltage, 3.1 kV; the capillary temperature was 275 ◦C with a sheath gas flow rate at 40 and auxiliary gas flow rate at 10 (arbitrary unit as provided by the software settings). The capillary voltage was 36 V and the tube lens voltage 110 V. MS data handling software (Xcalibur QualBrowser software, Thermo Fischer Scientific) was used to obtain the confirmation of the synthetic peptide by the exact m/z value of the ion species detected.

The peptides were quantified also by UV-Vis. In particular, peptide solutions of approximately 1mg/mL were quantitated using a Thermo Scientific™ NanoDrop™ One microvolume UV-Vis Spectrophotometer (Thermo Fisher Scientific, Waltham, MA, USA). The 31 quantitation method was chosen, where an extinction coefficient ε_{205} of 31 $mL \cdot mg^{-1} \cdot cm^{-1}$ is assumed[33].

Peptide 4g - H-PraKTTKS-NH$_2$

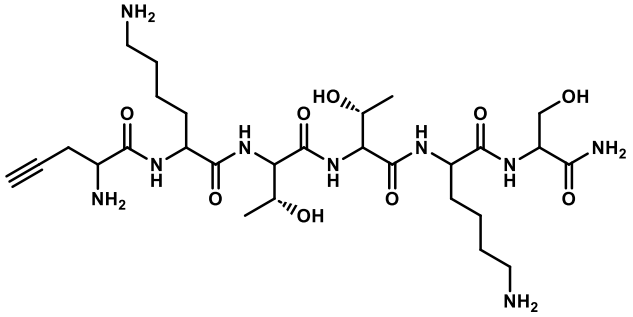

Resin: Fmoc Rink Amide AM (1g, loading 0.52 mmol/g)

Automatic synthesis: SWELL, FMOC DEP, Fmoc-Ser(tBu)-OH COUPLING **x2**, FMOC DEP, Fmoc-Lys(Boc)-OH COUPLING **x2**, FMOC DEP, Fmoc-Thr(tBu)-OH COUPLING **x2**, FMOC DEP, Fmoc-Thr(tBu)-OH COUPLING **x2**, FMOC DEP, Fmoc-Lys(Boc)-OH COUPLING **x2**, FMOC DEP, Fmoc-Pra-OH COUPLING **x2**, FMOC DEP, CLEAVAGE.

The peptide was purified with a gradient of 1-25%B in 60min (A: H_2O + 0.05% TFA, B: CH_3CN).

Purity 4g: 95% **UV-Vis quantification**: 40%

Peptide 5a - H-CKKLLKWLLKLL-NH$_2$

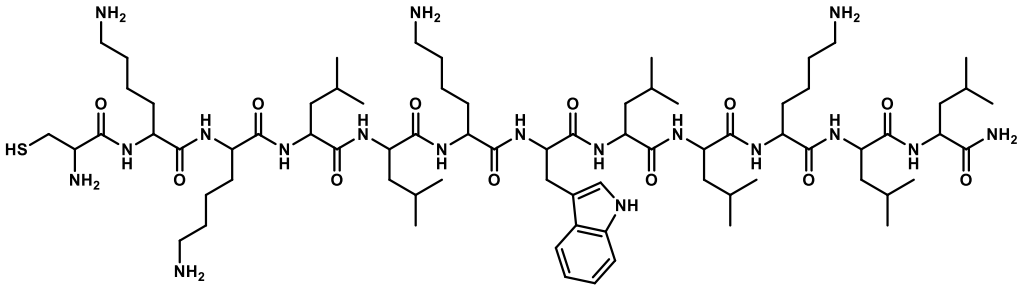

Resin: Fmoc Rink Amide AM (1g, loading 0.52 mmol/g)

Automatic synthesis: SWELL, FMOC DEP, Fmoc-Leu-OH COUPLING **x2**, FMOC DEP, Fmoc-Leu-OH COUPLING **x2**, FMOC DEP, Fmoc-Lys(Boc)-OH COUPLING **x2**, FMOC DEP, Fmoc-Leu-OH COUPLING **x2**, FMOC DEP, Fmoc-Leu-OH COUPLING **x2**, FMOC DEP, Fmoc-Trp(Boc)-OH COUPLING **x2**, FMOC DEP, Fmoc-Lys(Boc)-OH COUPLING **x2**, FMOC DEP, Fmoc-Leu-OH COUPLING **x2**, FMOC DEP, Fmoc-Leu-OH COUPLING **x2**, FMOC DEP, Fmoc-Lys(Boc)-OH COUPLING **x2**, FMOC DEP, Fmoc-Lys(Boc)-OH COUPLING **x2**, FMOC DEP, Fmoc-Cys(Trt)-OH COUPLING **x2**, FMOC DEP, CLEAVAGE.

The peptide was purified with a gradient of gradient 20-35%B in 10min then 35-75%B in 60min (A: H_2O + 0.05% TFA, B: CH_3CN).

Purity 5a: 97% **UV-Vis quantification**: 60%

3.4.2 Chitosan modification

Chitosan purification

High molecular weight chitosan powder was pre-hydrated in water, for 24 h at 4 ◦ C under magnetic stirring. Then, acetic acid was added up to a concentration of 1%. The slurry was left stirring overnight at room temperature. The resulting gel was filtered through a 20µm pore size filter and chitosan was then precipitated through dropwise addition of aqueous 1M NaOH, while stirring. The regenerated chitosan was washed with distilled and deionized water by centrifugation until neutrality, freeze-dried and grounded in a laboratory mill (IKA) to yield a fine powder.

CHO grafting on chitosan

Chitosan (25mg) was added to 2mL of a solution containing 20U of laccase (0.5 U/mg) per gram of chitosan and 8%$_{wt}$ of TEMPO in sodium acetate/acetic acid buffer (pH 5, 50mM). After 1 day of stirring, 10 drops of 1M NaOH were added to the solution to precipitate the dissolved chitosan. The precipitated solid was recovered by centrifugation (2500 rpm x 10min) and washed 3 times with a basic solution (2mL of H_2O + 10 drops of 1M NaOH) and 5 times with H_2O. The solid was left under vacuum at 37°C for the night and stored at room temperature.

Azide grafting on chitosan

Chitosan (450mg) was added to a solution containing 3eq of ISA·HCl and 4.5eq of K_2CO_3 in 43mL of water, and left stirring. The day after, NaOH 1M was added to the solution up to pH 12. The precipitated solid was recovered by centrifugation (2500 rpm x 10min) and washed five times with 0.1M NaOH and five times with H_2O. The solid was left under vacuum at 37°C for the night and stored at room temperature.

CHO grafting on chitosan-N_3

Chitosan-N_3 (400mg) was added to 30mL of a solution containing 20U of laccase (0.5 U/mg) per gram of material and 8%$_{wt}$ of TEMPO in sodium acetate/acetic acid buffer (pH 5, 50mM). After 1 day of stirring, 1M NaOHwas added to the solution up to pH 12. The precipitated solid was recovered by centrifugation (2500 rpm x 10min) and washed five times with 0.1M NaOH and five times with H_2O. The solid was left under vacuum at 37°C for the night and stored at room temperature.

3.4.3 Peptide-Chitosan conjugations - Preliminary

CHO-chitosan-N_3 + Cys3.1

The amount of aldehyde present was assumed at 10% of the available sites (for more details see *Chapter 4.2.2*), therefore CHO-chitosan-N_3 (20mg) was added to a 1.5mM solution of **Cys3.1** (1.5eq, with respect to the moles of aldehyde) and 1.5eq of TCEP in sodium acetate/acetic acid buffer (pH 4.5, 50mM). The day after, 1M NaOH was added to the solution up to pH 12. The precipitated solid was recovered by centrifugation (2500 rpm x 10min) and washed five times with 0.1M NaOH and five times with H_2O. The solid was left under vacuum at 37°C overnight and stored at room temperature.

CHO-chitosan-N_3 + PraPP4

The amount of grafted azide was assumed to be equivalent to the moles of repeating units. Four stock solutions of $CuSO_4 \cdot 5H_2O$, THPTA, sodium ascorbate and aminoguanidine hydrochloride were prepared in water. 236 µL of the copper solution were added to 602 µL of the THPTA solution, after which 2.357 mL of sodium ascorbate and 3.246 mL of aminoguanidine hydrochloride were mixed. Finally, the Cu/THPTA and ascorbate/aminoguanidine solutions were added to CHO-chitosan-N_3 (20mg) and peptide **4g** dissolved in water. After 2 days of stirring, 1M NaOHwas added to the solution up to pH 12. The precipitated solid was recovered by centrifugation (2500 rpm x 10min twice) and washed three times with 0.1M EDTA and three times with H_2O.

	Peptide **4g**	$CuSO_4 \cdot 5H_2O$	THPTA	Sodium ascorbate	Aminoguanidine hydrochloride
Molar equivalents	0.25eq*	0.25eq*	5eq**	50eq**	1eq***
Stock solution concentration	-	27.7 mg/mL	94.6 mg/mL	94.6 mg/mL	44.6 mg/mL
V used	-	236 µL	602 µL	2.357 mL	3.246 mL
Final concentration	1.25mM	1.25mM	6.25 mM	62.5 mM	62.5 mM

***Table 3.7**: reaction conditions for the synthesis of CHO-chitosan-**PP4**. *calculated with respect to the moles of azide. **calculated with respect to the moles of copper. ***calculated with respect to the moles of sodium ascorbate.*

The solid was left under vacuum at 37°C overnight and stored at room temperature.

The residual azides on CHO-chitosan-**PP4** were capped by performing the azide-alkyne reaction with an excess of propargylamine in the same conditions as the peptide.

	Propargylamine	$CuSO_4 \cdot 5H_2O$	THPTA	Sodium ascorbate	Aminoguanidine Hydrochloride
Molar equivalents	100eq*	0.25eq*	5eq**	50eq**	1eq***
Stock solution concentration	-	32.4 mg/mL	87.5 mg/mL	84.4 mg/mL	59.0 mg/mL
V used	-	202 µL	650 µL	3.074 mL	2.453 mL
Final concentration	500mM	1.25mM	6.25 mM	62.5 mM	62.5 mM

Table 3.8*: reaction conditions for the capping of the N_3 remaining in CHO-chitosan-**PP4**. *calculated with respect to the moles of azide. **calculated with respect to the moles of copper. ***calculated with respect to the moles of sodium ascorbate.*

The capped solid was left under vacuum at 37°C overnight and stored at room temperature.

3.1-chitosan-PP4

*From CHO-chitosan-**PP4***

The amount of aldehyde present was assumed at 10% of the available sites (for more details *Chapter 4.2.2*), therefore half of the solid obtained after the capping of CHO-chitosan-**PP4** (12.5mg) was added to a 1.5mM solution of **5a** (1.5eq, with respect to the moles of aldehyde) and 1.5eq of TCEP in sodium acetate/acetic acid buffer (pH 4.5, 50mM). The day after, NaOH 1M was added to the solution up to pH 12. The precipitated solid was recovered by centrifugation (2500 rpm x 10min) and washed five times with 0.1M NaOH and five times with H_2O. The solid was left under vacuum at 37°C overnight and stored at room temperature.

*From **3.1**-chitosan-N_3*

	Peptide **4g**	$CuSO_4 \cdot 5H_2O$	THPTA	Sodium ascorbate	Aminoguanidine Hydrochloride
Molar equivalents	0.25eq*	0.25eq*	5eq**	50eq**	1eq***
Stock solution concentration	-	27.7 mg/mL	94.6 mg/mL	94.6 mg/mL	44.6 mg/mL
V used	-	122 µL	310 µL	1.215 mL	1.673 mL
Final concentration	1.25mM	1.25mM	6.25 mM	62.5 mM	62.5 mM

Table 3.9*: reaction conditions for the synthesis of **3.1**-chitosan-**PP4**. *calculated with respect to the moles of azide. **calculated with respect to the moles of copper. ***calculated with respect to the moles of sodium ascorbate.*

The amount of grafted azide was assumed to be equivalent to the moles of repeating units. The same four stock solutions used to synthesize uncapped CHO-chitosan-**PP4** were used. In particular, the Cu/THPTA and ascorbate/aminoguanidine solutions were added to half the mass of the solid obtained

in the synthesis of **3.1**-chitosan-N_3 (15mg) and peptide **4g** dissolved in water. After 2 days of stirring, 1M NaOH was added to the solution up to pH 12. The precipitated solid was recovered by centrifugation (2500 rpm x 10min twice) and washed three times with 0.1M EDTA, 5% $NaHCO_3$, H_2O. The solid was left under vacuum at 37°C overnight and stored at room temperature.

3.4.4 Peptide-Chitosan conjugations

Conjugation to Cys3.1

The amount of aldehyde present was assumed at 10% of the available sites (for more details *Chapter 4.2.2*). Chitosan (100mg) or CHO-chitosan-N_3 (200mg) were added to a 2mM solution of peptide **5a** (1.5eq, with respect to the moles of aldehyde) and 1.5eq of TCEP in sodium acetate/acetic acid buffer (pH 4.5, 50mM). After 1 day of stirring, 1M NaOH was added dropwise until the formation of a precipitate. The solid was centrifuged (2500 rpm x 10min) and washed three times with 0.1M NaOH and three times with H_2O. Then, the solid was dispersed in H_2O, recovered by lyophilization, and stored at room temperature.

Conjugation to PraPP4

	Peptide **4g**	$CuSO_4 \cdot 5H_2O$	THPTA	Sodium ascorbate	Aminoguanidine Hydrochloride
Molar equivalents	0.25eq*	0.25eq*	5eq**	50eq**	1eq***
Stock solution concentration	2.50 mg/mL	44.5 mg/mL	72.3 mg/mL	119.4 mg/mL	52.4 mg/mL
Final concentration	1.25mM	1.25mM	6.25 mM	62.5 mM	62.5 mM
Volume added to chitosan	40 mL	870 µL	4.7 mL	12.8 mL	16.4 mL
Volume added to CHO-chitosan-N_3	35 mL	758 µL	4.1 mL	11.2 mL	14.2 mL
Volume added to **3.1**-chitosan-N_3	35 mL	758 µL	4.1 mL	11.2 mL	14.2 mL

Table 3.10*: reaction conditions for the synthesis of CHO-chitosan-**PP4**, **3.1**-chitosan-**PP4** and the control with unmodified chitosan. *calculated with respect to the moles of azide. **calculated with respect to the moles of copper. ***calculated with respect to the moles of sodium ascorbate.*

The amount of grafted azide was assumed to be equivalent to the moles of repeating units. Five stock solutions of: peptide **4g**, $CuSO_4 \cdot 5H_2O$, THPTA, sodium ascorbate and aminoguanidine were prepared in water. Then, 5eq of THPTA were added to $CuSO_4 \cdot 5H_2O$, and 1eq of aminoguanidine was added to sodium ascorbate. Next, Cu/THPTA and ascorbate/aminoguanidine solutions were added to chitosan (100mg), CHO-chitosan-N_3 (100mg), or half of the mass of **3.1**-chitosan-N_3 (148.1 mg) and peptide **4g** solution. After 2 days of stirring, 1M NaOH was added to the solution up to pH 12. The precipitated solid was recovered by centrifugation (2500 rpm x 10min twice) and washed three times with 0.1M EDTA, 5%

$NaHCO_3$ and H_2O. The solid was dispersed in H_2O, recovered by lyophilization, and stored at room temperature.

Capping of the azides

The residual azides on **3.1**-chitosan-N_3 and CHO-chitosan-**PP4** were capped by performing the azide-alkyne reaction with an excess of pent-1-yne in the same conditions used for peptide **4g**.

	Pent-1-yne	$CuSO_4 \cdot 5H_2O$	THPTA	Sodium ascorbate	Aminoguanidine Hydrochloride
Molar equivalents	80eq*	0.25eq*	5eq**	50eq**	1eq***
Stock solution concentration	-	42.5 mg/mL	69.5 mg/mL	111.5 mg/mL	48.7 mg/mL
Final concentration	800mM	1.0 mM	5.0 mM	50.0 mM	50.0 mM
Volume added to CHO-chitosan-**PP4**	3.4 mL	635 µL	3.374 mL	9.6 mL	12 mL
Volume added to **3.1**-chitosan-N_3	3.4 mL	635 µL	3.374 mL	9.6 mL	12 mL

Table 3.11*: reaction conditions for the capping of the N_3 remaining in CHO-chitosan-**PP4**, and **3.1**-chitosan-N_3. *calculated with respect to the moles of azide. **calculated with respect to the moles of copper. ***calculated with respect to the moles of sodium ascorbate.*

After 2 days of stirring, 1M NaOH was added to the solution up to pH 12. The precipitated solid was recovered by centrifugation (13000 rpm x 5min x2) and washed three times with 0.1M EDTA, 5% $NaHCO_3$ and H_2O. The solid was dispersed in H_2O, recovered by lyophilization, and stored at room temperature.

3.4.5 Amino acid analysis

Sample preparation: Aqueous HCl (6M) was added to weighed samples of the materials as per Table X. The resulting solutions were stirred at 120 °C for 24 h. Then, the solved was removed under reduced pressure using a rotatory evaporator , and the residues were sent for amino acid analysis (AAA) at the *Serveis Cientificotècnics* of the University of Barcelona.

Sample	Mass (mg)	Volume of 6M HCl (µL)
Chitosan	1.92	200
CHO-chitosan-N_3	2.24	200
Chitosan + **Cys3.1**	5.59	400
3.1-Chitosan	2.05	200
Chitosan + **PraPP4**	3.00	200
CHO-Chitosan-**PP4**	3.27	100
3.1-Chitosan-**PP4**	3.20	200

Table 3.12*: Preparation of the samples of AAA.*

Amino acid analysis: 1000 µL of 20 mM aqueous HCl were added to the tubes containing the hydrolyzed residue. The samples were subsequently shaken for 24 h on an orbital shaker and sonicated in an ultrasonic bath. The solutions were filtered through a PVDF syringe filter (0.45 µm). Finally, dilutions of these samples were prepared in HPLC-grade water, adding norleucine (Nle) and 2.5 mM α-aminobutyric acid (AABA) as internal standards. An aliquot of the final solution was derivatized with 6-aminoquinolyl-*N*-hydroxysuccinimidyl carbamate according to the Waters AccQ-Tag method. The derivatized amino acids were analyzed by HPLC with UV detection (λ = 254 nm).

Instrument: HPLC (WATERS 600 with detector WATERS 2487).

3.4.6 Antibacterial tests

Spin coating

50 µL of a 0.4% sample solution in 0.1M acetic acid were spin coated on a TCPE disc (diameter 13mm) for 60 sec using 9000 rpm with an acceleration of 1500 rpm. This procedure was repeated twice on each side of the TCPE disk. The disc was added to 500 µL of 0.1M NaOH, and the solution was stirred for 5 min. Then, NaOH solution was removed and the disc washed twice with 500 µL of H_2O. The sample was dried under a gentle stream of argon and stored in a desiccator.

This procedure was performed for chitosan, chitosan+**Cys3.1**, **3.1**-chitosan and **3.1**-chitosan-**PP4** that were synthetized as described in *Section 3.4.4*.

Antibacterial tests

A suspension of *S. aureus* (ATCC 25923) or *P. aeruginosa* (ATCC 27853) in phosphate buffered saline (PBS 1X; 10 µL, 10^6 CFU mL^{-1}) was deposited onto the spin coated discs and then covered with a sterile TCPE coverslip (13 mm diameter) to promote contact between bacteria and surface. After incubation at 37°C for 3 h, coverslips were gently removed and samples were rinsed twice with sterile-filtered aqueous PBS (200 µL). Then, samples were prepared for CFU counting after sonication. The same procedure was performed on sterile TCPE discs as a control. The procedure was performed in three independent triplicates using two discs coated with materials from the same batch.

CFU counting

The washing solution was sonicated and then the bacteria were recovered. Serial dilutions were plated on agar for CFU counting. Data is presented as mean ± standard deviation, and p values below 0.05 were considered statistically significant.

References

1 Bernkop-Schnürch, A. & Dünnhaupt, S. Chitosan-based drug delivery systems. *European journal of pharmaceutics and biopharmaceutics* **81**, 463-469 (2012).
2 Dash, M., Chiellini, F., Ottenbrite, R. M. & Chiellini, E. Chitosan—A versatile semi-synthetic polymer in biomedical applications. *Progress in polymer science* **36**, 981-1014 (2011).
3 Berger, J. *et al.* Structure and interactions in covalently and ionically crosslinked chitosan hydrogels for biomedical applications. *European journal of pharmaceutics and biopharmaceutics* **57**, 19-34 (2004).
4 Barbosa, M., Vale, N., Costa, F. M., Martins, M. C. L. & Gomes, P. Tethering antimicrobial peptides onto chitosan: Optimization of azide-alkyne "click" reaction conditions. *Carbohydrate polymers* **165**, 384-393 (2017).
5 Barbosa, M. *et al.* Antimicrobial coatings prepared from Dhvar-5-click-grafted chitosan powders. *Acta Biomaterialia* **84**, 242-256 (2019).
6 Huq, T. *et al.* Sources, production and commercial applications of fungal chitosan: A review. *Journal of Bioresources and Bioproducts* **7**, 85-98 (2022).
7 Salmon, S. & Hudson, S. M. Crystal morphology, biosynthesis, and physical assembly of cellulose, chitin, and chitosan. *Journal of Macromolecular Science, Part C: Polymer Reviews* **37**, 199-276 (1997).
8 Gheorghiță, D. *et al.* Chitosan-based biomaterials for hemostatic applications: a review of recent advances. *International journal of molecular sciences* **24**, 10540 (2023).
9 Li, J. & Zhuang, S. Antibacterial activity of chitosan and its derivatives and their interaction mechanism with bacteria: Current state and perspectives. *European Polymer Journal* **138**, 109984 (2020).
10 Ahmed, S. & Ikram, S. Chitosan based scaffolds and their applications in wound healing. *Achievements in the life sciences* **10**, 27-37 (2016).
11 Patrulea, V., Ostafe, V., Borchard, G. & Jordan, O. Chitosan as a starting material for wound healing applications. *European Journal of Pharmaceutics and Biopharmaceutics* **97**, 417-426 (2015).
12 Oliveira, J. R., Martins, M. C. L., Mafra, L. & Gomes, P. Synthesis of an O-alkynyl-chitosan and its chemoselective conjugation with a PEG-like amino-azide through click chemistry. *Carbohydrate Polymers* **87**, 240-249 (2012).
13 Castro, V., Blanco-Canosa, J. B., Rodriguez, H. & Albericio, F. Imidazole-1-sulfonyl azide-based diazo-transfer reaction for the preparation of azido solid supports for solid-phase synthesis. *ACS combinatorial science* **15**, 331-334 (2013).
14 da Silva, S. B., Krolicka, M., van den Broek, L. A., Frissen, A. E. & Boeriu, C. G. Water-soluble chitosan derivatives and pH-responsive hydrogels by selective C-6 oxidation mediated by TEMPO-laccase redox system. *Carbohydrate Polymers* **186**, 299-309 (2018).
15 Kang, S. J., Won, H. S., Choi, W. S. & Lee, B. J. De novo generation of antimicrobial LK peptides with a single tryptophan at the critical amphipathic interface. *Journal of Peptide Science: An Official Publication of the European Peptide Society* **15**, 583-588 (2009).
16 Teo, S. W. *et al.* Identification of an ultra-short peptide with potent Pseudomonas aeruginosa activity for development as a topical antibacterial agent. *International Journal of Peptide Research and Therapeutics* **25**, 359-366 (2019).
17 Ng, S. M. S. *et al.* Screening for a potent antibacterial peptide to treat mupirocin-resistant MRSA skin infections. *International Journal of Peptide Research and Therapeutics* **23**, 481-491 (2017).
18 Mendes, R. J. *et al.* In vitro evaluation of five antimicrobial peptides against the plant pathogen Erwinia amylovora. *Biomolecules* **11**, 554 (2021).
19 Mariz-Ponte, N. *et al.* A synergic potential of antimicrobial peptides against Pseudomonas syringae pv. actinidiae. *Molecules* **26**, 1461 (2021).
20 Gomes, A. *et al.* Turning a collagenesis-inducing peptide into a potent antibacterial and antibiofilm agent against multidrug-resistant gram-negative bacteria. *Frontiers in Microbiology* **10**, 1915 (2019).
21 Kachooeian, M. *et al.* Matrixyl patch vs matrixyl cream: a comparative in vivo investigation of matrixyl (MTI) effect on wound healing. *ACS omega* **7**, 24695-24704 (2022).
22 Park, H., An, E. & Lee, A.-R. C. Effect of Palmitoyl-Pentapeptide (Pal-KTTKS) on Wound Contractile Process in Relation with Connective Tissue Growth Factor and a-Smooth Muscle Actin Expression. *Tissue Engineering and Regenerative Medicine* **14**, 73-80 (2017).
23 Aracri, E., Valls, C. & Vidal, T. Paper strength improvement by oxidative modification of sisal cellulose fibers with laccase–TEMPO system: influence of the process variables. *Carbohydrate polymers* **88**, 830-837 (2012).
24 Albini, F., Biondi, B., Lastella, L. & Peggion, C. Oxime and thiazolidine chemoselective ligation reactions: a green method for cotton functionalization. *Cellulose* **30**, 5573-5587 (2023).
25 Amer, H. *et al.* Synthesis and characterization of periodate-oxidized polysaccharides: dialdehyde xylan (DAX). *Biomacromolecules* **17**, 2972-2980 (2016).
26 Kim, U.-J., Kuga, S., Wada, M., Okano, T. & Kondo, T. Periodate oxidation of crystalline cellulose. *Biomacromolecules* **1**, 488-492 (2000).
27 Alves, P. M. *et al.* Thiol–norbornene photoclick chemistry for grafting antimicrobial peptides onto chitosan to create antibacterial biomaterials. *ACS Applied Polymer Materials* **4**, 5012-5026 (2022).
28 Chouhan, G. & James, K. CuAAC macrocyclization: high intramolecular selectivity through the use of copper–tris (triazole) ligand complexes. *Organic Letters* **13**, 2754-2757 (2011).

29 Chan, T. R., Hilgraf, R., Sharpless, K. B. & Fokin, V. V. Polytriazoles as copper (I)-stabilizing ligands in catalysis. *Organic letters* **6**, 2853-2855 (2004).
30 Presolski, S. I., Hong, V. P. & Finn, M. Copper-catalyzed azide–alkyne click chemistry for bioconjugation. *Current protocols in chemical biology* **3**, 153-162 (2011).
31 Amaral, I., Granja, P. & Barbosa, M. Chemical modification of chitosan by phosphorylation: an XPS, FT-IR and SEM study. *Journal of Biomaterials Science, Polymer Edition* **16**, 1575-1593 (2005).
32 Atherton, E. *et al.* A mild procedure for solid phase peptide synthesis: use of fluorenylmethoxycarbonylamino-acids. *Journal of the Chemical Society, Chemical Communications*, 537-539 (1978).
33 Loughrey, S., Mannion, J. & Matlock, B. in *Using the NanoDrop one to quantify protein and peptide preparations at 205 nm.* (Thermo Fisher Scientific Wilmington, DE, 2021).

Chapter IV:

Nanofibrous Textiles with Antibacterial and Skin-regenerative Properties Based on Hyaluronic Acid and Peptides

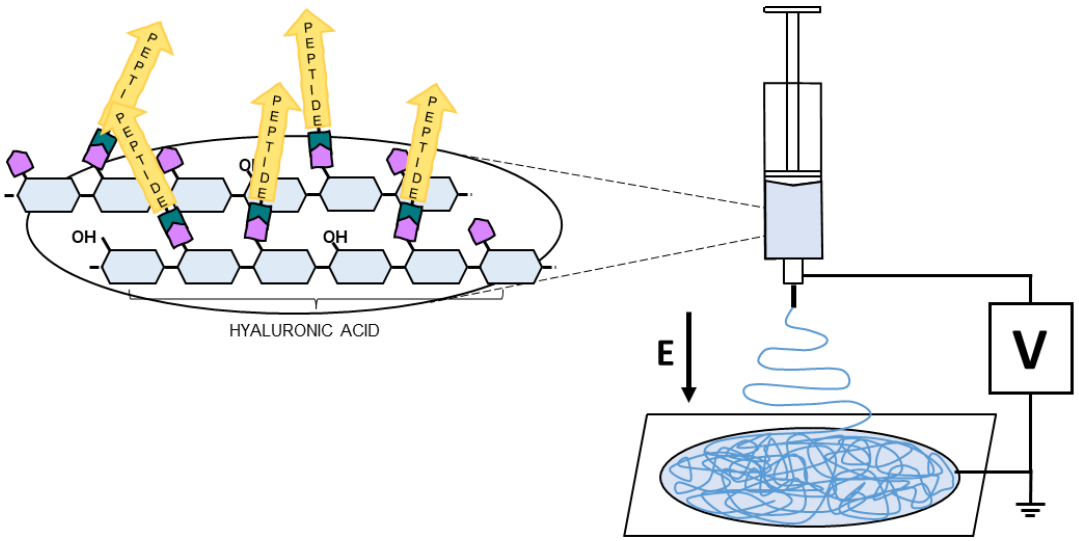

Acknowledgements:

- Prof. Giovanna Batoni and Prof. Semih Esin from the University of Pisa for the anti-inflammatory and cytotoxicity tests.
- Dr. Chiara Rinoldi from I.R.A. – Istituto di Ricerche Applicate for mentoring me about the electrospinning technique and for the antibacterial tests on the electrospun materials.
- Dr. Renato Schiesari for some of the FT-IR measurements.

4.1 Introduction

In the context of active wound healing dressings, hyaluronic acid is a very promising material due to its intrinsic anti-inflammatory activity, its active role at the wound site, and its high biocompatibility and biodegradability. On the other hand, peptides are great molecules for the functionalization of materials due to their wide range of activity that can be tuned by changes in the amino acidic sequence. Few authors have investigated a covalent bond to merge the properties of hyaluronic acid and peptides[1-4]. Of particular interest are the study of *Elder et al.*[2] and the very recent report of *Petit et al*[1]. In the former[2], the authors successfully bound the anti-inflammatory peptide WP9QY to hyaluronic acid via an amide bond. The resulting conjugate demonstrated an enhanced binding affinity for TNFα compared to the peptide alone. The latter[1], exploits thiol–acrylate conjugation to covalently bind the hybrid peptide **PP4-3.1** (*Chapter 3.1.2*) to acrylate-hyaluronic acid for the treatment of chronic wounds. The hydrogel formulated with this conjugate resulted active against Gram-positive and Gram-negative bacteria, and able to enhance cell adhesion.

In this chapter the focus is on the use of the thiazolidine bond[5,6] (*Chapter 1.4.1*) as a method to provide additional functionalities to hyaluronic acid using peptides as the active molecules. Since nanostructured hyaluronic acid could have enhanced wound healing potential, the use of electrospinning for the production of hyaluronic acid-based textiles will also be explored. Particular attention is given to the use of environmentally friendly solvents and procedures wherever possible in the production process.

4.1.1 Hyaluronic acid

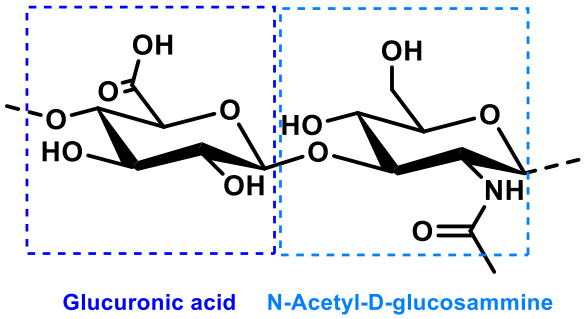

Hyaluronic acid (HA) is a well-studied natural polysaccharide present in all vertebrate animals, and originates in almost all body tissues and fluids[7]. It is a linear polymer, and its repeating unit is a disaccharide of β-1→4-D-glucuronic acid and β-1→3-N-acetyl-D-glucosamine[8], making it a hydrophilic polyanionic polymer. HA is a critical component of the extracellular matrix and, depending on its molecular weight, HA demonstrates a different set of properties: in general, low molecular weight HA (2-50 kDa) activates the proinflammation cytokines, whereas high molecular weight HA (>1250 kDa) has an anti-inflammatory and antiangiogenic activity[9,10]. Moreover, in a paper from *Lee et al.*[10] HA of 100-500 kDa (medium) was found to increase the expression of macrophages genes. The role of mono- to tetra-saccharides of HA in

inflammation was investigated by *Han et al.*[11]: the tetra-saccharide was demonstrated to enhance inflammation, but the di-saccharide was found to inhibit liposaccharide induced inflammation *in vivo*.

Hyaluronic acid is omnipresent in all stages of wound healing, being actively involved in the regulation of the tissue repair process[12]. During the *inflammatory phase*, fragments of HA accumulate at the site of the wound facilitating the deposition of fibrinogen and the infiltration of neutrophils, and stimulate the initial inflammatory response. During the *proliferative phase*, HA promotes angiogenesis. Finally, during *reepithelization* and *maturation*, high molecular HA promotes mitosis, and stimulates newly divided cells to migrate upward from their basal origin[13]. To this regard the work of *D'Agostino et al.*[14], demonstrated that both HA with a molecular weight of 90 kDa (low) and of 1400 kDa (high) induce wound closure and are non-toxic and non-inflammatory. The authors prove that the use of complexes of the two types of HA was even more beneficial to wound closure, probably due to their longer half-lives *in vivo*. In addition, they show that only HA with a molecular weight lower than 6kDa impairs the wound healing process[15].

Hyaluronic acid can be degraded in vivo by enzymatic processes (e.g hyaluronidases) and by oxidative degradation (e.g. reactive oxygen species), as well as by acidic depolymerization. HA is of particular interest due to its high water absorption capacity, that gives unique viscoelastic properties to its solution, but that can also be exploited for the absorption of exudates in wound sites[9,13].

Overall, this biopolymer is a great material in the biomedical field due to its high biocompatibility and biodegradability, but also its intrinsic anti-inflammatory properties and is favorable role in the wound healing process. In fact, it is widely used in fields[7] ranging from cosmetics, to tissue engineering, but also cancer treatment, or intra-articular injection for osteoarthritis[16] .

Aldehyde grafting on Hyaluronic acid

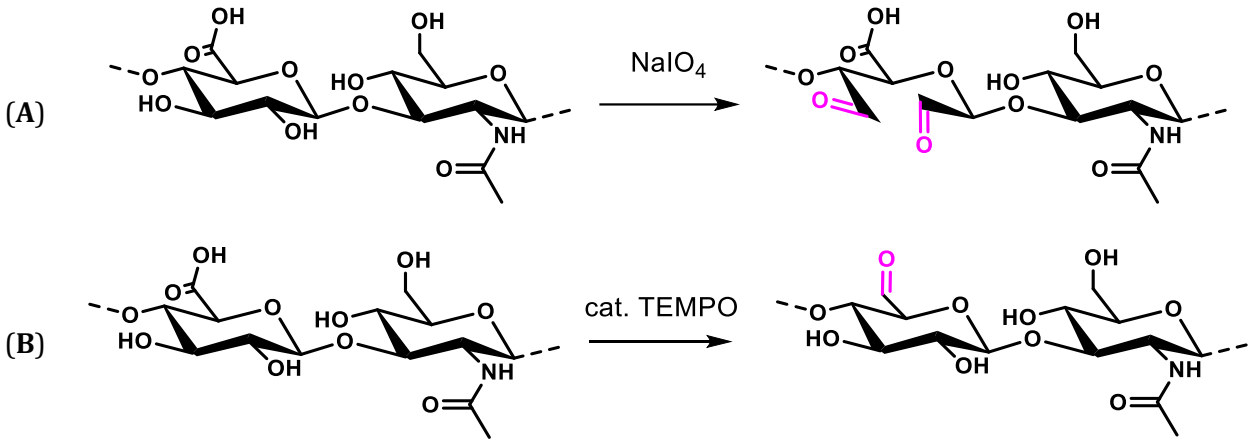

Figure 4.1*: Schematic representation of the introduction of aldehydes on hyaluronic acid using (**A**) $NaIO_4$ (**B**) TEMPO catalyzed reaction.*

The most common procedure to introduce an aldehyde moiety into hyaluronic acid involves the oxidation of the vicinal diols of the glucuronic acid moiety to aldehyde using $NaIO_4$[17-22] (Fig. 4.1A).

However there are reports of TEMPO catalyzed reactions for the selective conversion of the C_6-OH to aldehyde[18,23,24] (Fig. 4.1B).

It is important to note that the reaction conditions and yields of the $NaIO_4$ oxidation on hyaluronic acid (Table 4.1) vary depending on the reference and are not completely coherent one with the other:

Reference	Year	Eq $NaIO_4$	Time	Reported Yield
Jia et al.[22]	2004	2.3	2h	67%
Su et al.[21]	2010	1	24h	87%
Liu et al.[20]	2018	0.5	24h	33%
Qian et al.[19]	2019	0.5	overnight	24%
Shan et al.[18]	2021	0.1-0.7	2h	10%
Maiz- Fernández et al.[17]	2022	1	2h	24%

***Table 4.1**: Reaction conditions in relevant literature reports for the oxidation of HA with $NaIO_4$.*

As shown in Figure 4.1A, drawback of $NaIO_4$ is the opening of the glucuronic ring, that results in an alteration of the backbone structure of the polymer. Thus, a study by *Shan et al*.[18] investigated the use of a TEMPO/TCC catalyzed oxidation as a milder alternative to $NaIO_4$. Using DMF as the solvent and low molecular hyaluronic acid as the substrate (61 kDa), they managed to reach a maximal degree of oxidation (DO) of over 70% (0.05eq TEMPO, 0.76 eq TCC, reaction time 4h), which is higher than all the DO they obtained when using 0.1 to 0.7eq of $NaIO_4$ (reaction time 2h). However, to this author knowledge up to date there has not been any report on the applicability of the TEMPO/laccase/O_2 catalytic system[25] (*Chapter 2.2.3*) to hyaluronic acid.

4.1.2 The Peptides

In this chapter the peptides were selected with the perspective of an industrial scale-up of the whole process. Therefore, besides having an activity relevant for wound healing, they needed to have a short sequence, a minimal number of different amino acids, and be soluble in the solvents used for the conjugation reactions and electrospinning.

Ac-SDKP

Ac-SDKP, also known as goralatide or seraspenide, is a naturally occurring peptide that was first isolated from calf bone marrow[26]. In humans, it is mainly present in highly vascular and hematopoietic organs, and its concentration in tissues is regulated by its release by the action of propyl oligopeptidase (POP) from the N-terminal sequence of its precursor, a small ubiquitous protein with 43 amino acids called thymosin-beta 4 (Tβ4), and its degradation by the angiotensin-converting enzyme (ACE). Ac-SDKP was originally described as an inhibitor of hematopoietic stem cells proliferation[26], but its activity was demonstrated to be wider, including **anti-inflammatory**, and **anti-fibrotic**, **pro-angiogenic**, and **immunomodulatory effects** [27-29].

Its anti-inflammatory activity is thought to be due to an inhibition of the differentiation of bone marrow stem cells to macrophages, the activation and migration of macrophages, as well as the release of the proinflammatory cytokine TNF-α by activated macrophages[30]. On the other hand, the Ac-SDKP-mediated inhibition of transforming growth factor TGF-β signaling pathways results in reduced fibroblasts proliferation and collagen synthesis, indicating the mechanism of its anti-fibrotic effect[27,29]. The mechanism of Ac-SDKP pro-angiogenic activity is not clearly understood, however this type of activity was demonstrated to be comparable to that of HARP, a potent inductor of angiogenesis both *in vitro* and *in vivo,* at nanomolar concentrations, using chicken models [31].

In the work of *Cai et al*.[28] the use of Ac-SDKP as an anti-inflammatory agent were investigated on mice models with induced chronic obstructive pulmonary disease pathophysiology (COPD). Ac-SDKP was administered one time/week for 4 weeks, via intra-tracheal administration. The amount of pro-inflammatory cytokines in the serum of the mice treated with the peptide resulted significantly lower than the untreated COPD-mice, bringing the TNF-α and IL-1β levels to values comparable to the control group.

The angiogenic activity of Ac-SDKP makes it particularly interesting in the context of wound healing and skin treatments. In particular, a study by *Fromes et al*.[32] investigated the efficacy of Ac-SDKP subcutaneous injections (2.5mg/kg/injection; 5mg/kg/day) in healing skin injuries in rat skin flaps models. As argumented by the authors, an adequate blood supply is needed for the skin flap to survive and avoid necrosis, and indeed the injuries treated with the peptide resulted more vascularized than the controls. More specifically, the higher the vascularization the lower was the incidence of necrosis and higher re-epithelialization rates, suggesting that **Ac-SDKP can enhance the reconstructive process of the skin**. Another study from the same group[33,34] suggested the use of Ac-SDKP as an anti-ageing agent due to its ability to stimulate the growth of human keratinocytes and fibroblasts in vitro at concentrations that range from 10^{-7} to 10^{-11} M, but more importantly, topical treatment of *ex vivo* cultured skin explants with 10^{-5} M Ac-SDKP increases the thickness of the epidermis and upregulates the synthesis of keratins, fibronectin, collagen III and IV as well as the glycoaminoglycans (GAGs).

RWRWRW

The peptide sequence H-RWRWRW-NH_2, also known as $(RW)_3$, is one of the shortest synthetic antimicrobial peptides discovered so far, and was first studied by *Strøm et al*.[35,36] The authors were inspired by the studies on bovine lactoferricin, where substitution of Lys with Arg and the introduction of Trp in the sequence improved the antibacterial activity of lactoferricin analogues. Thus, they synthesized a set of peptides rich in Arg and aromatic amino acids, aiming for the shortest sequence with significant antimicrobial activity.

	MIC (μM)			
Sequence	***E. coli***	***P. aeruginosa***	***S. aureus***	**EC_{50} *(μM)***
RWRWRW-NH_2	5	20	5	N.h.
WWRWRW-NH_2	10	20	5	590
YWRWRW-NH_2	20	50	10	600
RWRYRW-NH_2	50	80	10	N.h.
WRWRWR-NH_2	10	-	7.5	-
RRRWWW-NH_2	5	-	5	-
RWWWRR-NH_2	25	-	5	-
WWRRRW-NH_2	25	-	10	-

***Table 4.2**: MIC and EC_{50} of the hexapeptides as reported in Strøm et al.[35,36] "N.h." no hemolytic activity was found up to 1000 μg/ml; "-"value not tested.*

As shown in Table 4.2, the order of the amino acids in peptides with three Arg and three Trp was demonstrated not to be particularly relevant on the activity against *S.aureus*, but relevant on the activity against *E. coli*[36]. Thus, out of the hexapeptides synthesized by *Strøm et al*[35,36], $(RW)_3$ was the most promising in terms of low hemolysis and high antibacterial activity, particularly against *S. aureus* and methicillin-resistant *S. aureus*[37]. Further studies found $(RW)_3$ to be the minimal pharmacophore and the best peptide in terms of selectivity for bacteria over blood cells amongst a series of $(RW)_n$ peptides[38], and revealed the low cytotoxicity of the peptide against human cancer cell lines, human T-cell lymphoblasts or rat kidney epithelial cells[37,39].

The mechanism of action of $(RW)_3$ was studied on *B. subtilis* and involves an interaction and consequent disruption of the cytoplasmic membrane. In particular, $(RW)_3$ was not found to either permeabilize the membrane, induce pore formation, or ion release. Indeed, its integration in the membrane, that is likely promoted by the cationic Arg residues, deforms the lipid bilayer and delocalizes essential proteins involved in respiration and cell wall biosynthesis, causing membrane depolarization. Since the authors did not find a specific ligand-receptor interaction the lipid bilayer itself is most probably the target of the peptide[40]. In addition, $(RW)_3$ displayed fast killing kinetics with only 3% of *B. subtilis* surviving after 10 min from sumministration, making the development of bacterial resistance unlikely[39].

Considering these promising characteristics, $(RW)_3$ was used as the lead structure for further development in several studies and the following data emerged (Table 4.3)[37,39,41-43]:

- $(RW)_3$ D-enantiomer demonstrates a lower MIC against *S.aureus*, while maintaining the same activity against *E.coli* (21 μM) , *A. baumannii* (21 μM) and *B.subtilis* (1.3 μM)[37]. Furthermore, a systematic L-to-D exchange scan of $(RW)_3K(C_{8-10})$ revealed that most of the diastereomeric peptides have an optimized spectrum of activity, and all of them showed lower hemolytic properties that in some cases reached a 0% hemolysis at concentrations up to 20-fold the MIC,

making the substitution with D-amino acids a valid strategy to lower hemolysis while maintaining the antibacterial activity[44].

- Acetylation at the N-terminus of $(RW)_3$ impacted negatively the activity against *E.coli and B.subtilis*. The same results were obtained when $(RW)_3$ D-enantiomer was acetylated at the same site[37]. On the other hand, lipidation with chains of eight to fourteen carbons on the side chain of an additional lysine improved the peptide activity against all the tested strains (*E. coli, A. baumannii, P. aeruginosa, S. aureus* and *B. subtilis*). The attachment of the lipid at the C-terminal or N-terminal end of the peptide did not make a significant difference in the antibacterial activity. Unfortunately, all the lipidated and active peptides showed an increase in their hemolytic activity with hemolysis values at 250 μg/mL from 20% of $K(C_8)$-$(RW)_3$ to the 50% of all the other peptides lipidated with chains of eight to fourteen carbons, which is notably higher than the 10% observed for the parent peptide[43]. Interestingly, the mode of action of $K(RW)_3$, $(RW)_3K$, $K(C_8)$-$(RW)_3$ and $(RW)_3$-$K(C_8)$ against *S.subtilis* was found to be comparable to the mode of $(RW)_3$ and involving an alteration of the bacterial membrane structure[42].
- The use of $(RW)_3$ in murine models uncovered an unexpected toxicity of the peptide. In particular at doses of 25 mg/kg body weight, the mouse died within few minutes from the injection, while lower doses caused excitement and indisposition in the animal. Since the response to the peptide was acute and immediately after administration, the authors excluded direct cytotoxicity as the cause. However, preliminary tests excluded also an anaphylactic shock and precipitation of $(RW)_3$ in the blood. Further analysis revealed erythrocyte damage whose severity was misjudged by a standard absorption-based hemolysis assay[39].

  Interestingly *Zhang et al.*[41] reported the use of a modified analogue of the peptide ($PcG_3K_5(RW)_3$, where Pc is a zinc phthalocyanine) for the treatment of wounds in mice. In particular, the phthalocyanine provided the peptide with a removable lipophilic moiety that did not negatively impact the cytotoxicity to human fibroblasts or hemolysis. In addition, the modified peptide was safely injected intravenously and cleared from liver and kidneys within 72 hours.

	MIC (μM)					
	Gram-negative			*Gram-positive*		
Sequence	*E. coli*	*A. baumannii*	*P. aeruginosa*	*S. aureus*	*B. subtilis*	Ref
$RWRWRW\text{-}NH_2$	21	21-85	n.a.	11	1.3	[37,43]
$Ac\text{-}RWRWRW\text{-}NH_2$	45	-	-	-	45	[37]
$K\text{-}RWRWRW\text{-}NH_2$	18	n.a.	n.a.	9-18	2	[43]
$K(C_8)\text{-}RWRWRW\text{-}NH_2$	5	9-18	9	1	0.6-1.1	[43]
$RWRWRW\text{-}K\text{-}NH_2$	18	n.a.	n.a.	18	5	[43]
$RWRWRW\text{-}K(C_8)\text{-}NH_2$	2-5	5-9	18-37	2	0-6-1.1	[43]

rwrwrw-NH_2	21	21	n.a.	5.3	1.3	[37]
Ac-rwrwrw-NH_2	90	-	-	-	90	[37]
rWrwRW-K(C_8)	36	18-36	73	9.1	1.1	[44]
rWrWrw-K(C_8)	36	18	73	9.1	1.1	[44]
rwRWrw-K(C_8)	18-36	36	73	4.6	1.1	[44]
rWrwRw-K(C_8)	73	18-36	73	9.1	1.1	[44]
rwRwRw-K(C_8)	n.a	n.a	n.a	9.1	1.1	[44]
Pc-GGGKKKKKRWRWRW-NH_2	16.1	-	-	16.1	-	[41]

***Table 4.3**: Antibacterial activity of relevant modified analogues of $(RW)_3$ reported in Albada et al.[37,43,44] and Zhang et al.[41] "n.a." means no antibacterial activity was found; "-" means that the value was not tested. When a range of values is presented instead of a single value means that different MICs were found.*

Overall, $(RW)_3$ shows promising characteristics for an antibacterial peptide, such as short sequence, activity against both Gram-negative and Gram-positive bacteria and low cytotoxicity in vitro. Its main disadvantage is the toxicity toward blood cells, but this can been addressed with the substitution with D-amino acids.

4.1.3 Electrospinning

Electrospinning is an technique used for the production of nanometric polymer fibers that was first patented by *Formhals*[45-49] around 100 years ago, but has re-emerged in the last few decades, testified by a growing production of scientific literature on the matter[50]. What makes electrospinning particularly attractive is the adaptability of the system to large variety of starting materials, matched to a relatively easy and cost-effective setup[50,51]. In addition, the fiber diameter and the thickness of the sheets could be finely tuned, making it a good candidate for mass production[9].

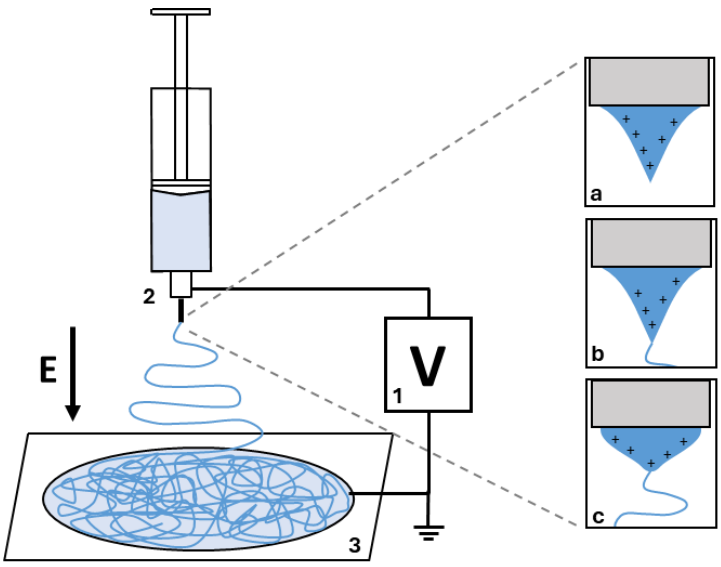

***Figure 4.2**: Schematics of a typical electrospinning apparatus, including: (**1**) high voltage supply, (**2**) syringe needle, and (**3**) collector. (**a**) Formation of Taylor cone, (b) Taylor cone ejects polymer jet, (c) Surface tension causes relaxation of the shape.*

The typical electrospinning set-up requires three main features (Fig. 4.2): a high voltage supply, a capillary tube connected to a needle or pipette, and a grounded collector (made of a conductive metal)[50-

[54]. Briefly, the polymer solution or melt is forced through the needle by gravity or by a pump, the needle and the collector are kept at a relatively short distance from each other (10-50cm), and a high voltage electric field is created between the two. The high voltage applied to the needle charges the polymer solution, and when it reaches a critical value the drop starts elongating to form the typical conical protrusion known as Taylor cone[55] (Fig. 4.2a). When the repulsive electrostatic force overcomes the surface tension, a jet of the fluid is released from the cone and the directs toward the collector, which is oppositely charged (Fig. 4.2b). The jet is subjected to an instability and elongation, and by the time it reaches the collector, the solvent evaporates and dry continuous fibers are deposited. In the case of the melt the released jet solidifies in the air (Fig. 4.2c) [50,51].

It is important to notice that fiber formation and morphology are highly dependent on a lot of parameters, that can be divided in *solution variables* (e.g concentration, polymer molecular weight, viscosity, surface tension, charge density, conductivity, volatility), and *process variables* (e.g. electrode shape, electrode material, electric field strength, electrode-collector distance, solution flow rate, temperature, relative humidity). Therefore the electrospinning of polymers, especially of polysaccharides, is not always straightforward[53,54]. In addition, the main disadvantage of this technique is the rate of production when compared to the popular industrial fiber spinning process (30m/min against the 200-1500 m/min of yarn dry spinning)[52]. However, this can be partially circumvented by the employment of multiple spinneret system[52].

The production of any type of non-woven nanofibrous textile is of particular interest because the high area-to-volume ratio of fibers with a diameter smaller than 100 nm demonstrate properties that were not present in the bulk material, such as remarkable strength of higher surface reactivity[56], but also capture a greater amount of exudates due to greater contact surface[9]. In addition, the use of biocompatible and/or biodegradable biopolymers has been investigated in the last years in the field of regenerative medicine. In fact, electrospun polysaccharides can recreate a structured three-dimensional environment similar to the extracellular matrix where human cells could attach and organize[57], allowing for an enhanced growth of cells at the wound site and potentially without the formation of scar tissue[51]. Moreover, pore sizes from 500nm to 1μm, typical of non-woven nanofibrous membranes, are small enough to mechanically protect the wound from bacterial penetration[51].

Electrospinning of Hyaluronic Acid

Adding the great biological properties of hyaluronic acid to an electrospun material is of great interest for the development of high performance dressings[9]. In fact, beside resembling the extracellular matrix, hyaluronic acid nanofibers create an easy-to-handle material equipped with good hemostatic properties that can act as a template for cell growth. However, the electrospinning of hyaluronic acid is particularly difficult to achieve, mainly due to the high viscosity and high surface tension of aqueous hyaluronic acid solutions. Indeed, the former makes the jet unstable and does not allow the formation of homogeneous

and fully dried fibers, the latter induces the necessity of much higher electrostatic forces that do not allow for a continuous process[9,13].

To circumvent these problems, two main approaches have been explored: (**1**) changes from the typical electrospinning set-up, or (**2**) changes to the solution. One example of the former is co-electrospinning (dual jet technique, emulsion, or co-axial technique), where two polymers solutions create a core-shell nanofiber with the electrospinnable polymer in the shell and the other filling the core[9,13]. Blow-assisted electrospinning[58] results particularly effective when using aqueous solutions of high molecular weight hyaluronic acid (3500 kDa). This technique uses a tangential high rate air flow (70ft^3/h) to assists the electric field in the pulling of the solution, and the use of heated air (optimal temperature 57°C) decreases the solution viscosity and fastens the water evaporation rate. This permits the formation of pure electrospun hyaluronic acid fibers[58,59]. Approaches to decrease the viscosity and surface tension of hyaluronic acid solutions include: the use of organic solvents (e.g. DMF, formic acid, CH_2Cl_2, DMSO), the introduction of surfactants, but also the mix with electrospinnable polymers (e.g. PVA, PCL, PEO, PU)[9,13].

Polyethylene oxide (PEO, or polyethylene glycol) is an optimal polymer to add for the electrospinning of hyaluronic acid. In fact, water solutions of PEO are easy to electrospin in standard conditions[60-62], the polymer is highly biocompatible and biodegradable[63,64], and it is already widely used in biomedical devices (e.g. tissue engineering, medical implants) but also as coating in several FDA approved drug nanodelivery systems[63]. In Table 4.4, the electrospinning conditions of relevant PEO/HA solutions are reported.

Solution	Solvent	Parameters	Ref
0.5% HA (1300kDa)/1.75% PCL (80kDa)	Formic Acid	Co-axial electrospinning with PEO (2000 kDa). 20kV[a], 15cm[b]	65
- 6% HA (8.7 kDa)/2% PEO (900kDa) - 4% HA (8.7 kDa)/4% PEO (900kDa) - 2% HA (8.7 kDa)/6% PEO (900kDa)	Aqueous acetic acid	The glass syringe was fitted with a copper positive electrode inside which was used to generate a transverse built-in electric field. 18kV[a], 18cm[b], RH 20-30%[c], 0.5mL/h[d]	66
- 0.1-0.2-0.3% HA (600-1000 kDa)/12% PEO (200kDa) - 0.2% HA (600-1000 kDa)/12% PEO (200kDa)/ 1% kanamycin	Water	10kV/-5kV[a], 15 cm[b], RH 30-35%[c]	67
HA (12000 kDa):Chitosan:PEO (900 KDa) in proportion 45:45:10	80% Acetic Acid Formic Acid	25kV[a], 14 cm[b], 1mlL/h[d]	68
1% HA (2000 kDa)/0.5-1-2% PEO(1000kDa)	Water	20kV[a], 15 cm[b].	69
5% CHO-HA*/5% PEO (1000 kDa)/1%Triton X	5% DMSO in water	8kV[a], 15 cm[b], 1.2mlL/h[d]	70
1.5% HA (1800-2000 kDa)/ 1% PEO(2000 kDa)	Water	3kV/cm[a], 0.2-1.0 mlL/h[d]. PEO is washed after electrospinning	71

Table 4.4: *Electrospinning conditions of relevant PEO/HA blends. *hyaluronic acid oxidized with $NaIO_4$ [a] Applied voltage, [b] needle-collector distance, [c] relative humidity in the electrospinning chamber, [d] flow of the solution.*

The systems developed by *Ahire et al.*[67] and *Chen et al.*[69] are particularly relevant because they managed to use the standard electrospinning set-up to electrospin PEO/HA solutions in water. In addition, *Ahire et al.*[67] managed to produce a HA-based antibacterial material by adding an antibiotic molecule (kanamycin) to the electrospun solution. Interestingly, *Raye et al.*[71] recently reported a heat-quench method to partially remove PEO from the electrospun matrix, leaving mainly HA gel fibers to be used as wound dressings. Finally, of particular value is the work of *Yang et al.*[70], where the antimicrobial peptide ε-polylysine was used both as cross-linking and antibacterial agent on electrospun mats made of oxidized hyaluronic acid and PEO.

Electrospinning for Peptide Delivery

The production of electrospun materials based solely on peptides is starting to be explored, but is still at the early stages due to a series of disadvantages posed by the intrinsic nature of peptides. In fact, the high viscosity needed for the electrospinning with peptides is achievable only at concentrations in the range of 10-50% (most polymers merely require 2-10%), and only specific solvents (e.g. HFIP, TFA) are able to allow an optimal electrospinning[72]. On the other hand, a much more common approach for the delivery of peptides via electrospinning is their grafting on electrospinnable materials[73,74]. In fact, the conjugation of peptides to nanofibers could offer protection against degradation, enhance the bioavailability, and allow for a precise control over their release and the site of action. For this purpose, a variety of peptides, conjugation techniques and polymers have been explored over the last years[73]. Two main general approaches are currently used: grafting prior or after electrospinning. The former, allows the control of both the amount and special presentation of the peptides, but could burn the bioactive species. The latter, permits a more tailored approach, but adds more steps to the process and may affect the scaffold properties[74]. Relevant examples are the works of *Dwivedi et al.*[75,76] and *Nogueira et al*.[77]. In the first the authors coated the epidermal growth factor peptide to electrospun fibers of PLGA/Gelatin, demonstrating its efficacy in fastening the closure of diabetic ulcers in mice. In the second, the antimicrobial peptide Cys-LC-LL-37 was coated by disulfide bonds to electrospun fibers of polypropylene grafted with cysteine, managing to produce a material active against *S.aureus*.

4.2 Results and Discussion

Considering the success of peptide conjugation by the thiazolidine bond in the previous chapters, the use of the same bond with a different polysaccharidic substrate is herein explored. Hyaluronic acid by itself has a great potential in biomedical applications due to its intrinsic anti-inflammatory and wound healing properties. However, the solubility of HA in the solvent that is routinely used for thiazolidine bond formation poses additional challenges to the recovery of the material after reaction and it also complicates its characterization.

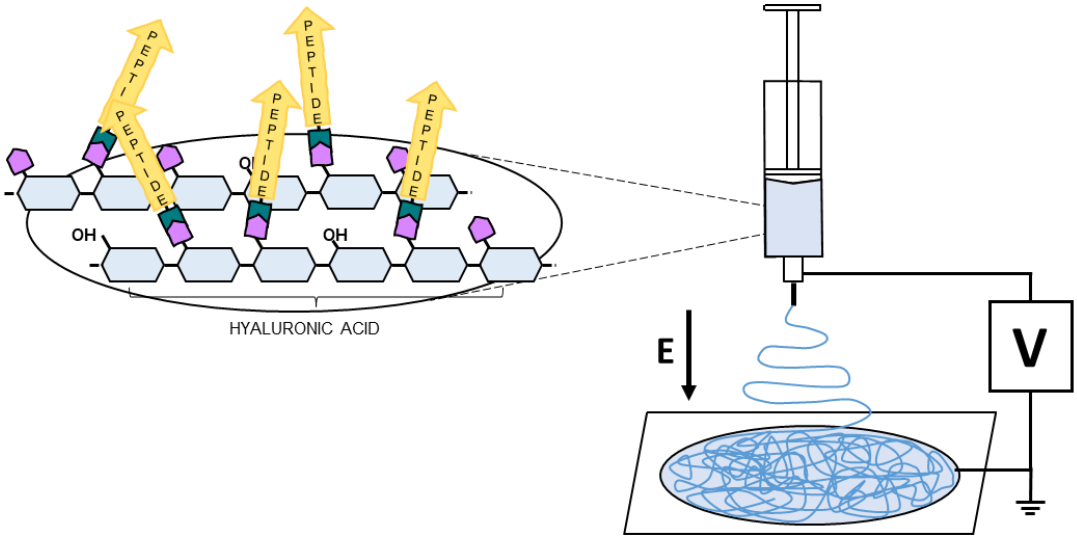

***Figure 4.3**: Schematic representation of the process used to produce peptide-HA based wound dressings. Hyaluronic acid backbone is in blue, the peptide in yellow and the cysteine and the aldehyde needed for the thiazolidine are represented in green and pink, respectively.*

To create a final material that could be used as a gauze for skin lesions, the electrospinning technique was employed. In fact, besides being an easy-to-handle material, nanofibrous hyaluronic acid could enhance the wound healing properties of the hyaluronic acid. To further amplify the activity of the polymer, two peptides were covalently linked to hyaluronic acid: the skin regenerative peptide Ac-SDKP (**6a**) and the antibacterial peptide $(RW)_3$ (**7a**).

4.2.1 Choice of Peptides

In this project, the peptides selected as the active molecules to be conjugated to hyaluronic acid were chosen with the perspective of an industrial scale-up of the whole process. Therefore, they needed to have a short sequence with a minimal number of amino acids, and be soluble in water-based solvents. The former is to minimize the costs of the synthesis, if possible also by cutting the cost for the purification, but also minimizes the hindrance at the ligation site. The latter is to allow the thiazolidine reaction to take place under ideal conditions: slightly acidic water at a pH of 4.5[5,6]. In addition, the peptides needed an activity relevant in the wound healing context. The skin regenerative peptide Ac-

SDKP (**6a**), beside fitting the scale-up criteria, has already been used and demonstrated to be beneficial for wound healing in rat skin flaps models[32]. Similarly, the antibacterial peptide $(RW)_3$ (**7a**) fits the scale-up criteria and shows promising characteristics, such as broad-spectrum activity, non-specific mechanism of action and low cytotoxicity *in vitro*. Its main disadvantage is the reported toxicity toward blood cells in *in vivo* models[39], but this could be addressed with the substitution with D-amino acids[44]. In Table 4.5, the characteristics of the two sets of peptides are summarized:

Peptide	Short name	Sequence	Nr residues	Purity	MW (g/mol)
SDKP analogues					
6a	SDKP	Ac-SDKP-NH_2	4	96.9 %	486.43
6b	CWSDKP	H-**C**W**W**SDKP-NH_2	6	99.4%	733.84
6c	Pal-SDKP-K(WC)	C_{16}-SDKPK(**W**C)-NH_2	7	97.7%	1100.43
6d	Pal-K(WC) SDKP	C_{16}-K(**W**C)SDKP-NH_2	7	99.8%	1100.43
$(RW)_3$ analogues					
7a	$(RW)_3$	H-R**W**R**W**R**W**- NH_2	6	89.1 %	1044.24
7b	cys$(RW)_3$	H-**C**R**W**R**W**R**W**- NH_2	7	93.7 %	1147.38

***Table 4.5**: List of the synthesized peptides. Cysteine is highlighted in green, Trp in bold. Details about the synthesis and HPLC-MS characterization are in Section 4.3.2 and in Chapter 5.4.1, respectively.*

Peptides **6b** to **6d** and peptide **7b** are analogues of Ac-SDKP and $(RW)_3$ that can be conjugated to oxidized hyaluronic acid (CHO-HA, *Section 4.2.2*), respectively. In fact, the β-amino thiol characteristic of cysteine selectively reacts with aldehydes present on CHO-HA to form the typical thiazolidine ring. A way to quantify, at any moment, the amount of peptide present on the peptide-HA conjugate is the addition of a chromophore to the active sequence. Trp is the aromatic amino acid with the highest extinction coefficient ($\varepsilon_{Trp\text{-}280nm}$ in H_2O = 5630 $M^{-1}cm^{-1}$)[78]. Therefore, the amino acid was added to the sequence of all the SDKP analogues. Peptide **7a** naturally present Trp in its sequence so it was not added to peptide **7b**.

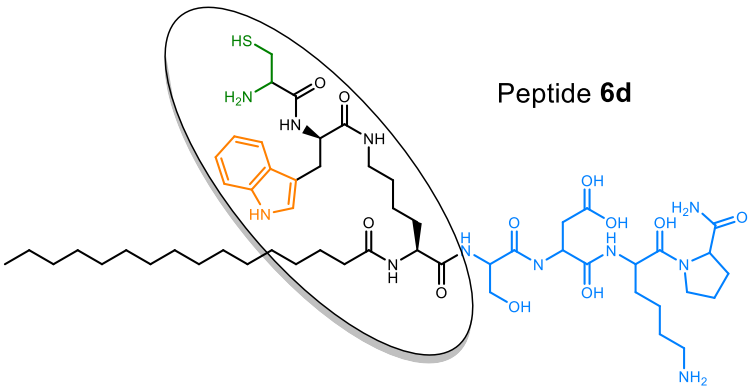

***Figure 4.4**: Chemical structure of peptide **6d**. Highlighted is the "conjugation arm" made of Lys(Trp-Cys). In blue is the active sequence SDKP, in orange the chromophore and in green the β-amino thiol .*

One of the main challenges in the large scale application of peptides is their fast degradability in the presence of proteases. A strategy to avoid this is the addition of acyl chains to the peptide sequence.

Taking into consideration the cytotoxicity of peptide **4f** (H-CWKTTKSK(Pal)-NH_2, *Chapter 2.2.1*), in this case the palmitoyl chain was introduced at the N-terminus of peptides **6c** and **6d**, and the additional Trp and Cys were introduced at the side chain of an additional lysine. This was possible by the use of a Dde-Lys(Fmoc)-OH and Fmoc-Cys(Boc)-OH during the synthesis: the Fmoc protecting group of Lys was removed by standard protocol (20% piperidine in DMF), then Trp and Cys were attached to Lys side chain, and the deprotection of the Dde protecting group was performed with a strategy that is orthogonal to both Fmoc and Boc removal (2% hydrazine in DMF).

To summarize, peptide **6b** has the additional Cys-Trp moiety at the N-terminus, and peptides **6c** and **6d** differ in the position of the "conjugation arm" made of Lys(Trp-Cys).

All peptides were synthesized in high purity by solid phase peptide synthesis using the Fmoc/Boc strategy. The cleavage from the resin was performed by acidic treatment with TFA. In this way also the side chain protecting groups of amino acids could be removed simultaneously. The peptides were recovered by precipitation and washed in cold diethyl ether. When necessary, medium pressure flash chromatography was performed to further purify the peptides (*Section 4.3.2*). All synthetized peptides were characterized by HPLC-MS (*Chapter 5.4.1*).

Protease Resistance of SDKP analogues

As previously stated, one of the limitations to the widespread use of peptides is their instability to protease degradation. To assess whether the palmitoylation improved the resistance to proteases, peptides **6a**, **6c**, and **6d** were put in contact with human serum for 24h. At selected timepoints an aliquot of the peptide-serum solution was quenched in EtOH and analyzed by HPLC (Fig.4.5 and *Chapter 5.4.2*).

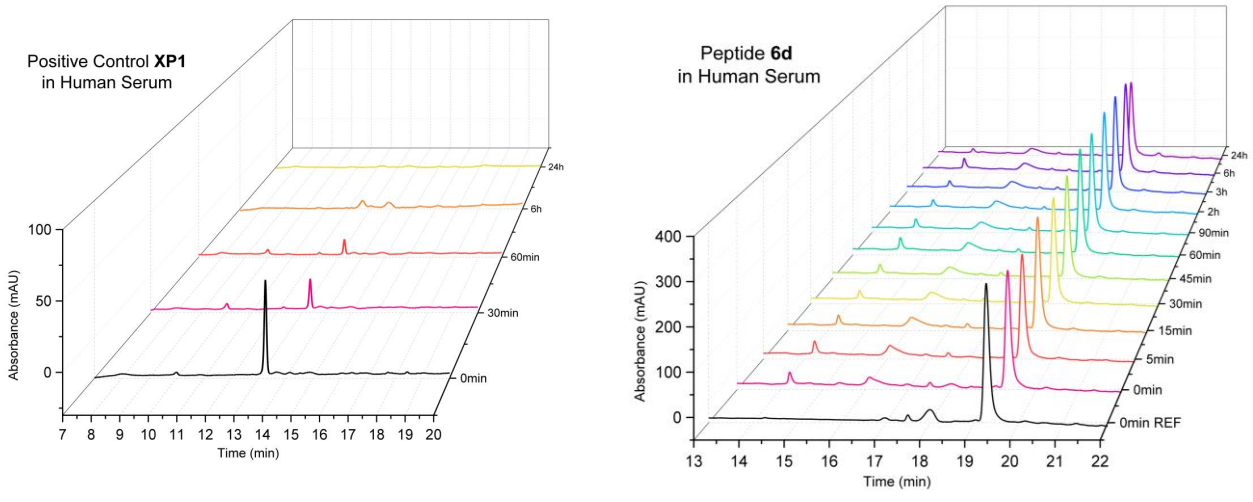

(A) **(B)**

Figure 4.5: *HPLC profiles of the human serum degradation of (**A**) the positive control **XP1** and (**B**) peptide **6d** over time, reported as an example. Ref represent the profile of the negative control of peptide **6d**. The profiles of the other peptides and their controls are reported in Chapter 5.4.2.*

The area of the chromatographic peak was correlated to the amount of intact peptide still present in solution. As a negative control, the peptides were incubated in the buffer used for the degradation without adding human serum. As a positive control, the C-terminal portion of natural Endonuclease V involved in the DNA repair mechanism that occurs after DNA damage caused by ultraviolet radiation (peptide XP1), whose fast degradation is already reported in the literature[79], was put in the same conditions as the SDKP analogues. The results are expressed in Figure 4.6 as percentage of intact peptide in solution overtime.

Unfortunately, the hydrophilicity of peptide **6a** did not allow for a complete analysis of its HPLC chromatograms. In fact, the peak of the peptide at 2.7min (gradient 0-30%B using a binary elution system with A: 0.05% TFA in CH_3CN/H_2O 1:9 v/v, and B: 0.05% TFA in CH_3CN/ H_2O 9:1 v/v) overlapped the injection peak. In any case, the results of the palmitoylated peptide can be compared to the positive control that was completely degraded after only 6h.

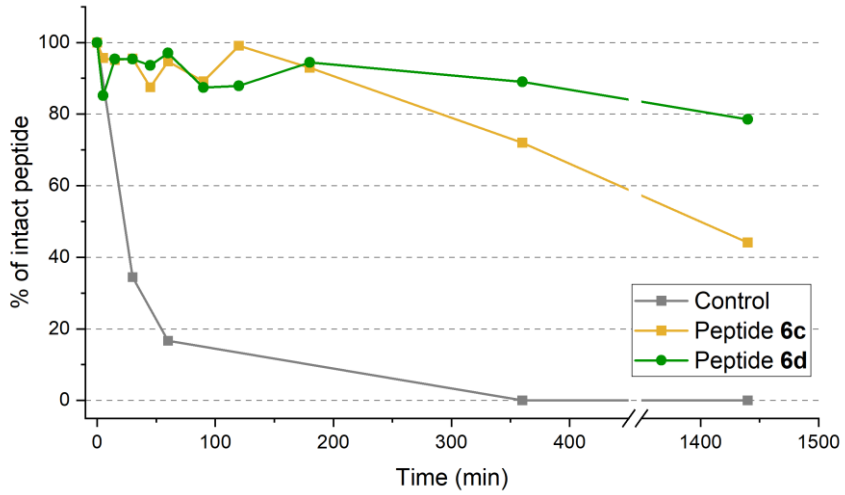

Figure 4.6: *Proteolytic degradation of the peptides* ***6c****,* ***6d*** *and the control (peptide XP1) in human serum, represented as the percentage of intact peptide over time calculated as the HPLC-peak area. The control is a peptide known to be easy to degrade in human serum*[79]*.*

As shown in Figure 4.6, the addition of palmitoyl to both peptide **6c** and **6d** improved their resistance against human proteases, with peptide **6d** seeming slightly more resistant than its counterpart peptide **6c**. In fact, even after 24h the peptides were still present in solution with a percentage of intact peptide of 78% and 44% respectively. Probably, the presence of the Lys(Trp-Cys) "conjugation arm" at the N-terminus made the recognition of the peptide by the proteases more difficult.

Biological Activity

The cytotoxicity of peptides **6a** and **6b** was tested at the University of Pisa and both peptides were confirmed not cytotoxic to human THP-1 cells (Fig. 4.7).

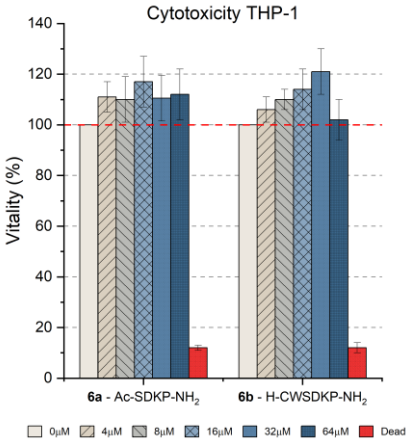

***Figure 4.7**: Cytotoxicity to THP-1 cells of peptides **6a** and **6b**.*

To evaluate whether the modified peptides maintained the same activity of peptide **6a**, the anti-inflammatory activity of peptide **6b** was preliminary tested *in vitro* on THP-1 cells at the University of Pisa. Unfortunately, the anti-inflammatory activity detected *in vivo* by *Cai et al.*[28] could not be detected in peptide **6a,** but **6b** exhibited a slight anti-inflammatory effect at 64μM. In fact, when the peptide was in presence of an antibody (LPS) the concentration of the cytokines IL-8, IL-1β and TNFα was lower than the control and the sample with peptide **6a** (Fig. S4.25, *Chapter 5.4.7*).

4.2.2 CHO grafting on Hyaluronic Acid

The most common way to convert the hydroxyl groups present on polysaccharides to aldehydes is the $NaIO_4$ oxidation. Since the reaction involves two vicinal diols, it causes the opening of the monosaccharide ring and a consequent loss in the molecular weight of the polymer. Even though the reaction takes place in the most environmentally friendly solvent, water, the reagent in itself is extremely harmful to both humans and aquatic organisms. In addition, the reaction conditions have not been thoroughly explored in the literature when hyaluronic acid is used as a substrate. Meanwhile, the TEMPO/laccase/O_2 catalyzed oxidation of primary alcohols is a milder method that is selective for primary hydroxyls that is quite established for polysaccharides such as cellulose or chitosan. However, in the context of hyaluronic acid, even though TEMPO has already been used to catalyze the oxidation of C_6-OH, the solvent that was employed was DMF[18]. In addition, the regeneration of the catalyst with laccase (to the best of this author knowledge) has never been explored in this context.

For these reasons, to evaluate the best conditions in terms of minimal loss of molecular weight and maximization of the aldehydes, the two reactions were compared varying the reaction time and the amounts of reagents. The two oxidation methods were tested on hyaluronic acid with a molecular weightof 2300 kDa and of 50 kDa. For simplicity, from this point on the former will be referred to as high molecular weight (HMW-HA) and the latter as low molecular weight (LMW-HA)

In the case of the $NaIO_4$ oxidation, an amount of 0.5eq and 2 eq of reagent were employed, using water as the solvent:

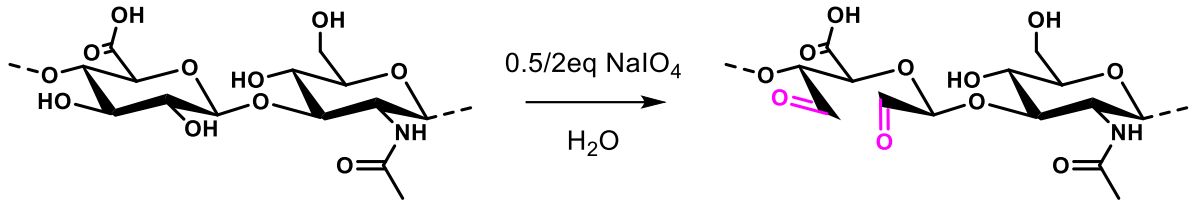

***Figure 4.8**: Schematic representation of the $NaIO_4$ oxidation of hyaluronic acid.*

The TEMPO/laccase/O_2 system was tested in NaOAc/AcOH buffer (50mM, pH 5) using TEMPO/laccase at 8%/20U or 8%/60U. Both conditions were tested with and without air bubbling (Fig. 4.12).

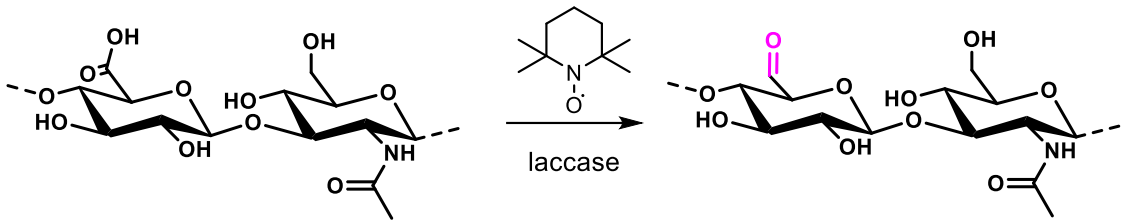

***Figure 4.9**: Schematic representation of the TEMPO/laccase/O_2 catalyzed oxidation of hyaluronic acid.*

Both $NaIO_4$ and TEMPO/laccase/O_2 reactions were monitored for 5 days. At 1h, 3h, 8h, 24h, 48h and 5days, an aliquot of the solution was quenched with an excess of ethylene glycol or EtOH, respectively. Oxidized hyaluronic acid (CHO-HA) was recovered by lyophilization after purification with membrane dialysis. The reactions with the most promising conditions were performed in triplicates to assure the replicability of the results.

^{1}H-NMR - Aldehyde quantification

The presence of the aldehyde on CHO-HA was confirmed by the appearance of a new band around 1730 cm^{-1} at the FT-IR spectra, that corresponds to the aldehyde C=O stretching[25,26]. Interestingly the aldehyde is visible just after 1h of reaction both with $NaIO_4$ and TEMPO/laccase oxidations (Fig. 4.10 and Fig. S4.13-S4.14, *Chapter 5.4.4*).

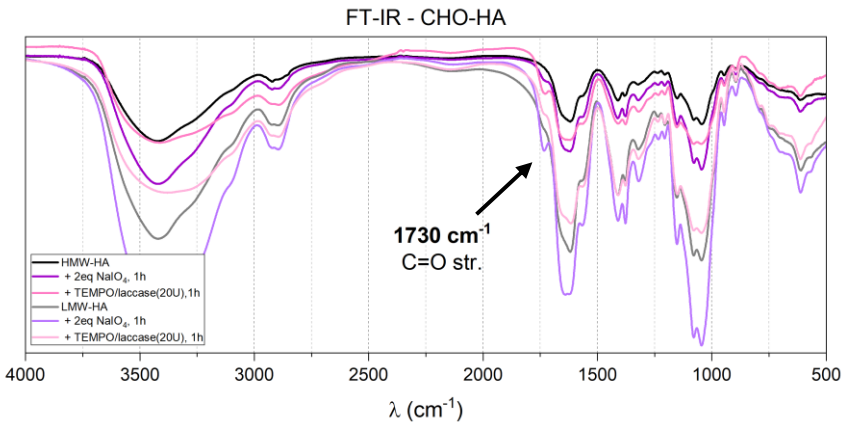

***Figure 4.10**: FT-IR spectra of high and low molecular weight CHO-HA obtained from the reaction with 2eq of $NaIO_4$ (purples) and 8%$_{wt}$/20U of TEMPO/laccase/O_2 (pinks). The profiles of the other timepoints are reported in chapter 5.4.3.*

The aldehydes grafted on CHO-HA using $NaIO_4$ can be quantified by ^{1}H-NMR using the signals of the hemiacetals that form at the C_2 and C_3 carbons of the glucuronic acid (4.8-5.2 ppm)[17,20]. The area of the peak of the methyl of the amide at C_1 is used as standard for calculating the area of the hemiacetals peaks (Fig. 4.11). In the same way, the aldehydes grafted on CHO-HA using the TEMPO/laccase/O_2 system were quantified by the proton of the hemiacetals that form at the C_6 of the N-acetyl-D-glucosamine monomer (5.2 ppm, Fig. 4.11).

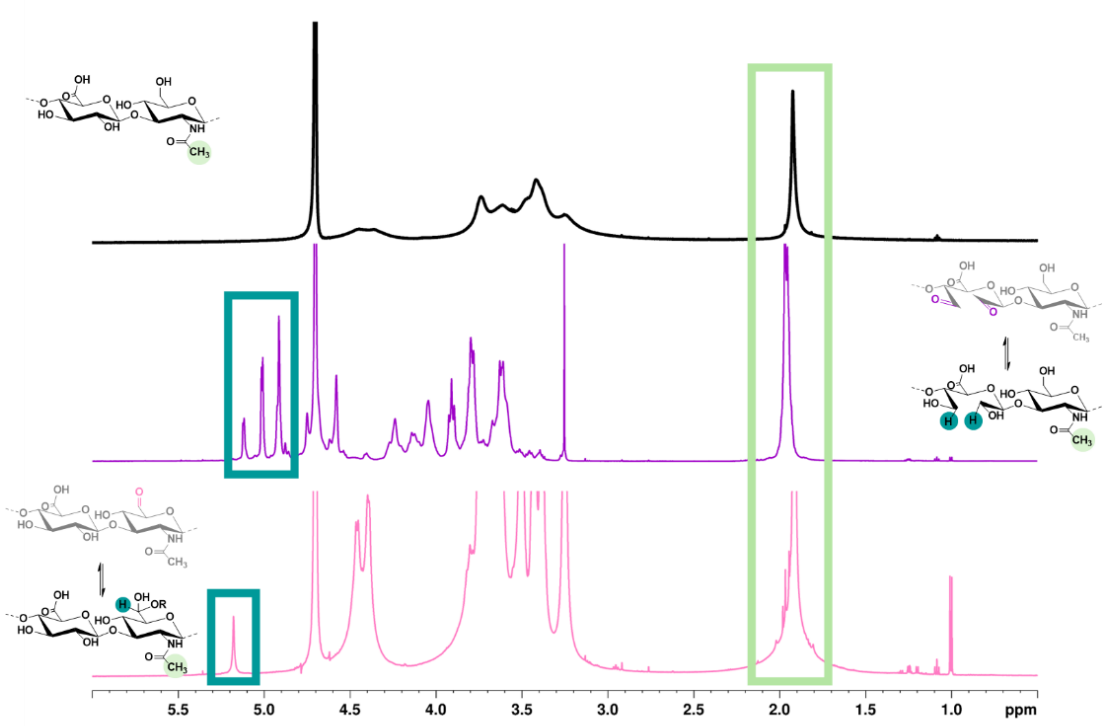

***Figure 4.11**: ^{1}H-NMR (600 MHz) of hyaluronic acid and CHO-HA after 5days of reaction with NaIO4 or TEMPO/laccase. Reported as an example. (Dissolved in D_2O)*

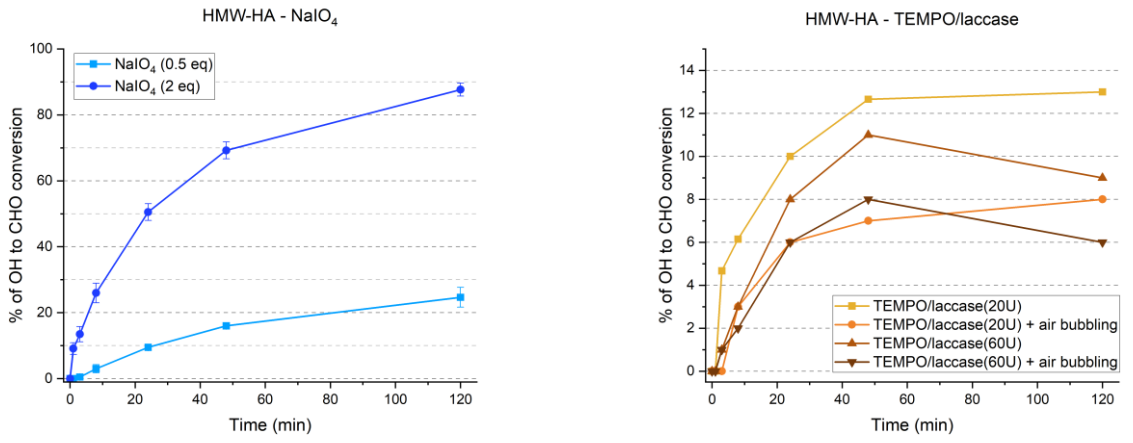

(A) **(B)**

***Figure 4.12:** Percentage of conversion of hydroxyl to aldehyde using **(A)** $NaIO_4$, **(B)** TEMPO/laccase/O_2 (TEMPO is always at 8%$_{wt}$) and HA-HMW as the substrate. The detailed calculations are reported in Chapter 5.4.4.*

Figure 4.12 shows the progress of the reactions over time calculated as the percentage of reactive hydroxyls that are converted into aldehydes. In the case of $NaIO_4$, when using 2eq after 5days almost all

(88%) of the C_2-C_3 diols are converted. When using 0.5eq the reaction is much less efficient: the 25% of conversion that was obtained in 24h with the previous conditions needs 5days to be reached. The best results of the TEMPO/laccase/O_2 catalyzed oxidation are obtained with 20U of laccase. Even though, after 5days only 13% of the C_6-OH was converted to aldehydes. In addition, increasing the amount of laccase or adding air bubbling to the solution reduced the yield of the reaction.

When using LMW-HA as the substrate, only the best conditions (2eq of $NaIO_4$ and 20U of laccase) were tested, and the results were very similar to that of HMW-HA (Table S4.3 and S4.4, *Chapter 5.4.4*).

The amount of aldehydes per gram of hyaluronic acid after 5 days is reported in Table 4.6 (the other timepoints are reported in *Chapter 5.4.4*). The highest amount of aldehydes is obtained using 0.2 eq of $NaIO_4$, even though the results are worse than the data reported by *Maiz-Fernández et al.[17] (24%. 1eq., 2h)*, *Su et al.[21] (87%. 1eq., 24h)*, and *Jia et al. (67%. 2eq., 2h)[22]*. On the other hand, when using 0.5eq of $NaIO_4$, the amount of aldehydes is coherent with the literature[18-20].

Substrate	Oxidizing Reagent	Conversion OH to CHO	CHO (mmol/g_{HA})
HMW-HA	0.5 eq $NaIO_4$*	24.7 ± 3.0 %	1.30 ± 0.16
HMW-HA	2 eq $NaIO_4$*	87.6 ± 2.0%	4.62 ± 0.10
HMW-HA	TEMPO/laccase(20U)*	13.0 ± 0.5 %	0.69 ± 0.01
HMW-HA	TEMPO/laccase(20U) + air bubbling	8.0 %	0.42
HMW-HA	TEMPO/laccase(60U)	9.0 %	0.47
HMW-HA	TEMPO/laccase(60U) + air bubbling	6.0 %	0.32
LMW-HA	2 eq $NaIO_4$*	85.7 ± 0.2%	4.52 ± 0.01
LMW-HA	TEMPO/laccase(20U)*	12.0 ± 0.0%	0.63 ± 0.00

***Table 4.6**: Quantification of the aldehydes **after 5 days of reaction**. TEMPO is always at 8%$_{wt}$. *reaction performed in triplicates. The complete dataset is reported in chapter 5.4.4.*

The quantity of aldehydes formed by the catalytic TEMPO/laccase reaction is coherent with the results obtained with cellulose, as reported in the literature[25] or in *Chapter 2*. The results are particularly encouraging when considering that, since only acetyl-D-glucosamine possesses a C_6-OH, hyaluronic acid presents half the reactive hydroxyl than cellulose, but results with a comparable amount of aldehydes. This could be because in the case of hyaluronic acid, the reaction is homogeneous, which probably makes more sites available for the reaction.

GPC Analysis - Molecular Weight over time

The molecular weight of the samples was evaluated by gel permeation chromatography (GPC). As shown in Figure 4.13, both methods break down HMW and LMW hyaluronic acid. However, $NaIO_4$ is more aggressive: the molecular weight of HMW-HA after 1h with 0.5eq is around 650 kDa, with 2eq is at 250 kDa, whereas the with TEMPO/laccase is still at 850 kDa. Even at the latest timepoints, the

TEMPO/laccase systems is confirmed to be milder with a minimum of 94 kDa after 5days against the 24 kDa and 11 kDa of 0.5eq and 2eq of $NaIO_4$, respectively.

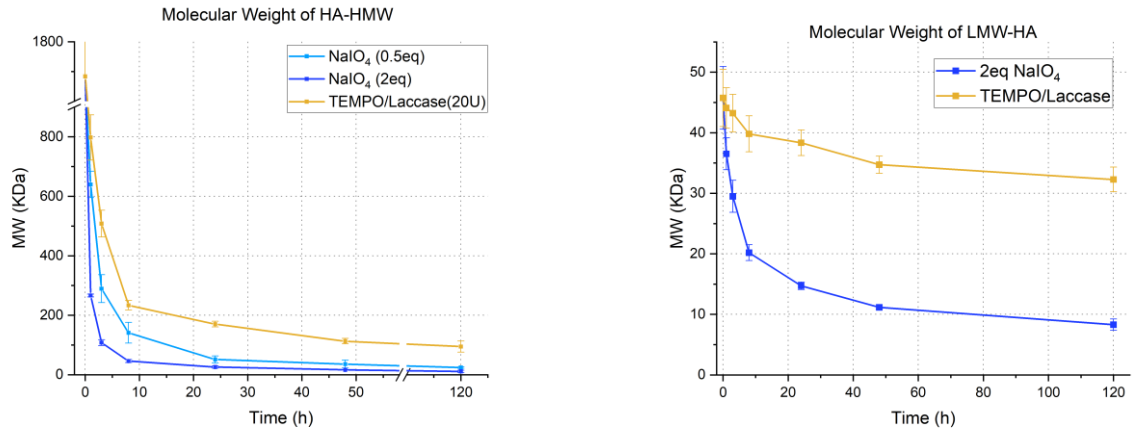

(A) **(B)**

***Figure 4.13**: Molecular weight of CHO-HA over the time of reaction when using $NaIO_4$ (blue) or the TEMPO/laccase/O_2 system (yellow) for the oxidation. (**A**) HMW-HA or (**B**) LMW-HA were used as the substrate. Detailed data reported on Chapter 5.4.5.*

The results are even more drastic when considering LMW-HA. The TEMPO/laccase system accounts for a loss of 15kDa after 5 days, whereas $NaIO_4$ causes a drop of 40 kDa. In addition, we demonstrated that neither of the solvents (water and the acetic acid buffer) have a role in the degradation of hyaluronic acid (Fig. S4.19, *Chapter 5.4.5*)

Biological Activity of CHO-HA

The cytotoxicity of hyaluronic acid of high and low molecular weight and their oxidized derivatives was tested at the University of Pisa: the grafting of the aldehyde did not impact negatively to the cytotoxicity of the materials (Fig. 4.14).

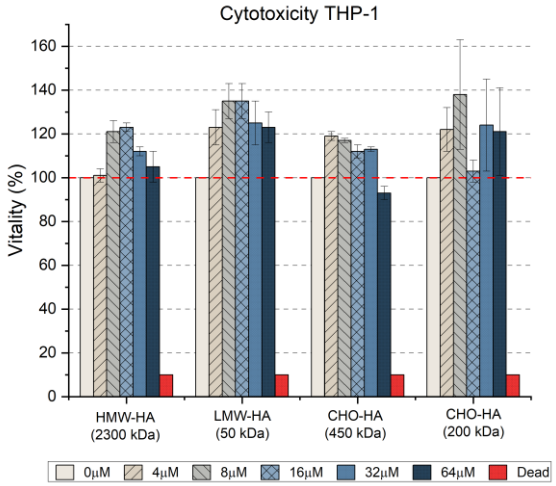

***Figure 4.14**: Cytotoxicity to THP-1 cells of HMW-HA (2300 kDa), LMW-HA (50kDa) and CHO-HA obtained from TEMPO/laccase oxidation for 3h (450 kDa) and 8h (200 kDa).*

To evaluate whether CHO-HA acid maintained the same activity of unmodified HA, their anti-inflammatory activity was preliminary tested *in vitro* on THP-1 cells. Overall, CHO-HA was found to have

a higher anti-inflammatory activity than hyaluronic acid. In fact, when the samples were in presence of the antibody LPS, the concentration of the cytokines IL-6, IL-10, IL-1β and TNFα was much lower than the control and lower or comparable to the one of HA. This is particularly impressive, when considering that the concentration of the CHO-HA samples was half the one of HA (Fig. S4.26, *Chapter 5.4.7*).

CHO-HA for electrospinning

Considering the results of the previous sections, the TEMPO/laccase/O_2 system was employed to introduce the aldehydes on hyaluronic acid that will be used for the conjugation with the peptides and subsequently for electrospinning. Both HMW-HA and LMW-HA were used as substrates in batches of 3g. In order to maximize the number of aldehydes without losing too much in molecular weight, hyaluronic acid was in contact with TEMPO and laccase (8%wt/20U) for 2 days.

Substrate	Reaction Conditions	MW[a]	Conversion OH to CHO	CHO mmol/g
HMW CHO-HA	TEMPO/Laccase (8%wt/20U), 2days	345 kDa	17%.	0.44
LMW CHO-HA		40 kDa	18%	0.47

Table 4.7*: Characterization of HMW and LMW CHO-HA. [a] measured after reaction. [1]H-NMR (600mHz) spectra reported in Figure S4.18, Chapter 5.4.4.*

The loss in molecular weight is in agreement with the results of the previous sections. However, the molecular weight of HMW CHO-HA is slightly higher (345 kDa against 112 ± 9 kDa). This is probably due to the use of a different batch of the same hyaluronic acid and/or the different batch of laccase. On the other hand, the amount of aldehydes is coherent with the previous results.

For simplicity, the oxidized materials (CHO-HA) synthesized using the procedure described in this section, will hereafter be referred to as HMW CHO-HA and LMW CHO-HA.

4.2.3 Peptide-HA Conjugates – Preliminary

The thiazolidine bond requires a β-amino thiol and an aldehyde to form (*Chapter 1.4.1*). The former was introduced on the peptides as a cysteine during solid phase peptide synthesis. The latter is formed by TEMPO/laccase/O_2 catalyzed oxidation of the C_6-OH of hyaluronic acid.

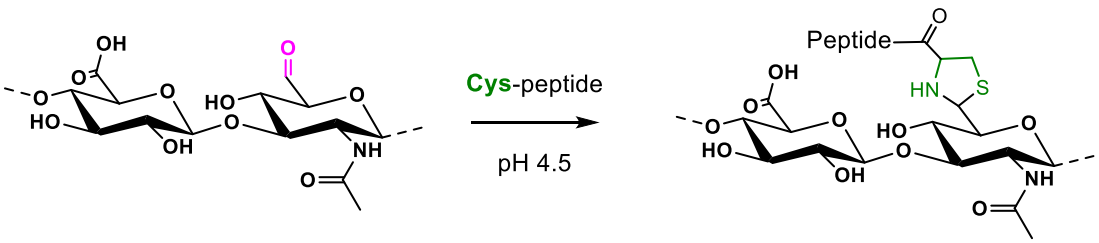

Figure 4.15*: Schematic representation of the thiazolidine between a cys-peptide and hyaluronic acid.*

As stated in the previous chapters, the aldehydes present on the polysaccharide surface do not have a vicinal C-terminal ester. Thus, the final intramolecular O- to N-acyl transfer described in *Chapter 1.4.1*

does not take place and the reaction stops with the formation of the heterocyclic ring. The reaction takes place at a slightly acidic pH to avoid the reaction of the aldehyde with other nucleophiles present in the peptide. The presence of a reducing agent (TCEP) is needed to prevent the formation of the peptide dimer through the disulfide bond between the Cys residues of two peptide molecules. Moreover, given the high chemoselectivity of this reaction, the peptide reacts without the need for protecting groups.

The two peptides selected to test the reaction were **6b** (H-CWSDKP-NH_2) for the skin regenerative properties and **7b** (HCRWRWRW-NH_2) for the antibacterial properties.

	Substrate	**Peptide**	**Amount of added peptide (mmol/g_{HA})**	**Solvent**	**Peptide loading* (mmol/g_{HA})**
r1 - ctrl	HMW-HA	**6b**	0.62	NaOAc/AcOH **buffer** (50mM, pH 4.5)	0.07
r1	HMW CHO-HA		0.63		0.19
r2 - ctrl	HMW-HA		0.55	H_2O	0.02
r2	HMW CHO-HA		0.58		0.19
r3 - ctrl	HMW-HA	**7b**	0.57	**25% CH_3CN** in NaOAc/AcOH buffer (50mM, pH 4.5)	-
r3	HMW CHO-HA		0.58		0.60
r4	HMW CHO-HA		0.60		-
r5 - ctrl	LMW-HA		0.62		-
r5	LMW CHO-HA		0.59		0.16

***Table 4.8**: **Reaction conditions for the preliminary tests** on the conjugation of peptides to hyaluronic acid, reaction time 1day. *calculated by UV-Vis. "-" the measure could not be performed due to the insolubility of the substrate.*

The absorbance of the Trp in the peptide chains was used to quantify the amount of peptide on the materials. To perform the measure, weighted samples of **r1**, **r2** and their controls were dissolved in a known amount of water, while **r3** and **r5** were dissolved in 0.1M NaOH. The material obtained from the controls of **r3** and **r5,** and **r4** could not be completely dissolved in water, CH_3CN (from 10% to 100% in water) or NaOH (0.1-1M) making the quantification unfeasible.

The reaction with peptide **6b** was first tested in the slightly acidic buffer (NaOAc/AcOH, 50mM, pH 4.5) used for the conjugations with cotton (*Chapter 2.2*). The same peptide solution was added to a solution unmodified hyaluronic acid and one of CHO-HA that were dissolved overnight in the buffer (Table 4.8). The amount of peptide in the reaction vessel was of 2 eq with respect to the mmoles of aldehydes present in CHO-HA. Considering the results obtained in the previous chapters, the reaction was carried out for 24h. Then, the solution was purified by dialysis, and the solid recovered by lyophilization. However, it is important to note that, in this case, the time of reaction cannot be precisely determined because, after the selected reaction time, the solution is put in a dialysis membrane and remains in contact with an unknow amount of peptide for two days. The very low amount of peptide found in the controls with unmodified hyaluronic acid confirms the success of the reaction, and the 0.19 mmol/g found in both **r1**

and **r2** are coherent with the results obtained when using the thiazolidine to bind peptides to cotton (*Chapter 2.2*), and with the amount of free aldehyde sites present on CHO-HA. When using water as the solvent no significant differences in the peptide loading were found.

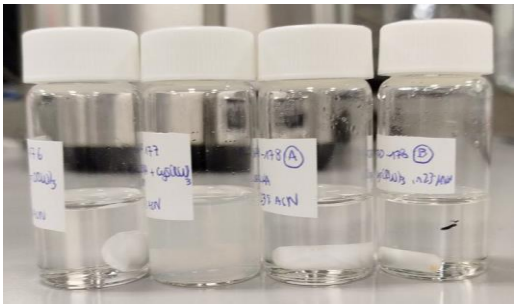

***Figure 4.16**: **reaction 5** and its controls. From left to right: 3mL of **7b** + 5mL of HMW-HA, 3mL of **7b** + 5mL of HMW CHO-HA, 3mL solvent + 5mL of HMW CHO-HA, and 3mL of **7b** + 5mL of solvent. In all samples the solvent is 25% CH_3CN in NaOAc/AcOH buffer (50mM, pH 4.5).*

Similar reaction conditions were used with peptide **7b,** however the reaction revealed to be more challenging. Peptide **7a** was reported to be soluble in water[39], however neither peptide **7a** nor **7b** were found to be soluble in water or the acetate buffer. Therefore, a solution containing the minimal amount of CH_3CN needed to dissolve peptide **7b** (25%) in the acetate buffer was used as the solvent. Moreover, when the peptide solution (2eq with respect to the aldehydes) was added to CHO-HA (**r3** and **r5**) a precipitate formed. To check that this behavior was due to the interaction between the peptide and CHO-HA, in reaction **5**, in addition to the control with unmodified hyaluronic acid, two more controls were added. In the first, the same amount of solvent used for peptide solution was added to the CHO-HA solution. In the second, the same peptide solution that was used in **r5** and **r5-ctrl** was added to the solvent used to dissolve CHO-HA In both cases, no precipitation was observed (Fig. 4.16). This behavior is confirmed by **r4**, where the solution is added to dry peptide and dry CHO-HA, and CHO-HA does never fully dissolve as it did when alone.

Anyhow, the presence of peptide **7b** is confirmed by the UV-Vis analysis. In the absence of the control the success of the reaction is not fully confirmed. In particular, in **r3** the amount of peptide is higher than the aldehydes present on CHO-HA suggesting that some of the peptide is adsorbed on the material and/or was not completely removed by dialysis. In **r5** the amount of peptide is compatible with the results with peptide **6b**.

4.2.4 Peptide-HA Conjugates for electrospinning

To minimize the amount of material to synthetize for the electrospinning tests, HMW CHO-HA was used in bigger batches (250mg) as a substrate for both peptide **6b** and **7b**. In fact, the minimal amount of LMW CHO-HA needed for an electrospinning test is ten-fold the amount of HMW CHO-HA (*Section 4.2.5*), and thus was used only for conjugation with peptide **6b**, whose preliminary results were more consistent.

	Substrate	Peptide	Amount of added peptide (mmol/g_{HA})	Solvent	Peptide loading[a] (mmol/g_{HA})
r6 - ctrl	HMW-HA	**6b**	0.55	H_2O	0.08
r6	HMW CHO-HA		0.56		0.24
r7 – ctrl	LMW-HA		0.57		0.06
r7	LMW CHO-HA		0.60		0.19
r8 – ctrl	HMW-HA	**7b**	0.59	**25% CH_3CN** in NaOAc/AcOH buffer (50mM, pH 4.5)	0.05*
r8	HMW CHO-HA		0.59		0.61

***Table 4.9**: Reaction conditions for **the peptide-HA conjugates** used **for electrospinning** and their controls with unmodified hyaluronic acid, reaction time 1day. [a]calculated by UV-Vis. * the solid was not completely dissolved, measure not accurate.*

For all conjugations the following conditions were set: (***1***) reaction time: 24h, (***2***) 2eq of peptide with respect to the aldehydes, and (***3***) 2eq of TCEP.

Since in **r2** there were no significant differences with **r1**, water was used as the solvent for the reactions with peptide **6b**. On the other hand, for **r8** 25% CH_3CN in NaOAc/AcOH buffer (50mM, pH 4.5) was confirmed as the solvent for peptide **7b**. Reaction **r7** presented the same precipitation problems of **r3** and **r5**.

FT-IR characterization

The presence of the peptides on both unmodified HA and CHO-HA was verified by the appearance of the *amide I* and *amide II* bands of the peptide backbone (1630 and 1550 cm^{-1}, respectively) at FT-IR (Fig. 4.16, and S4.16-4.17 of *Chapter 5.4.3*). In addition, the presence of free aldehydes is highlighted by the signal at 1730 cm^{-1} corresponding to the C=O stretching of the aldehyde. Interestingly, in the spectra of HMW CHO-HA this signal is not visible, probably due to the formation of hemiacetals[80,81].

(A)

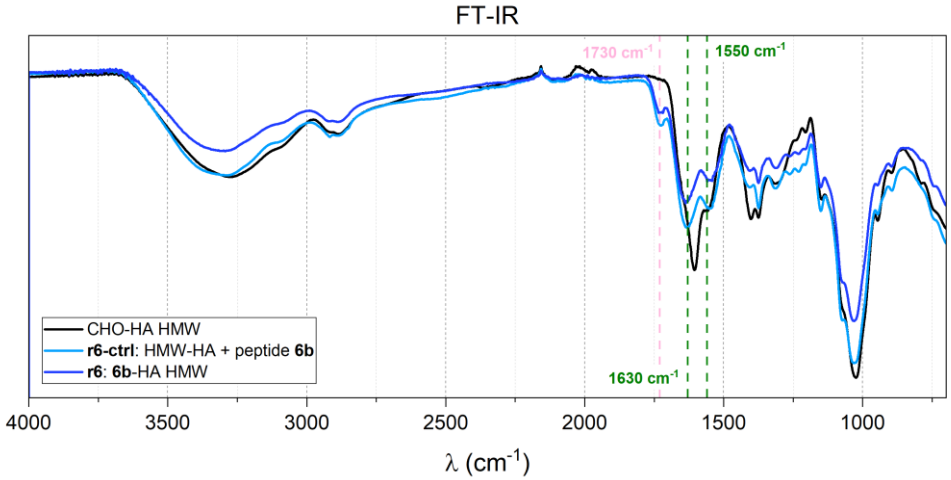

(B)

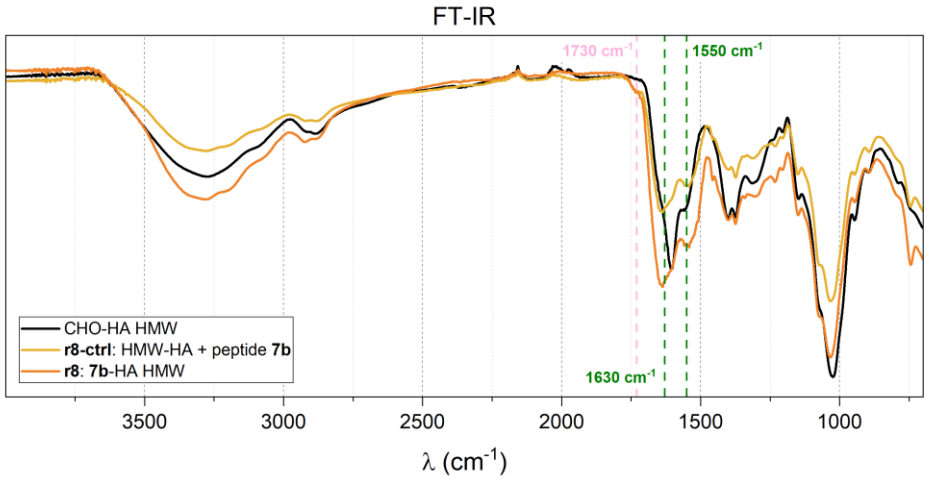

***Figure 4.16**: FT-IR spectra of the materials obtained from **r6** and **r7**, and their controls.*

Unfortunately, FT-IR does not give information about the amount of peptide present on the materials.

UV-Vis - Peptide Quantification

To quantify the peptide on the materials, the weighted samples of **r6**, **r7** and their controls were dissolved in water at a known concentration, while **r8** was dissolved in a carbonate buffer (100mM, pH 9.6). The material obtained from the control of **r8** (**r8-ctrl**) was not completely dissolved in the carbonate buffer, so the absorbance measurement of the **r8-ctrl** solution is not reliable. As shown in Table 4.9, the loading results obtained from the UV-Vis analysis are consistent with previous results: the thiazolidine bond formation is confirmed with peptide **6b**, but the success of the reaction with **7b** cannot be definitively confirmed with this technique.

GPC Analysis – Molecular Weight of the Conjugates

The GPC analysis of the low molecular weight samples is of particular interest, especially when the molecular weight of **r7** is compared to its controls. In fact, **r7** presents a significant increase in molecular weight, that can be attributed to the presence of the peptide on the material, confirming the success of the reaction with peptide **6b**.

Reaction	Description	MW
-	LMW-HA	45 kDa
-	LMW CHO-HA	40 kDa
r7 – ctrl	LMW-HA + pep **6b**	38 kDa
r7	LMW CHO-HA + pep **6b**	77 kDa
-	HMW-HA	1683 kDa
-	HMW CHO-HA	345 kDa
r6 - ctrl	HMW-HA + pep **6b**	184 kDa
r6	HMW CHO-HA + pep **6b**	220 kDa
r8 – ctrl	HMW-HA + pep **7b**	349 kDa

r8	HMW CHO-HA + pep **7b**	289 kDa
r9 - ctrl	HMW-HA in H_2O for 1day	581 kDa
r9	HMW-HA + TCEP in H_2O for 1day	311 kDa

***Table 4.10**: Molecular Weight of the peptide-HA conjugates and their controls. Calculated by GPC analysis.*

In the case of high molecular weight samples, this difference is not noticeable because the analysis revealed a slight decrease in the molecular weight of the conjugates, and an intense decrease in the molecular weight of unmodified HMW-HA that was in contact with the peptides and TCEP. Since the solvent does not have a role in the degradation of HA (Fig. S4.19, *Chapter 5.4.5*), this could be due to the presence of TCEP. In fact, when HMW-HA is left in contact with the same amount of TCEP that is used for the reactions with the peptides, the molecular weight after 1 day is much lower than the control (Reaction 9).

For simplicity in the following section the materials from **r6**, **r7** and **r8** will only be referred as ***6b**-HA HMW*, ***6b**-HA LMW* and ***7b**-HA,* respectively.

4.2.5 Electrospinning

The electrospinning technique was employed to produce a textile based on hyaluronic acid. In order to minimize the environmental impact of the process, improve the safety of the final product, and minimize the risks for the operators, water-based solvents were employed to prepare the solutions to electrospin.

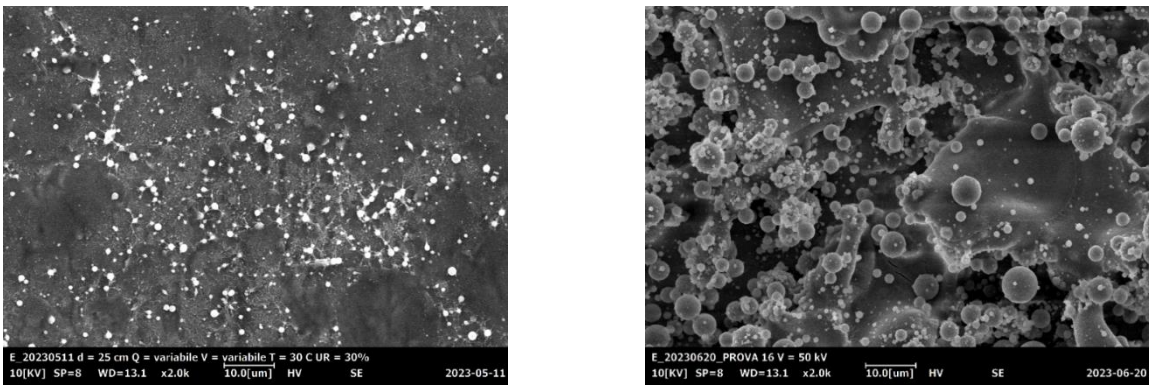

(A) **(B)**

***Figure 4.17**: SEM image after electrospinning of (**A**) 1% HMW-HA in H_2O, (**B**) 10% LMW-HA, 3%EtOH in H_2O.*

Preliminary tests were performed both to fine-tune the electrospinning set up and to explore the feasibility of the electrospinning hyaluronic acid in water. As stated in the literature, the high viscosity and high surface tension made the electrospinning of solutions of pure hyaluronic acid (HMW or LMW) in water is not feasible, independently of the selected concentration. At low concentrations (5% HA-LMW) the low viscosity of the solution caused dropping of the solution from the needle, impeding the process. At high concentrations (20% LMW-HA, 1% HMW-HA) a polymer jet could be formed but it was not stable and caused accumulation of polymer solution on the collector. At a concentration of 10%

LMW-HA, a stable jet was formed but the SEM analysis revealed that no fibers were formed; only spheres were formed, which collapsed when additional layers of polymer were electrospun over them (Fig. 4.17B). The addition of 3% EtOH[82] to the solutions did not improve the electrospinning process.

Therefore, to electrospin CHO-HA we decided to add the electrospinnable and biocompatible polymer PEO (MW of 1000 kDa) to the solution. Out of all the tested concentrations, 3% PEO was the best to form a stable polymer jet during the process and fibers on nanometric dimensions (Fig. S4.20, *Chapter 5.4.6*). Thus, this concentration was added to all the solutions described hereafter.

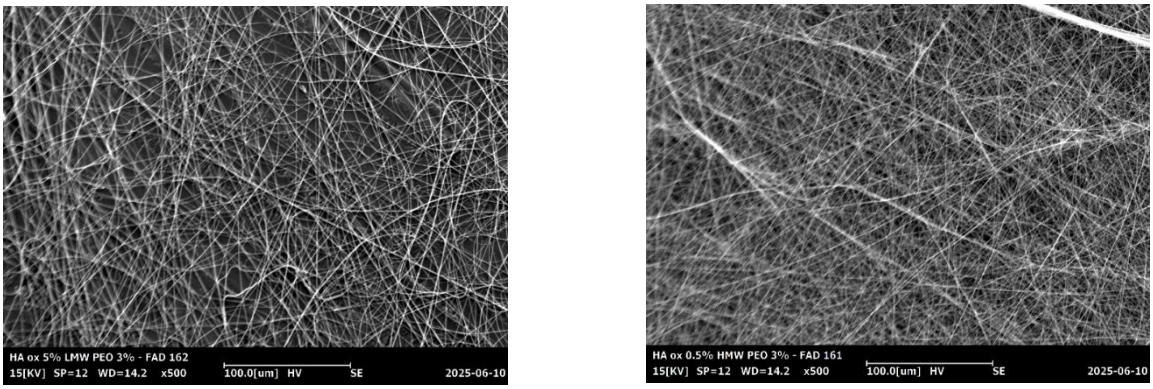

(**A**) (**B**)

Figure 4.18: *SEM image after electrospinning of (**A**) 5% LMW CHO-HA, 3% PEO in H_2O, (**B**) 0.5% HMW CHO-HA, 3% PEO in H_2O.*

In the case of LMW CHO-HA, the electrospinning of solutions in concentrations of 5% and 7% was tested, but only the former managed to form a stable jet and fibers. In the case of HMW CHO-HA, concentrations from 0.5% to 1.5% were tested: at the higher concentrations (1.5-1-0.75% HMW-HA + 3% PEO) fibers were formed but the electrospinning process was not stable and caused the accumulation of the polymer and drops of solvent on the collector. A concentration of 0.5% HMW-HA proved to be ideal for electrospinning (Fig. 4.18 and Fig. S4.21, *Chapter 5.4.6*).

Taking these results into consideration, for the electrospinning of the peptide-HA conjugates, a concentration of 0.5% (and 3%PEO) was selected for the samples of HMW, and a concentration of 5% (and 3% PEO) for the samples of LMW.

Name	Sample	PEO	Solvent	Voltage	Feed rate
ES-01	5% LMW CHO-HA	3%	H_2O	18 kV	1 ml/h
ES-02	0.5% HMW CHO-HA		H_2O	18 kV	1 ml/h
ES-03	0.5% **6b**-HA HMW		H_2O	18 kV	1 ml/h
ES-04	0.5% HA HMW + peptide **6b**		H_2O	18 kV	1 ml/h
ES-05	0.5% **7b**-HA		Alkaline H_2O	18 kV	1 ml/h
ES-06	0.5% HA HMW + peptide **7b**		25% CH_3CN in H_2O	14 kV	1 ml/h

Table 4.11*: List of the successful electrospinning conditions used. Needels of 20G were used. The needle-collector distance, the temperature and the relative humidity of the electrospinning chamber were always set at 25cm, 30°C and of 30%, respectively.*

The same electrospinning conditions used for HMW CHO-HA were ideal for the electrospinning of the HMW conjugates, **6b**-HA HMW and **7b**-HA (Table 4.11 and Fig. 4.19). Surprisingly, a solution of 5% **6b**-HA LMW and 3% PEO could not be electrospun at the same conditions of LMW CHO-HA: the solution failed to form a stable jet and instead dispersed as a spray. This could be due to the too low viscosity of the solution.

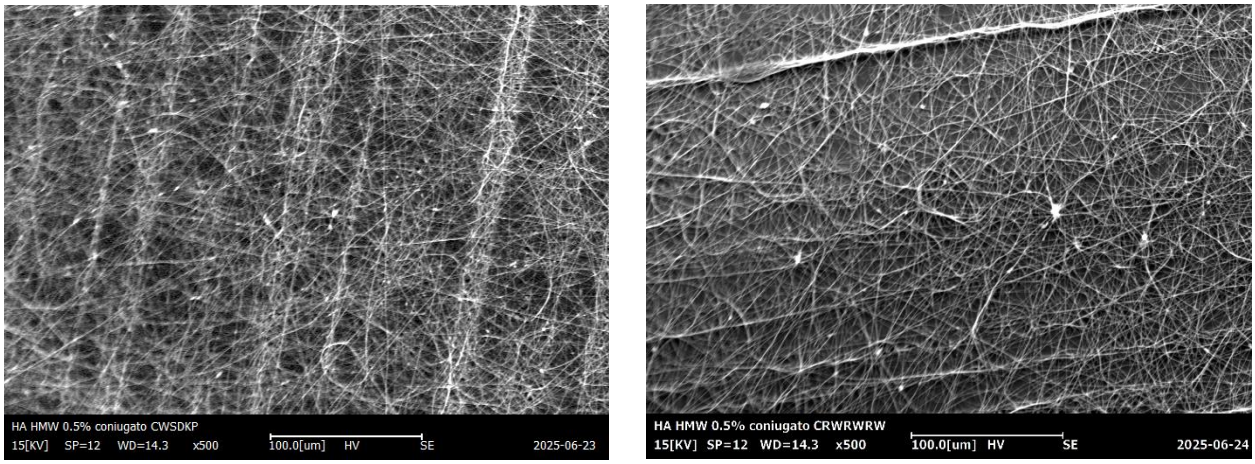

(**A**) (**B**)

Figure 4.19: *SEM image after the electrospinning of (**A**) ES-03: 0.5% **6b**-HA HMW, 3% PEO in H_2O, (**B**) ES-05: 0.5% **7b**-HA HMW, 3% PEO in $NaHCO_3/NaH_2CO_3$ buffer (pH 9.6). The SEM of the other samples is reported in Fig. S4.22, Chapter 5.4.6.*

As controls for **6b**-HA HMW and **7b**-HA, solutions of HMW CHO-HA (with 3% PEO) and 0.2 mmol/g of peptide **6b** or 0.6 mmol/g of peptide **7b** were electrospun. Since **6b** is not soluble in water, the electrospinning of the first solution was performed in 25% CH_3CN in H_2O (SEM images reported in Fig. S4.22B and D, *Chapter 5.4.6*).

These results are of particular interest because we managed to electrospin CHO-HA using only water as the solvent and with concentrations of PEO that are lower than most of the reported[67,70]. In addition, we demonstrate that the presence of peptides does not impact the optimized electrospinning system.

For simplicity in the following sections the electrospun materials will be referred to with the sample name reported in Table 4.11.

4.2.6 Antibacterial Activity

To qualitatively evaluate whether the antibacterial properties of peptide **7b** were maintained after the conjugation to CHO-HA and after being subjected to electrospinning process, the final materials **r8**, **ES-05** and **ES-06** were put in contact with *S. aureus* (ATCC 6538). In particular, solutions containing 2mg/mL of material and *S. aureus* in concentrations of 10^7 CFU/mL or 10^6 CFU/mL were plated for 24h at 37°C. Free peptide **7b** and electrospun CHO-HA HMW (**ES-02**) were used as controls. In particular, in the peptide control, the same amount of peptide **7b** present on the ES-05 and ES-06 samples (0.171µmol) was added to a PBS solution.

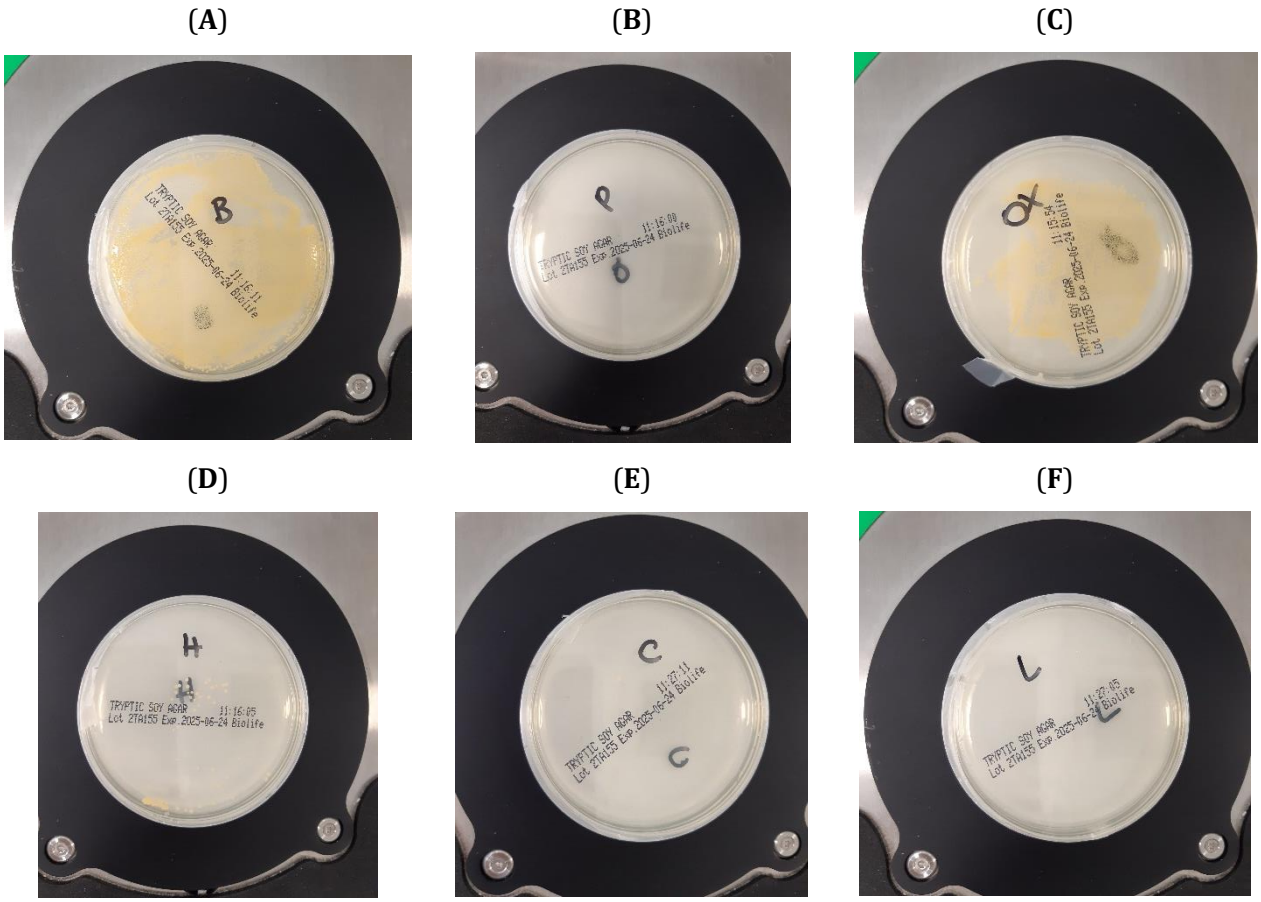

***Figure 4.20**: Growth of S. aureus (10⁶ CFU/mL) when in contact with (**A**) PBS, (**B**) peptide **7b**, (**C**) ES-02: CHO-HA HMW, (**D**) **r8**: **7b**-HA conjugate, (**E**) ES-05: electrospun **7b**-HA conjugate, (**F**) ES-06: HA + **7b** electrospun.*

The results obtained when using 10^7 CFU/mL or 10^6 CFU/mL of *S. aureus* were similar (Fig. 4.20 and S4.27, *Chapter 5.4.8*), and suggest that the antibacterial properties of the peptide were not affected by the conjugation to CHO-HA or electrospinning. In fact, in all the samples were the peptide was present the bacterial growth was inhibited, regardless of whether it was free (Fig. 4.20B), conjugated (Fig. 4.20D and E) or electrospun (Fig. 4.20E and F). In addition, in the control with only electrospun CHO-HA (ES-02) the bacterial growth inhibition did not occur, as expected.

4.3 Conclusions and Future Perspectives

Hyaluronic acid as a great potential in the context of wound healing due to its fundamental role at the wound site. Whereas the versatility of peptides makes them good functionalizing agents, especially in an industrial context where the automatization of processes is essential. Therefore, combining the properties of peptides and hyaluronic acid would create a material with the right balance of properties that could fasten the healing of damaged skin or aid closure of chronical wounds. Moreover, the formation of electrospun nanofibers of the peptide-HA conjugate could further improve the efficacy of the material as wound dressing by providing better hemostatic properties and acting as a template for cell growth.

In this chapter we selected the sequences of a skin regenerative (Ac-SDKP-NH_2) and an antibacterial peptide (H-RWRWRW-NH_2) to use as active molecules for the thiazolidine binding to hyaluronic acid. Two sets of analogues were synthesized in order to have peptides equipped with the β-amino thiol needed for the conjugation, but also a UV-Vis active probe for the quantification of the peptide on the material. In the case of Ac-SDKP, the addition of a palmitoyl was successfully employed as a method to avoid degradation. Interestingly the position of the chain (N-terminus or C-terminus) modified the degradation kinetics of the peptides.

Two methods for the introduction of the aldehyde necessary for the thiazolidine conjugation were explored with hyaluronic acid. The systematic study that we performed awarded $NaIO_4$ as the best oxidizing agent in terms of the amount of formed aldehydes. However, using lower amounts of reagent in this type of reaction had a highly negative effect on the yield. Taking this and the environmental hazard of $NaIO_4$ into consideration, we selected the TEMPO/laccase/O_2 catalyzed system for the larger-scale oxidations. In fact, even though the yields of the reaction are much lower than $NaIO_4$, this system has a lower impact on the integrity of the polysaccharide chain, as measured by molecular weight. In addition, we managed to reach aldehyde loading comparable to the results obtained with cotton cellulose (0.69 ± 0.01 mmol/g_{HA}).

The comparison of the peptide loading on CHO-HA (0.24mmol/g_{HA}) and on unmodified hyaluronic acid (0.08 mmol/g_{HA}) confirms the success of the thiazolidine conjugation with an analogue of Ac-SDKP, peptide **6b**. Unfortunately, the insolubility of the control for the conjugation with peptide **7b**, did not allow to prove the success of the thiazolidine reaction between CHO-HA and the antibacterial peptide.

We managed to produce different electrospun material based on oxidized hyaluronic acid, PEO and peptides. In particular, the addition of 3% PEO to solutions of CHO-HA of high and low molecular weight allowed the electrospinning of water-based solutions. Interestingly the addition of peptides, by conjugation or freely in the solution, did not impact the electrospinning parameters. Thus, electrospun

materials of ***6b**-HA HMW*, ***7b**-HA,* and their controls with the peptides dissolved in the hyaluronic acid/PEO solutions were produced. Preliminary tests on the antibacterial properties of the materials containing the antibacterial peptide **7b** were encouraging. In fact, both the conjugation of the peptide and its electrospinning did not impact its ability to inhibit the growth of *S.aureus*. Scratch tests on the electrospun materials with peptide **6b** are scheduled for the future.

Overall, this project is at an early stage of development, but it has shown great potential. In fact, we managed to produce an electrospun peptide-HA conjugate material with peptide loading comparable to the ones obtained with cotton and chitosan. The antibacterial properties of peptide **7b** were maintained after electrospinning. However, the conjugation with peptide **7b** could not be proven, and an implementation in the set-up of this reaction is needed. In future, it could be interesting to test the thiazolidine reaction in solvents in which hyaluronic acid is insoluble. This could be achieved by performing heterogeneous reactions (similar to those performed with cotton), to avoid the dialysis step and recover the material only by filtration or centrifugation. Another way to avoid purification steps could be to test the reaction with no excess of peptide and electrospin the reaction solution directly.

4.4 Methods

4.4.1 Instruments

HPLC for peptides: Phenomenex C_{18} reverse phase column (4.6 × 250 mm, 5 μ, 100 Å) using a VWR HITACHI Chromaster instrument with spectrophotometric detection at λ = 214 nm and λ = 280 nm.

ESI–MS: Agilent technologies 1260 Infinity II instrument equipped with an Agilent technologies quadrupole LC–MS 6130.

Preparative HPLC for peptide purification: preparative RP-HPLC on a Phenomenex C_{18} column (22.1 mm × 250 mm, 10 μm, 300 Å) using an Akta Pure GE Healthcare (Little Chalfont, U.K.) LC system equipped with an ultraviolet detector (flow rate of 15 mL/min) and a binary elution system (A: H_2O, B: CH_3CN/H_2O [9:1 (v/v)].

UV-Vis: SPECTROstarNano microplate reader (BMG LABTECH). 5mg of the materials were dissolved in a known amount of water and the absorbance of the solution at 280nm was recorded

FT-IR: Thermo Scientific Nicolet Is-10

GPC: Viscotek GPCmax - Advanced GPC/SEC + Viscotek TDA 305-040 Triple Detector Array (Refractive Index, Viscosimeter, LALS/RALS) equipped with the following colums: A6000M, GENERAL MIXED AQ 300x8mm + A7000, AQ GPC/SEC COL 300x8mm. Eluent 0.1M $NaNO_3$ + 0.02% NaN_3. Samples concentration 1 mg/mL for the high molecular weight samples, and 5mg/mL for the low molecular weight samples.

SEM: COXEM EM-30AXN / Xplore 30C

NMR: The ^{1}H-NMR spectra of hyaluronic acid and CHO-HA were recorded using a Bruker AVANCENEO-600 spectrometer (600mHz). HMW CHO-HA and LMW CHO-HA samples were dissolved overnight in D_2O at concentrations of 1 mg/mL and 5 mg/mL, respectively.

4.3.2 Peptide Synthesis

All peptides were synthesized by solid phase synthesis using standard by Fmoc strategy[83]. The synthesis can be rationalized with the following steps:

- SWELLING: degassed DMF is added to the resin and the dispersion stirred for 30min. Then, DMF is removed.
- AA COUPLING: To activate the amino acid, 3eq (with respect to the mmol of binding sites on the resin) of protected amino acid and 3eq of Oxima Pure are dissolved in DMF. Then, 3eq of DIC are added and the solution is left stirring for 3-5min. The activated amino acid solution is added to

the resin and the dispersion is left stirring. After 50min, the solution is filtered and the resin is washed 5 times with DMF. The last amino acid of the sequence is also washed 5 times with DCM.

- Palmitic acid COUPLING: To activate palmitic acid, 3eq (with respect to the mmol of binding sites on the resin) of palmitic acid and 3eq of Oxime are dissolved in DMF. Then, 3eq of DIC are added and the solution is left stirring for 3-5min. The activated palmitic acid solution is added to the resin and the dispersion is left stirring. After 2h, the solution is filtered and the resin is washed 5 times with DMF.
- FMOC DEPROTECTION: the resin is submerged in a solution of 20% piperidine in DMF for 5min. This procedure is repeated a second time for 15min. Then, the resin is washed 5 times with DMF.
- DDE DEPROTECTION: the resin is submerged in a solution of 2% hydrazine in DMF for 5min. This procedure is repeated 5 times. Then, the resin is washed 5 times with DMF.
- ACETILATION: A solution of acetic anhydride in DMF (10 eq with respect to the mmol of binding sites in the resin) and DIPEA (2eq with respect to acetic anhydride) are added to the resin. After 1h, the solution is filtered and the resin is washed 5 times with DMF and DCM.
- CLEAVAGE: a solution of TFA/TIS/H_2O (95:2.5:2.5) is added to the resin and the dispersion is stirred for 2.5h. When the peptide sequence has a cys, a solution of TFA/TIS/H_2O/DODT (94:1:2.5:2.5) is used. Then, a 10-fold excess of cold Et_2O is added to the filtered solution to precipitate the peptide. The solid is recovered by centrifugation (5500 rpm x 5min) and washed 3 times with Et_2O.

All the peptides were kept in a desiccator under reduced pressure for two days and then stored in the fridge.

*Peptide **6a**: Ac-SDKP-NH_2*

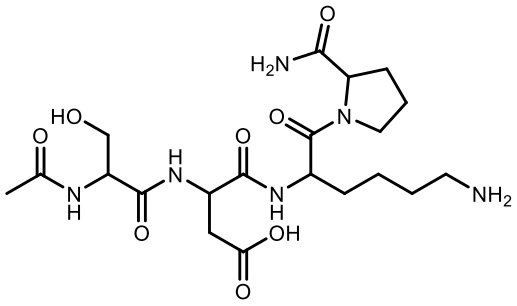

Resin: Fmoc Rink Amide AM (200mg, loading 0.62 mmol/g)

Manual synthesis: SWELL, FMOC DEP, Fmoc-Pro-OH COUPLING, FMOC DEP, Fmoc-Lys(Boc)-OH COUPLING, FMOC DEP, Fmoc-Asp(OtBu)-OH COUPLING, FMOC DEP, Fmoc-Ser(tBu)-OH COUPLING, FMOC DEP, ACETILATION **x2**, CLEAVAGE.

Purity **6a**: 96.9%

*Peptide **6b**: H-CWSDKP-NH₂*

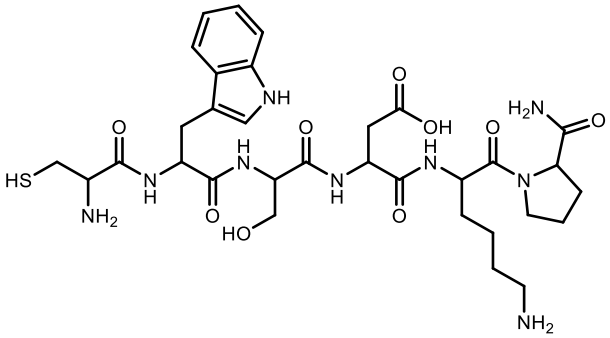

Resin: Fmoc Rink Amide AM (1g, loading 0.52 mmol/g)

Manual synthesis: SWELL, FMOC DEP, Fmoc-Pro-OH COUPLING **x2**, FMOC DEP, Fmoc-Lys(Boc)-OH COUPLING **x2**, FMOC DEP, Fmoc-Asp(OtBu)-OH COUPLING **x2**, FMOC DEP, Fmoc-Ser(tBu)-OH COUPLING **x2**, FMOC DEP, , Fmoc-Trp(Boc)-OH COUPLING **x2**, FMOC DEP, , Fmoc-Cys(Trt)-OH COUPLING **x2**, FMOC DEP, CLEAVAGE.

Purity **6b**: 99.4%

*Peptide **6c**: Pal-SDKPK(WC)-NH₂*

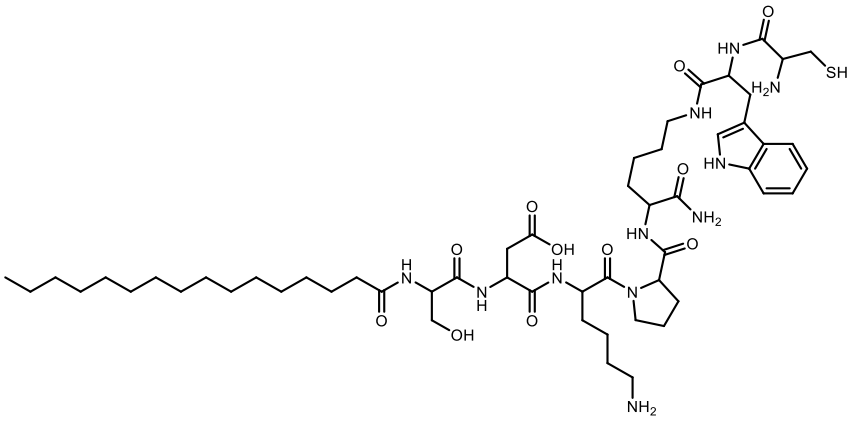

Resin: Fmoc Rink Amide AM (200mg, loading 0.61 mmol/g)

Manual synthesis: SWELL, FMOC DEP, Dde-Lys(Fmoc)-OH COUPLING, FMOC DEP, Fmoc-Trp(Boc)-OH COUPLING, FMOC DEP, Boc-Cys(Trt)-OH COUPLING, DDE DEP, Fmoc-Pro-OH COUPLING, FMOC DEP, Fmoc-Lys(Boc)-OH COUPLING, FMOC DEP, Fmoc-Asp(OtBu)-OH COUPLING, FMOC DEP, Fmoc-Ser(tBu)-OH COUPLING, FMOC DEP, Palmitic Acid COUPLING **x2**, CLEAVAGE.

The peptide was purified with a preparative HPLC, gradient 40-90%B in 50min (A: H_2O + 0.05% TFA, B: CH_3CN/ H_2O 9:1+ 0.05% TFA).

Purity **6c**: 97.7%

*Peptide **6d:** Pal-K(WC)SDKP-NH_2*

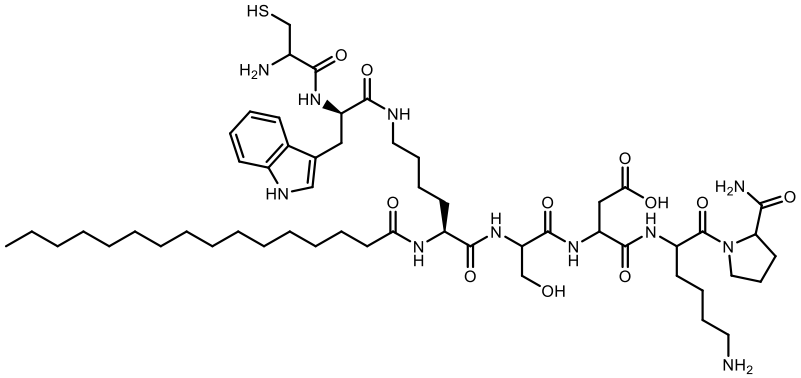

Resin: Fmoc Rink Amide AM (300mg, loading 0.52 mmol/g)

Automatic synthesis: SWELL, FMOC DEP, Fmoc-Pro-OH COUPLING, FMOC DEP, Fmoc-Lys(Boc)-OH COUPLING, FMOC DEP, Fmoc-Asp(OtBu)-OH COUPLING, FMOC DEP, Fmoc-Ser(tBu)-OH COUPLING, FMOC DEP, Dde-Lys(Fmoc) COUPLING, FMOC DEP, Fmoc-Trp(Boc)-OH COUPLING, FMOC DEP, Boc-Cys(Trt)-OH COUPLING, DDE DEP, Palmitic acid COUPLING **x2**, CLEAVAGE.

Peptide **6d** was purified with a preparative HPLC, gradient 35-75%B in 30min (A: H_2O + 0.05% TFA, B: CH_3CN/ H_2O 9:1+ 0.05% TFA).

Purity **6d**: 99.8%

*Peptide **7a** and **7b:** H-RWRWRW- NH_2 and H-CRWRWRW- NH_2*

(**7a**)

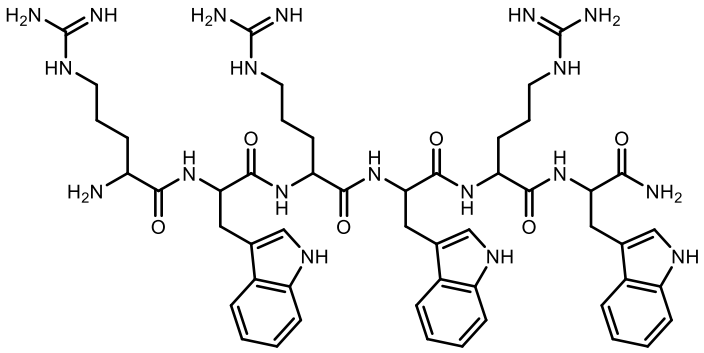

(**7b**)

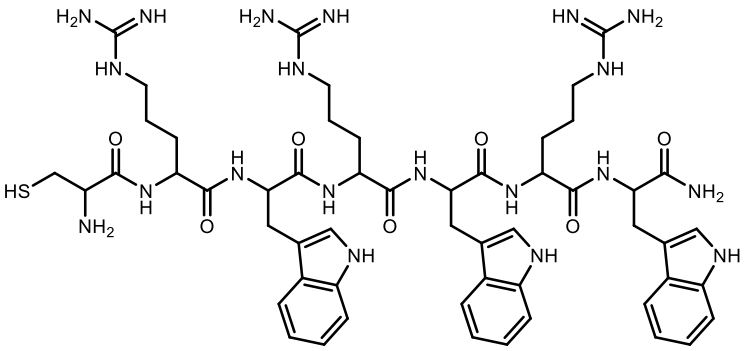

Resin: Fmoc Rink Amide AM (1g, loading 0.52 mmol/g)

Automatic synthesis: SWELL, FMOC DEP, Fmoc-Trp(Boc)-OH COUPLING **x2**, FMOC DEP, Fmoc-Lys(Boc)-OH COUPLING **x2**, FMOC DEP, Fmoc-Trp(Boc)-OH COUPLING **x2**, FMOC DEP, Fmoc-Lys(Boc)-OH COUPLING **x2**, FMOC DEP, Fmoc-Trp(Boc)-OH COUPLING **x2**, FMOC DEP, Fmoc-Lys(Boc)-OH COUPLING **x2**, FMOC DEP.

- 100mg of resin for peptide **7a**: CLEAVAGE.
- The remaining resin for peptide **7b**: Fmoc-Cys(Trt)-OH COUPLING **x2**, FMOC DEP, CLEAVAGE.

The peptides were purified with a preparative HPLC, gradient 15-55%B in 35min (A: H_2O + 0.05% TFA, B: CH_3CN/ H_2O 9:1+ 0.05% TFA).

Purity **7a**: 89.1%

Purity **7b**: 93.7%

4.3.3 Peptide Resistance in Human Serum

The resistance of peptides **6a**, **6c**, and **6d** against serum proteases was tested using the following solutions:

- *Control*: 40 µL of a 5mg/mL solution of the peptide in DMSO was added to 1.25 mL of HEPES buffer (25mM, pH 7.2)
- *Sample*: 40 µL of a 5mg/mL solution of the peptide in DMSO and 250µL of human serum were added to 1mL of HEPES buffer (25mM, pH 7.2)

At 0min, 5min, 15min, 30min, 45min, 60min, 90min, 2h, 3h, 6h and 24h, 100 µL were sampled from the *Sample* and precipitated in 200 µL of EtOH, centrifuged, and 50µL of the supernatant ware injected in HPLC. To ascertain that the buffer did not interfere with the measure at 0min, 30min, 60min, 6h and 24h the same procedure was done also to the *Control*.

4.3.4 CHO grafting on Hyaluronic Acid

$NaIO_4$ oxidation

Hyaluronic acid (300mg) was dissolved overnight in 60mL of H_2O MilliQ. The day after, 2eq of $NaIO_4$ (with respect to the monomer of hyaluronic acid) were added to the solution under stirring. At 1h, 3h, 8h, 24h, 48h and 120h, 10mL of the solution were withdrawn from the solution, put in a vial with 200µL of ethylene glycol. After 1h of stirring, the solution in the vial was dialyzed against water for at least 2 days with a Spectra/Por membrane (cutoff 3.5kDa). The solid was recovered from the solution by lyophilization.

This reaction was performed in a triplicate both on high (2300kDa) and low (50 kDa) molecular weight hyaluronic acid. In the case of HMW hyaluronic acid, the reaction was performed also with 0.5eq in triplicates.

TEMPO/laccase catalyzed oxidation

Hyaluronic acid (300mg) was dissolved overnight in 40mL of acetic acid/sodium acetate buffer (pH 5). The day after, 20U or 60U of laccase (0.84U/mg) and TEMPO (8%$_{w/w}$) were dissolved in 20mL of the buffer and added to the hyaluronic acid solution. The solution stirred in an opened round bottom flask. At 1h, 3h, 8h, 24h, 48h and 120h, 10mL of the solution were withdrawn from the solution, precipitated in a 4-fold excess of EtOH and centrifuged (4500 rpm x 5min). Then the obtained solid was dissolved in 10mL of H_2O milliQ and dialyzed against water for at least 2 days with a Spectra/Por membrane (cutoff 100kDa for HMW-HA, 3.5kDa for LMW-HA). The solid was recovered from the solution by lyophilization.

HA molecular weight	Laccase	TEMPO	Air bubbling	Time of reaction
2300 KDa (HMW)	20 U	8%	-	5days*
	60U		-	
	20U		yes	
	60U		yes	
50kDa (LMW)	20U	8%	-	5days*

***Table 4.12**: Tested reaction conditions for the TEMPO/laccase catalyzed oxidation.*Timepoints at 1h, 3h, 8h, 24h, 48h and 120h.*

This reaction with 20U of laccase without air bubbling were performed in triplicate with high (2300kDa) and low (50 kDa) molecular weight hyaluronic acid.

Stability of hyaluronic acid in the solvent

Test 1: Hyaluronic acid (2300kDa, 300mg) was dissolved overnight in 60mL of H_2O MilliQ or acetic acid/sodium acetate buffer (pH 4.5). At 1h, 3h, 8h, 24h, 48h and 120h, 10mL of the solution were withdrawn from the solution and dialyzed against water for at least 2 days with a Spectra/Por membrane (cutoff 3.5kDa). The solid was recovered from the solution by lyophilization.

Test 2: Hyaluronic acid (2300kDa, 300mg) was dissolved overnight in 60mL of H_2O MilliQ. At 1h, 3h, 8h, 24h, 48h and 120h, 10mL of the solution were withdrawn from the. The solid was recovered from the solution by lyophilization.

CHO-HA for electrospinning

HMW CHO-HA: Hyaluronic acid (2300kDa, 3g) was dissolved overnight in 300 mL of acetic acid/sodium acetate buffer (pH 4.5). The day after, 20U of laccase (1.4U/mg) were added to the solution. Then, TEMPO (8%$_{w/w}$) was dissolved in 100mL of the buffer, added to the hyaluronic acid solution. After 2 days of stirring, a 4-fold excess of EtOH was added to the solution, and the dispersion was centrifuged (9000rpm x 1h, at 4°C). The obtained solid was dissolved in H_2O milliQ and dialyzed against water for 2 days with a Spectra/Por membrane (cutoff 100kDa). The solid was recovered from the solution by lyophilization.

LMW CHO-HA: Hyaluronic acid (50kDa, 3g) was dissolved overnight in 200 mL of acetic acid/sodium acetate buffer (pH 4.5). The day after, 20U of laccase (1.4U/mg) and TEMPO (8%$_{w/w}$) were added to the solution. After 2 days of stirring, a 4-fold excess of EtOH was added to the solution, and the dispersion was centrifuged (9000 rpm x 1h, at 4°C). The obtained solid was dissolved in H_2O milliQ and dialyzed against water for 2 days with a Spectra/Por membrane (cutoff 3.5kDa). The solid was recovered from the solution by lyophilization.

4.3.5 Peptide-HA conjugations

Peptide 6b

Reaction 1: Hyaluronic acid (2300kDa, 60mg) and CHO-HA (HMW, 60mg) were dissolved overnight in 10mL of acetic acid/sodium acetate buffer (pH 4.5). Then, 4eq of peptide **6b** (with respect to the mmoles of aldehydes on CHO-HA) and 4eq of TCEP were dissolved in 20 mL of the buffer. 10mL of the peptide solution were added to the hyaluronic acid and CHO-HA solution. At 5min, 30min, 1h, 3h, 8h and 24h, 3mL of the solution were withdrawn from the solutions, and dialyzed against water for 2 days with a Spectra/Por membrane (cutoff 3.5kDa). The solid was recovered by lyophilization.

Reaction 2: Hyaluronic acid (2300kDa, 60mg) and CHO-HA (HMW, 60mg) were dissolved overnight in 10mL H_2O milliQ. Then, 4eq of peptide **6b** (with respect to the mmoles of aldehydes on CHO-HA) and 4eq of TCEP were dissolved in 20 mL of the buffer. 10mL of the peptide solution were added to the hyaluronic acid and CHO-HA solution. After 24h, the solutions were dialyzed against water for 2 days with a Spectra/Por membrane (cutoff 3.5kDa). The solid was recovered by lyophilization.

Peptide 7b

Reaction 3: Hyaluronic acid (2300kDa, 60mg) and CHO-HA (HMW, 60mg) were dissolved overnight in 10mL of a solution of CH_3CN in acetic acid/sodium acetate buffer (25:75). Then, 4eq of peptide **7b** (with respect to the mmoles of aldehydes on CHO-HA) and 4eq of TCEP were dissolved in 16 mL of the buffer. 8mL of the peptide solution were added to the hyaluronic acid and CHO-HA solution. After 24h, the solutions were dialyzed against 25% CH_3CN (1day) and water (1day) with a Spectra/Por membrane (cutoff 3.5kDa). The solid was recovered by lyophilization.

Reaction 4: 20mL of a solution of CH_3CN in acetic acid/sodium acetate buffer (25:75) were added to CHO-HA (HMW, 60mg), 2eq of peptide **7b** (with respect to the mmoles of aldehydes) and 4eq of TCEP. After 24h of stirring, the dispersion was dialyzed against 25% CH_3CN (1day) and water (1day) with a Spectra/Por membrane (cutoff 3.5kDa). The solid was recovered by lyophilization.

Reaction 5: Hyaluronic acid (50kDa, 25mg) and CHO-HA (LMW, 50mg) were dissolved in a solution of CH_3CN in acetic acid/sodium acetate buffer (25:75), in a concentration of 5mg/mL (5mL). 44µmol of peptide **7b** and TCEP were dissolved in 9mL of 25% CH_3CN. 3mL of the peptide solution were added to the hyaluronic acid solution, to half of the CHO-HA solution and to 5 mL of the solvent. The four solutions

(HA+peptide, CHO-HA+peptide, CHO-HA, and peptide) were stirred for 24h, then they were dialyzed against 25% CH_3CN (1day) and water (1day) with a Spectra/Por membrane (cutoff 3.5kDa). The solids were recovered by lyophilization.

Conjugates for electrospinning

*Reaction 6 (**6b**-HA HMW*): Hyaluronic acid (2300kDa, 50mg) and CHO-HA (HMW, 250mg) were dissolved overnight in H_2O milliQ in a concentration of 5mg/mL. Then, peptide **6b** (130mg,) and TCEP (50mg) were dissolved in 30mL of H_2O milliQ. 5mL of the peptide solution were added to the hyaluronic acid solution and the remaining to the CHO-HA solution (2eq of peptide with respect to the aldehydes). After 24h, the solutions were dialyzed with a Spectra/Por membrane (cutoff 3.5kDa). The solid was recovered by lyophilization.

*Reaction 7 (**6b**-HA LMW)*: Hyaluronic acid (50kDa, 50mg) and CHO-HA (LMW, 450mg) were dissolved overnight in H_2O milliQ in a concentration of 5mg/mL. Then, peptide **6b** (10mg,) and TCEP (40mg) were dissolved in 30mL of H_2O milliQ. 3mL of the peptide solution were added to the hyaluronic acid solution and the remaining to the CHO-HA solution (2eq of peptide with respect to the aldehydes). After 24h, the solutions were dialyzed with a Spectra/Por membrane (cutoff 3.5kDa). The solid was recovered by lyophilization.

*Reaction 8 (**7b**-HA)*: Hyaluronic acid (2300kDa, 50mg) and CHO-HA (HMW, 250mg) were dissolved overnight in a solution of CH_3CN in acetic acid/sodium acetate buffer (25:75) in a concentration of 5mg/mL. Then, peptide **7b** (200mg,) and TCEP (50mg) were dissolved in 30mL of 25% CH_3CN. 5mL of the peptide solution were added to the hyaluronic acid solution and the remaining to the CHO-HA solution (2eq of peptide with respect to the aldehydes). After 24h, the solutions were against 25% CH_3CN (1day) and water (1day) with a Spectra/Por membrane (cutoff 3.5kDa). The solid was recovered by lyophilization.

Reaction 9: Hyaluronic acid (2300kDa, 80mg) was dissolved overnight in 20mL of H_2O MilliQ. 10ml of the solution were left stirring (*control*), 15mg of TCEP were added to the other 10mL of the solution,. After 24h, the two solutions were dialyzed against water for 2 days with a Spectra/Por membrane (cutoff 3.5kDa). The solid was recovered from the solution by lyophilization.

4.3.6 Electrospinning

All the electrospinning tests were performed at I.R.A. – Istituto di Ricerche Applicate (Usmate Velate, MB) using a FLUIDNATEK® LE-500 Pilot-scale electrospinning machine by Bionicia. For the SEM images of the electrospun materials refer to *chapter 5.4.6*. In the following section polyethylene oxide (1000kDa) will be referred as PEO, and hyaluronic acid of 2300 kDa and 50kDa will be referred as HMW-HA and LMW-HA, respectively.

Hyaluronic Acid and PEO

The following solutions were electrospun varying the voltage (10-30kV), the flux (0.5-1 mL/h), and the needle-collector distance (30-15 cm), maintaining the temperature at 30°C:

- 1% HMW-HA in H_2O
- 5-10-20% LMW-HA in H_2O
- 10-20% LMW-HA, 3%EtOH in H_2O
- 0.5-1-2-3-5-7% PEO in H_2O
- 3% PEO in $NaHCO_3/NaH_2CO_3$ buffer (pH 9.6)
- 3% PEO in CH_3CN/H_2O (25:75)
- 1% HMW-HA, 2% PEO in H_2O
- 1.5% HMW-HA, 2.5% PEO in H_2O
- 0.75% HMW-HA, 1.25% PEO in H_2O

Electrospinning of CHO-HA

The following solutions were electrospun varying the voltage (14-20kV), and maintaining the flux at 1ml/min, the needle-collector distance at 25cm and the temperature at 30°C:

- **ES-01**: 5% LMW CHO-HA, 3% PEO in H_2O
- 7% LMW CHO-HA, 3% PEO in H_2O
- 1.5% HMW CHO-HA, 3% PEO in H_2O
- 1% HMW CHO-HA, 3% PEO in H_2O
- 0.75% HMW CHO-HA, 3% PEO in H_2O
- **ES-02:** 0.5% HMW CHO-HA, 3% PEO in H_2O

Electrospinning of the conjugates

The following solutions were electrospun varying the voltage (14-20kV), and maintaining the flux at 1ml/min, the needle-collector distance at 25cm and the temperature at 30°C:

- 5% ***6b****-HA LMW*, 3% PEO in H_2O
- **ES-03:** 0.5% ***6b****-HA HMW*, 3% PEO in H_2O
- **ES-04:** 0.5% HMW-HA, 3% PEO and 0.2mmol/g_{HA} of peptide **6b** in H_2O
- **ES-05:** 0.5% ***7b****-HA HMW*, 3% PEO in $NaHCO_3/NaH_2CO_3$ buffer (pH 9.6)
- **ES-06:** 0.5% HMW-HA, 3% PEO and 0.6mmol/g_{HA} of peptide **7b** in CH_3CN/H_2O (25:75)

4.3.7 Antibacterial tests

A dried pellet of *S. aureus* (ATCC 6538, $4.7*10^7$ colonies) was dissolved in 3mL of sterile PBS buffer and plated overnight at 30°C. The day after, one colony was added to 3mL of sterile Muller–Hinton broth and

left at 37°C for 24h. Then, 500µL of the 10^7 CFU/mL solution of *S.aureus* were added to 500µL of the *sample* solution that was previously filtered (0.22 µm):

- *Control*: PBS buffer
- *Peptide **7b***: 23µL of a 72mM solution of peptide **7b** in DMSO were added to 5mL of PBS buffer (342µM)
- *CHO*-HA HMW: 2mg of **ES-02** dissolved in 500µL of PBS buffer
- ***7b**-HA HMW*: 2mg of electrospun **ES-05** dissolved in 500µL of PBS buffer
- ***7b** + HA HMW:* 2mg of electrospun **ES-06** dissolved in 500µL of PBS buffer

Then, 500µL of the mixed solutions were plated for 24h at 37°C. All samples were prepared in triplicates.

The same procedure was repeated for peptide **7b**, CHO-HA HMW, **r8** (**7b**-HA), **ES-02**, **ES-06** and **ES-07** using *S.aureus* in a concentration of 10^6 CFU/mL.

References

1 Petit, N. *et al.* Development of a bioactive hyaluronic acid hydrogel functionalised with antimicrobial peptides for the treatment of chronic wounds. *Biomaterials Science* (2025).

2 Elder, A. N., Hannes, S. K., Atoyebi, S. F. & Washburn, N. R. Effects on peptide binding affinity for TNFα by PEGylation and conjugation to hyaluronic acid. *European polymer journal* **49**, 2968-2975 (2013).

3 Schanté, C. E., Zuber, G., Herlin, C. & Vandamme, T. F. Improvement of hyaluronic acid enzymatic stability by the grafting of amino-acids. *Carbohydrate polymers* **87**, 2211-2216 (2012).

4 Schanté, C., Zuber, G., Herlin, C. & Vandamme, T. F. Synthesis of N-alanyl-hyaluronamide with high degree of substitution for enhanced resistance to hyaluronidase-mediated digestion. *Carbohydrate polymers* **86**, 747-752 (2011).

5 Liu, C.-F. & Tam, J. P. Chemical ligation approach to form a peptide bond between unprotected peptide segments. Concept and model study. *Journal of the American Chemical Society* **116**, 4149-4153 (1994).

6 Tam, J. P., Rao, C., Liu, C. F. & Sha, J. Specificity and formation of unusual amino acids of an amide ligation strategy for unprotected peptides. *International Journal of Peptide and Protein Research* **45**, 209-216 (1995).

7 Yasin, A. *et al.* Advances in hyaluronic acid for biomedical applications. *Frontiers in Bioengineering and Biotechnology* **10**, 910290 (2022).

8 Weissmann, B. & Meyer, K. The structure of hyalobiuronic acid and of hyaluronic acid from umbilical Cord1, 2. *Journal of the american chemical society* **76**, 1753-1757 (1954).

9 Castro, K. C., Campos, M. G. N. & Mei, L. H. I. Hyaluronic acid electrospinning: Challenges, applications in wound dressings and new perspectives. *International Journal of Biological Macromolecules* **173**, 251-266 (2021).

10 Lee, B. M., Park, S. J., Noh, I. & Kim, C.-H. The effects of the molecular weights of hyaluronic acid on the immune responses. *Biomaterials Research* **25**, 27 (2021).

11 Han, W. *et al.* The anti-inflammatory activity of specific-sized hyaluronic acid oligosaccharides. *Carbohydrate Polymers* **276**, 118699 (2022).

12 Litwiniuk, M., Krejner, A., Speyrer, M. S., Gauto, A. R. & Grzela, T. Hyaluronic acid in inflammation and tissue regeneration. *Wounds* **28**, 78-88 (2016).

13 Valachová, K., El Meligy, M. A. & Šoltés, L. Hyaluronic acid and chitosan-based electrospun wound dressings: Problems and solutions. *International Journal of Biological Macromolecules* **206**, 74-91 (2022).

14 D'Agostino, A. *et al.* In vitro analysis of the effects on wound healing of high-and low-molecular weight chains of hyaluronan and their hybrid H-HA/L-HA complexes. *BMC Cell Biology* **16**, 19 (2015).

15 D'Agostino, A. *et al.* Is molecular size a discriminating factor in hyaluronan interaction with human cells? *Carbohydrate polymers* **157**, 21-30 (2017).

16 Altman, R. *et al.* Anti-inflammatory effects of intra-articular hyaluronic acid: a systematic review. *Cartilage* **10**, 43-52 (2019).

17 Maiz-Fernández, S., Pérez-Álvarez, L., Silván, U., Vilas-Vilela, J. L. & Lanceros-Méndez, S. Dynamic and self-healable chitosan/hyaluronic acid-based in situ-forming hydrogels. *Gels* **8**, 477 (2022).

18 Shan, J. *et al.* Tempo/tcc as a chemo selective alternative for the oxidation of hyaluronic acid. *Molecules* **26**, 5963 (2021).

19 Qian, C. *et al.* Injectable and self-healing polysaccharide-based hydrogel for pH-responsive drug release. *International journal of biological macromolecules* **123**, 140-148 (2019).

20 Liu, C. *et al.* Glycol chitosan/oxidized hyaluronic acid hydrogels functionalized with cartilage extracellular matrix particles and incorporating BMSCs for cartilage repair. *Artificial cells, nanomedicine, and biotechnology* **46**, 721-732 (2018).

21 Su, W.-Y., Chen, Y.-C. & Lin, F.-H. Injectable oxidized hyaluronic acid/adipic acid dihydrazide hydrogel for nucleus pulposus regeneration. *Acta biomaterialia* **6**, 3044-3055 (2010).

22 Jia, X. *et al.* Synthesis and characterization of in situ cross-linkable hyaluronic acid-based hydrogels with potential application for vocal fold regeneration. *Macromolecules* **37**, 3239-3248 (2004).

23 Buffa, R. *et al.* (Google Patents, 2016).

24 Angelin, M., Hermansson, M., Dong, H. & Ramström, O. (Wiley Online Library, 2006).

25 Aracri, E., Valls, C. & Vidal, T. Paper strength improvement by oxidative modification of sisal cellulose fibers with laccase–TEMPO system: influence of the process variables. *Carbohydrate polymers* **88**, 830-837 (2012).

26 Lenfant, M. *et al.* Inhibitor of hematopoietic pluripotent stem cell proliferation: purification and determination of its structure. *Proceedings of the National Academy of Sciences* **86**, 779-782 (1989).

27 Kumar, N. & Yin, C. The anti-inflammatory peptide Ac-SDKP: Synthesis, role in ACE inhibition, and its therapeutic potential in hypertension and cardiovascular diseases. *Pharmacological research* **134**, 268-279 (2018).

28 Cai, J., Chen, Q., Mehrabi Nasab, E. & Athari, S. S. Immunomodulatory effect of N-acetyl-seryl-aspartyl-proline and vasoactive intestinal peptide on chronic obstructive pulmonary disease pathophysiology. *Fundamental & Clinical Pharmacology* **36**, 1005-1010 (2022).

29 Dadar, M. *et al.* Antiinflammatory peptides: current knowledge and promising prospects. *Inflammation Research* **68**, 125-145 (2019).

30 Sharma, U. *et al.* Novel anti-inflammatory mechanisms of N-Acetyl-Ser-Asp-Lys-Pro in hypertension-induced target organ damage. *American Journal of Physiology-Heart and Circulatory Physiology* **294**, H1226-H1232 (2008).

31 Liu, J.-M. *et al.* The tetrapeptide AcSDKP, an inhibitor of primitive hematopoietic cell proliferation, induces angiogenesis in vitro and in vivo. *Blood, The Journal of the American Society of Hematology* **101**, 3014-3020 (2003).

32 Fromes, Y., Liu, J. M., Kovacevic, M., Bignon, J. & Wdzieczak-Bakala, J. The tetrapeptide acetyl-serine-aspartyl-lysine-proline improves skin flap survival and accelerates wound healing. *Wound repair and regeneration* **14**, 306-312 (2006).

33 Hajem, N. *et al.* The regulatory role of the tetrapeptide A c SDKP in skin and hair physiology and the prevention of ageing effects in these tissues–a potential cosmetic role. *International journal of cosmetic science* **35**, 286-298 (2013).

34 Bakala, J., Lallemand, J.-Y., Liu, J.-M. & Bignon, J. (Google Patents, 2014).

35 Strøm, M. B., Rekdal, Ø. & Svendsen, J. S. Antimicrobial activity of short arginine-and tryptophan-rich peptides. *Journal of peptide science: an official publication of the European Peptide Society* **8**, 431-437 (2002).

36 Strøm, M. B. *et al.* The pharmacophore of short cationic antibacterial peptides. *Journal of medicinal chemistry* **46**, 1567-1570 (2003).

37 Albada, H. B. *et al.* Modulating the activity of short arginine-tryptophan containing antibacterial peptides with N-terminal metallocenoyl groups. *Beilstein journal of organic chemistry* **8**, 1753-1764 (2012).

38 Liu, Z. *et al.* Length effects in antimicrobial peptides of the (RW) n series. *Antimicrobial agents and chemotherapy* **51**, 597-603 (2007).

39 Wenzel, M. *et al.* Towards profiles of resistance development and toxicity for the small cationic hexapeptide RWRWRW-NH2. *Frontiers in Cell and Developmental Biology* **4**, 86 (2016).

40 Wenzel, M. *et al.* Small cationic antimicrobial peptides delocalize peripheral membrane proteins. *Proceedings of the National Academy of Sciences* **111**, E1409-E1418 (2014).

41 Zhang, D. *et al.* Development of a potent antimicrobial peptide with photodynamic activity. *Frontiers in Microbiology* **12**, 624465 (2021).

42 Wenzel, M. *et al.* Influence of lipidation on the mode of action of a small RW-rich antimicrobial peptide. *Biochimica et Biophysica Acta (BBA)-Biomembranes* **1858**, 1004-1011 (2016).

43 Albada, H. B. *et al.* Tuning the activity of a short Arg-Trp antimicrobial peptide by lipidation of a C-or N-terminal lysine side-chain. *ACS medicinal chemistry letters* **3**, 980-984 (2012).

44 Albada, H. B. *et al.* Short antibacterial peptides with significantly reduced hemolytic activity can be identified by a systematic L-to-D exchange scan of their amino acid residues. *ACS Combinatorial Science* **15**, 585-592 (2013).

45 Formhals, A. (US patent 1975504, 1934).

46 Formhals, A. (US patent 2160962, 1939).

47 Formhals, A. (US patent 2187306, 1940).

48 Formhals, A. (US patent, 2323025, 1943).

49 Formhals, A. (US patent, 2349950, 1944).

50 Schiffman, J. D. & Schauer, C. L. A review: electrospinning of biopolymer nanofibers and their applications. *Polymer reviews* **48**, 317-352 (2008).

51 Huang, Z.-M., Zhang, Y.-Z., Kotaki, M. & Ramakrishna, S. A review on polymer nanofibers by electrospinning and their applications in nanocomposites. *Composites science and technology* **63**, 2223-2253 (2003).

52 Teo, W. E. & Ramakrishna, S. A review on electrospinning design and nanofibre assemblies. *Nanotechnology* **17**, R89 (2006).

53 Burger, C., Hsiao, B. S. & Chu, B. Nanofibrous materials and their applications. *Annu. Rev. Mater. Res.* **36**, 333-368 (2006).

54 Subbiah, T., Bhat, G. S., Tock, R. W., Parameswaran, S. & Ramkumar, S. S. Electrospinning of nanofibers. *Journal of applied polymer science* **96**, 557-569 (2005).

55 Taylor, G. I. Electrically driven jets. *Proceedings of the Royal Society of London. A. Mathematical and Physical Sciences* **313**, 453-475 (1969).

56 He, J.-H., Wan, Y.-Q. & Xu, L. Nano-effects, quantum-like properties in electrospun nanofibers. *Chaos, Solitons & Fractals* **33**, 26-37 (2007).

57 Laurencin, C. T., Ambrosio, A. M., Borden, M. D. & Cooper Jr, J. A. Tissue engineering: orthopedic applications. *Annual review of biomedical engineering* **1**, 19-46 (1999).

58 Um, I. C., Fang, D., Hsiao, B. S., Okamoto, A. & Chu, B. Electro-spinning and electro-blowing of hyaluronic acid. *Biomacromolecules* **5**, 1428-1436 (2004).

59 Wang, X. *et al.* Formation of water-resistant hyaluronic acid nanofibers by blowing-assisted electro-spinning and non-toxic post treatments. *Polymer* **46**, 4853-4867 (2005).

60 Shin, Y., Hohman, M., Brenner, M. & Rutledge, G. Experimental characterization of electrospinning: the electrically forced jet and instabilities. *Polymer* **42**, 09955-09967 (2001).

61 Deitzel, J. M., Kleinmeyer, J. D., Hirvonen, J. K. & Tan, N. B. Controlled deposition of electrospun poly (ethylene oxide) fibers. *Polymer* **42**, 8163-8170 (2001).

62 Deitzel, J. M., Kleinmeyer, J., Harris, D. & Tan, N. B. The effect of processing variables on the morphology of electrospun nanofibers and textiles. *Polymer* **42**, 261-272 (2001).

63 Sankaranarayanan, S. A., Murugappan, S., Eswar, K., Padmakumar, A. & Rengan, A. K. in *Synthetic Polymers in Drug and Biotherapeutics Delivery* 197-234 (Elsevier, 2025).

64 Gilding, D. & Reed, A. Biodegradable polymers for use in surgery—poly (ethylene oxide) poly (ethylene terephthalate)(PEO/PET) copolymers: 1. *Polymer* **20**, 1454-1458 (1979).

65 Chen, C.-H., Chen, S.-H., Shalumon, K. & Chen, J.-P. Dual functional core–sheath electrospun hyaluronic acid/polycaprolactone nanofibrous membranes embedded with silver nanoparticles for prevention of peritendinous adhesion. *Acta biomaterialia* **26**, 225-235 (2015).

66 Chen, G., Guo, J., Nie, J. & Ma, G. Preparation, characterization, and application of PEO/HA core shell nanofibers based on electric field induced phase separation during electrospinning. *Polymer* **83**, 12-19 (2016).
67 Ahire, J., Robertson, D., van Reenen, A. & Dicks, L. Polyethylene oxide (PEO)-hyaluronic acid (HA) nanofibers with kanamycin inhibits the growth of Listeria monocytogenes. *Biomedicine & Pharmacotherapy* **86**, 143-148 (2017).
68 Bazmandeh, A. Z., Mirzaei, E., Fadaie, M., Shirian, S. & Ghasemi, Y. Dual spinneret electrospun nanofibrous/gel structure of chitosan-gelatin/chitosan-hyaluronic acid as a wound dressing: In-vitro and in-vivo studies. *International journal of biological macromolecules* **162**, 359-373 (2020).
69 Chen, H. *et al.* Molecular interaction, chain conformation, and rheological modification during electrospinning of hyaluronic acid aqueous solution. *Membranes* **10**, 217 (2020).
70 Yang, Q., Xie, Z., Hu, J. & Liu, Y. Hyaluronic acid nanofiber mats loaded with antimicrobial peptide towards wound dressing applications. *Materials Science and Engineering: C* **128**, 112319 (2021).
71 Raje, K., Tanaka, S. & Fujita, S. Biocompatible native hyaluronan nanofibers fabricated via aqueous PEO-assisted electrospinning and heat-quench process. *ACS omega* **9**, 40010-40018 (2024).
72 Bucci, R., Georgilis, E., Bittner, A. M., Gelmi, M. L. & Clerici, F. Peptide-based electrospun fibers: Current status and emerging developments. *Nanomaterials* **11**, 1262 (2021).
73 Kamaraj, S., Kandasamy, R. & Alagarsamy, S. Electrospinning: A New Frontier in Peptide Therapeutics. *AAPS PharmSciTech* **26**, 69 (2025).
74 Bucci, R. *et al.* Peptide grafting strategies before and after electrospinning of nanofibers. *Acta Biomaterialia* **122**, 82-100 (2020).
75 Dwivedi, C. *et al.* In vivo biocompatibility of electrospun biodegradable dual carrier (antibiotic+ growth factor) in a mouse model—Implications for rapid wound healing. *Pharmaceutics* **11**, 180 (2019).
76 Dwivedi, C. *et al.* In vivo diabetic wound healing with nanofibrous scaffolds modified with gentamicin and recombinant human epidermal growth factor. *Journal of biomedical materials research Part A* **106**, 641-651 (2018).
77 Nogueira, F., Teixeira, P. & Gouveia, I. C. Electrospinning polypropylene with an amino acid as a strategy to bind the antimicrobial peptide Cys-LC-LL-37. *Journal of Materials Science* **53**, 4655-4664 (2018).
78 Pace, C. N., Vajdos, F., Fee, L., Grimsley, G. & Gray, T. How to measure and predict the molar absorption coefficient of a protein. *Protein science* **4**, 2411-2423 (1995).
79 Biondi, B. *et al.* Structural and biological characterization of shortened derivatives of the cathelicidin PMAP-36. (2023).
80 Amer, H. *et al.* Synthesis and characterization of periodate-oxidized polysaccharides: dialdehyde xylan (DAX). *Biomacromolecules* **17**, 2972-2980 (2016).
81 Kim, U.-J., Kuga, S., Wada, M., Okano, T. & Kondo, T. Periodate oxidation of crystalline cellulose. *Biomacromolecules* **1**, 488-492 (2000).
82 Sun, J., Perry, S. L. & Schiffman, J. D. Electrospinning nanofibers from chitosan/hyaluronic acid complex coacervates. *Biomacromolecules* **20**, 4191-4198 (2019).
83 Atherton, E. *et al.* A mild procedure for solid phase peptide synthesis: use of fluorenylmethoxycarbonylamino-acids. *Journal of the Chemical Society, Chemical Communications*, 537-539 (1978).

Chapter V

Supporting Information

5.1 Materials

Reagents and solvents

Brand	Reagents and solvents
Aldrich	TEMPO, Fmoc-Gly-OH, Fmoc-Trp(Boc)-OH, TCEP
Carlo Erba	Methanol, Acetonitrile, Hydrazine, NaH_2PO_4, KH_2PO_4, $NaHCO_3$, $NaClO_2$
Eurisotop	D_2O
Fujifilm Irvine Scientific	VA-086
GL Biochem	Fmoc-Arg(Pbf)-OH, Fmoc-Leu-OH, Fmoc-Ile-OH, Fmoc-Val-OH, Fmoc-Pro-OH
Honeywell	Piperidine, DODT
Iris biotech	Fmoc Rink Amide AM, Fmoc-Cys(Trt)-OH, Fmoc-Lys(Boc)-OH, Fmoc-His(Boc)-OH, Fmoc-Ala-OH, Fmoc-D-Ala-OH, Fmoc-Thr(tBu)-OH, Fmoc-Ser(tBu)-OH, Dde-Lys(Fmoc)-OH, Fmoc-Pra-OH, Fmoc-Asp(OtBu)-OH, HOBt, HBTU, Oxima Pure, DIC, HCTU
Piave Maitex Srl	Cotton
Riedel-den Haen	Sodium acetate, Sodium ascorbate
Sigma	Schiff reagent, Laccase from "Trametes Versicolor", DIPEA
Sigma-Aldrich	Acetone, Acetic acid, Diethylether, Hydrochloric acid, Ethanol, DMF, DCM, TFA, TIS, DMSO, 1-pentyne, Propargylamine, Boc-Aminooxiacetic acid-OH, Fmoc-Lys(Dde)-OH, Palmitic acid, Carbic anhydride, Aminoguanidine, HEPES, NMM, MTBE, ISA·HCl, THPTA, EDTA, $NaIO_4$, NaCl, KOH, NaOH, KCl, Na_2CO_3, K_2CO_3, $CuSO_4 \cdot 5H_2O$, Kaiser test kit.

5.2 Supporting Images – Chapter II

5.2.1 Chromatograms (HPLC) of the synthesized peptides

Peptide 1a and 1b

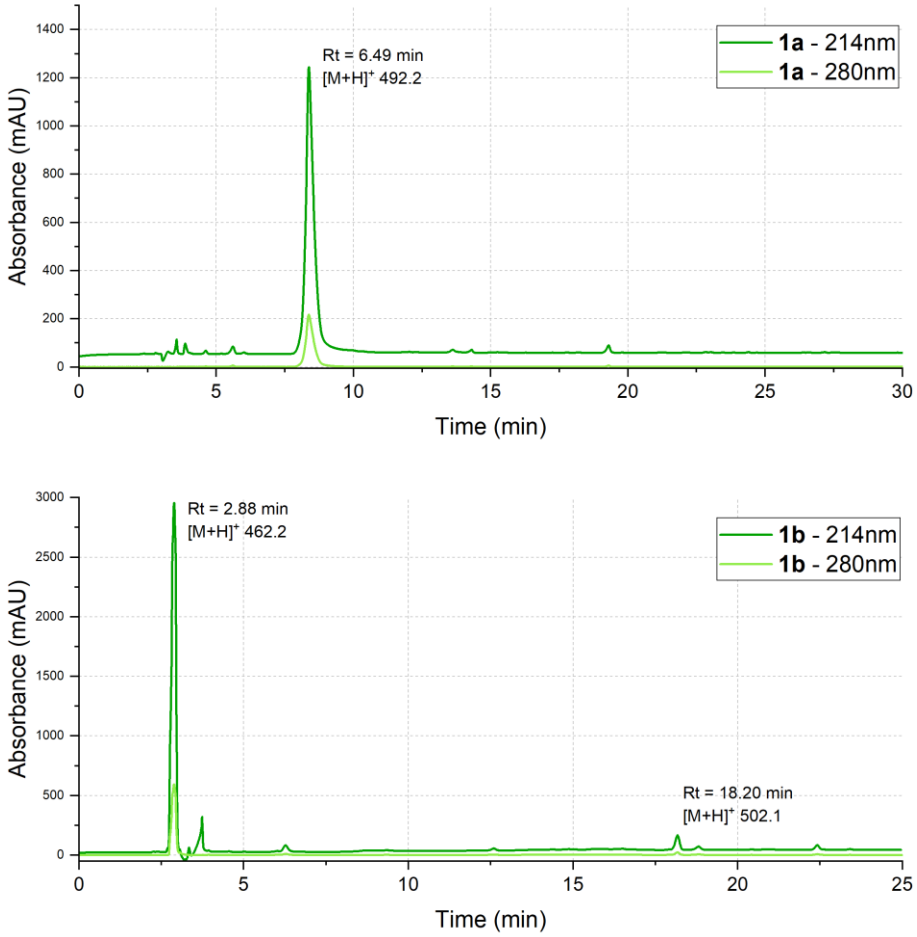

***Figure S2.1**: HPLC trace of peptide **1a** (H-CGWK-NH_2**)** and **1b** (H-AxGWK-NH_2). Gradient 0-30%B in 30min using a binary elution system with A: 0.05% TFA in CH_3CN/H_2O (1:9 v/v) and B: 0.05% TFA in CH_3CN/ H_2O (9:1 v/v).*

Peptide 2a, 2b and 2c

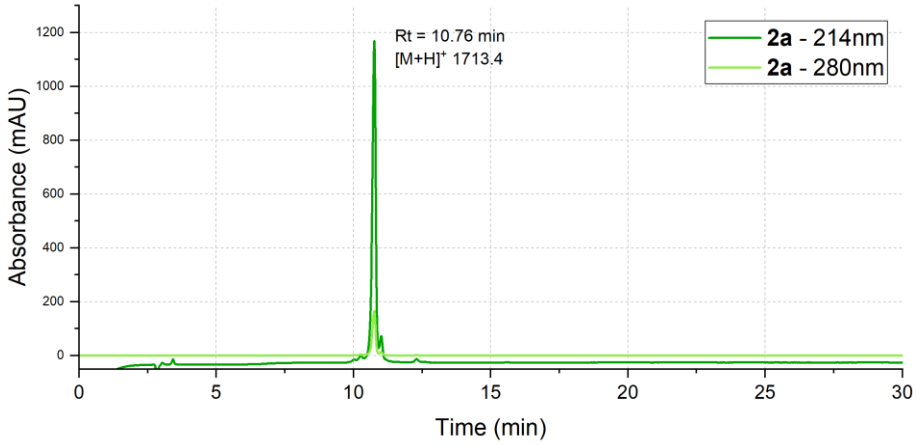

***Figure S2.2:** HPLC trace of peptide **2a** (H-CKRLKKIGKVLKWI-NH_2). Gradient of 10-60%B in 30min using a binary elution system with A: 0.05% TFA in CH_3CN/H_2O (1:9 v/v) and B: 0.05% TFA in CH_3CN/ H_2O (9:1 v/v).*

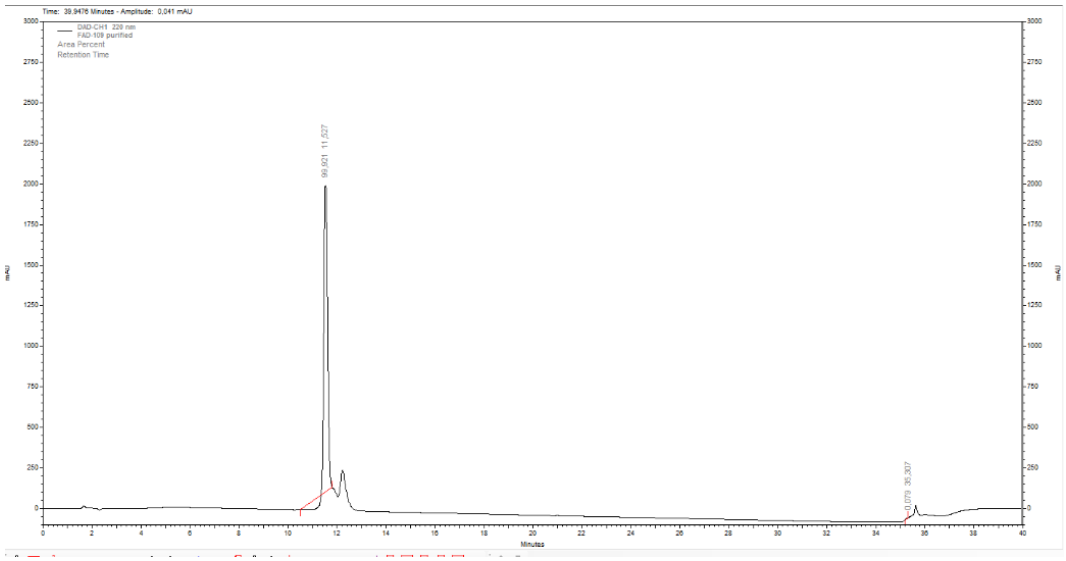

Figure S2.3: *HPLC trace of peptide* ***2b*** *(H-KRLKKIGKVLKWIC-NH_2). Gradient 1-100%B in 30min. Binary elution system with A: 0.05% TFA in H_2O and B: 0.05% TFA in CH_3CN.*

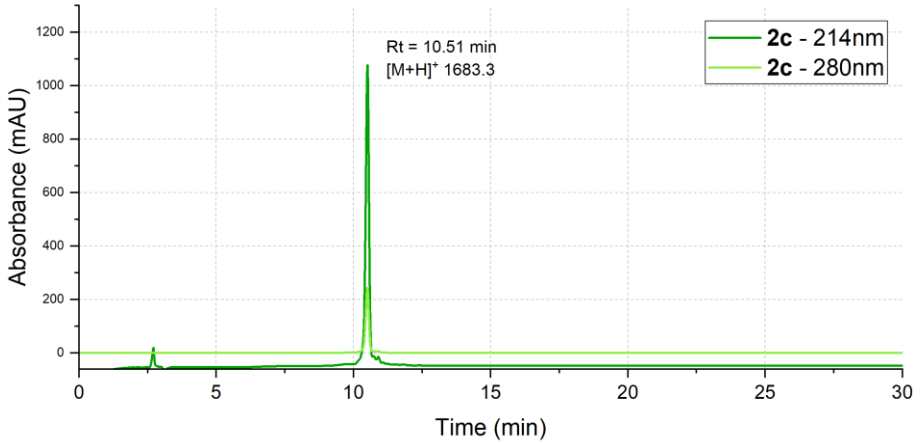

Figure S2.4: *HPLC trace of peptide* ***2c*** *(H-A_xKRLKKIGKVLKWI-NH_2). Gradient 20-60%B in 30min using a binary elution system with A: 0.05% TFA in CH_3CN/H_2O (1:9 v/v) and B: 0.05% TFA in CH_3CN/ H_2O (9:1 v/v).*

Peptide 3a, 3b and 3c

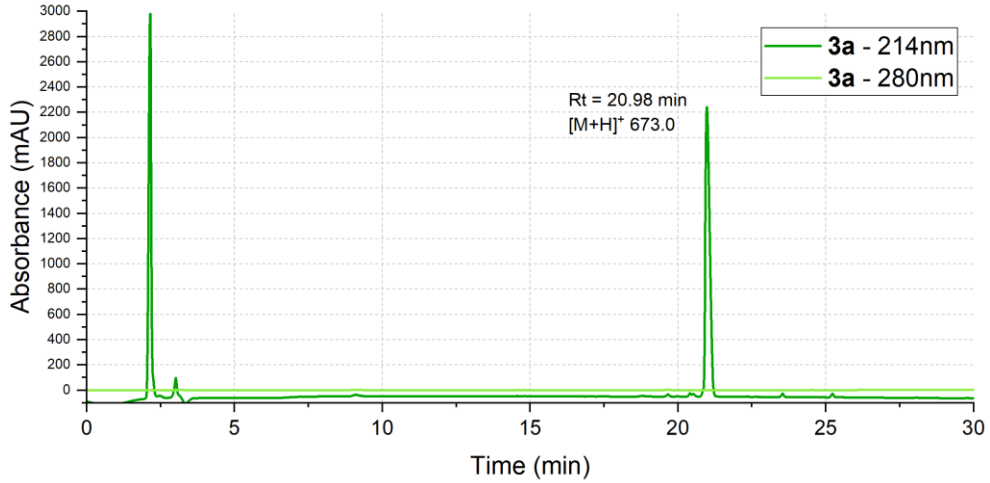

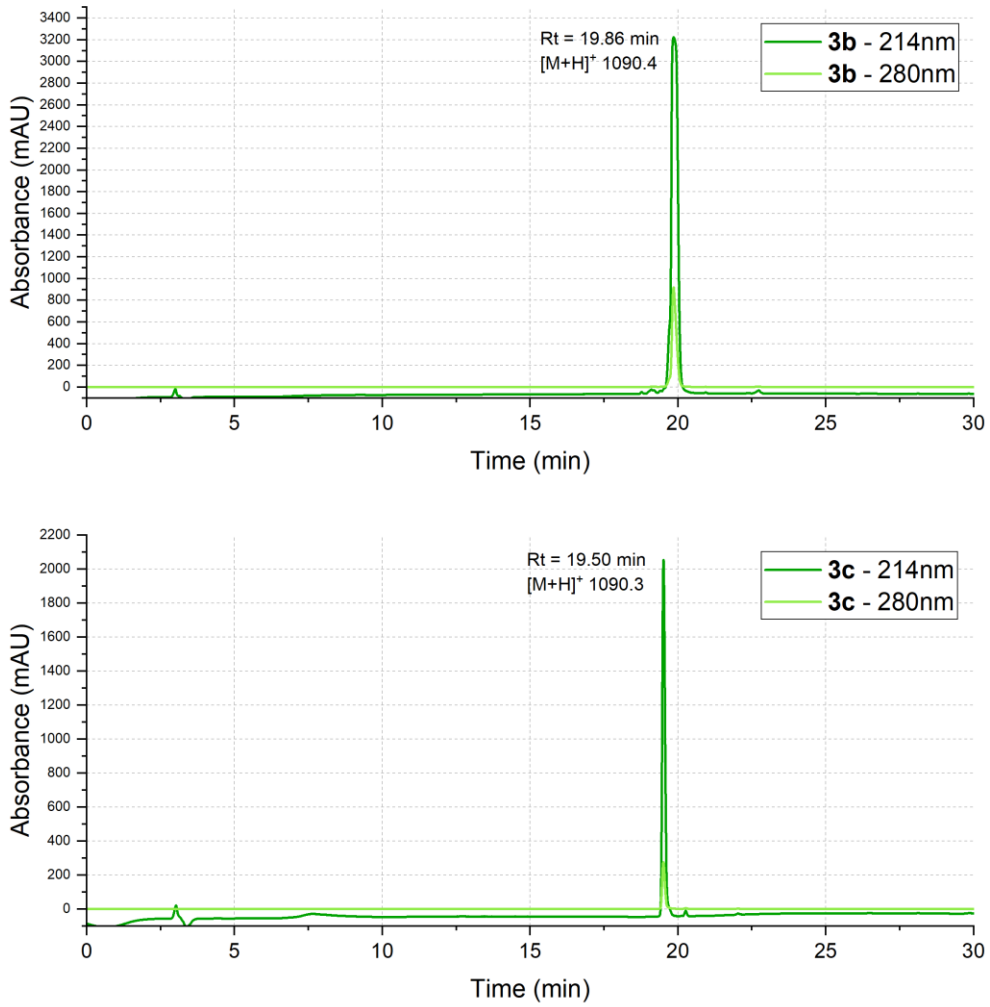

Figure S2.5: *HPLC trace of peptide* ***3a*** *(Pal-HAaH-NH_2),* ***3b*** *(Pal-K(WC)HAaH-NH_2) and* ***3c*** *(Pal- HAaHK(WC)-NH_2). Gradient 5-95%B in 30min using a binary elution system with A: 0.05% TFA in CH_3CN/H_2O (1:9 v/v) and B: 0.05% TFA in CH_3CN/ H_2O (9:1 v/v).*

Peptide 4a, 4b and 4c

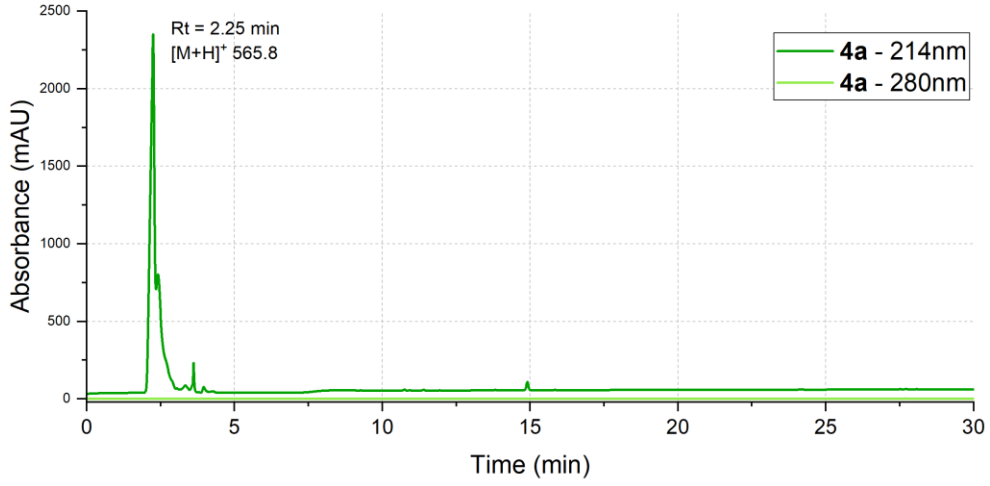

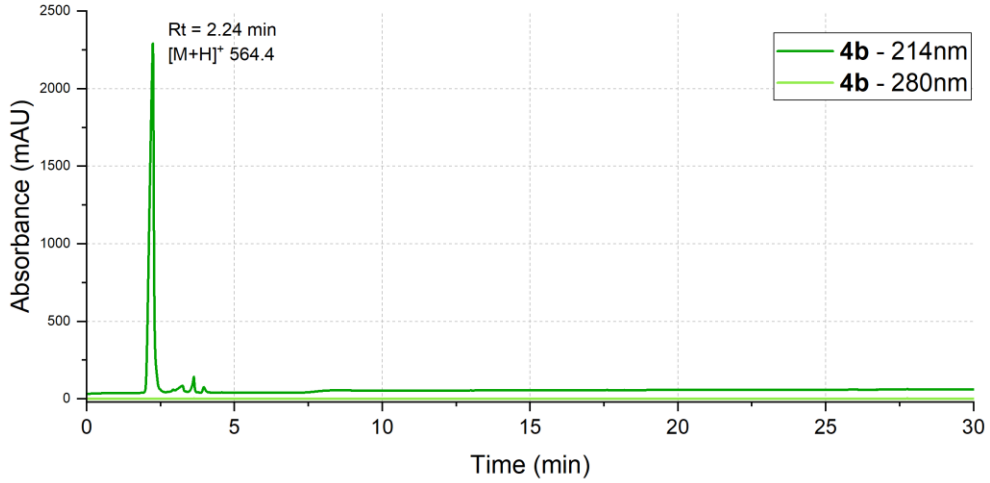

***Figure S2.6**: HPLC trace of peptide **4a** (H-KTTKS-OH), **4b** (H-KTTKS-NH_2) Gradient 0-80%B in 30min using a binary elution system with A: 0.05% TFA in CH_3CN/H_2O (1:9 v/v) and B: 0.05% TFA in CH_3CN/ H_2O (9:1 v/v).*

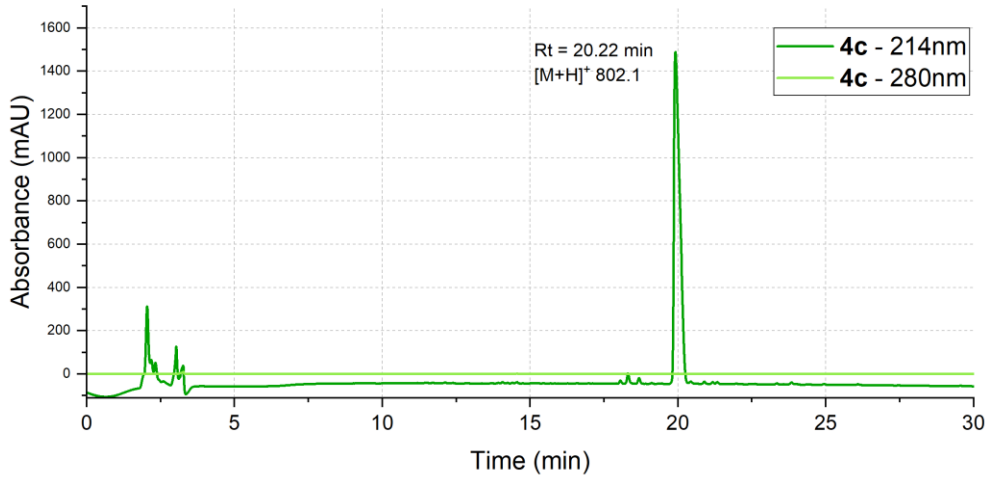

***Figure S2.7:** HPLC trace of peptide **4c** (Pal-KTTKS-OH). Gradient 5-95%B in 30min using a binary elution system with A: 0.05% TFA in CH_3CN/H_2O (1:9 v/v) and B: 0.05% TFA in CH_3CN/ H_2O (9:1 v/v).*

Peptide 4d, 4e and 4f

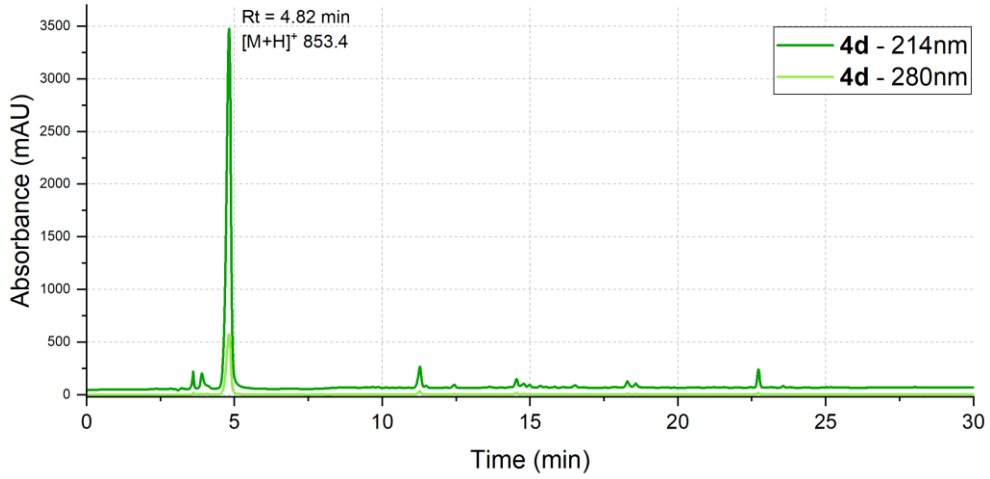

***Figure S2.8:** HPLC trace of peptide **4d** (H-CWKTTKS-NH_2). Gradient 0-50%B in 30min using a binary elution system with A: 0.05% TFA in CH_3CN/H_2O (1:9 v/v) and B: 0.05% TFA in CH_3CN/ H_2O (9:1 v/v).*

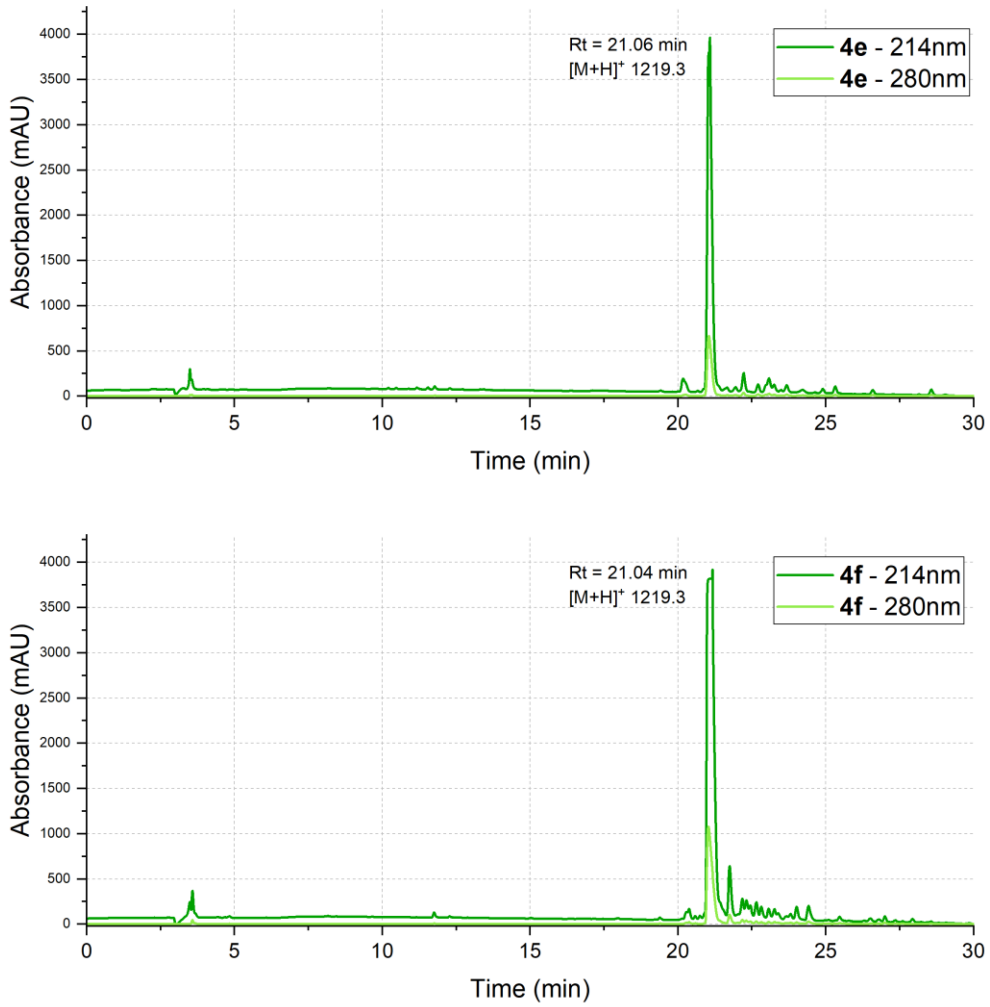

Figure S2.9: *HPLC trace of peptide* ***4e*** *(H-CWK(Pal)KTTKS-NH_2) and* ***4f*** *(H-CWKTTKSK(Pal)-NH_2). Gradient 5-95%B in 30min using a binary elution system with A: 0.05% TFA in CH_3CN/H_2O (1:9 v/v) and B: 0.05% TFA in CH_3CN/ H_2O (9:1 v/v).*

5.2.2 Peptide Loading overtime

Project 1: Model Peptides for Oxime and Thiazolidine Chemoselective Ligation Reactions

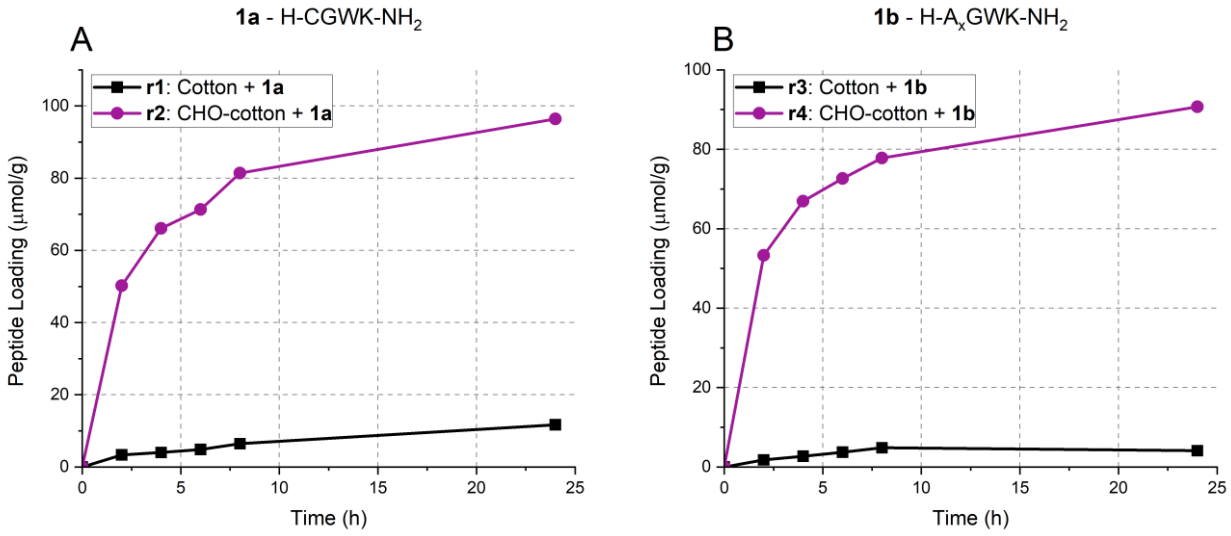

Figure S2.10**: Peptide Loading overtime for **(A) r1** and **r2 (B) r3** and **r4

Project 2: Multiple Cotton Functionalization by Thiazolidine bond

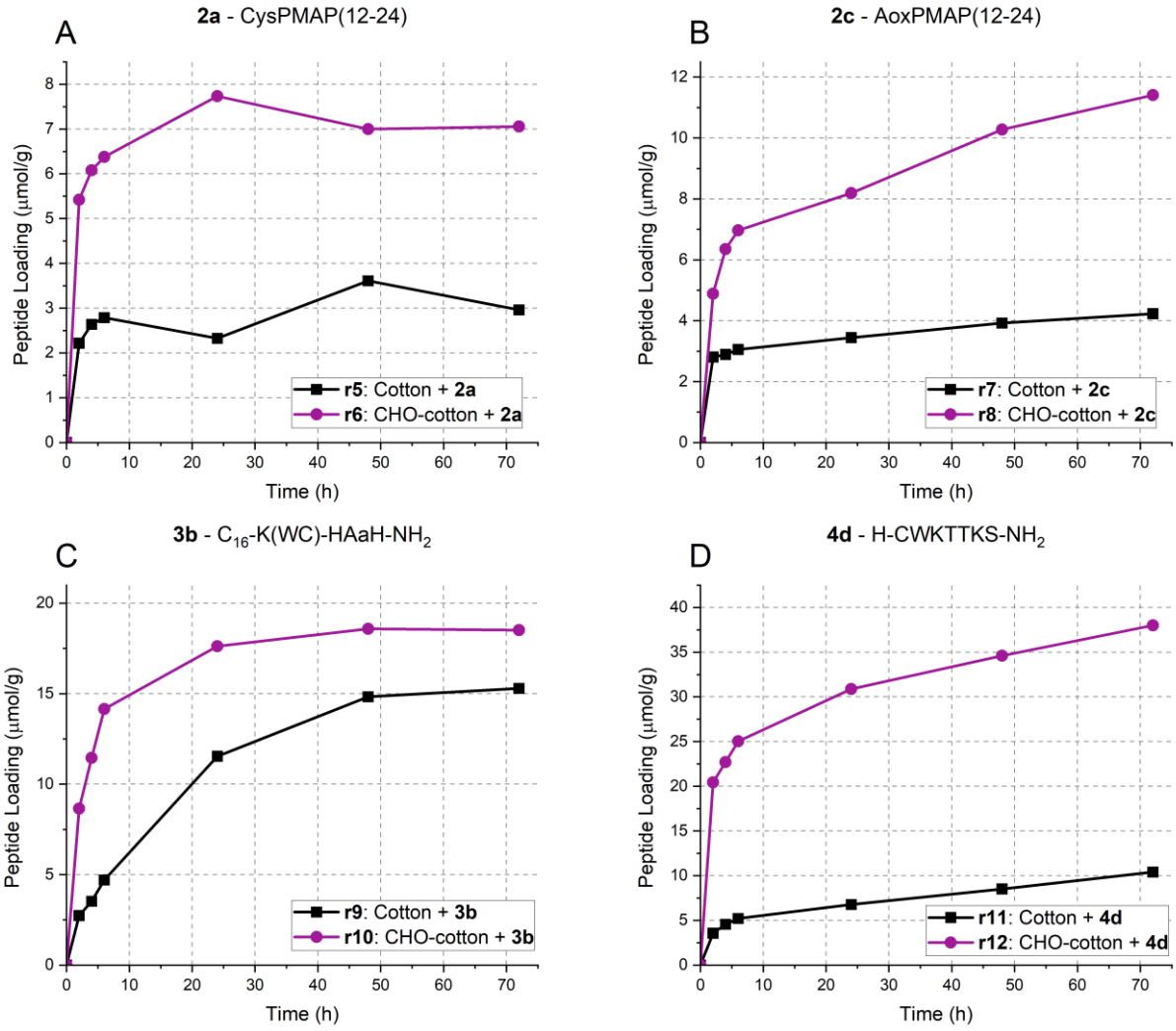

Figure S2.11:** Peptide Loading overtime for the preliminary reactions **(A) r5** and **r6, (B) r7** and **r8, (C) r9** and **r10**, and **(D) r11** and **r12

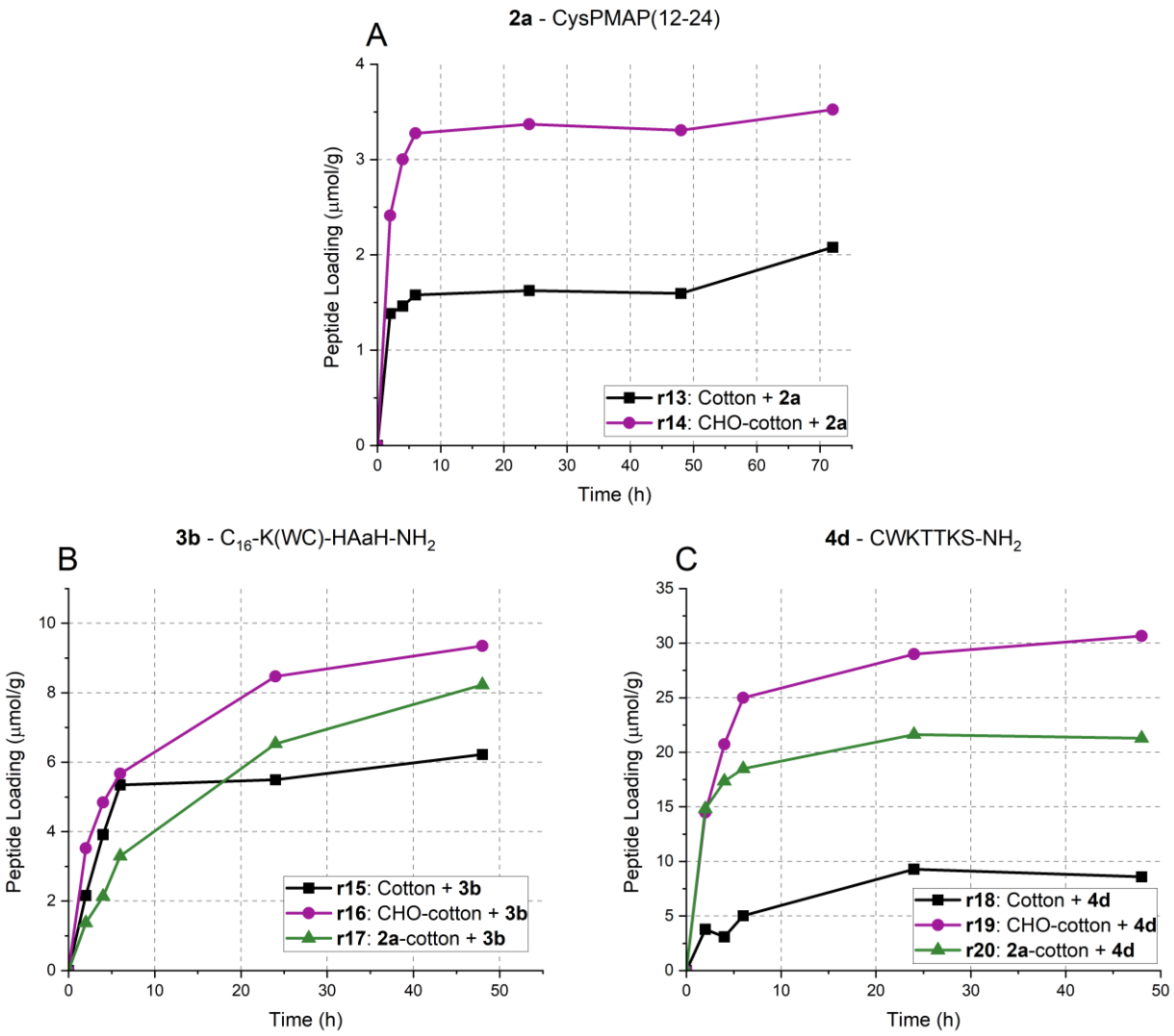

***Figure S2.12**: Peptide Loading of the double functionalization in **(A) r13** and **r14, (B) r15, r16** and **r17,** and **(C) r18, r19** and **r20**.*

5.2.3 FT-IR Spectra – Project 2

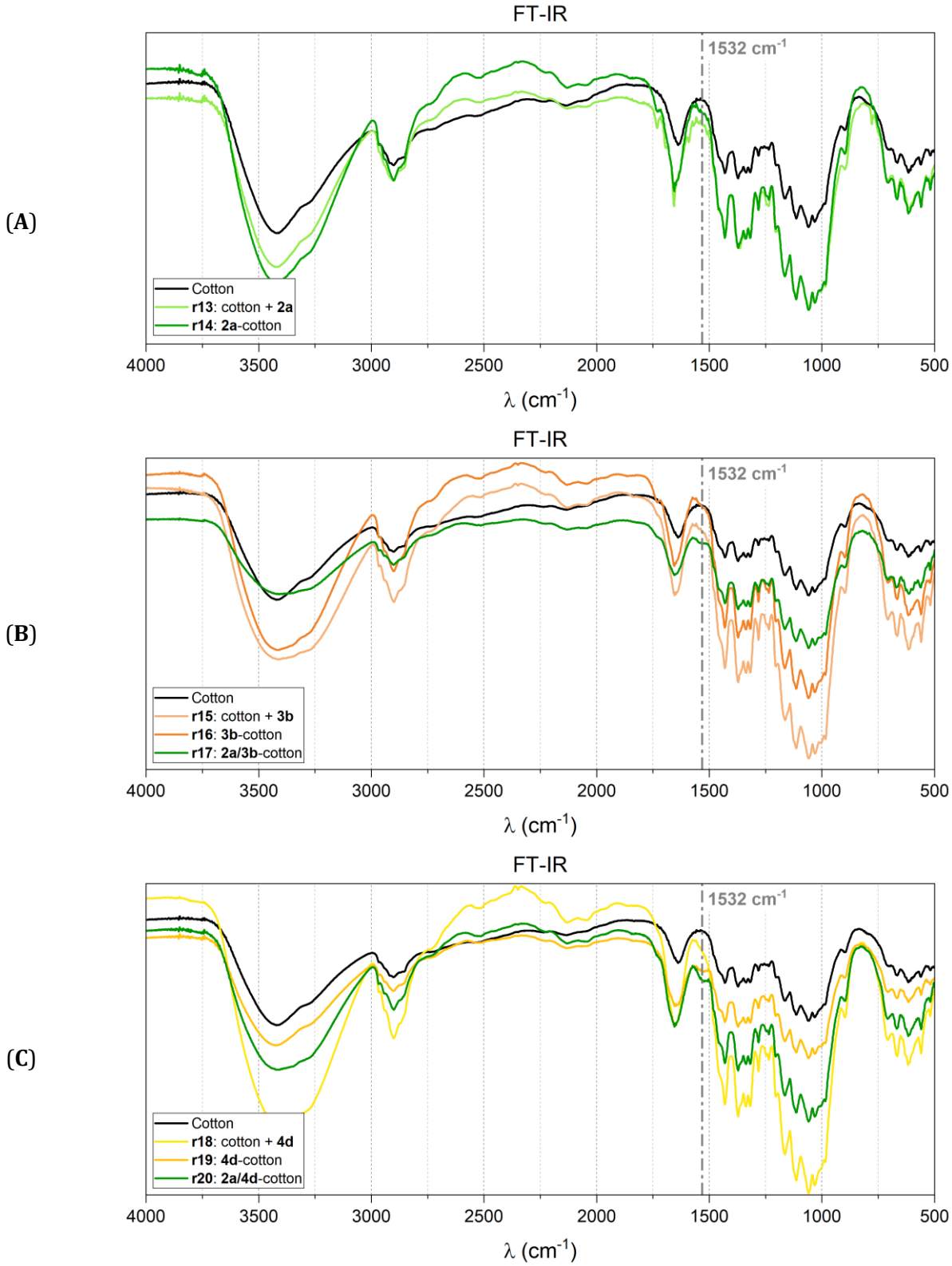

***Figure S2.13**: FT-IR spectra of cotton and of (A) **r13** and **r14**, (B) **r15**, **r16** and **r17**, and (C) **r18**, **r19** and **r20**.*

5.2.4 FT-IR Spectra – Project 3

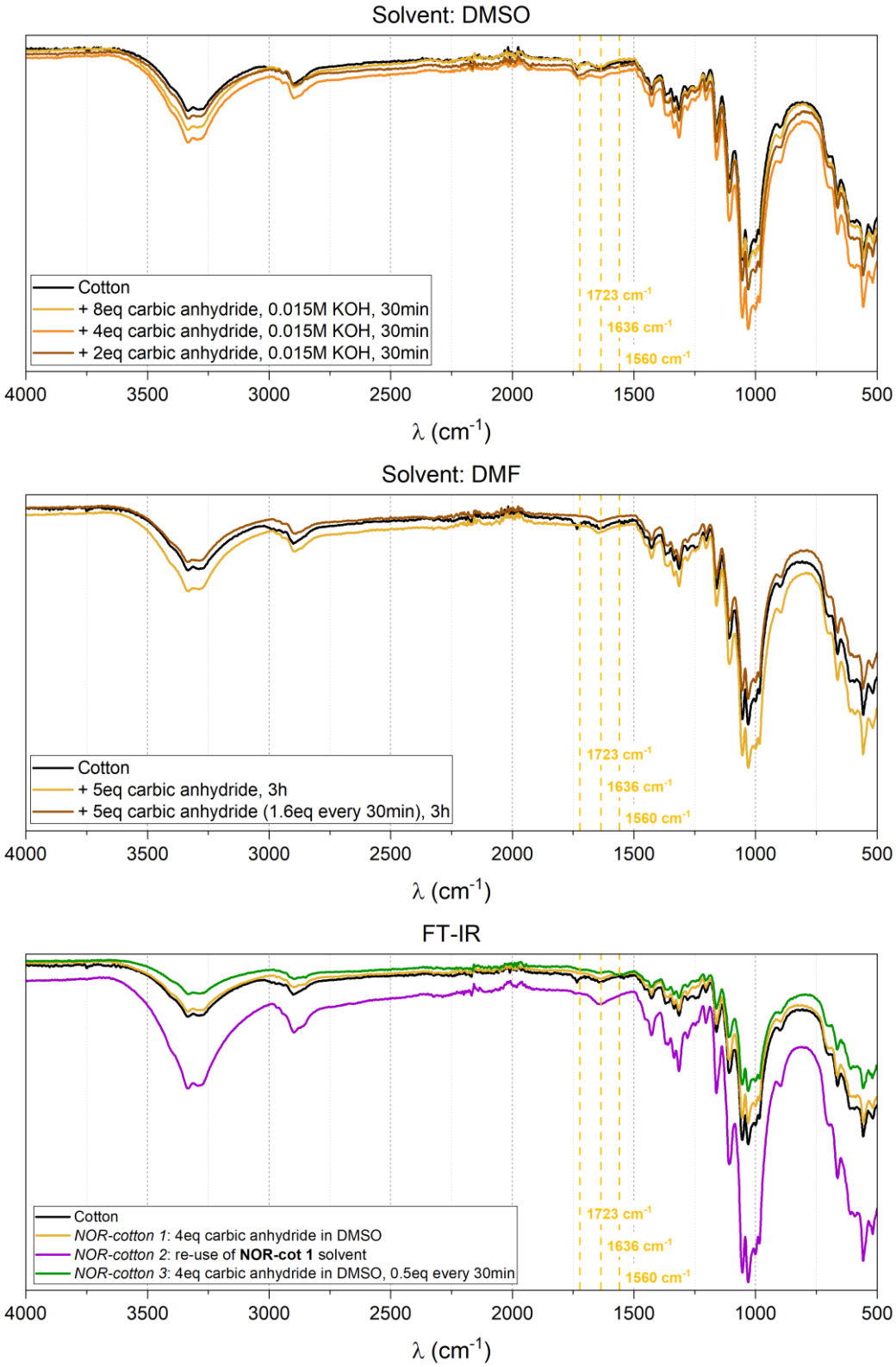

Figure S2.14: *FT-IR spectra of (A) put in contact with carbic anhydride using DMSO as the solvent. (B) cotton put in contact with carbic anhydride using DMF as the solvent (C) big batches of NOR-cotton synthesized by reaction with carbic anhydride in DMSO.*

(A)

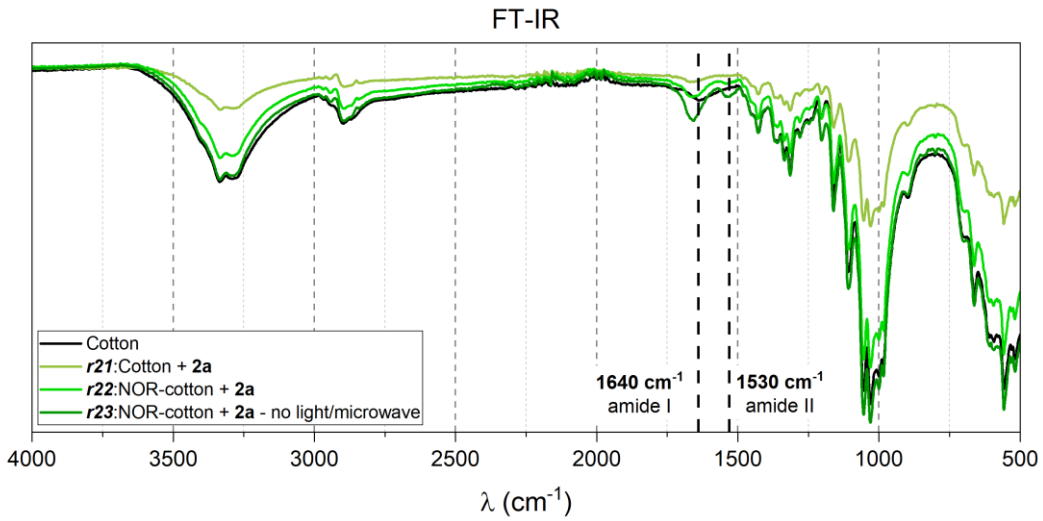

(B)

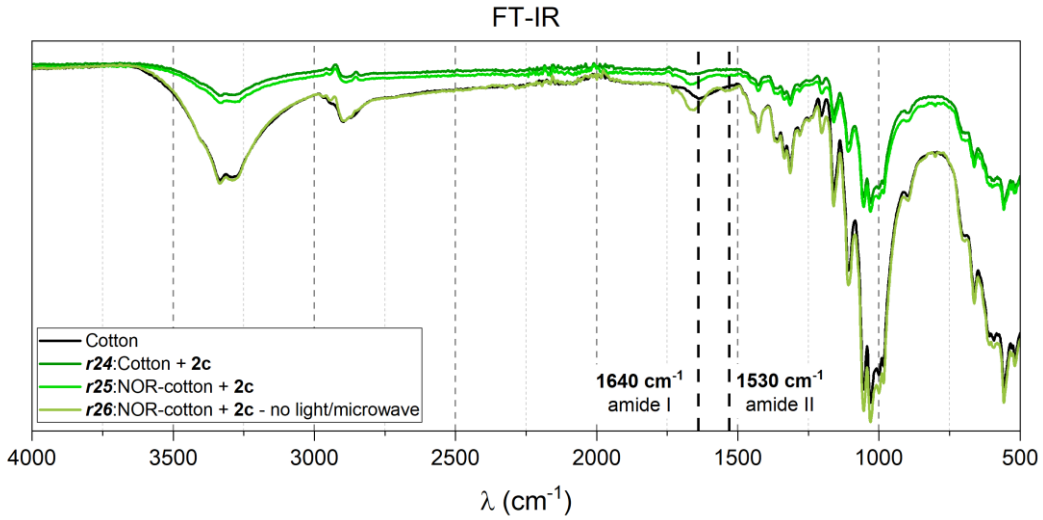

Figure S2.15: *FT-IR spectra of the materials from (**A**) reactions with peptide **2a** (H-CKRLKKIGKVLKWI-NH₂): **r21**, **r22**, and **r23**, (**B**) reactions with peptide **2c** (H-KRLKKIGKVLKWIC-NH₂): **r24**, **r25** and **r26**.*

5.2.5 Amino acid analysis

The following tables show the results of amino acid analyses of the test samples (as nmol of amino acid in the hydrolysis tube), the theoretical ratio of amino acids according to the sequence provided and the calculated relative proportion, as well as the amount of peptide (nmol hydrolyzed). The amino acids marked with an asterisk were used for the calculation.

r21: Cotton + 2a

AA	nmol (in the hydrolyzed residue)	Theoretical amount	Experimental
Gly	13.123	1	1.78
Cys	n.d.	1	-
Val	11.155	1	1.51
Ile	13.780	2	1.87 (*)
Leu	34.121	2	4.62
Lys	38.058	5	5.16 (*)
Arg	7.218	1	0.98 (*)
Calculated peptide amount (nmol)			7.382

r22: CHO-cotton + 2a

AA	nmol (in the hydrolyzed residue)	Theoretical amount	Experimental
Gly	32.441	1	1.36
Cys	n.d.	1	-
Val	30.414	1	1.28
Ile	44.607	2	1.87 (*)
Leu	54.745	2	2.30
Lys	120.641	5	5.06 (*)
Arg	25.345	1	1.06 (*)
Calculated peptide amount (nmol)			23.824

r23: CHO-cotton + 2a – no UV/mW

AA	nmol (in the hydrolyzed residue)	Theoretical amount	Experimental
Gly	32.793	1	1.47
Cys	n.d.	1	-
Val	23.148	1	1.04 (*)
Ile	32.793	2	1.47
Leu	43.403	2	1.95 (*)
Lys	110.918	5	4.98 (*)
Arg	23.148	1	1.04 (*)
Calculated peptide amount (nmol)			22.291

r24: Cotton + 2b

AA	nmol (in the hydrolyzed residue)	Theoretical amount	Experimental
Gly	17.697	1	2.14
Cys	n.d.	1	-
Val	15.337	1	1.86
Ile	17.697	2	2.14 (*)
Leu	27.135	2	3.29
Lys	40.113	5	4.86 (*)
Arg	10.618	1	1.29
Calculated peptide amount (nmol)			8.259

r25: CHO-cotton + 2b

AA	nmol (in the hydrolyzed residue)	Theoretical amount	Experimental
Gly	28.102	1	1.42
Cys	n.d.	1	-
Val	24.860	1	1.26
Ile	32.425	2	1.64
Leu	41.072	2	2.08 (*)
Lys	95.115	5	4.82 (*)
Arg	21.617	1	1.10 (*)
Calculated peptide amount (nmol)			19.725

r26: CHO-cotton + 2b – no UV/mW

AA	nmol (in the hydrolyzed residue)	Theoretical amount	Experimental
Gly	26.940	1	1.57
Cys	n.d.	1	-
Val	21.552	1	1.25
Ile	34.124	2	1.99 (*)
Leu	46.695	2	2.72
Lys	86.207	5	5.01 (*)
Arg	19.756	1	1.15
Calculated peptide amount (nmol)			17.190

5.2.6 XPS Analysis

Nitrogen

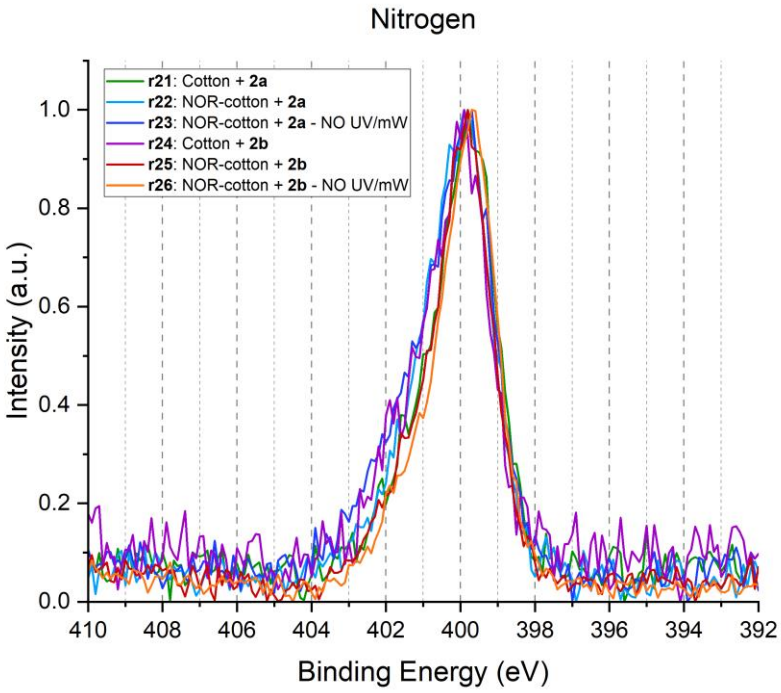

***Figure S2.16**: XPS spectra of the N1s region.*

Sulfur

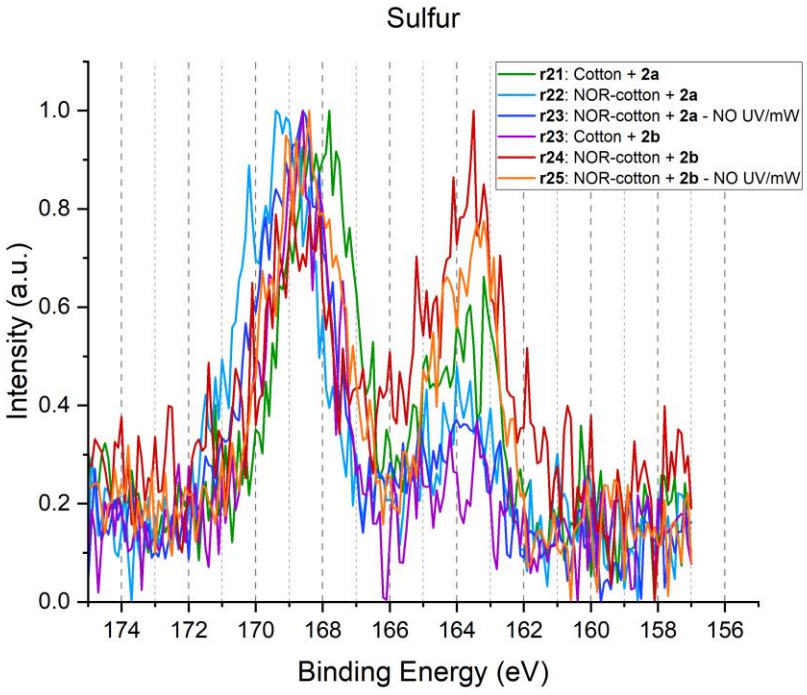

***Figure S2.17**: XPS spectra of the S2p region.*

Carbon

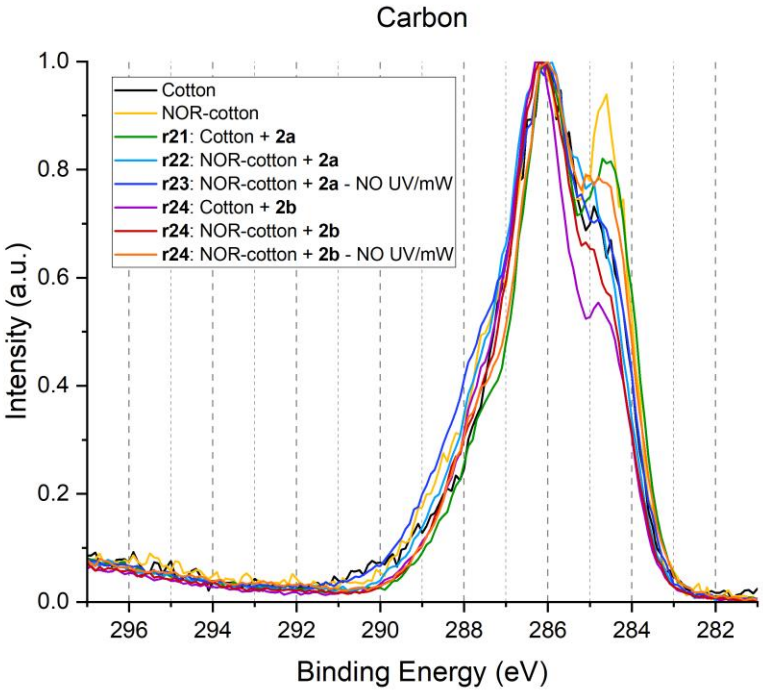

***Figure S2.18**: XPS spectra of the C1s region.*

Oxygen

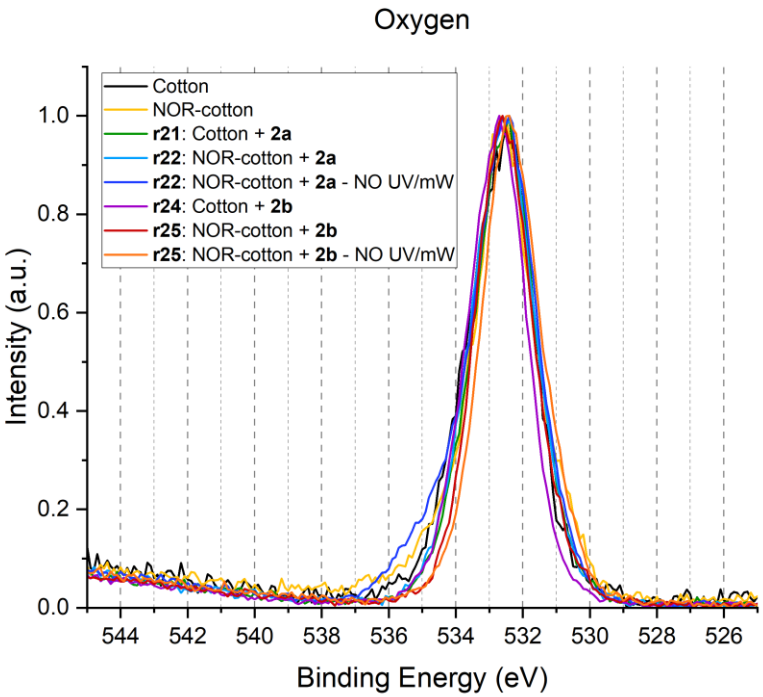

***Figure S2.19**: XPS spectra of the O1s region.*

5.2.7 Antibacterial tests - Optical Density measurements

The samples were sent to the University of Trieste where the following procedure was carried out:

CHO-cotton and peptide-cotton conjugate samples (ca. 15mg) were first sterilized by submerging the materials in 1 mL of EtOH 70% (v/v in water) for 1 hour in the wells of a 24-well plate (Sarstedt- Italy). The ethanol was then removed working under sterile conditions, letting the cotton dry in the same wells for 2 hours under the sterile air flow of the microbiology hood, then let sit overnight. In the same day, reference bacterial strain of *Acinetobacter baumannii* ATCC 19606 (American Type Culture Collection (ATCC) in Manassas, VA, USA) was grown in sterile Muller–Hinton broth (MHB) (Difco Inc., Becton Dickinson, Sparks, MD, USA) at 37 ◦ C for approximately 18 hours under shacking (140 rpm).

The next day, the bacterial culture was diluted 1:30 in fresh MHB and again shaken at 140 rpm for ~2 hours to reach the mid-log phase (OD ~0.3 at 600 nm). A mid-log bacterial culture was diluted to 10^6 CFU/mL, and finally 1 mL of this bacterial suspension was dispensed into each well of a 24-well plate containing cotton samples except for medium sterility control. The plate was incubated at 37°C for 24 hours.

The optical density OD_{600} of the medium containing bacteria in the presence of cotton samples and of the sterility control was measured with a spectrophotometer, after diluting the bacterial samples 1:10. The measured OD_{600} values were then multiplied by the respective dilution factor to calculate the actual bacterial concentration in each well in the presence of cotton discs.

The procedure was performed in three independent triplicates using three pieces of material from the same batch.

	Measure 1		*Measure 2*		*Measure 3*			*AVERAGE*	
Sample	**OD_{600}**	**Biofilm Growth (%)**	**OD_{600}**	**Biofilm Growth (%)**	**OD_{600}**	**Biofilm Growth (%)**		**Biofilm Growth (%)**	**Error**
ctrl	0.159	100	0.344	100	0.306	100		100	0.00
CHO-cot	0.272	171	0.377	110	0.344	112		131	34.7
r5	0.157	98.7	0	0	0.187	61.1		53.3	49.8
r14	0.075	47.2	0.001	0.291	0.004	1.31		16.3	26.8
r19	0.273	171	0.355	103	0.298	97.4		124	41.3
r20	0.006	3.77	0.001	0.291	0.172	56.2		20.1	31.3
NOR-cot	0.273	172	0.425	124	0.327	107		134	33.7
r21	0.195	123	0.001	0.291	0.253	82.7		68.5	62.4
r22	0.003	1.89	0.003	0.872	0.002	0.654		1.12	0.658
r24	0.196	123	0.012	3.49	0.223	72.8		66.5	60.1
r25	0.017	10.6	0.002	0.581	0.161	52.6		21.3	27.6

Table S2.1*: Results of the biofilm growth assay with Acinetobacter baumannii (ATCC 19606). The control (ctrl) is the bacterial solution without any added cotton samples. Results expressed in optical density of the solution measured at 600 nm (OD_{600}) and percentage of biofilm growth calculated as the ratio between the OD_{600} of the sample and the control multiplied by 100. In red are highlighted the measurement not in agreement with the set of data. Error calculated as the standard deviation of the three measurements.*

5.3 Supporting Images – Chapter III

5.3.1 Chromatograms (HPLC-MS) of the synthesized peptides

Peptide 4g – PraPP4

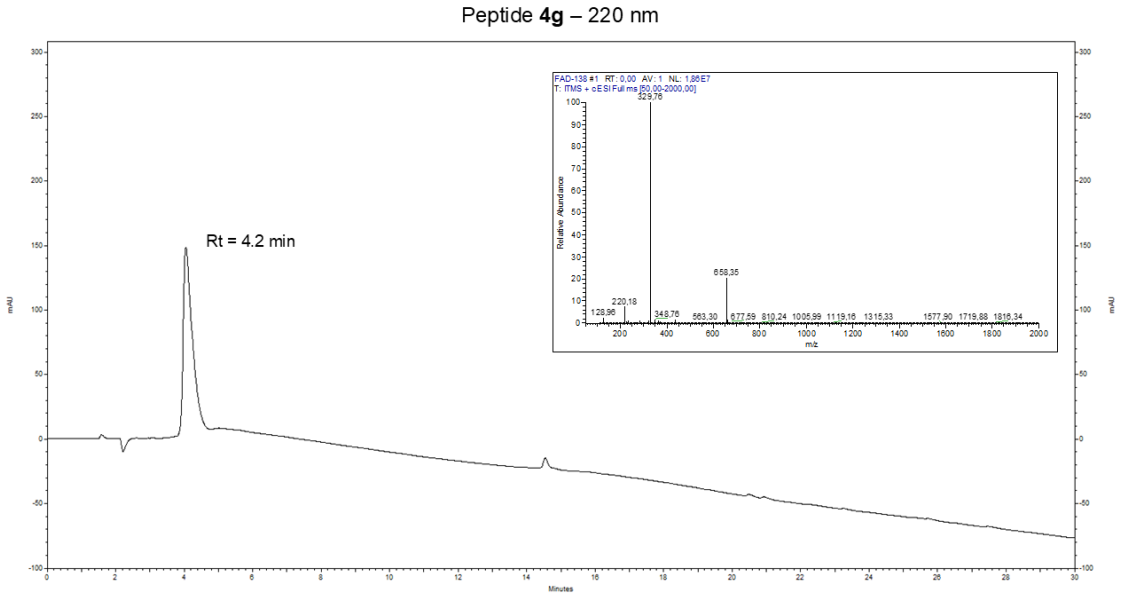

***Figure S3.1**: HPLC trace of peptide **4g** (H-PraKTTKS-NH_2). Gradient 1-100%B in 30min using a binary elution system with A: 0.05% TFA in H_2O B: 0.05% TFA in CH_3CN.*

Peptide 5a – Cys3.1

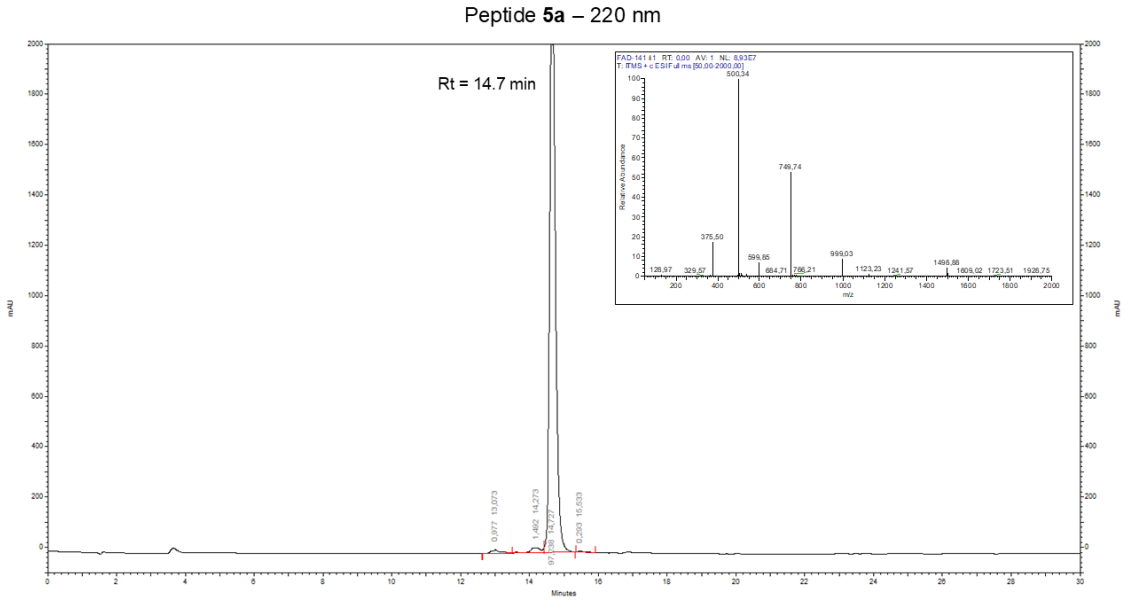

***Figure S3.2**: HPLC trace of peptide **4g** (H-CKKLLKWLLKLL- NH_2). Gradient 1-100%B in 30min using a binary elution system with A: 0.05% TFA in H_2O B: 0.05% TFA in CH_3CN.*

5.3.2 FT-IR Spectra of modified chitosan

Modified chitosan

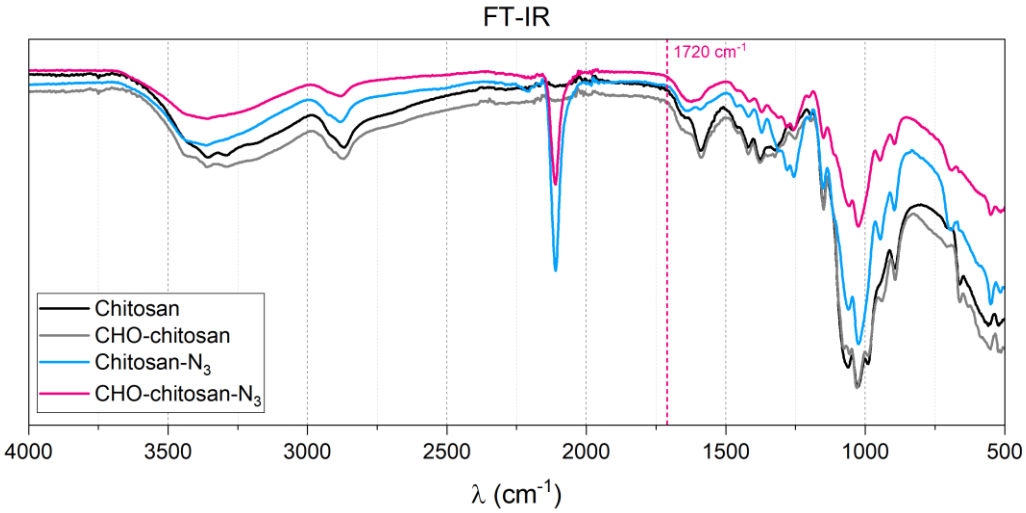

***Figure S3.3**: FT-IR spectra of chitosan (black), CHO-chitosan (grey), chitosan-N_3 (blue), CHO-chitosan-N_3 (pink).*

Peptide-chitosan conjugations

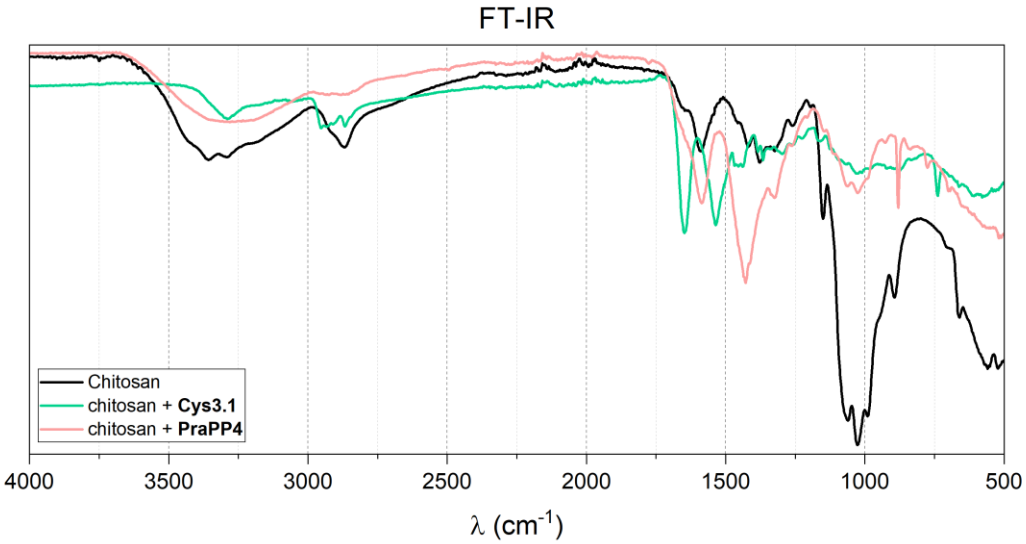

***Figure S3.4:** FT-IR spectra of the controls: chitosan+**Cys3.1** (green) and chitosan+**PraPP4** (light pink).*

5.3.3 Schiff test

(A) **(B)** **(C)**

***Figure S3.5**: Shiff test on (**A**) left chitosan, right CHO-chitosan (**B**) from left to right, chitosan, chitosan-N_3 and CHO-chitosan-N_3. And (**C**) chitosan (upper) CHO-chitosan-N_3 (lower).*

5.3.4 XPS Analysis

Qualitative analysis

Nitrogen

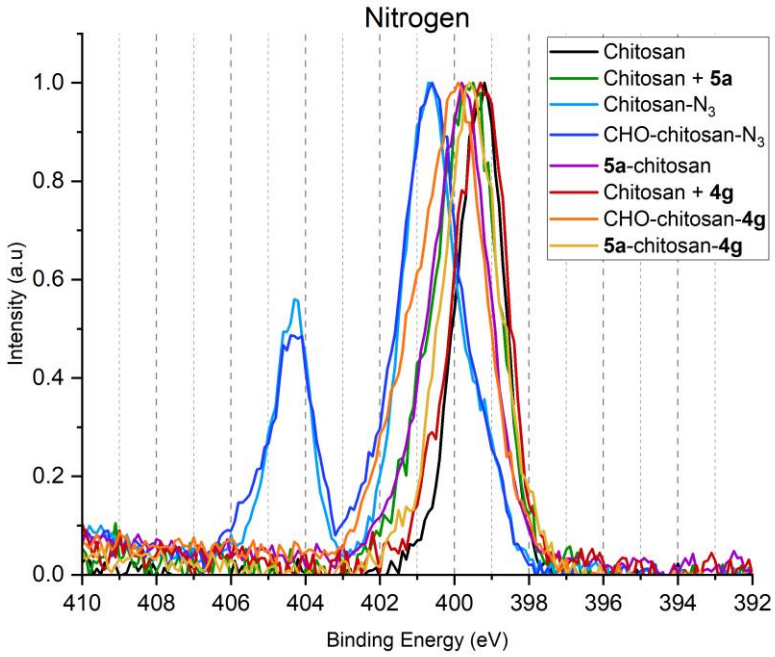

***Figure S3.6**: XPS spectra of the materials in the N1s region.*

From the interpolation of the curves the following data could be extracted:

	Atomic %			
	C-N/CO-N	**CO-N-CO / N-CO-O**	**NH_3^+**	**N^-=N^+=N^-**
	399.5 eV	**400.0 eV**	**400.9 eV**	**404.4 eV**
Chitosan	100	-	-	-
Chitosan-**N_3**	16.8	-	58.3	24.9
CHO-chitosan-**N_3**	24.3	-	50.2	25.4
Chitosan + **cys3.1**	72.5	27.5	-	-
3.1-chitosan	68.0	32.0	-	-
Chitosan + **PraPP4**	87.2	12.8	-	-
CHO-chitosan-**PP4**	24.9	54.6	20.6 (401.5)	-
3.1-chitosan-**PP4**	90.6	9.4 (400.8 eV)	-	-

Carbon

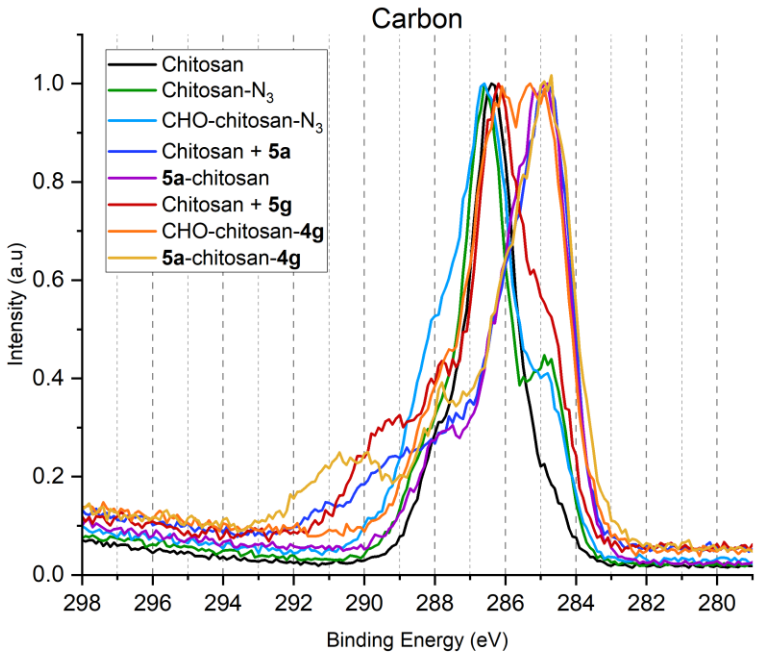

Figure S3.7*: XPS spectra of the materials the C1s region.*

From the interpolation of the curves the following data could be extracted:

	Atomic %			
	C-C / C-H	**C-O-C/ C-NH$_2$ / C-OH**	**O-C-O / N-C=O**	**N-CO-O**
	285.0 eV	**286.5 eV**	**287.8 eV**	**289.4 eV**
Chitosan	13.7	67.1	19.2	
Chitosan-**N$_3$**	24.38	54.1	21.6	
CHO-chitosan-**N$_3$**	15.5	52.5	32.9	
Chitosan + **cys3.1**	53.3	20.4	13.3	13.0
3.1-chitosan	61.6	22.5	15.9	
Chitosan + **PraPP4**	24.0	45.0	15.2	15.8
CHO-chitosan-**PP4**	41.5	37.3	11.5	9.7
3.1-chitosan-**PP4**	48.6	25.8	14.8	11.8

Oxygen

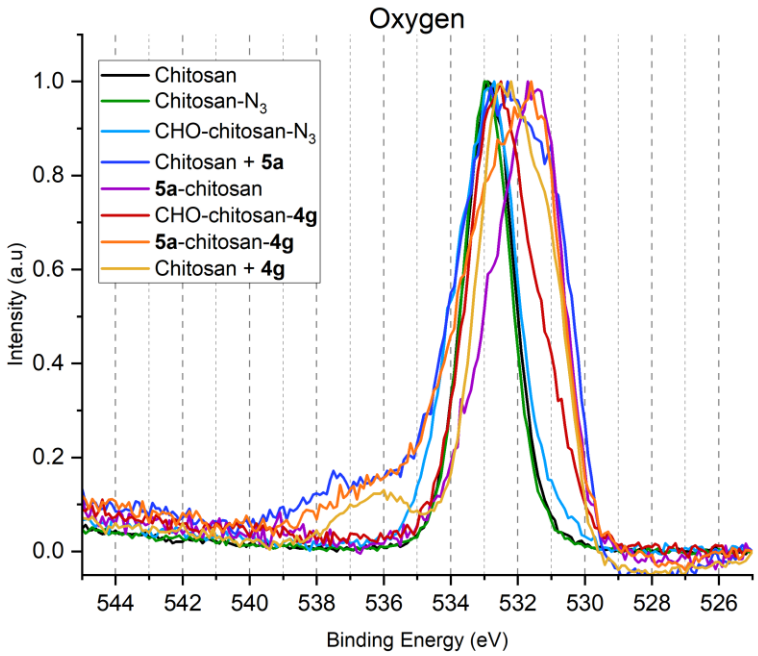

Figure S3.8*: XPS spectra of the materials O1s region.*

From the interpolation of the curves the following data could be extracted:

	Atomic %				
	N-C=O	**C-O-C / C-OH**	**O-C-O**		
	531 eV	**532.8 eV**	**534 eV**	**536 eV**	**537 eV**
Chitosan	-	100	-	-	-
Chitosan-**N3**	-	100	-	-	-
CHO-chitosan-**N3**	4.2	82.3	13.5	-	
Chitosan + **cys3.1**	31.9	43.7	15.9	-	8.5
3.1-chitosan	51.1	43.8	5.1	-	-
Chitosan + **PraPP4**	30.9	61.0	-	8.1	-
CHO-chitosan-**PP4**	20.8	72.7	6.5	-	-
3.1-chitosan-**PP4**	30.1	46.6	14.8	8.4	-

5.3.5 Amino acid analysis

The following tables show the results of the sample amino acid analysis (as nmol of amino acid in the hydrolysis tube), the theoretical ratio of amino acids according to the sequence provided and the calculated relative proportion, as well as the amount of peptide (nmol hydrolyzed). The amino acids marked with an asterisk were used for the calculation. Peaks not matching the amino acids in the peptide were also detected. For chitosan and CHO-chitosan-N_3, which theoretically contain no peptide content, the nmol of amino acids corresponding to the detected peaks are shown. The chromatogram for chitosan shows peaks that do not coincide with the amino acid retention times.

Chitosan+Cys3.1

AA	nmol (in the hydrolyzed residue)	Theoretical amount	Experimental
Cys	312.500	1	0.19
Leu	10083.330	6	5.99 (*)
Lys	6750.000	4	4.01 (*)
Calculated peptide amount (nmol)			1683.333

3.1-Chitosan

AA	nmol (in the hydrolyzed residue)	Theoretical amount	Experimental
Cys	301.724	1	0.38
Leu	4849.138	6	6.11 (*)
Lys	3081.897	4	3.89 (*)
Calculated peptide amount (nmol)			793.103

Chitosan+PraPP4

AA	nmol (in the hydrolyzed residue)	Theoretical amount	Experimental
Thr	19.802	2	2.11 (*)
Ser	19.802	1	2.11
Lys	17.822	2	1.89 (*)
Calculated peptide amount (nmol)			9.406

CHO-chitosan-PP4

AA	nmol (in the hydrolyzed residue)	Theoretical amount	Experimental
Thr	323.214	2	1.99 (*)
Ser	151.786	1	0.93 (*)
Lys	337.500	2	2.08 (*)
Calculated peptide amount (nmol)			162.500

3.1-chitosan-PP4

		Cys3.1	PraPP4		
AA	Total Experimental amount	Theoretical amount	Experimental (H-Pra-KTTKS NH_2 subtraction)	Theoretical amount	Experimental
Thr	216.667	-	0.18	2	1.90 (*)
Ser	125.000	-	0.11	1	1.10 (*)
Cys	n.d.	1	-	-	-
Leu	7083.334 (*)	6	-	-	-
Lys	4341.667	4	-0.32	2	-3.34
Calculated peptide amount (nmol)		1180.556	113.889		

Data Elaboration

Sample	Mass (mg)	nmol 3.1	mass 3.1 (mg)	nmol PP4	Loading 3.1 (mmol/g)	Loading PP4 (mmol/g)
Chitosan+ **Cys3.1**	5.59	1683.333	2.520	-	0.548	-
3.1-chitosan	2.05	793.103	1.187	-	0.919	-
Chitosan+**PraPP4**	3.00	-	-	9.406	-	0.003
CHO-chitosan-**PP4**	3.27	-	-	162.500	-	0.051
3.1-chitosan-**PP4**	3.20	1180.556	1.767	133.889	0.824	0.043

5.3.6 Raw Data of Antibacterial tests

	Measure 1		Measure 2		Measure 3		Average	
	CFU/mL						Mean (CFU/mL)	Error
Inoculum (S.aureus)	$7.1x10^6$	$8.0x10^6$	$5.6x10^6$	$2.5x10^6$	$5.3x10^5$	$2.3x10^6$	$4.3x10^6$	$3.0x10^6$
Ctrl (3h in PBS)	$2.7x10^6$	$1.8x10^6$	$3.4x10^6$	$1.6x10^6$	$2.5x10^6$	$1.2x10^6$	$1.8x10^6$	$8.1x10^5$
TCPE	-	-	$4.8x10^5$	$5.2x10^5$	$4.3x10^5$	$5.2x10^5$	$3.8x10^5$	$4.6x10^4$
Chitosan	$6.3x10^3$	$7.5x10^3$	$1.6x10^3$	$1.7x10^3$	$6.0x10^2$	$4.0x10^2$	$2.9x10^3$	$3.0x10^3$
Chitosan + Cys3.1	$1.0x10^4$	$1.7x10^4$	$1.2x10^4$	$1.1x10^4$	$2.0x10^4$	$1.7x10^4$	$1.0x10^4$	$4.1x10^3$
3.1-chitosan	0	0	$2.0x10^2$	0	0	0	$3.3x10^1$	$8.2x10^1$
3.1-chitosan-PP4	$4.7x10^3$	$5.1x10^3$	$2.0x10^3$	$1.1x10^3$	$2.1x10^3$	$1.1x10^3$	$2.3x10^3$	$1.8x10^3$

***Figure S3.9**: Results of Bacterial Growth of S. aureus (ATCC 25923) after forced contact with spin-coated surfaces of the materials. Error calculated as the standard deviation of all the measurements.*

	Measure 1		Measure 2		Measure 3		Average	
	CFU/mL						Mean (CFU/mL)	Error
Inoculum (P. aeruginosa)	$1.0x10^6$	$1.2x10^6$	$5.0x10^5$	$1.0x10^6$	$7.0x10^5$	$5.3x10^6$	$7.4\ x10^5$	$2.8\ x10^5$
Ctrl (3h in PBS)	$7.0x10^5$	$6.0x10^5$	$4.0x10^5$	$5.0x10^5$	$8.0x10^5$	$3.0x10^5$	$4.4\ x10^5$	$1.6\ x10^5$
TCPE	$5.0x10^5$	$6.0x10^5$	$8.0x10^5$	$1.5x10^5$	$2.1x10^5$	$1.1x10^5$	$2.4\ x10^5$	$2.2\ x10^5$
Chitosan	$1.0x10^4$	$1.2x10^4$	$1.6x10^4$	$1.2x10^4$	$2.1x10^4$	$1.7x10^4$	$1.0\ x10^4$	$4.4\ x10^3$
Chitosan + Cys3.1	$3.0x10^4$	$2.5x10^4$	$1.1x10^4$	$5.0x10^3$	$8.0x10^3$	$3.0x10^3$	$1.4\ x10^4$	$1.1\ x10^4$
3.1-chitosan	$1.5x10^3$	$1.3x10^3$	$1.2x10^3$	$3.0x10^2$	$7.0x10^2$	$9.0x10^2$	$8.6\ x10^2$	$4.9\ x10^4$
3.1-chitosan-PP4	$1.0x10^3$	$1.2x10^3$	$x10^3$	$8.0x10^3$	$1.1x10^4$	$6.0x10^3$	$5.2\ x10^3$	$2.3\ x10^3$

***Figure S3.10**: Results of Bacterial Growth of P.aeruginosa (ATCC 27853) after forced contact with spin-coated surfaces of the materials. Error calculated as the standard deviation of all the measurements.*

5.4 Supporting Images – Chapter IV

5.4.1 Chromatograms (HPLC) of the synthesized peptides

Peptide 6a

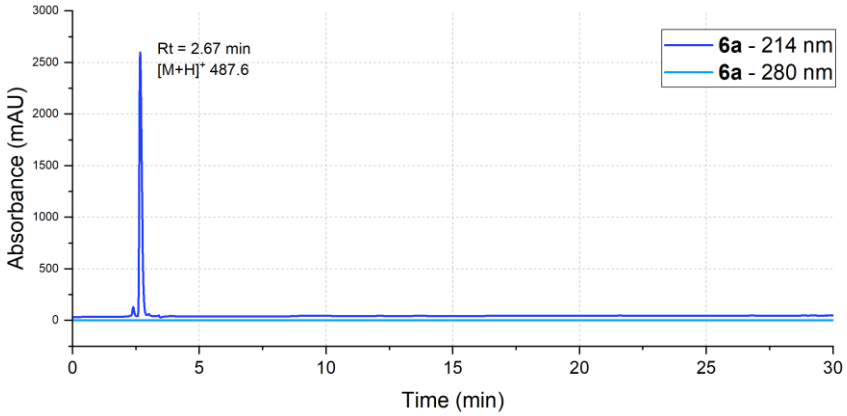

***Figure S4.1**: HPLC trace of peptide **6a** (Ac-SDKP-NH_2). Gradient 0-30%B in 30min using a binary elution system with A: 0.05% TFA in CH_3CN/H_2O (1:9 v/v) and B: 0.05% TFA in CH_3CN/ H_2O (9:1 v/v).*

Peptide 6b

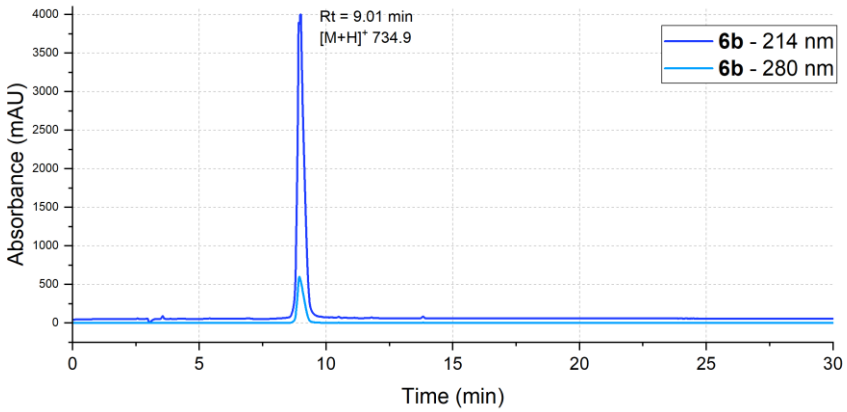

***Figure S4.2**: HPLC trace of peptide **6b** (H-CWSDKP-NH_2). Gradient 0-50%B in 30min using a binary elution system with A: 0.05% TFA in CH_3CN/H_2O (1:9 v/v) and B: 0.05% TFA in CH_3CN/ H_2O (9:1 v/v).*

Peptide 6c

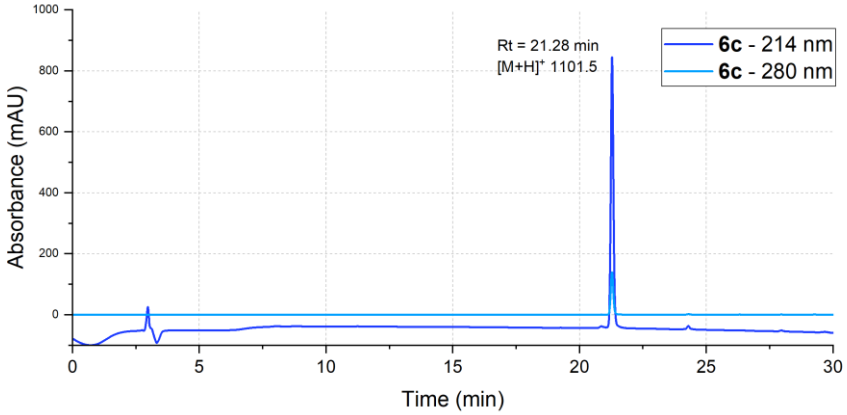

***Figure S4.3:** HPLC trace of peptide **6c** (Pal-SDKPK(WC)-NH_2). Gradient 5-95%B in 30min using a binary elution system with A: 0.05% TFA in CH_3CN/H_2O (1:9 v/v) and B: 0.05% TFA in CH_3CN/ H_2O (9:1 v/v).*

Peptide 6d

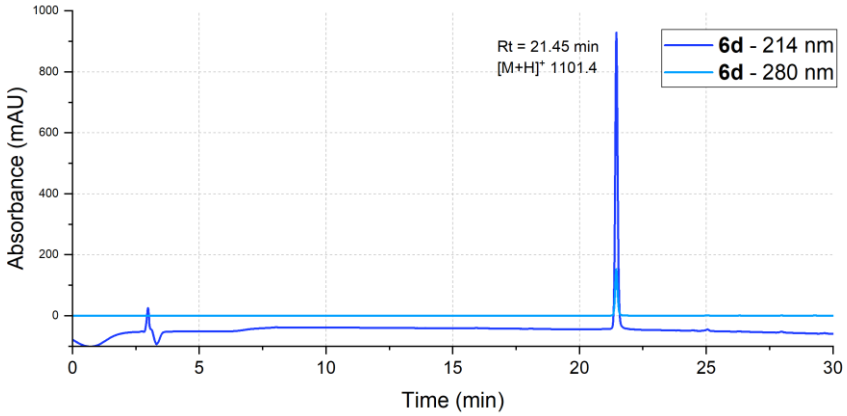

***Figure S4.4**: HPLC trace of peptide **6d** (Pal- K(WC)SDKP-NH_2). Gradient 5-95%B in 30min using a binary elution system with A: 0.05% TFA in CH_3CN/H_2O (1:9 v/v) and B: 0.05% TFA in CH_3CN/ H_2O (9:1 v/v).*

Peptide 7a

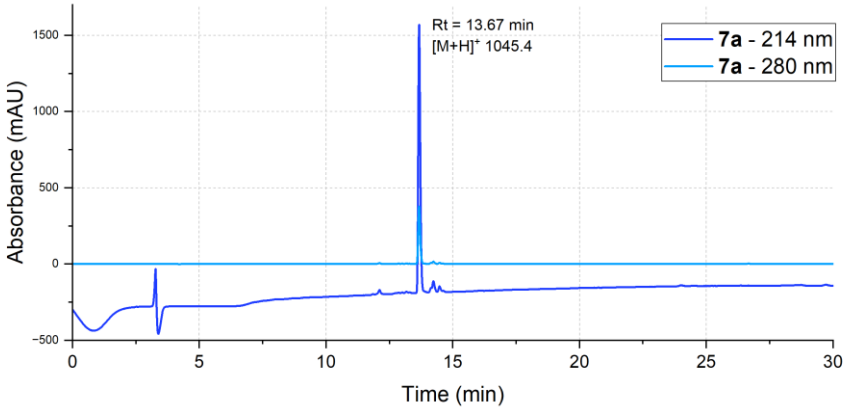

***Figure S4.6:** HPLC trace of peptide **6e** (H-RWRWRW-NH_2). Gradient 5-45%B in 30min using a binary elution system with A: 0.05% TFA in CH_3CN/H_2O (1:9 v/v) and B: 0.05% TFA in CH_3CN/ H_2O (9:1 v/v).*

Peptide 7b

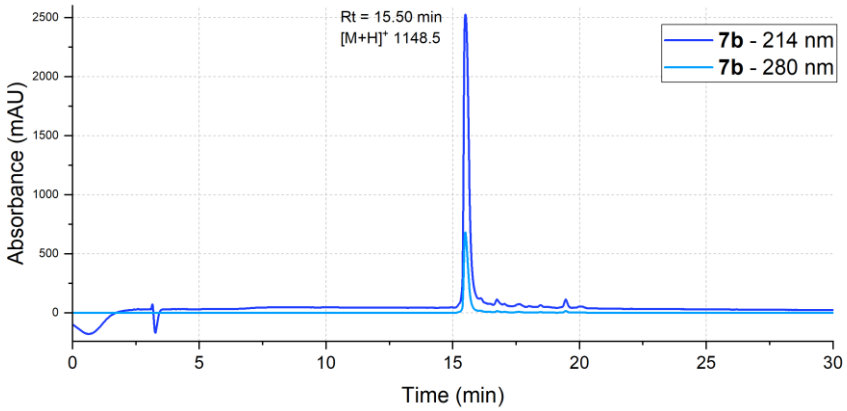

***Figure S4.7**: HPLC trace of peptide **6e (H-CRWRWRW-NH_2)**. Gradient 5-95%B in 30min using a binary elution system with A: 0.05% TFA in CH_3CN/H_2O (1:9 v/v) and B: 0.05% TFA in CH_3CN/ H_2O (9:1 v/v).*

5.4.2 HPLC of the degradations in human serum

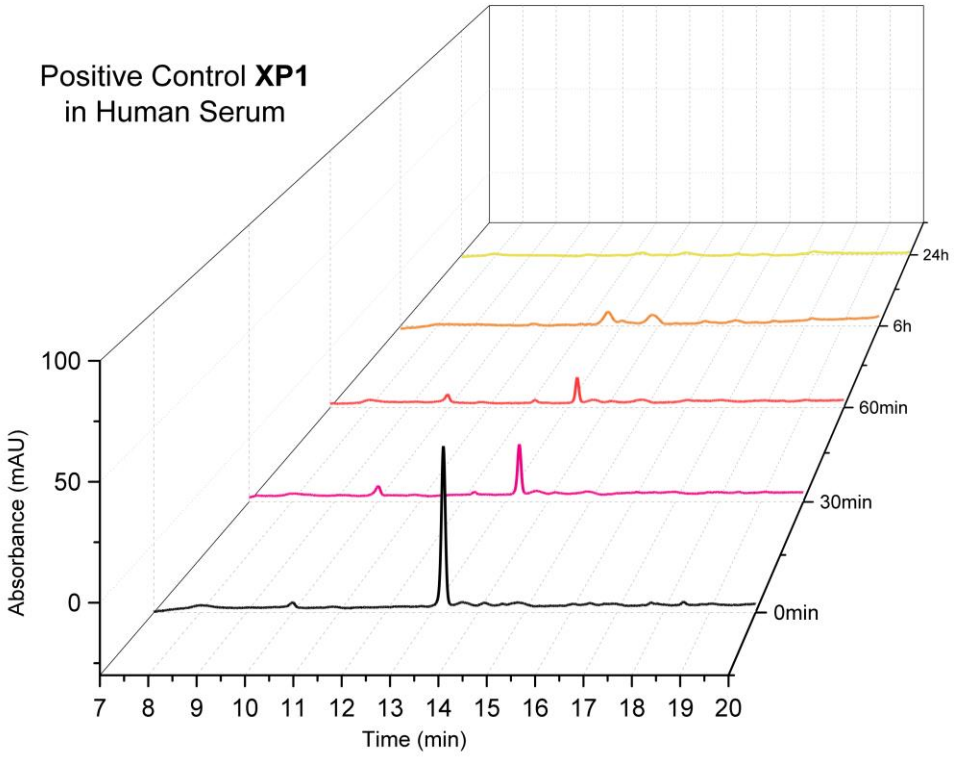

***Figure S4.8**: HPLC trace (214nm) of peptide **XP1** (H-WYKYGKAIYA-NH_2) degradations test. Gradient 5-95%B in 30min using a binary elution system with A: 0.05% TFA in CH_3CN/H_2O (1:9 v/v) and B: 0.05% TFA in CH_3CN/ H_2O (9:1 v/v).*

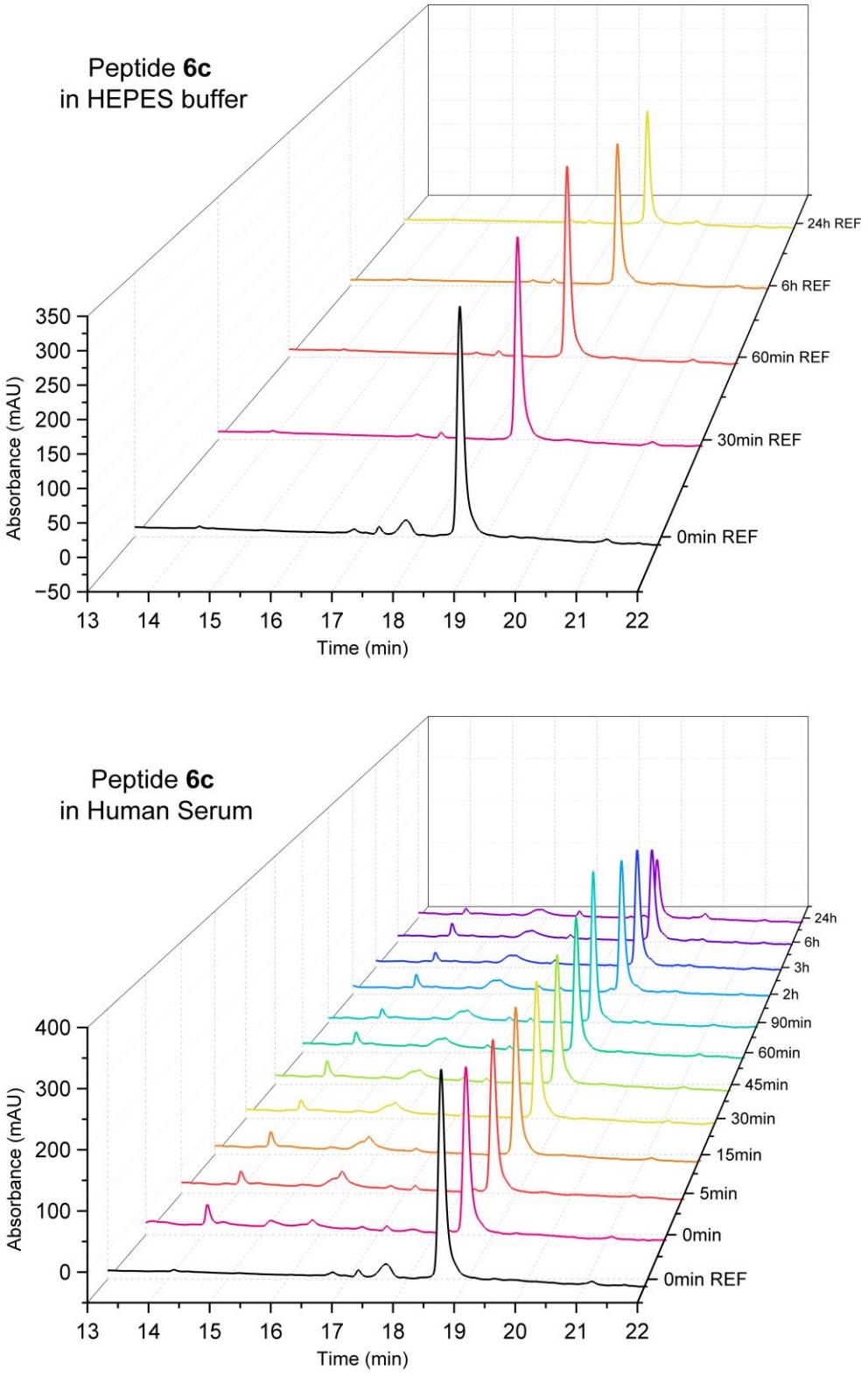

***Figure S4.10**: HPLC trace (214nm) of peptide **6c** degradations test. Gradient 5-95%B in 30min using a binary elution system with A: 0.05% TFA in CH_3CN/H_2O (1:9 v/v) and B: 0.05% TFA in CH_3CN/ H_2O (9:1 v/v).*

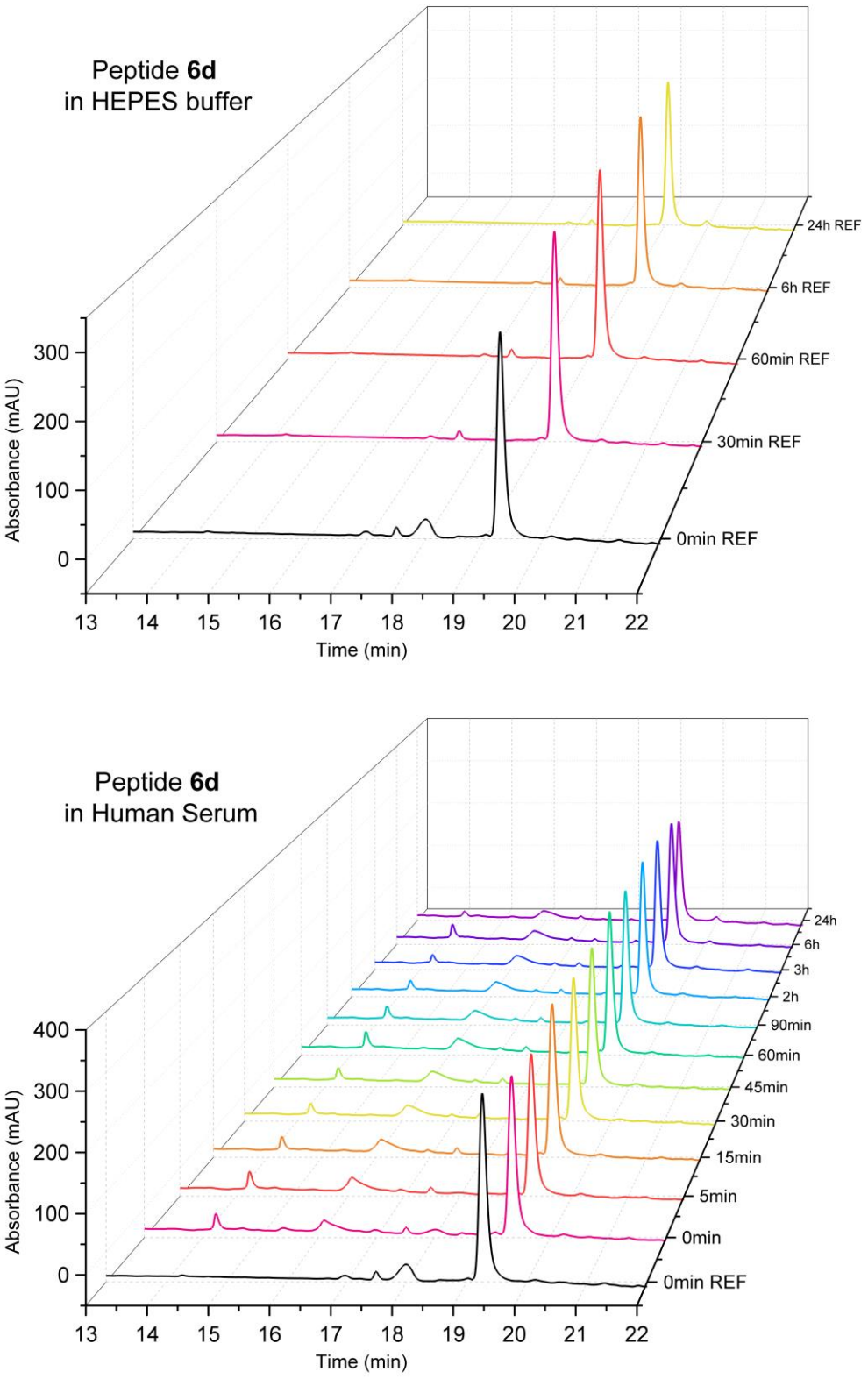

***Figure S4.11**: HPLC trace (214nm) of peptide **6d** degradations test. Gradient 5-95%B in 30min using a binary elution system with A: 0.05% TFA in CH_3CN/H_2O (1:9 v/v) and B: 0.05% TFA in CH_3CN/ H_2O (9:1 v/v).*

5.4.3 FT-IR Spectra

CHO-HA – $NaIO_4$

(A)

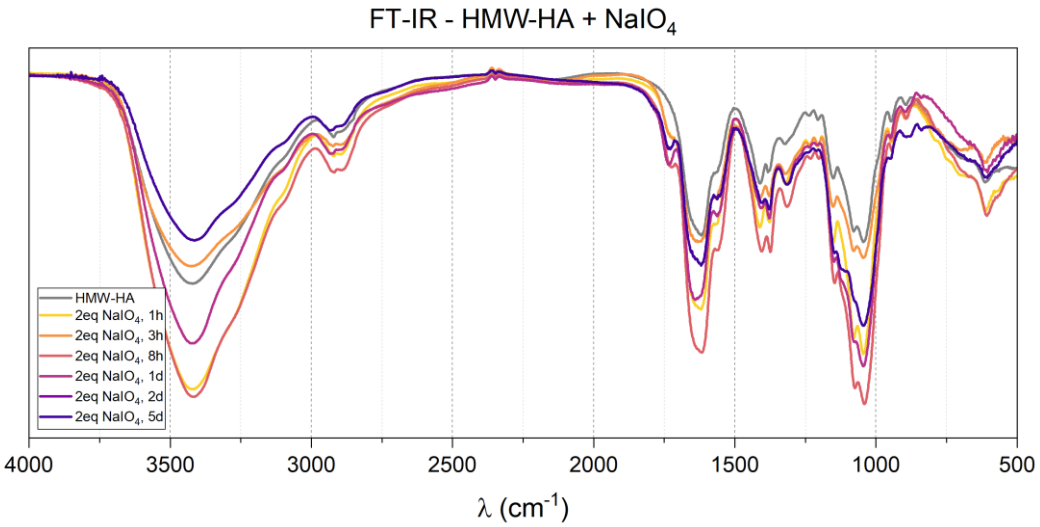

(B)

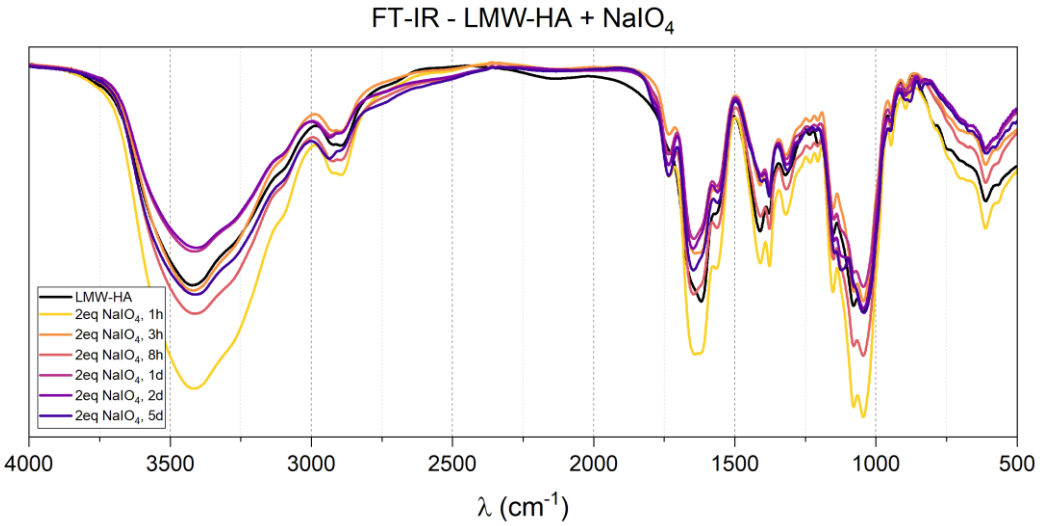

***Figure S4.13**: FT-IR spectra of oxidized (**A**) HMW-HA (**B**) LMW-HA, over the time of the $NaIO_4$ reaction (2eq).*

CHO-HA – TEMPO/laccase/O_2

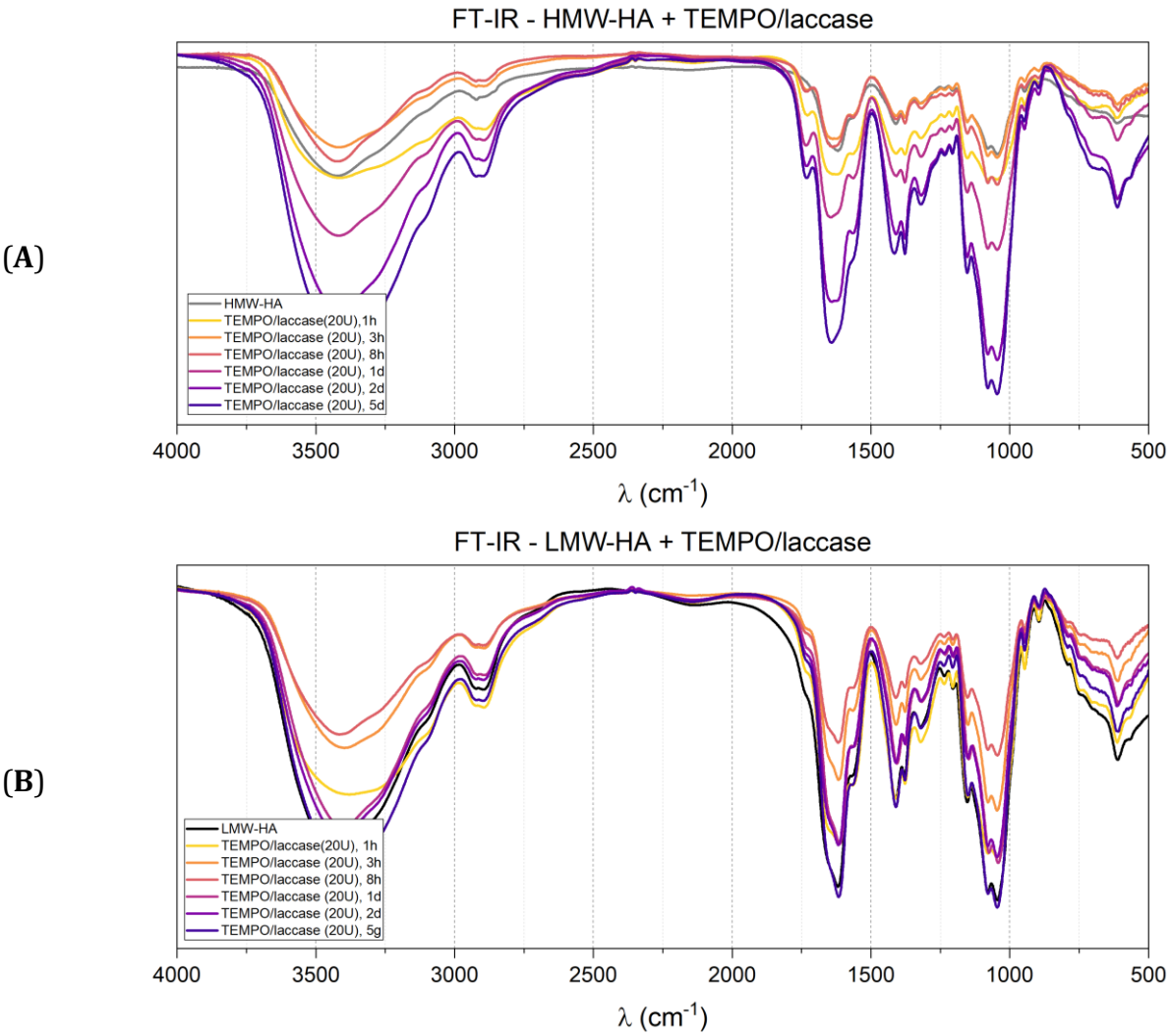

***Figure S4.14**: FT-IR spectra of oxidized (**A**) HMW-HA (**B**) LMW-HA, over the time of TEMPO/laccase/O_2 catalyzed oxidation reaction. TEMPO 8%wt and laccase 20U.*

CHO-HA for electrospinning

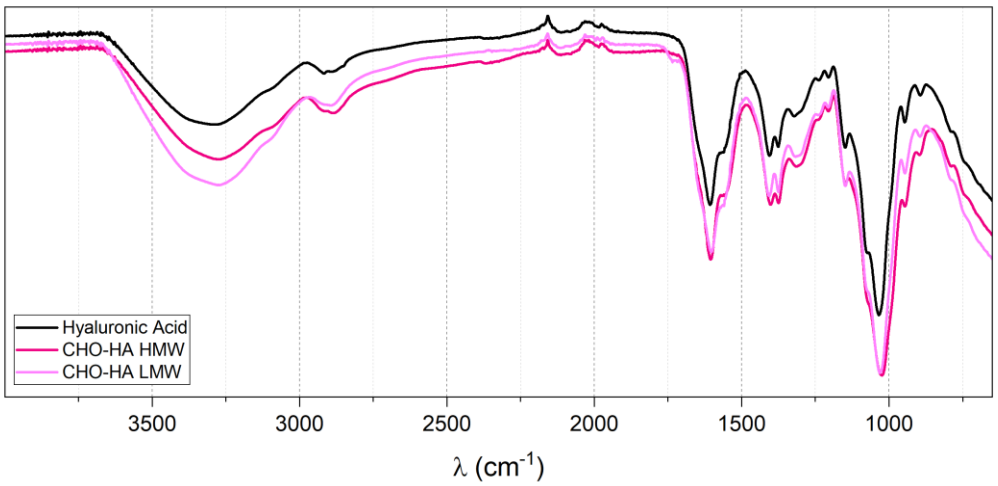

***Figure S4.15**: FT-IR spectra of oxidized hyaluronic acid, CHO-HA HMW and CHO-HA LMW used for electrospinning.*

(A)

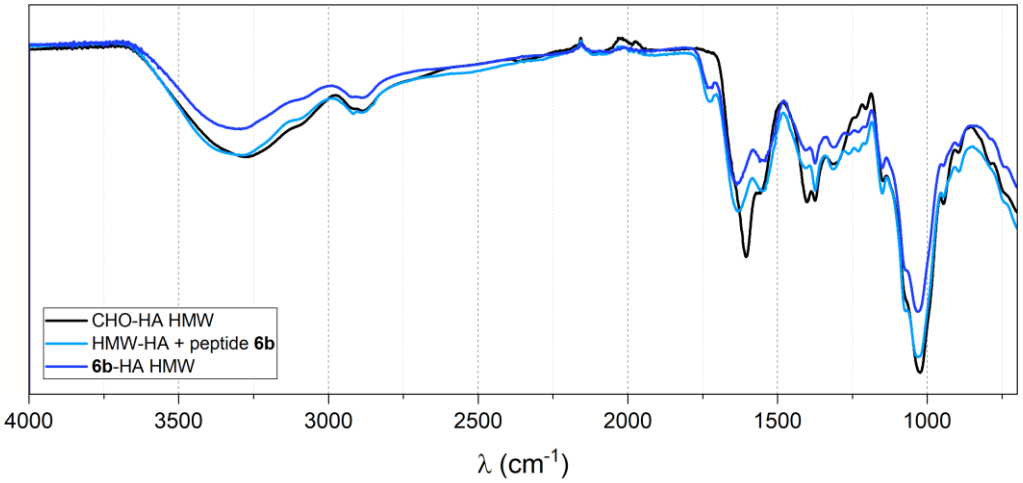

(B)

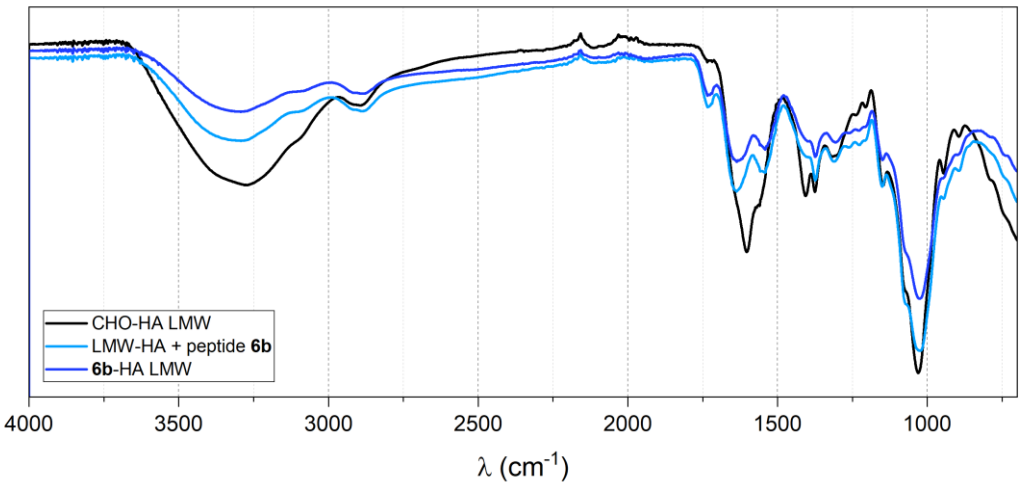

***Figure S4.16**: FT-IR spectra of the conjugate between peptide **6b** and (**A**) HMW HA and CHO-HA, (**B**) LMW HA and CHO-HA.*

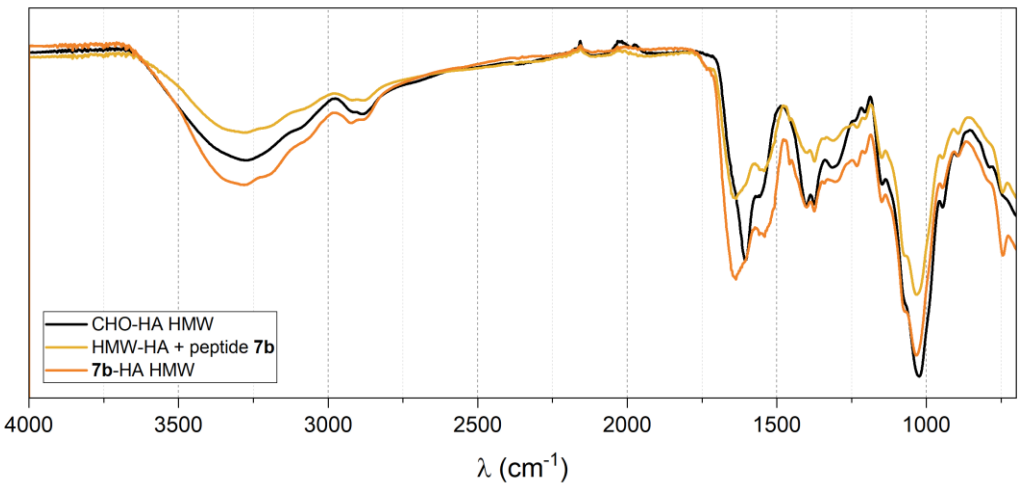

***Figure S4.17**: FT-IR spectra of the conjugate between peptide **7b** and CHO-HA HMW.*

5.4.4 ^{1}H-NMR results

HMW CHO-HA

Time	Area hemiacetal	Error		% of conversion OH to CHO	CHO (mmol/g)
$NaIO_4$, 0.5 eq					
1h	0.000	0.000		0.0	0.00
3h	0.010	0.005		0.5	0.03
8h	0.060	0.025		3.0	0.16
24h	0.190	0.015		9.5	0.50
48h	0.320	0.010		16.0	0.84
120h	0.493	0.060		24.7	1.30
$NaIO_4$, 2eq					
1h	0.182	0.035		9.1	0.48
3h	0.269	0.046		13.5	0.71
8h	0.520	0.059		26.0	1.37
24h	1.011	0.051		50.5	2.66
48h	1.384	0.052		69.2	3.65
120h	1.753	0.039		87.6	4.62

Table S4.1: *Calculation of the amount of aldehyde present on CHO-HA (HMW) grafted using $NaIO_4$. The area is an average of three independent measurements of three independent experiments. Error is calculated as the difference between the highest and lowest value divided by two.*

Time	Area hemiacetal	Error		% of conversion OH to CHO	CHO (mmol/g)
TEMPO 8%wt /laccase 20U					
1h	0.000*	0.000		0.0	0.00
3h	0.047*	0.025		4.7	0.25
8h	0.061*	0.022		6.1	0.32
24h	0.100*	0.015		10.0	0.53
48h	0.127*	0.007		12.7	0.67
120h	0.130*	0.005		13.0	0.69
TEMPO 8%wt /laccase 20U + air bubbling					
1h	0	-		0.0	0.00
3h	0	-		0.0	0.00
8h	0.03	-		3.0	0.16
24h	0.06	-		6.0	0.32
48h	0.07	-		7.0	0.37
120h	0.08	-		8.0	0.42
TEMPO 8%wt /laccase 60U					
1h	0	-		0.0	0.00
3h	0.01	-		1.0	0.05
8h	0.03	-		3.0	0.16
24h	0.08	-		8.0	0.42
48h	0.11	-		11.0	0.58
120h	0.09	-		9.0	0.47
TEMPO 8%wt /laccase 60U + air bubbling					
1h	0	-		0.0	0.00
3h	0.01	-		1.0	0.05
8h	0.02	-		2.0	0.11
24h	0.06	-		6.0	0.32
48h	0.08	-		8.0	0.42
120h	0.06	-		6.0	0.32

Table S4.2: *Calculation of the amount of aldehyde present on CHO-HA (HMW) grafted using the TEMPO/laccase/O_2 catalyzed reaction * average of three independent measurements of three independent experiments. Error is calculated as the difference between the highest and lowest value divided by two.*

LMW CHO-HA

Time	Area hemiacetal	Error		% of conversion OH to CHO	CHO (mmol/g)
$NaIO_4$, 2 eq					
1h	0.151	0.000		7.5	0.40
3h	0.277	0.030		13.8	0.73
8h	0.511	0.026		25.5	1.35
24h	0.940	0.015		47.0	2.48
48h	1.329	0.012		66.4	3.50
120h	1.713	0.005		85.7	4.52

Table S4.3: *Calculation of the amount of aldehyde present on CHO-HA (LMW) grafted using $NaIO_4$. The area is an average of three independent measurements of three independent experiments. Error is calculated as the difference between the highest and lowest value divided by two.*

Time	Area hemiacetal	Error		% of conversion OH to CHO	CHO (mmol/g)
TEMPO 8%wt /laccase 20U					
1h	0.000	0.000		0.0	0.00
3h	0.008	0.003		0.8	0.04
8h	0.024	0.020		2.4	0.12
24h	0.075	0.018		7.5	0.40
48h	0.098	0.028		9.8	0.52
120h	0.120	0.000		12.0	0.63

Table S4.4: *Calculation of the amount of aldehyde present on CHO-HA (LMW) grafted using the TEMPO/laccase/O_2 catalyzed reaction. The area is an average of three independent measurements of three independent experiments. Error is calculated as the difference between the highest and lowest value divided by two.*

CHO-HA for electrospinning

(A)

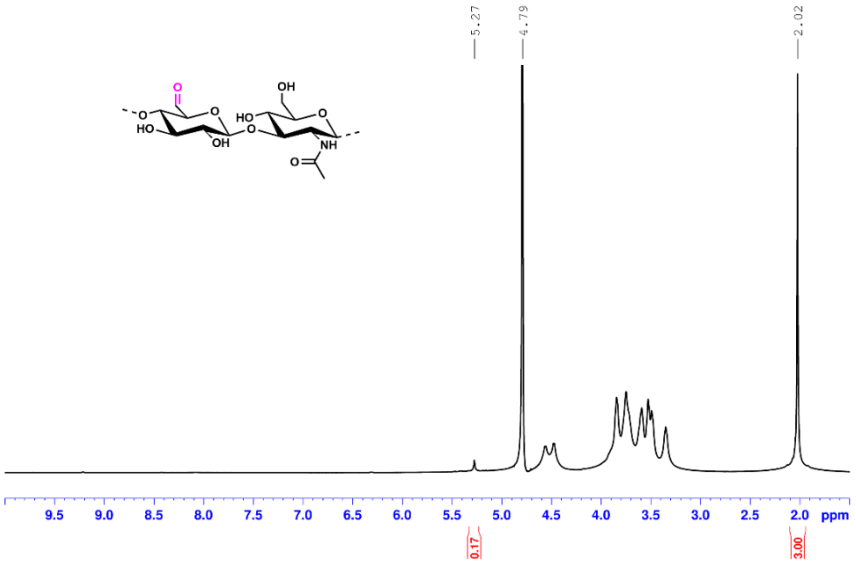

(B)

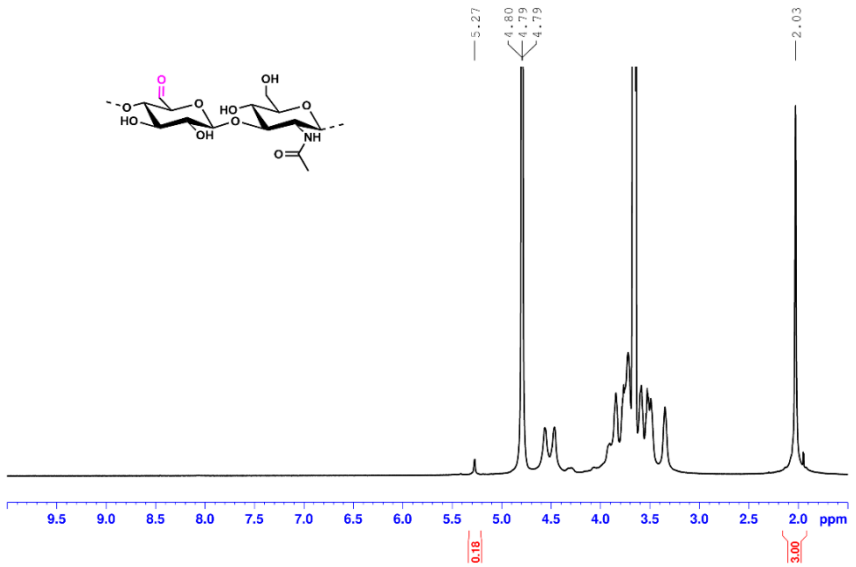

***Figure S4.18**: 1H-NMR (600 MHz) spectra of (**A**) CHO-HA HMW (**B**) CHO-HA LMW.*

Time	Area hemiacetal	Error		% of conversion OH to CHO	CHO (mmol/g)
TEMPO 8%wt /laccase 20U, 2days					
HMW	0.17	-		17	0.44
LMW	0.18	-		18	0.47

***Table S4.5:** Calculation of the amount of aldehyde present on CHO-HA used for electrospinning*

5.4.5 Gel Permeation chromatography - Molecular weight

MW measured for unmodified HMW hyaluronic acid 1683 ± 324.

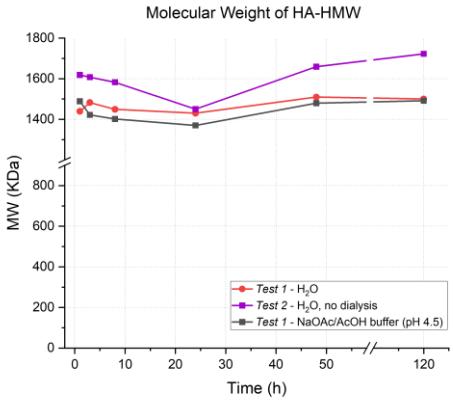

***Figure S4.19**: Molecular weight the time of hyaluronic acid in water and NaOAc/AcOH buffer (50mM, pH 5)*

MW measured for unmodified LMW hyaluronic acid 45.7 ± 4.7.

HMW CHO-HA

Time	MW measured (kDa)	Error (kDa)
$NaIO_4$, 0.5eq		
1h	639.8	44.5
3h	289.4	46.8
8h	141.2	34.8
24h	51.2	12.2
48h	35.9	13.6
120h	24.0	2.71
$NaIO_4$, 2 eq		
1h	266.5	4.6
3h	108.1	9.8
8h	45.9	5.1
24h	26.0	3.9
48h	16.5	0.8
120h	11.3	3.8

***Table S4.6**: MW over time of HMW CHO-HA grafted using $NaIO_4$. MW is an average of three independent measurements of three independent experiments. Error is calculated as the difference between the highest and lowest value divided by two.*

Time	MW measured (kDa)	Error (kDa)
TEMPO 8%wt /laccase 20U		
1h	797.8	76.3
3h	508.3	45.1
8h	233.7	15.7
24h	170.2	9.6
48h	112.9	9.0
120h	94.6	18.8

***Table S4.7**: MW over time of HMW CHO-HA grafted using TEMPO/laccase in 8%wt/20U_4. MW is an average of three independent measurements of three independent experiments. Error is calculated as the difference between the highest and lowest value divided by two.*

LMW CHO-HA

Time	MW measured (kDa)	Error (kDa)
$NaIO_4$, 2 eq		
1h	36.5	2.6
3h	29.5	2.6
8h	20.2	1.3

24h	14.7	0.6
48h	11.2	0.3
120h	8.3	0.9

Table S4.8*: MW over time of LMW CHO-HA grafted using $NaIO_4$. MW is an average of three independent measurements of three independent experiments. Error is calculated as the difference between the highest and lowest value divided by two.*

Time	MW measured (kDa)	Error (kDa)
TEMPO 8%wt /laccase 20U		
1h	44.1	3.3
3h	43.2	3.1
8h	39.8	2.9
24h	38.3	2.1
48h	34.7	1.4
120h	32.3	2.0

Table S4.9*: MW over time of LMW CHO-HA grafted using TEMPO/laccase in 8%wt/20U_4. MW is an average of three independent measurements of three independent experiments. Error is calculated as the difference between the highest and lowest value divided by two.*

5.4.6 SEM images of electrospun hyaluronic acid

Here are reported the SEM images of the solutions described in paragraph 4.2.5 and 4.3.6.

Electrospinning of Hyaluronic acid and PEO

We did not record any SEM image of the following because the solution could not be electrospun:

- 5-20% LMW in H_2O
- 5-20% LMW in H_2O, 3%EtOH in H_2O
- 10-20% HMW-HA, 3%EtOH in H_2O
- 5-7% PEO in H_2O
- 1.5% HMW-HA, 2.5% PEO in H_2O
- 0.75% HMW-HA, 1.25% PEO in H_2O

(A)

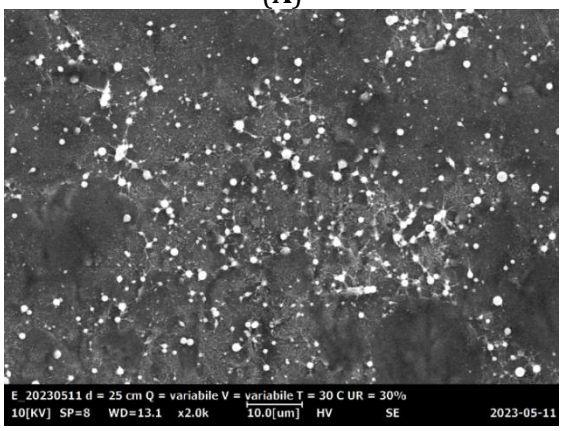

(B)

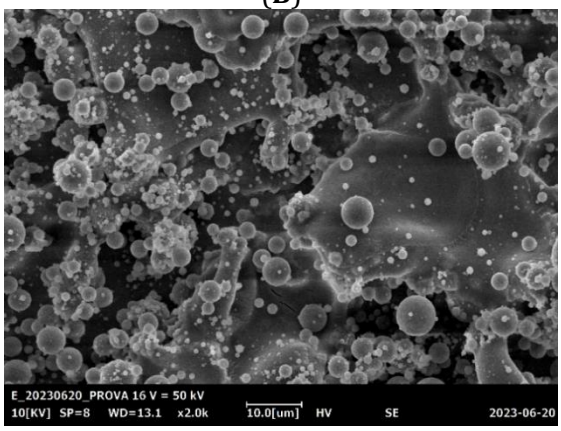

(C)

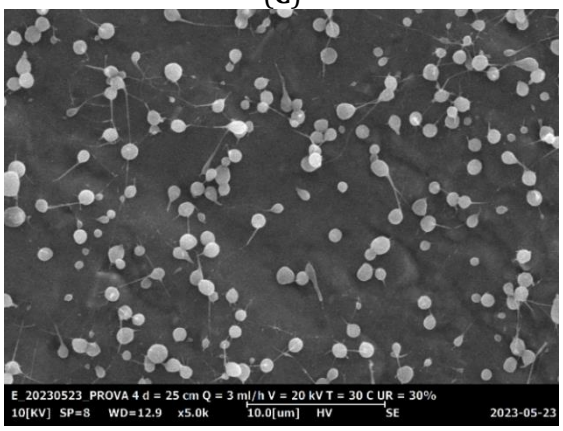

(D)

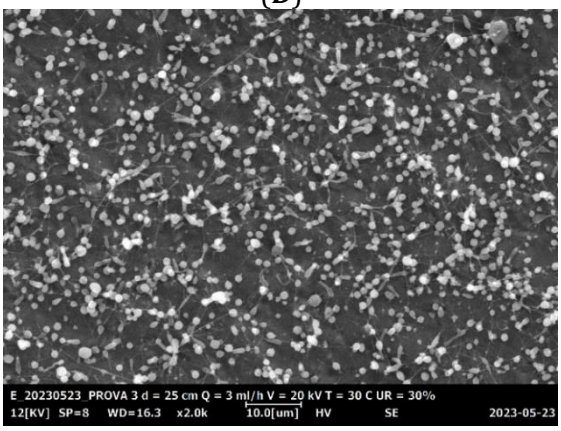

(E)

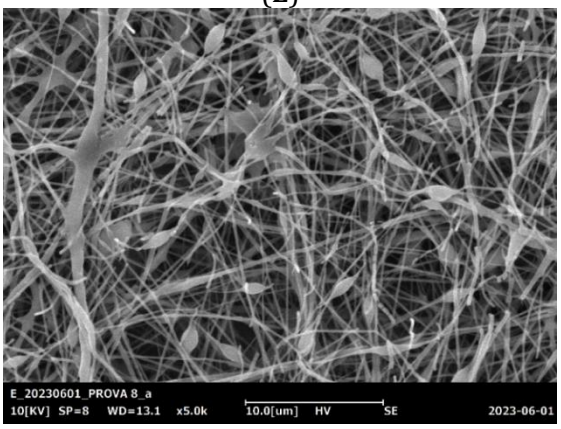

(F)

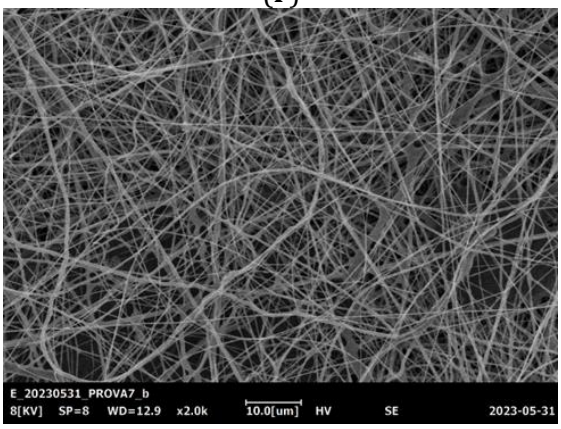

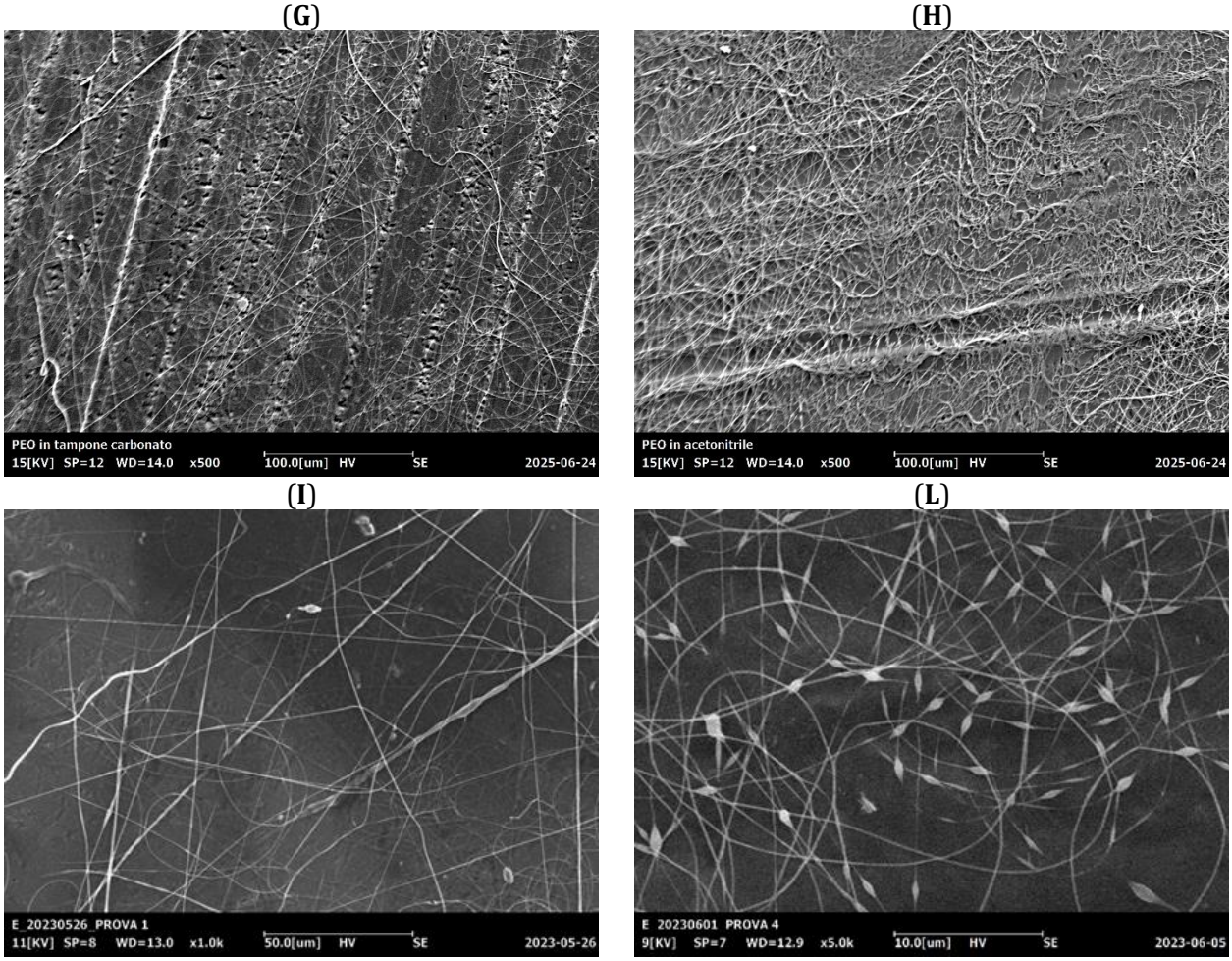

Figure S4.20: *SEM image after electrospinning of (**A**) 1% HMW-HA in H_2O, (**B**) 10% LMW-HA, 3%EtOH in H_2O, (**C**) 0.5% PEO in H_2O, (**D**) 1% PEO in H_2O, (**E**) 2% PEO in H_2O, (**F**) 3% PEO in H_2O, (**G**) 3% PEO in $NaHCO_3/NaH_2CO_3$ buffer, (**E**) 3% PEO in CH_3CN/H_2O (25:75), (**I**) 1% HMW-HA, 2% PEO in H_2O, (**L**) 0.75% HMW-HA, 1.25% PEO in H_2O.*

Electrospinning of CHO-HA

We did not record any SEM image of the following because the solution could not be electrospun:

- 7% LMW CHO-HA, 3% PEO in H_2O

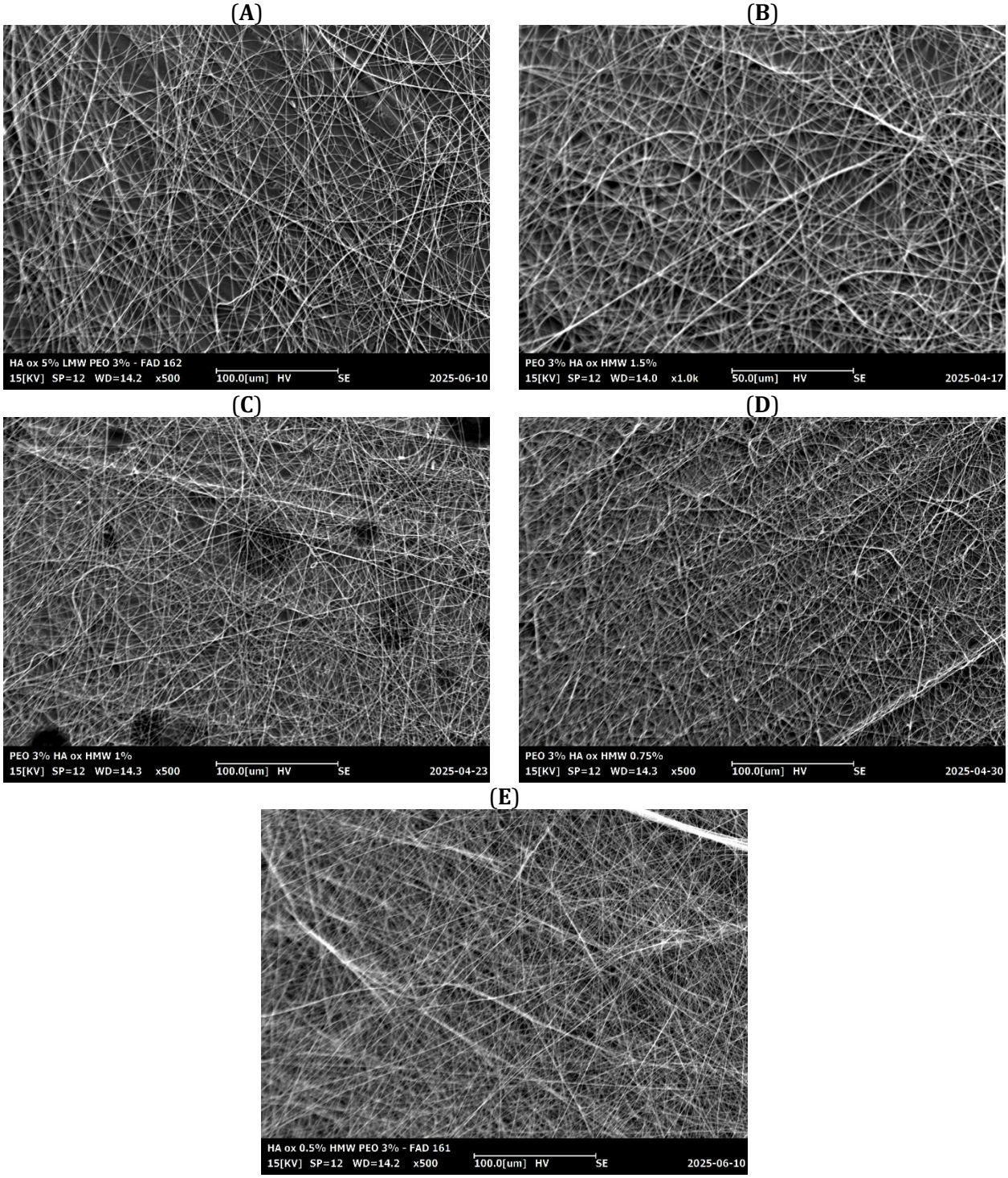

Figure S4.21: *SEM image after electrospinning of (**A**) 5% LMW CHO-HA, 3% PEO in H_2O, (**B**) 1.5% HMW CHO-HA, 3% PEO in H_2O, (**C**) 1% HMW CHO-HA, 3% PEO in H_2O, (**D**) 0.75% HMW CHO-HA, 3% PEO in H_2O, (**E**) 0.5% HMW CHO-HA, 3% PEO in H_2O.*

Electrospinning of the conjugates

We did not record any SEM image of the following because the solution could not be electrospun:

- 5% ***6b***-*HA LMW*, 3% PEO in H_2O

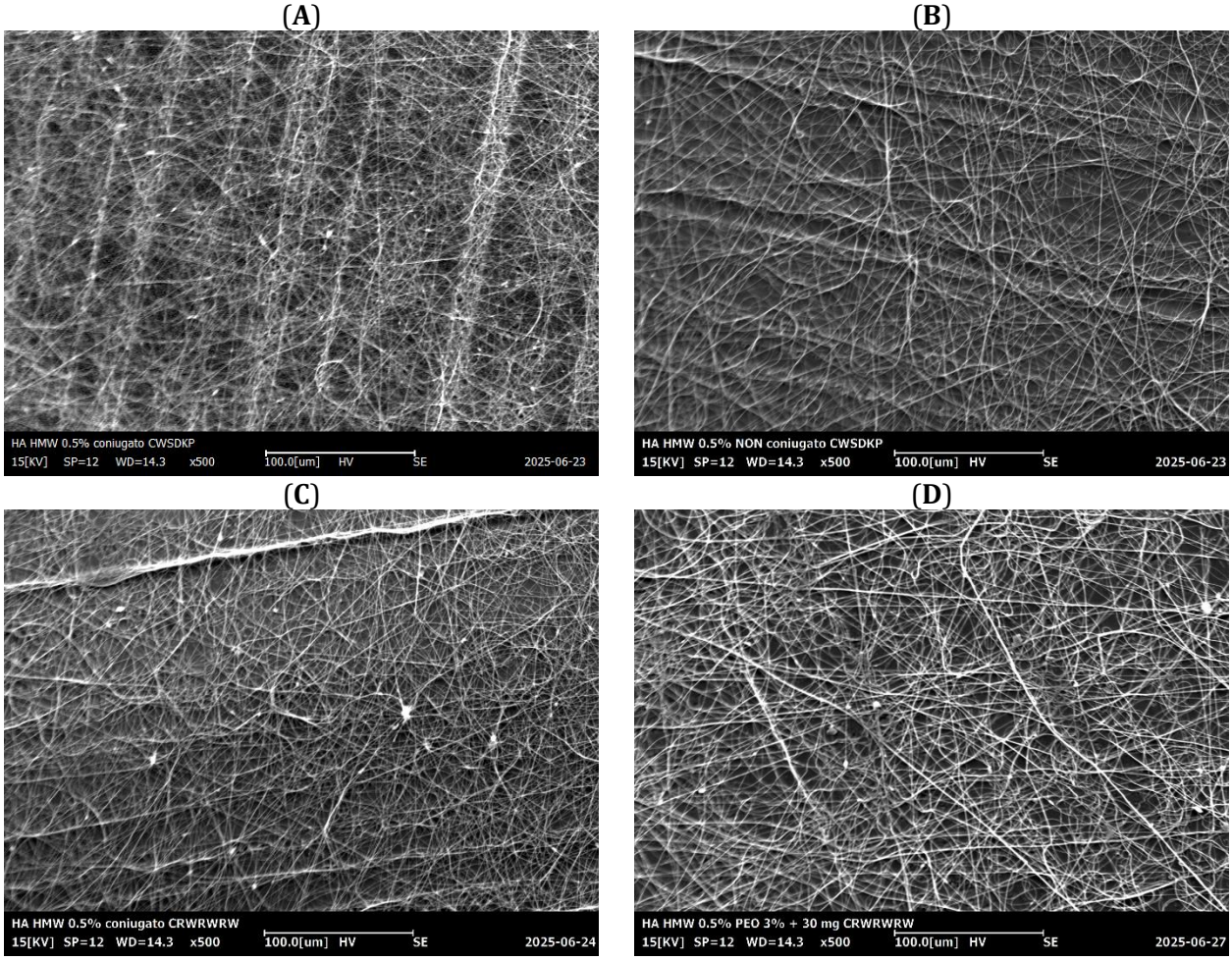

Figure S4.22: *SEM image after electrospinning of (**A**) 0.5% **6b**-HA HMW, 3% PEO in H_2O, (**B**) 0.5% HMW-HA, 3% PEO and 0.2mmol/g_{HA} of peptide **6b** in H_2O, (**C**) 0.5% **7b**-HA HMW, 3% PEO in $NaHCO_3/NaH_2CO_3$ buffer (pH 9.6), (**D**) 0.5% HMW-HA, 3% PEO and 0.6mmol/g_{HA} of peptide **7b** in CH_3CN/H_2O (25:75).*

5.4.7 Immunomodulatory activity

Pro-inflammatory Activity

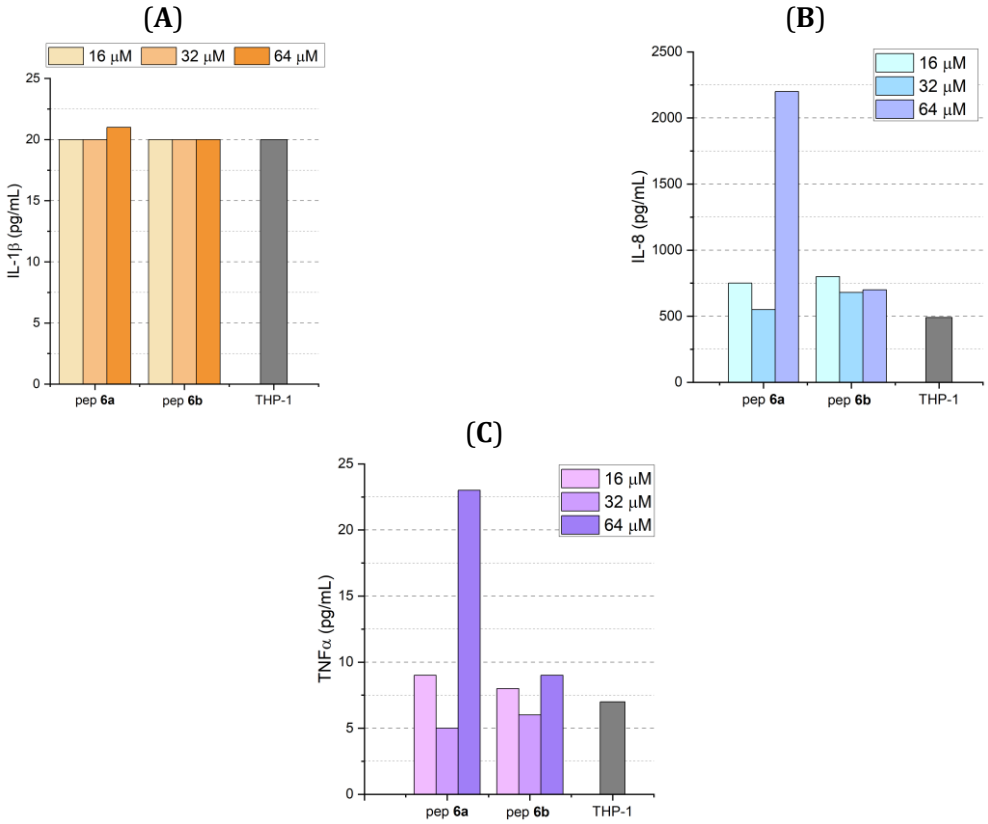

***Figure S4.23**: Measurement of cytokines in supernatants after 24 h of incubation of peptides **6a** (Ac-SDKP-NH_2) and **6b** (H-CWSDKP-NH_2), with the human macrophage line THP-1 differentiated with PMA. (**A**) IL-1β (**B**) IL-8 (**C**) TNFα.*

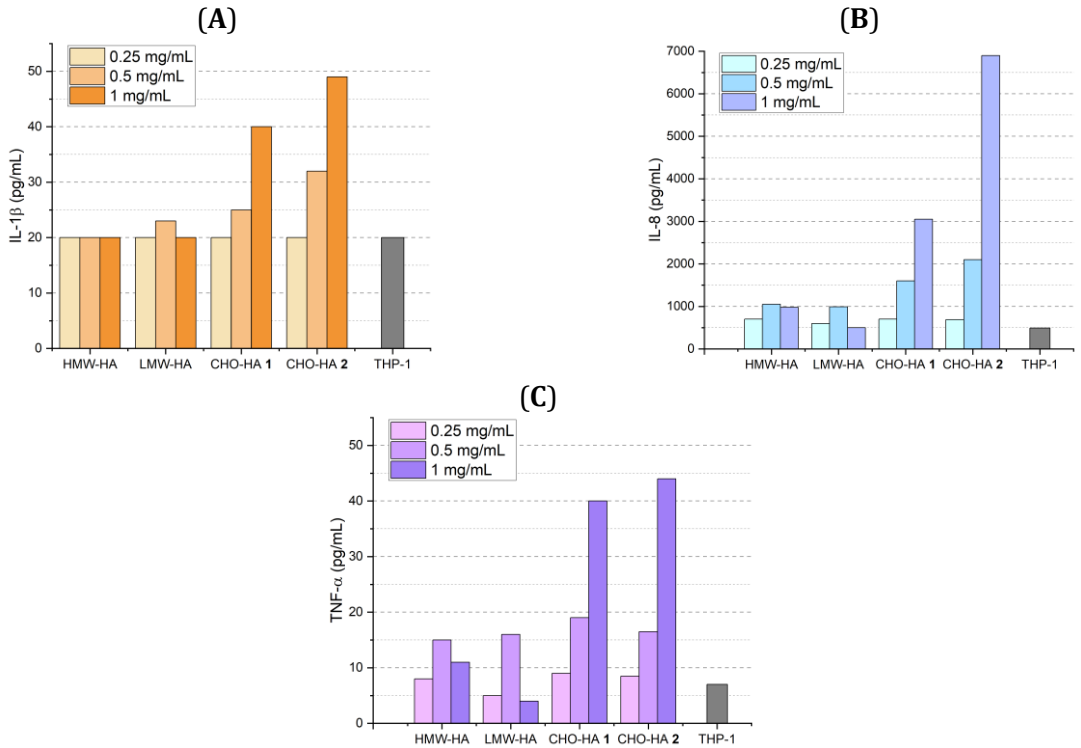

***Figure S4.24**: Measurement of cytokines in supernatants after 24 h of incubation of HMW.HA, LMW-HA and CHO-HA oxidized with TEMPO/laccase for 3h (**1**) and 8h (**2**), with the human macrophage line THP-1 differentiated with PMA. (**A**) IL-1β (**B**) IL-8 (**C**) TNFα.*

Anti-inflammatory Activity

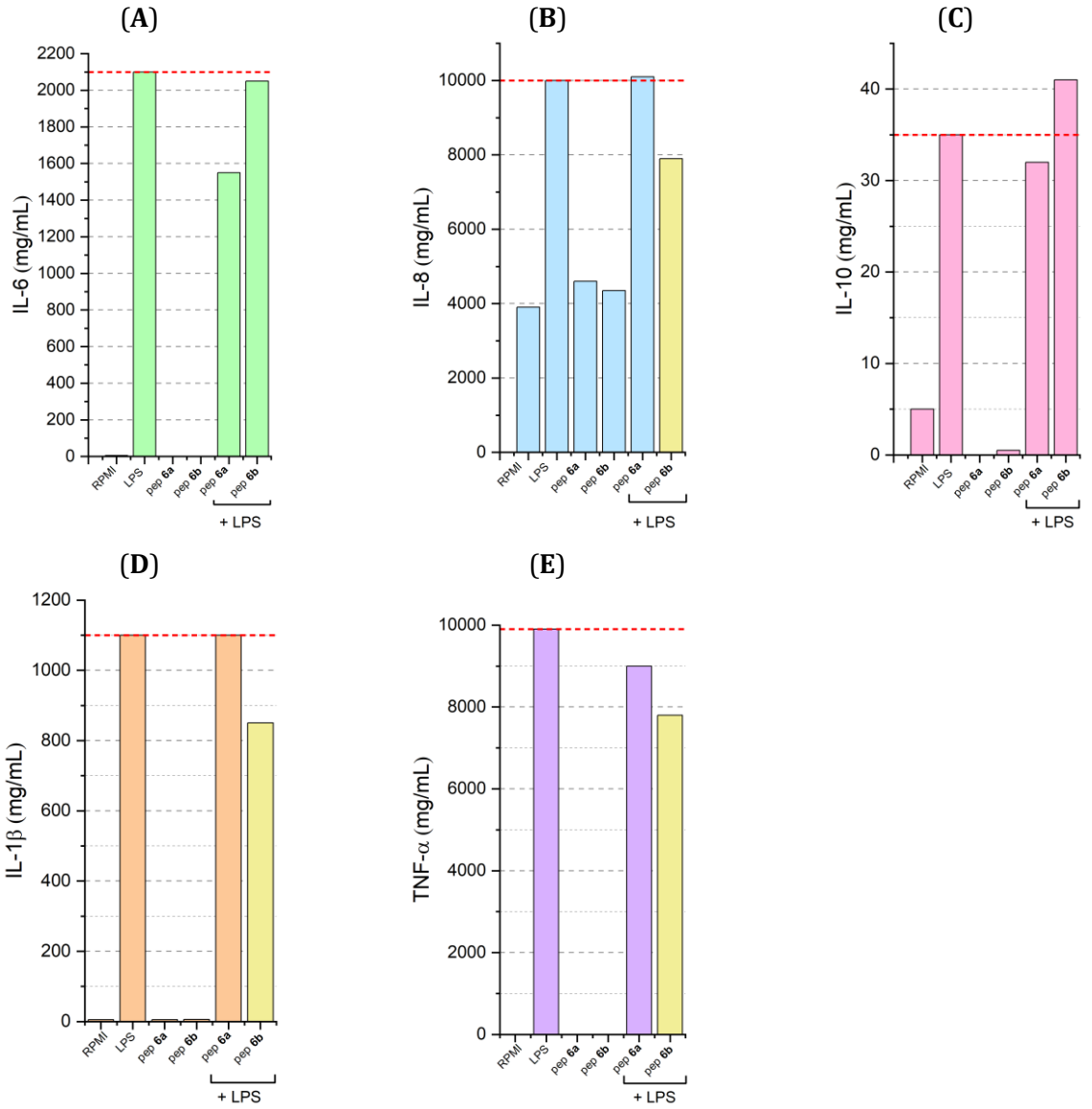

Figure S4.25*: Measurement of cytokines in 64 μM solutions of peptides* ***6a*** *(Ac-SDKP-NH_2) and* ***6b*** *(H-CWSDKP-NH_2). (**A**) IL-6 (**B**) IL-8 (**C**) IL-8 (**C**) IL-10 (**D**) IL-1β (**E**) TNFα. In yellow are highlighted the samples with potential anti-inflammatory activity.*

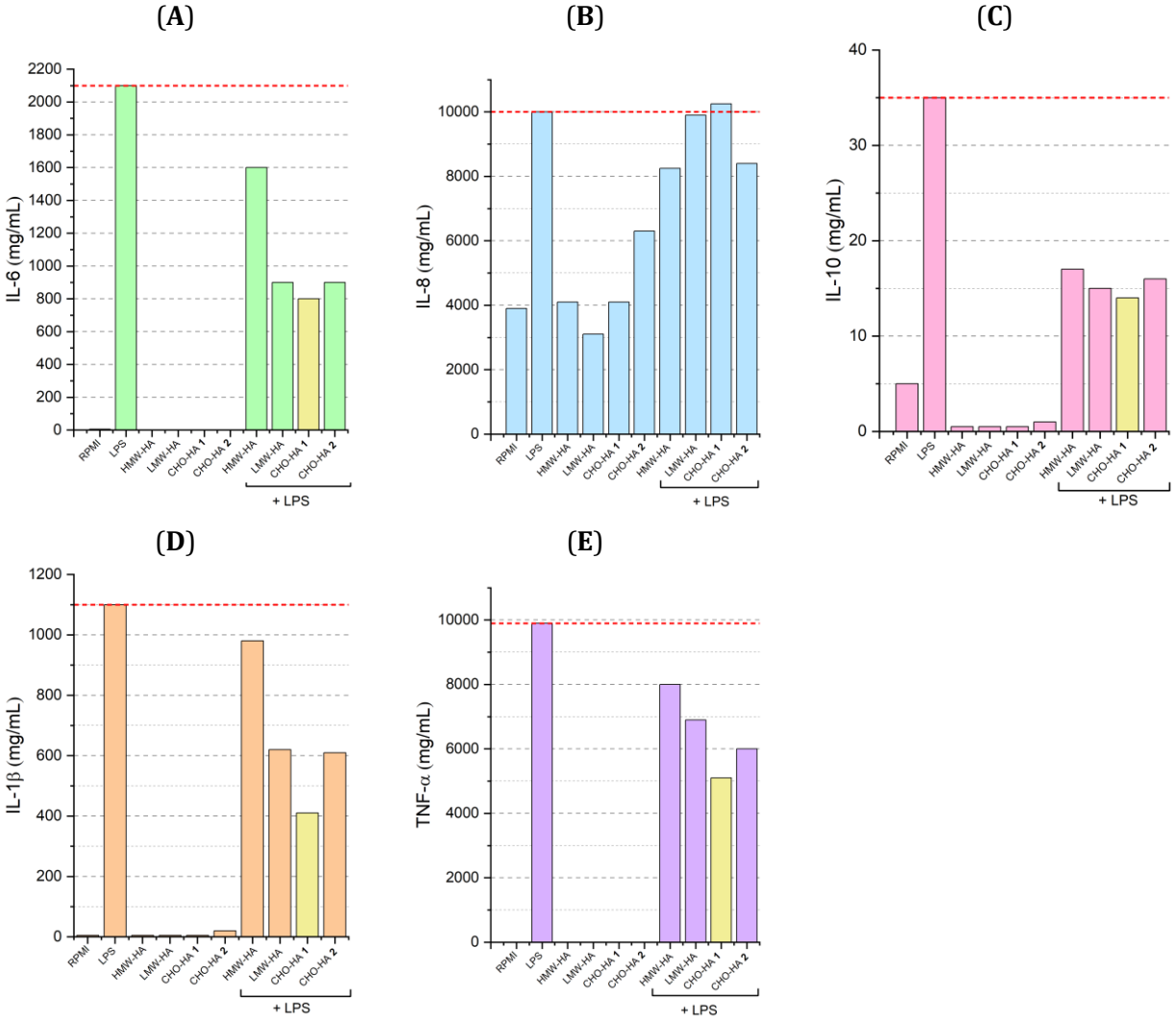

Figure S4.26: *Measurement of cytokines in solutions of HMW-HA (1mg/mL), LMW-HA (1mg/mL) and CHO-HA oxidized with TEMPO/laccase for 3h (**1,** 0.5mg/mL) and 8h (**2,** 0.5mg/mL). (**A**) IL-6 (**B**) IL-8 (**C**) IL-8 (**C**) IL-10 (**D**) IL-1β (**E**) TNFα. In yellow are highlighted the samples with the highest potential anti-inflammatory activity.*

5.4.8 Antibacterial Activity

Qualitative - 10^7 CFU/mL

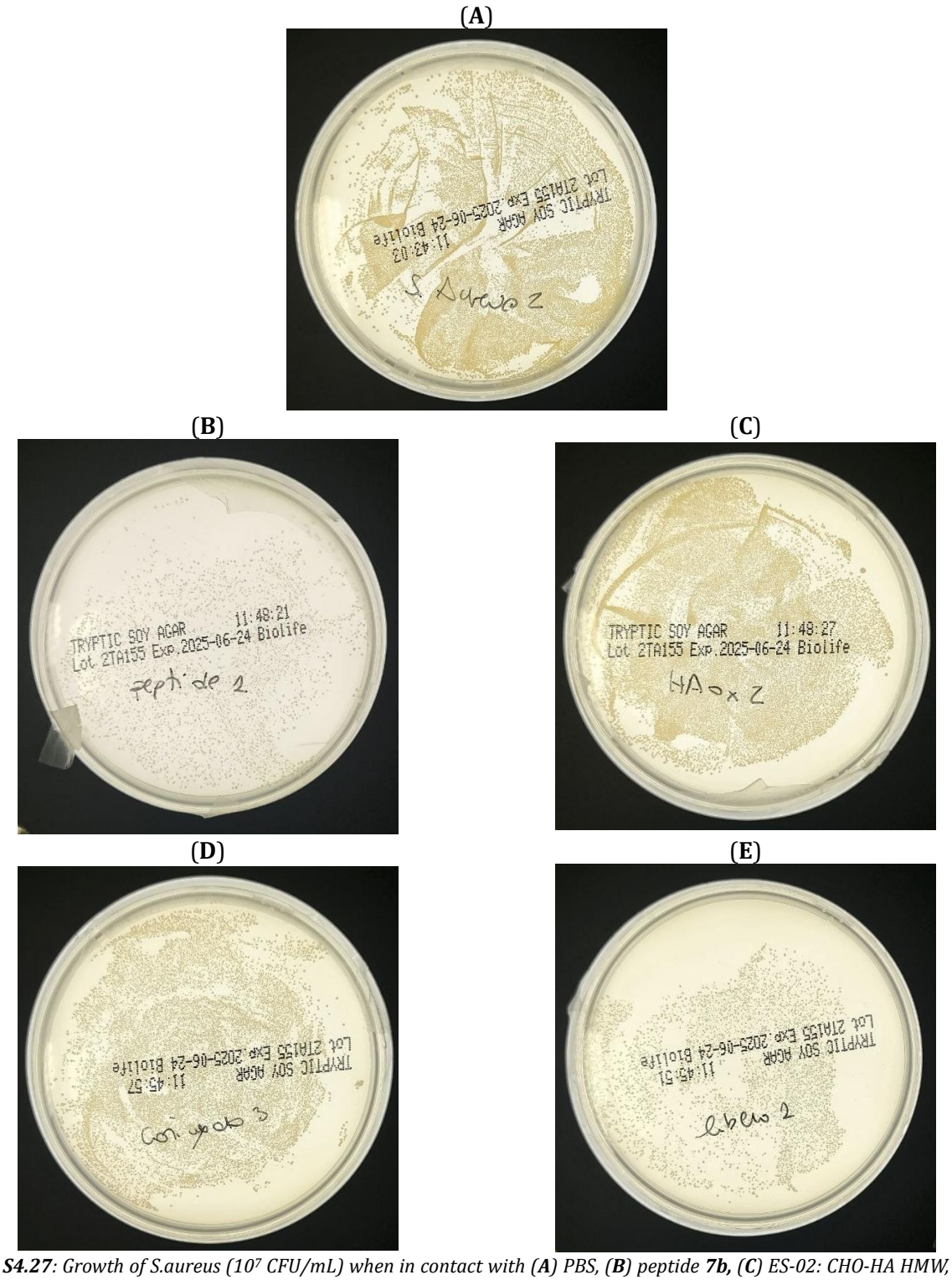

Figure S4.27*: Growth of S.aureus (10^7 CFU/mL) when in contact with (**A**) PBS, (**B**) peptide **7b**, (**C**) ES-02: CHO-HA HMW, (**D**) ES-05: electrospun **7b**-HA conjugate, (**E**) ES-06: HA + **7b** electrospun.*

Qualitative – 10^6 CFU/mL

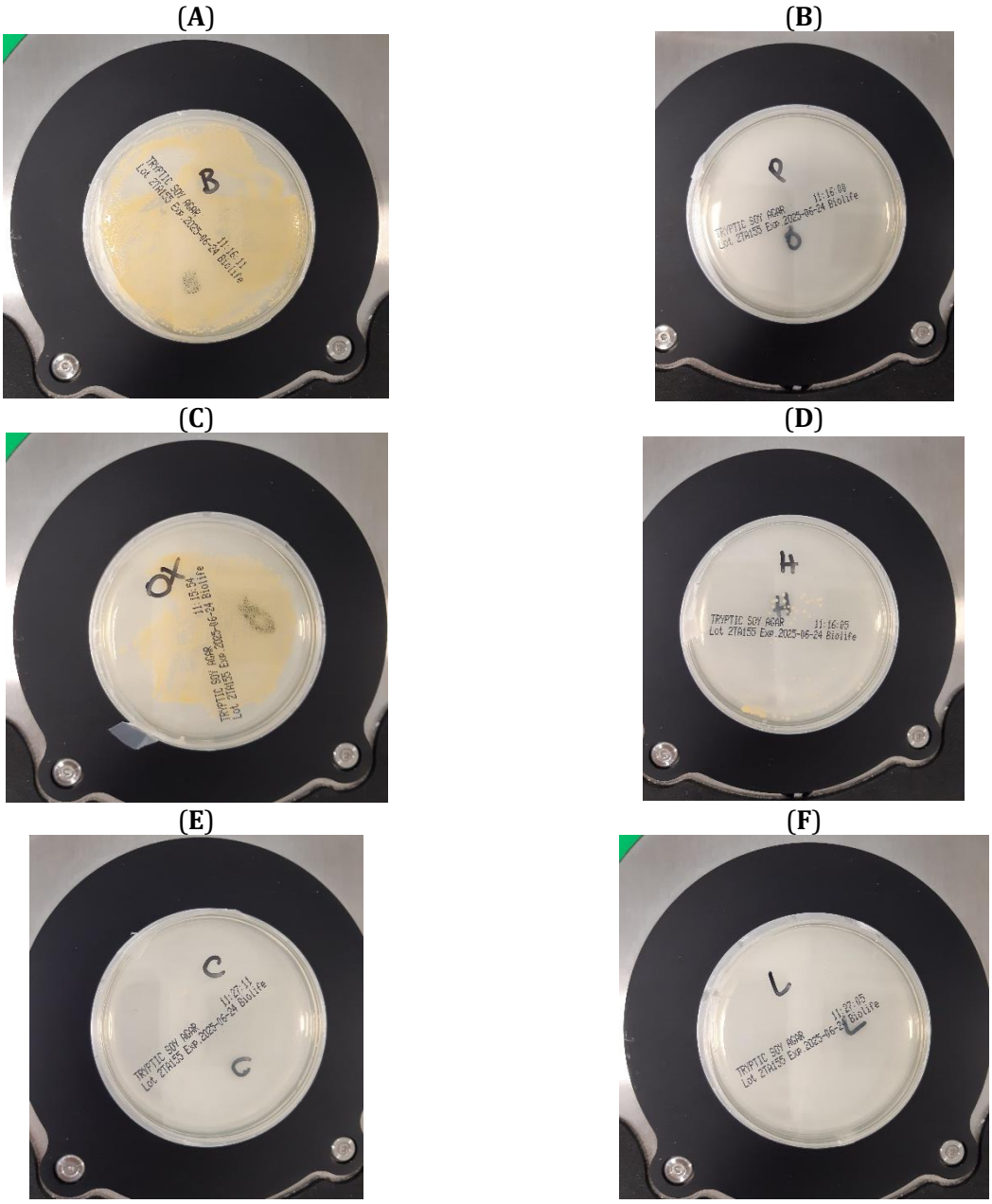

Figure S4.28: *Growth of S.aureus (10^6 CFU/mL) when in contact with (**A**) PBS, (**B**) peptide **7b**, (**C**) ES-02: CHO-HA HMW, (**D**) **r8**: **7b**-HA conjugate, (**E**) ES-05: electrospun **7b**-HA conjugate, (**F**) ES-06: HA + **7b** electrospun.*

Ringraziamenti

In conclusione di questo elaborato vorrei ringraziare e dare merito a tutte le persone che mi sono state accanto in questo percorso e hanno contribuito allo svolgimento del progetto di dottorato. Innanzitutto, ringrazio la mia supervisor, Prof. Cristina Peggion, per aver creduto in me ed avermi offerto l'opportunità di fare questo dottorato, ma anche per il supporto accademico e l'incoraggiamento ricevuti durante questi tre anni che mi hanno permesso di sviluppare un approccio alla ricerca continuo e approfondito. Qualunque dubbio avessi, la sua porta era sempre aperta!

Ringrazio anche il mio co-supervisor Lorenzo Beretta, che mi ha sempre accolto in I.R.A. con il sorriso e disponibilità ad ogni evenienza. In I.R.A mi sono sentita subito parte del *team R&D*, per questo vorrei in particolar modo ringraziare Giulia F, Chiara R, Federica P e le batteriacee©. Sono inoltre grata a Giulia MG e Federica per l'introduzione alla tecnica dell'electrospinning e a Chiara R per lo scrupoloso tutoraggio durante i mesi trascorsi in azienda.

I would like to thank Prof. Paula Gomes and Prof. Cristina Martins for hosting and welcoming me in their laboratories during my research period at the University of Porto. A special thanks also goes to Ana for tutoring me on every new lab equipment and for making me feel part of the group with Renato and Claudia. I felt so welcome that I did not want to leave Porto! I would also like to thank Paula P for showing me the world of an antibacterial testing lab at i3s. Obrigada!

Un sentito ringraziamento va al team dei biologi di Trieste (Prof. Marco Scocchi, Prof. Mario Mardirossian, Dott.ssa Adriana di Stasi e Dott. Luigi de Pascale) per la costante disponibilità ad un confronto e a test sui peptidi e materiali.

Un grande grazie è per tutto il BioOrganic Chemistry (sezione Fmoc) Group di Padova: Daniele, Luana, Chiara G, Claudia S, Matteo, Andrea, Sara, Alessia, Martina R (e Anna). Grazie a voi perché non siete mai stati solo colleghi, ma amici, compagni di brioches e allietatori di pranzi. Grazie a Luana, la mia prima compagna di laboratorio, per essere sempre disponibile ad insegnarmi procedure e strumenti, per tenermi aggiornata su tutte le scadenze, ma soprattutto per avermi accompagnato nelle missioni alla ricerca dei reagenti perduti. Grazie a Daniele per essere un ottimo compagno di cappa, un attentissimo catalogatore di reagenti e *partner in crime* nel design (a simmetria centrale) di presentazioni e poster. Grazie a Claudia S per essere stata la mia prima tutor per la sintesi dei peptidi, per i giorni trascorsi a cambiare gli eluenti dell'HPLC durante i test di degradazione e per aver condiviso con me gli sprint di energia di Daniele allo zoo di Praga. Grazie ad Andrea e Sara, che sono stati dei laureandi modello e con le loro domande mi hanno aiutato ad approfondire le mie conoscenze. Grazie a Chiara G e a Matteo per i piacevoli pranzi condivisi e per le serate di bouldering. Grazie anche ai Prof. Barbara Biondi e Prof. Ivan Guryanov per gli spunti di approfondimento e la disponibilità a spiegazioni in ogni occasione. Infine,

grazie al nostro membro onorario Anna per i suoi simpatici racconti durante il pranzo e per gli ottimi consigli di stile nelle presentazioni. È sempre un gran piacere chiacchierare con te! Grazie

Porgo una menzione d'onore agli amici che hanno condiviso dall'esterno questo dottorato. Giulia P per avere sempre un film trashino, dei mirtilli e delle patatine pronti all'uso. Vittoria per le carbonare con tiramisù, i sushi, gli spuntini al Mac, i gelati, gli hamburger, le pizze alle patatine (dopo il siciliano), i brunch e le tigelle, ma soprattutto per essere sempre venuta a trovarmi in qualsiasi posto finissi (incluso Paderno D'Adda). Alessandro e Martina M per le passeggiate serali a Padova, i pranzi durante i weekend e le gite all'IKEA.

Grazie alla mia famiglia. Ai miei genitori per avermi incoraggiato a proseguire nei miei studi e per avermi sempre supportato nelle mie decisioni. A mio fratello Emanuele perché probabilmente se non avesse detto quel "perché non chimica?" più di nove anni fa, non so se il mio percorso sarebbe arrivato a questo punto. A Francesco perché mi sei sempre stato accanto, non hai mai dubitato di me e delle mie capacità supportandomi nei momenti di difficoltà con deliziosi pasti e tanti pat-pat, ma soprattutto perché mi sproni ad essere una persona migliore sia nella vita che nel lavoro.

Infine, vorrei citare e ringraziare tutte le persone che hanno contribuito al lavoro di questa tesi con analisi ed esperimenti aggiuntivi. Senza di loro questo lavoro non avrebbe potuto essere portato a compimento. In particolare, grazie alla Dott.ssa Adriana Di Stasi per tutte le misure di attività antibatterica dei campioni di cotone e dei peptidi, ma anche per la disponibilità a test sugli analoghi di PP4 per la rigenerazione del collagene; grazie alla Dott.ssa Paula Parreira per i test effettuati sui campioni di chitosano; grazie alla Dott.ssa Chiara Rinoldi per i test antibatterici sui campioni di acido ialuronico; grazie alla Prof. Antonella Glisenti per essere sempre disponibile a eseguire analisi XPS sui campioni più disparati; grazie al Dott. Renato Schiesari per gli spettri FT-IR; ed infine grazie ai Prof. Giovanna Batoni e Prof. Semih Esin per le misure e le spiegazioni sull'attività antiinfiammatoria.